STRINGQFT

String-Theoretic Construction
of Quantum Field Theory

VOLUME XII

Type IIB Geometric Engineering

Xingyang Yu

StringQFT v1.0 / Source build candidate

Drafted with AI assistance under the supervision of the author.
Manuscript free to read. All rights reserved.

Contents

XII.1 Six-dimensional $(2,0)$ theories from ALE spaces **1**

XII.1.1 What becomes light when a sphere collapses? 1
XII.1.2 The compact spheres and their pairing 1
XII.1.3 The tension and charge of a wrapped D3 3
XII.1.4 Tensor vacua and the tensionless origin 6
XII.1.5 The local field theory limit 9
XII.1.6 An external circle turns strings into particles 11
XII.1.7 The gauge coupling remembers the radius 13
XII.1.8 Exercises 16

XII.2 Local threefolds and conifold particles **19**

XII.2.1 A particle at a shrinking sphere 19
XII.2.2 The cycles of a smoothed node 19
XII.2.3 Period integrals and the cutoff 23
XII.2.4 A loop around the node 26
XII.2.5 The wrapped D3 and its electric charge 28
XII.2.6 When the photon becomes dynamical 30
XII.2.7 The four-dimensional threshold 33
XII.2.8 Exercises 36

XII.3 Hypersurface singularities and the deformation spectrum **41**

XII.3.1 A singularity with two different deformations 41
XII.3.2 Which singularities enter the construction? 42
XII.3.3 The Jacobi algebra counts independent deformations 44
XII.3.4 The three-form sets the physical unit 46
XII.3.5 Reading a deformation spectrum 48
XII.3.6 A reusable family and its limits 51
XII.3.7 Two active coordinates and a lattice of parameters 54
XII.3.8 Holding sources fixed in a rank-four construction 56
XII.3.9 A rank-seven family with all coefficient roles 58
XII.3.10 Exercises 62

XII.4 Vanishing cycles, charge pairings, and a controlled BPS chamber **66**

XII.4.1 Which charges disappear? 66

XII.4.2 Distinguished paths and matching spheres 66
XII.4.3 The intersection of two three-spheres 69
XII.4.4 Periods and the rays at the real-root point 71
XII.4.5 Two elementary monodromies 73
XII.4.6 From a charge basis to a stable spectrum 76
XII.4.7 Changing the paths and rotating the half-plane 80
XII.4.8 Three spheres and a measurable null period 82
XII.4.9 Two maps and six indecomposable charges 85
XII.4.10 Which interval representations bind? 87
XII.4.11 Exercises 90

XII.5 Gauge sectors from ALE fibrations 94
XII.5.1 How an ALE fiber produces four-dimensional periods 94
XII.5.2 The threefold over the punctured sphere 94
XII.5.3 From a wrapped sphere to a spectral period 97
XII.5.4 Four masses and one interior coefficient 99
XII.5.5 The rank and the finite kinetic variation 102
XII.5.6 Pinching a weak gauge tube 104
XII.5.7 The weak vector and its four fundamentals 108
XII.5.8 Sending one flavor mass to infinity 111
XII.5.9 The irregular end and its finite Coulomb variation 113
XII.5.10 Compact periods that survive the confluence 115
XII.5.11 Exercises 118

XII.6 Marginal families and local limits 122
XII.6.1 Two ways to change a singularity 122
XII.6.2 The isolated part of the quartic family 123
XII.6.3 Which deformations carry a scale? 125
XII.6.4 From geometric parameters to physical couplings 127
XII.6.5 Zooming in on the tuned origin 128
XII.6.6 Parameters that survive the local limit 131
XII.6.7 Two masses and the choice of a critical fiber 134
XII.6.8 From quartic scaling to a node 136
XII.6.9 Turning on a relevant coupling 138
XII.6.10 Parameters of the local sector 140
XII.6.11 Nested scales and the surviving local sector 141
XII.6.12 Exercises 144

XII.7 Beyond hypersurfaces: complete intersections 148
XII.7.1 Two equations for the same physical question 148
XII.7.2 Finding the isolated threefold 148
XII.7.3 Independent changes of the defining equations 151
XII.7.4 The nine deformation directions 153
XII.7.5 The residue sets the physical scale 157
XII.7.6 Vacuum parameters, masses, and couplings 159
XII.7.7 Following a mass deformation 160

XII.7.8 The residue near a selected node . . . 164
XII.7.9 Tuning the quartic local singularity . . . 166
XII.7.10 Changing one exponent . . . 168
XII.7.11 Exercises . . . 172

XII.8 Four-dimensional $\mathcal{N} = 1$ engineering and geometric transitions 176
XII.8.1 From a wrapped brane to a glueball variable . . . 176
XII.8.2 A rigid sphere and its four-dimensional gauge fields . . . 176
XII.8.3 Which charge crosses the conifold transition? . . . 179
XII.8.4 Computing the compact and regulated periods . . . 181
XII.8.5 Flux pairing and the four-dimensional scale . . . 184
XII.8.6 One superpotential and the holomorphic vacua . . . 186
XII.8.7 Two cuts share one cutoff logarithm . . . 189
XII.8.8 The IIA and M-theory versions of the integer . . . 193
XII.8.9 Exercises . . . 194

XII.9 Atlas of direct IIB constructions 198
XII.9.1 What distinguishes two construction records? . . . 198
XII.9.2 Compact charges and relative periods . . . 198
XII.9.3 Equal Milnor rank and different parameter roles . . . 203
XII.9.4 Four ordinary ends and a weak tube . . . 206
XII.9.5 One quadric with and without flux . . . 209
XII.9.6 When the presentation or spacetime dimension changes . . . 211
XII.9.7 The atlas by construction route . . . 212
XII.9.8 Exercises . . . 216

Chapter XII.1

Six-dimensional $(2,0)$ theories from ALE spaces

XII.1.1 What becomes light when a sphere collapses?

Take a small two-sphere in the internal space and wrap a brane around it. If the brane has no remaining spatial direction, an observer outside the internal space sees a particle. If it has one remaining spatial direction, the observer sees a string. Shrinking the same sphere therefore lowers a particle mass in type IIA and a string tension in type IIB. Which of these objects becomes light determines the field theory we should look for.

We start from the resolution of an ADE surface singularity and follow the type-IIB string through two operations. The internal wrapping produces a string in six dimensions. Winding that string around an *external* circle produces a charged particle in five dimensions. We will track the charge, the energy and the fields that couple to these objects, using the two spheres of A_2 throughout. This will explain why the vector field appears after the circle reduction, even though a generic six-dimensional vacuum has tensor multiplets.

We use the D-brane action from Volume III and the ADE resolutions and calibrations from Volume III. From Volume I we need the distinction between a chiral tensor multiplet and a vector multiplet. We will recall the part of each construction needed for the calculation. Our target in six dimensions is the local interacting theory at the tensionless point. The tensor branch is how we approach it and identify the degrees of freedom that become light.

XII.1.2 The compact spheres and their pairing

How do the resolving spheres determine which charges a string can carry? Let X_Γ be a smooth hyperkähler ALE resolution of $\mathbb{C}^2/\Gamma$, for a nontrivial finite subgroup $\Gamma \subset SU(2)$. The space is noncompact and approaches $\mathbb{R}^4/\Gamma$ at infinity. We hold its asymptotic data

fixed. The part relevant to a wrapped brane is the compact homology of the resolution:

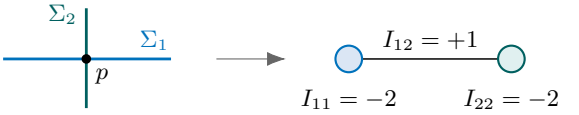
$$H_2(X_\Gamma, \mathbb{Z}) = \bigoplus_{i=1}^{r} \mathbb{Z}[\Sigma_i], \qquad r = \operatorname{rank} \mathfrak{g}_\Gamma. \tag{XII.1.1}$$

Here $\mathfrak{g}_\Gamma$ denotes the finite ADE Lie algebra associated with Γ. Each Σ_i is an exceptional sphere. The finite diagram records their intersections. The extra node of the affine McKay diagram does not add a compact homology generator.

To calculate the pairing, use a complex structure in which the exceptional spheres are holomorphic. Orient them and the surface by this complex structure. Adjunction for a smooth curve Σ_i of genus zero and trivial ambient canonical class K_X gives

$$-2 = 2g(\Sigma_i) - 2 = (K_X + \Sigma_i) \cdot \Sigma_i = \Sigma_i \cdot \Sigma_i. \tag{XII.1.2}$$

This is the intersection with a displaced representative, even though a sphere is drawn only once in Figure XII.1.1. Two distinct neighboring spheres meet once and transversely. The complex orientation gives that intersection a positive sign. With $I_{ij} = \Sigma_i \cdot \Sigma_j$, the diagonal is thus -2 and the off-diagonal entries are $+1$ for joined nodes and zero otherwise.



Branches near their intersection Finite intersection diagram

Figure XII.1.1: At left, lines represent the two complex branches near the single transverse intersection p of the exceptional spheres. The link at right records $I_{12} = 1$, and the node labels record the two self-intersections. It represents the intersection data rather than additional cycles.

For A_2, the group is $\mathbb{Z}_3$. The two matrices we will use are

$$I = \begin{pmatrix} -2 & 1 \\ 1 & -2 \end{pmatrix}, \qquad C = -I = \begin{pmatrix} 2 & -1 \\ -1 & 2 \end{pmatrix}. \tag{XII.1.3}$$

The positive form C is the Cartan matrix. To see the root normalization directly, take orthonormal vectors e_i in $\mathbb{R}^3$ and work in their sum-zero plane. The simple roots are

$$\alpha_1 = e_1 - e_2, \qquad \alpha_2 = e_2 - e_3, \qquad \alpha_i \cdot \alpha_j = C_{ij}. \tag{XII.1.4}$$

Consequently an oriented compact wrapping $q = n_1\Sigma_1 + n_2\Sigma_2$ has simple-charge coordinates (n_1, n_2). For $q' = \sum_i n_i'\Sigma_i$, the positive pairing on compact string charges is

$$(q, q') = -q \cdot q' = n^{\mathsf{T}} C n'. \tag{XII.1.5}$$

The minus sign converts the oriented geometric intersection into the positive root form. It does not reverse any individual brane charge.

For a single charge, the quadratic form makes positivity and the distinction between a charge and its coordinates concrete:

$$\|n_1\alpha_1 + n_2\alpha_2\|^2 = 2n_1^2 - 2n_1n_2 + 2n_2^2 = n_1^2 + n_2^2 + (n_1 - n_2)^2. \tag{XII.1.6}$$

For real n_i this vanishes only at the zero vector. For integral n_i, asking for a root means asking which nonzero compact charges have square two. Each of the three squares on the right is an integer square. Their sum can be two only if two are one and the third is zero. The solutions are

$$(n_1, n_2) = (1,0), (0,1), (1,1), (-1,0), (0,-1), (-1,-1). \tag{XII.1.7}$$

This recovers the six roots without mistaking every integral combination for a root. In particular, two simple charges individually have square two but their mutual pairing is negative, $(\Sigma_1, \Sigma_2) = -1$. That negative off-diagonal entry is compatible with a positive definite quadratic form. It says how the two nonorthogonal simple roots sit in the sum-zero plane.

Orientation provides another useful distinction. With $n = (1,1)$, the geometric self-intersection is -2 and the positive square is 2. Reversing the entire wrapping gives

$$q \longmapsto -q, \qquad n \longmapsto -n, \qquad (-n)^{\mathsf{T}} C (-n) = n^{\mathsf{T}} C n. \tag{XII.1.8}$$

The charge reverses while its square is preserved. The tension will have the same orientation independence, although its origin is a positive volume rather than an intersection number.

The difference between a lattice vector and a root will matter when we count the charges of the circle-reduced vector multiplets. For example,

$$\alpha_1 + \alpha_2 = e_1 - e_3, \qquad \|\alpha_1 + \alpha_2\|^2 = 2, \qquad \|\alpha_1 - \alpha_2\|^2 = 6. \tag{XII.1.9}$$

Both vectors have integral simple-root coefficients. Only the first is a root. The finite A_2 root set consists of these three positive roots $\alpha_1, \alpha_2, \alpha_1 + \alpha_2$ and their negatives. This enumeration does not assert a stable single string for every charge. Even the lattice itself must be distinguished from the lattice of linear functionals on it: $\det C = 3$, so the map to the integral dual defined by C is not unimodular. We will meet its inverse over the reals when choosing the six-dimensional tensor fields.

XII.1.3 The tension and charge of a wrapped D3

What does a brane on one of these spheres look like from outside? We use the product of flat six-dimensional spacetime with X_Γ, with mostly-plus metric, constant dilaton $g_s = e^\Phi$ and constant axion C_0. The background three-form fluxes vanish. A D3 with worldvolume $W_2 \times \Sigma_i$ has two external worldvolume directions, one time and one space. Its external image is a string, as in the upper panel of Figure XII.1.2. A D2 on the same internal sphere has just one external worldvolume direction. It produces a particle.

Write $\ell_s = \sqrt{\alpha'}$. On the positive Kähler resolution slice, the area $A_i = \int_{\Sigma_i} J$ is positive and the curve is calibrated by the Kähler form J. Choose vanishing flat

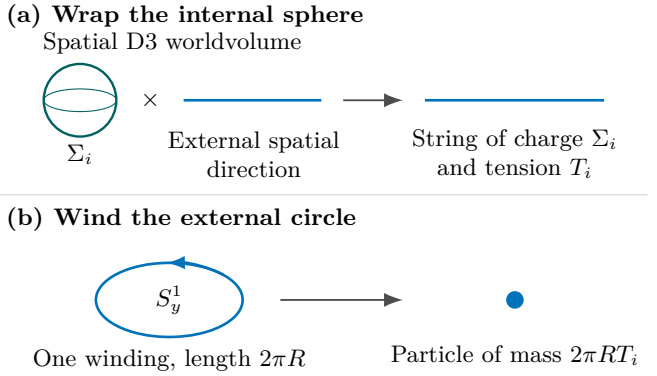


Figure XII.1.2: Two wrappings of different kinds. Above, a D3 wraps the internal sphere Σ_i and extends along one external spatial direction; time is suppressed. The external string carries the compact charge of the D3. Below, the external spatial direction is a circle of circumference $L = 2\pi R$. A single winding covers its full length. From the uncompactified five dimensions the configuration is a particle whose worldline couples to the reduced vector.

NSNS and RR two-form periods and zero gauge-invariant worldvolume flux and electric displacement. In this sector the static string-frame DBI matrix is block diagonal. If h is the induced Lorentzian metric on W_2 and k the induced Riemannian metric on Σ_i, then

$$\det \begin{pmatrix} h & 0 \\ 0 & k \end{pmatrix} = \det h \, \det k, \qquad \int_{\Sigma_i} \sqrt{\det k}\, d^2\sigma = A_i. \tag{XII.1.10}$$

Thus the internal integral multiplies the D3 energy per unit spatial three-volume by the wrapped area. The effective string action and tension are

$$S_{\text{DBI}} = -T_i \int_{W_2} d^2\sigma \, \sqrt{-\det h}, \qquad T_i = \tau_3 A_i = \frac{A_i}{(2\pi)^3 g_s \ell_s^4}. \tag{XII.1.11}$$

The factor g_s^{-1} belongs to the D3 tension τ_3. The area has units of length squared, so T_i has units of mass squared. Reversing the orientation of the internal wrapping will reverse its charge. The positive volume entering the DBI action is unchanged.

As a concrete scale choice, let $u > 0$ have units of mass and choose

$$(A_1, A_2) = (2\pi)^3 g_s \ell_s^4 u^2 (2, 3). \qquad (T_1, T_2) = (2, 3) u^2. \tag{XII.1.12}$$

The choice separates the two tension parameters. The DBI argument is a smooth, slowly varying calculation. Its use when a cycle becomes smaller than the string scale relies on continuation of the calibrated BPS tension in this sector. It is not a small-radius expansion of the classical D3 action at the singularity.

To find the charge of this string, we need the localized part of the RR four-form. On the smooth complete ALE space the normalizable harmonic two-forms span the real image of compactly supported cohomology in ordinary cohomology. The compact

Poincaré dual of Σ_i has a harmonic representative η_i. Its period over Σ_j and its wedge pairing with η_j are both given by I:

$$\int_{\Sigma_j} \eta_i = I_{ji}, \qquad \int_{X_\Gamma} \eta_i \wedge \eta_j = I_{ij}. \tag{XII.1.13}$$

To make a unit wrapping source a unit field, choose the period basis ω^i with unit period on Σ_i and zero on the other spheres. This means inverting the matrix of periods:

$$\omega^i = \sum_j \eta_j (I^{-1})_{ji}, \qquad \int_{\Sigma_j} \omega^i = \delta^i_j, \qquad \int_{X_\Gamma} \omega^i \wedge \omega^j = (I^{-1})_{ij}. \tag{XII.1.14}$$

For instance, on A_2 the coefficients of ω^1 in the η basis are $-2/3, -1/3$. Its periods are nevertheless $(1, 0)$. This basis change uses real harmonic forms. It does not turn the compact charge lattice into its integral dual.

We can obtain these fractions without guessing a dual basis. Write $\omega^1 = a\eta_1 + b\eta_2$. Requiring unit period on the first sphere and zero on the second gives the two simultaneous equations

$$\begin{pmatrix} -2 & 1 \\ 1 & -2 \end{pmatrix} \begin{pmatrix} a \\ b \end{pmatrix} = \begin{pmatrix} 1 \\ 0 \end{pmatrix}, \qquad \begin{pmatrix} a \\ b \end{pmatrix} = \begin{pmatrix} -2/3 \\ -1/3 \end{pmatrix}. \tag{XII.1.15}$$

For the second unit-period form the coefficients are interchanged. Thus the two forms are

$$\omega^1 = -\frac{2\eta_1 + \eta_2}{3}, \qquad \omega^2 = -\frac{\eta_1 + 2\eta_2}{3}. \tag{XII.1.16}$$

For example, $\int_{\Sigma_1} \omega^1 = (-2/3)(-2) + (-1/3)(1) = 1$. The fractional coefficients arise because the compact intersection matrix has determinant three; they are coefficients of differential forms, not fractional wrapping numbers. The source can still be an ordinary integral D3 wrapping.

The same change of basis must be made on both entries of a wedge pairing. In matrix notation the calculation is

$$\left(\int_X \omega^i \wedge \omega^j \right)_{ij} = (I^{-1})^{\mathsf{T}} I I^{-1} = I^{-1} = -C^{-1}. \tag{XII.1.17}$$

Using C in this expression would mix the basis of compact cycles with the basis of forms having unit periods on those cycles. A period is the evaluation of a form on a cycle; a norm pairs two objects of the same type. Keeping these operations distinct lets the Wess–Zumino integral below determine the integral charge without changing the harmonic norm matrix.

The middle-degree harmonic space is preserved by the internal Hodge star $*_4$. Its wedge pairing is negative definite in the chosen complex orientation. A nonzero $+1$ Hodge eigenmode would have positive self-pairing equal to its squared norm. Hence every normalizable mode has $*_4 \omega^i = -\omega^i$. In particular,

$$\int_{X_\Gamma} \omega^i \wedge *_4 \omega^j = (C^{-1})_{ij}, \qquad C^{-1}_{A_2} = \frac{1}{3} \begin{pmatrix} 2 & 1 \\ 1 & 2 \end{pmatrix}. \tag{XII.1.18}$$

This is the positive norm matrix of the harmonic modes in the unit-period basis. The compact string charges have the different Gram matrix (XII.1.5).

There is a useful positivity check directly in this basis. For real coefficients v_1, v_2, define $\omega(v) = v_1\omega^1 + v_2\omega^2$. Its norm is

$$\int_X \omega(v) \wedge *_4\omega(v) = \frac{2}{3}(v_1^2 + v_1v_2 + v_2^2) = \frac{1}{2}(v_1 + v_2)^2 + \frac{1}{6}(v_1 - v_2)^2. \qquad \text{(XII.1.19)}$$

Both eigen-directions have positive norm. A minus sign in the wedge pairing is therefore precisely what the anti-self-duality of the internal modes requires. This sign check uses the smooth ALE Hodge problem; it is not a computation of a tensor kinetic action at the singular origin.

Take the ten-dimensional orientation to be $\mathrm{vol}_6 \wedge \mathrm{vol}_4$ and impose $F_5 = + *_{10} F_5$. Work to linear order in the C_4 sector on the flux-free product, keeping the other potentials fixed at their background values on the zero two-form-period slice. Then the normalizable components are

$$C_4 = \frac{1}{\mu_3}\sum_i \mathcal{B}_i \wedge \omega^i, \qquad F_5 = \frac{1}{\mu_3}\sum_i H_i \wedge \omega^i, \qquad H_i = d\mathcal{B}_i. \qquad \text{(XII.1.20)}$$

Here $\mu_3 = g_s\tau_3$ is the RR charge of a positively oriented D3. The six-dimensional fields $\mathcal{B}_i$ come from C_4; they are distinct from the original NSNS two-form. For a product of an external three-form and an internal two-form the Hodge product sign is $(-1)^{2(6-3)} = +1$. Hence

$$*_{10}(H_i \wedge \omega^i) = (*_6H_i) \wedge (*_4\omega^i) = -(*_6H_i) \wedge \omega^i, \qquad *_6H_i = -H_i. \qquad \text{(XII.1.21)}$$

In Lorentzian signature $*_6^2 = +1$ on three-forms. This equation consistently keeps just one chirality. Its minus sign refers to the declared orientation.

The Wess–Zumino term now fixes which tensor is sourced. With positive external worldsheet orientation and $q = \sum_j n_j\Sigma_j$ internally,

$$\mu_3 \int_{W_2\times q} C_4 = \sum_i \left(\int_q \omega^i\right) \int_{W_2} \mathcal{B}_i = \sum_i n_i \int_{W_2} \mathcal{B}_i. \qquad \text{(XII.1.22)}$$

Thus a D3 on Σ_1 couples to $\mathcal{B}_1$, and one on Σ_2 couples to $\mathcal{B}_2$. The duality constraint ties the electric flux to the magnetic flux, rather than allowing them to be chosen independently. This is why the wrapped object is called a self-dual string. The name refers to the chiral electric and magnetic coupling and does not impose a separate positive sign in (XII.1.21).

XII.1.4 Tensor vacua and the tensionless origin

Which six-dimensional fields remain light when the wrapped strings have nonzero tension? The hyperkähler holonomy is contained in one $SU(2)$ factor of Spin(4). It preserves the spinors of one internal Weyl chirality. In the product spin decomposition we can write

$$\Gamma_{11} = \Gamma_{6,*} \otimes \Gamma_{4,*}, \qquad \chi_{10} = \chi_6\chi_4. \qquad \text{(XII.1.23)}$$

Here χ_d denotes a chirality eigenvalue in dimension d. Once the invariant internal sign χ_4 is fixed, both IIB spinors, which have the same χ_{10}, give the same χ_6. In IIA the two ten-dimensional signs are opposite, so the two surviving six-dimensional signs are opposite. Both reductions preserve sixteen real supercharges. We use the label $(2,0)$ for the chiral IIB case and $(1,1)$ for the nonchiral IIA case. These labels follow the supercharges; they are not a naming convention for the sign in (XII.1.21).

At a generic point on the tensor branch, the low-energy localized fields are r abelian tensor multiplets. For the chiral two-form, the transverse little group acts on a two-form in four transverse directions. The chirality condition halves the six independent components. Adding the scalars of the tensor multiplet gives

$$N_{\text{bosons}} = \frac{1}{2}\binom{4}{2} + 5 = 3 + 5 = 8 \quad \text{per tensor multiplet.} \tag{XII.1.24}$$

The two harmonic modes of A_2 count two tensor multiplets in this description. They do not count six-dimensional vector multiplets, and the rank of the algebra need not equal the number of charged root states.

In the A_2 example, the five scalar parameters associated with Σ_i have a simple geometric description. Write J^a for the three hyperkähler forms, with $J = J^3$ in the chosen complex structure, and let B_2, C_2 denote the NSNS and RR two-forms. The local coordinates are represented by

$$\boldsymbol{A}_i = \left(\int_{\Sigma_i} J^1, \int_{\Sigma_i} J^2, \int_{\Sigma_i} J^3\right), \qquad (b_i, c_i) = \frac{1}{4\pi^2\alpha'}\left(\int_{\Sigma_i} B_2, \int_{\Sigma_i} C_2\right). \tag{XII.1.25}$$

The triplet consists of metric periods, in units of area. The last two entries are dimensionless angular periods; they are represented here in a local lift near zero. They are coordinates on the branch, not five canonically normalized scalar components in a common unit. The tension formula (XII.1.11) uses the aligned slice $\boldsymbol{A}_i = (0, 0, A_i)$, $b_i = c_i = 0$ and the stated worldvolume sector.

At zero metric periods, the complex period entering the wrapped string's BPS tension is $c_i + \tau b_i$, where $\tau = C_0 + i/g_s$. Stay in the local lift and take $b_i = \delta$ with $0 < |\delta| \ll 1$ and $c_i = 0$. At fixed $g_s > 0$, $\mathrm{Im}(c_i + \tau b_i) = \delta/g_s$ is nonzero even at zero area. Thus the full origin requires tuning the two-form periods as well as the metric periods. To keep the string in a low-energy description at finite string scale, its tension must also be small compared with the fundamental string tension T_{F1}.

For the A series there is another useful way to organize these scalar directions. In the fivebrane description of the same local theory, use five-vectors X_i as tension coordinates for the three fivebranes of the A_2 example. Only differences enter the compact charge sector. Decompose the coordinates as

$$X_i = X_{\text{cm}} + x_i, \qquad X_{\text{cm}} = \frac{X_1 + X_2 + X_3}{3}, \qquad x_1 + x_2 + x_3 = 0. \tag{XII.1.26}$$

A common translation changes X_{cm} but preserves every root difference. The interacting theory therefore uses two independent relative five-vectors, modulo permutation of the three branes. Keeping X_{cm} would include a free tensor of the fivebrane system. There is no third normalizable tensor on the ordinary A_2 ALE resolution.

To solve for the relative positions, start with the two endpoint differences and eliminate x_1 and x_3 in favor of x_2. In one aligned direction,

$$x_1 = x_2 + t_1, \qquad x_3 = x_2 - t_2, \qquad 0 = x_1 + x_2 + x_3 = 3x_2 + t_1 - t_2. \tag{XII.1.27}$$

This fixes the otherwise invisible common translation. The inverse map is

$$\begin{pmatrix} x_1 \\ x_2 \\ x_3 \end{pmatrix} = \frac{1}{3} \begin{pmatrix} 2 & 1 \\ -1 & 1 \\ -1 & -2 \end{pmatrix} \begin{pmatrix} t_1 \\ t_2 \end{pmatrix}. \tag{XII.1.28}$$

The two columns sum to zero, as required. Multiplying on the left by the simple-root difference matrix returns (t_1, t_2). The construction applies separately to every component of the relative five-vectors. It does not put the three metric periods and two angular periods of (XII.1.25) into a common physical normalization.

Restrict the relative coordinates to the same aligned direction as the positive slice of (XII.1.12). Let $t_1 = x_1 - x_2$ and $t_2 = x_2 - x_3$ denote the components along that direction, so $t_i = T_i$ there. The sum constraint gives

$$(x_1, x_2, x_3) = \frac{1}{3}(2t_1 + t_2, -t_1 + t_2, -t_1 - 2t_2) = \frac{u^2}{3}(7, 1, -8) \tag{XII.1.29}$$

for the chosen example. Reading the endpoint differences gives the three positive-root periods,

$$Z_{\alpha_1} = t_1 = 2u^2, \qquad Z_{\alpha_2} = t_2 = 3u^2, \qquad Z_{\alpha_1+\alpha_2} = t_1 + t_2 = 5u^2. \tag{XII.1.30}$$

The last equality is a central-charge statement. On this aligned slice the sum is at the threshold of the two simple strings. It does not establish that an isolated single string of the sum charge exists in six dimensions.

Changing the relative tensions illustrates what this map retains. Choose the same positive slice but set $(t_1, t_2) = (1, 4)u^2$, keeping $t_1 + t_2$ unchanged. Then

$$(x_1, x_2, x_3) = (2, 1, -3)u^2, \qquad (Z_{\alpha_1}, Z_{\alpha_2}, Z_{\alpha_1+\alpha_2}) = (1, 4, 5)u^2. \tag{XII.1.31}$$

The first interval contracts and the second expands. The outer endpoint difference remains $5u^2$, while the two simple-string tensions change separately. Thus the sum-root period alone cannot specify a rank-two vacuum. Conversely, the two simple differences determine every root period on this aligned slice once the common center is removed.

Figure XII.1.3 also explains the difference between a partial coincidence and the full origin. Use the same labelled coordinates before quotienting by permutations. Taking $(t_1, t_2) = (2, -2)u^2$ gives

$$(x_1, x_2, x_3) = \frac{u^2}{3}(2, -4, 2). \tag{XII.1.32}$$

The first and third positions coincide, while the second is separated. The sum-root period vanishes although the two simple periods do not. This is an example in relative coordinates outside the positive calibrated chamber, not a negative physical area. The full origin instead has all three positions coincident in every component of the five-vector.

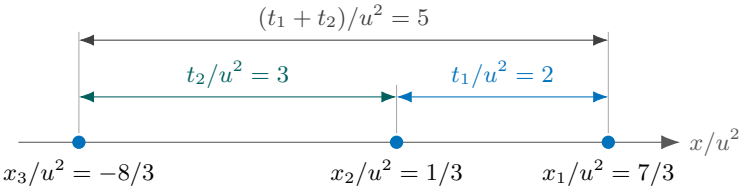


Figure XII.1.3: One aligned scalar direction of the A_2 branch, for $(t_1, t_2) = (2, 3)u^2$. The positive root periods are the lengths of the three indicated differences. The displayed positions are relative to the common center. A common shift would leave all three lengths unchanged.

A controlled approach to that origin keeps the two intervals positive and reduces both together. Introduce a dimensionless parameter $\lambda > 0$ within the already decoupled branch theory and take

$$\begin{gathered}(t_1, t_2) = \lambda(2, 3)u^2, \qquad (x_1, x_2, x_3) = \frac{\lambda u^2}{3}(7, 1, -8), \\ (Z_{\alpha_1}, Z_{\alpha_2}, Z_{\alpha_1+\alpha_2}) = \lambda(2, 3, 5)u^2.\end{gathered} \tag{XII.1.33}$$

Keep the other components zero along this path. All relative five-vectors then vanish as $\lambda \to 0$. By contrast, setting only the displayed component of one difference to zero would not produce coincidence if another component remained nonzero. The origin is a condition on the full branch coordinates, not merely on a drawing of one scalar direction.

At a generic vacuum the abelian tensor theory describes the far infrared. At the full origin the tensions vanish, and the approximation that kept only those free tensor fields no longer describes the local dynamics. The IIB construction identifies the decoupled theory there with the interacting ADE $(2, 0)$ SCFT. Setting the scalars to zero in a free tensor action would miss this change of degrees of freedom. To make the statement about a local field theory, we must also say what happens to the bulk string scale.

XII.1.5 The local field theory limit

How can the local strings remain in the calculation while the scale of the ambient string theory is removed? Fix an external energy E and first keep positive branch tensions T_i finite. In the common asymptotic string length convention, the fundamental string tension, the string mass scale and the ten-dimensional gravitational constant satisfy

$$T_{\mathrm{F1}} = \frac{1}{2\pi\ell_s^2}, \qquad M_s = \ell_s^{-1}, \qquad 2\kappa_{10}^2 = (2\pi)^7 g_s^2 \ell_s^8. \tag{XII.1.34}$$

The dimensionless measure of the gravitational interaction at this fixed energy is proportional to $\kappa_{10}^2 E^8$. The local tension, by contrast, depends on the ratio of the area to $g_s \ell_s^4$. The two quantities can scale independently.

To see this, let ε tend to zero through positive values and introduce exponents a, b, c by

$$g_s = g_0\varepsilon^a, \qquad \ell_s = \ell_0\varepsilon^b, \qquad A_i = A_i^{(0)}\varepsilon^c. \tag{XII.1.35}$$

Here $g_0, \ell_0, A_i^{(0)}$ are fixed positive constants. Substituting into the tension formula yields

$$T_i = \frac{A_i^{(0)}}{(2\pi)^3 g_0 \ell_0^4}\varepsilon^{c-a-4b}, \qquad \kappa_{10}^2 E^8 = \frac{(2\pi)^7 g_0^2 \ell_0^8 E^8}{2}\,\varepsilon^{2a+8b}. \tag{XII.1.36}$$

A finite nonzero tensor-branch tension requires $c = a + 4b$. In the weak-coupling paths below this has a consequence:

$$\frac{A_i}{\alpha'} = \frac{A_i^{(0)}}{\ell_0^2}\varepsilon^{c-2b} = \frac{A_i^{(0)}}{\ell_0^2}\varepsilon^{a+2b}. \tag{XII.1.37}$$

The cycles become small in string units. The argument follows the BPS tension of the wrapped brane; it cannot rely on a supergravity expansion in large cycle size all the way to the limit.

For the A_2 tensions in (XII.1.12), choose $A_i^{(0)}$ so that their ratio is $2:3$ and their two tension scales stay fixed. Compare the following choices of (a, b, c):

(a,b,c)	$\kappa_{10}^2 E^8$	M_s	T_{F1}	T_i
$(1,0,1)$	$\propto \varepsilon^2$	fixed	fixed	fixed
$(1,1,5)$	$\propto \varepsilon^{10}$	$\propto \varepsilon^{-1}$	$\propto \varepsilon^{-2}$	fixed

(XII.1.38)

Both suppress the bulk gravitational interaction. Only the second sends the ambient string scale above any fixed test energy. For example, keeping $a = b = 1$ but using $c = 4$ would make $T_i \propto \varepsilon^{-1}$. That path would remove the very finite-tension degrees of freedom whose approach to zero we wanted to study.

Dimensionless ratios show why removing gravity and removing the intrinsic string scale answer different questions. At fixed E and fixed nonzero T_i, the ratios to the ambient scales obey

$$\frac{E}{M_s} = E\ell_0\varepsilon^b, \qquad \frac{T_i}{T_{\mathrm{F1}}} = 2\pi T_i \ell_0^2 \varepsilon^{2b}, \qquad \kappa_{10}^2 E^8 \propto \varepsilon^{2a+8b}. \tag{XII.1.39}$$

The first two tend to zero only if $b > 0$ along these paths. At $b = 0$, reducing g_s suppresses gravity but does not change either ratio. A low-energy approximation at finite M_s still requires an independent choice of small E/M_s.

As a changed-input example, take $a = 2$ and $b = 1/2$. Finite T_i fixes $c = 4$, giving

$$(\kappa_{10}^2 E^8, M_s, T_{\mathrm{F1}}, T_i, A_i/\alpha') \;\propto\; (\varepsilon^8, \varepsilon^{-1/2}, \varepsilon^{-1}, 1, \varepsilon^3). \tag{XII.1.40}$$

The powers differ from the second row of (XII.1.38), but the retained and removed scales are the same. If we change only c to 5, the tension instead goes as ε. We would be approaching the origin while removing the ambient scale. This can be a chosen path, but it no longer preserves a nonzero branch tension during that operation. Keeping

these two tunings separate makes it possible to study a generic tensor vacuum first and then follow the parameter λ of (XII.1.33) to its origin.

At fixed ℓ_s the decoupled A-series construction retains an intrinsic string scale and gives the $(2,0)$ little string theory. Its low-energy limit at the origin, at $E \ll M_s$, is the local $(2,0)$ SCFT. The second path sends the intrinsic scale to infinity at fixed E. In either description the conformal point is reached by tuning the localized tensor parameters to zero. Keeping finite T_i during the scaling is a way to retain the tensor branch and track the approach to its origin. The planned discussion of little string theories returns to the theory at finite intrinsic string scale.

A noncompact ALE space has no normalizable constant internal wavefunction for a six-dimensional graviton. It still has a continuum of bulk modes. Suppression of $\kappa_{10}^2 E^8$ and loss of the constant mode do not establish that every coupling between the localized sector and that continuum vanishes. The field theory construction uses the physical decoupling of the localized sector as an input. The scale calculation tells us which limits are consistent with that input. We can now put an external circle in the local field theory without retaining the original fundamental string scale.

XII.1.6 An external circle turns strings into particles

Where does the vector field come from after compactification? Compactify a spatial direction y with periodic fermions and no twist. Use the physical radius R, the circumference $L = 2\pi R$ and the orientation $\mathrm{vol}_5 \wedge dy$. The lower panel of Figure XII.1.2 shows the external winding. The internal sphere and the external circle have different roles: the sphere labels the charge and sets the tension, whereas the circle converts tension into a rest mass.

The component of $\mathcal{B}_i$ with one circle index gives a vector potential. Define its five-dimensional normalization by integrating the component around the circle, so that a wrapped string retains its integral charge. For zero modes write

$$\mathcal{B}_i = B^{(5)}_{2,i} + \frac{1}{L}\mathcal{A}_i \wedge dy, \qquad \mathcal{A}_i = \int_0^L \mathcal{B}_{i,\mu y}\, dy\, dx^\mu. \tag{XII.1.41}$$

Here $B^{(5)}_{2,i}$ has both legs in the five uncompactified directions. The corresponding decomposition of the curvature is

$$H_i = H^{(5)}_{3,i} + \frac{1}{L}\mathcal{F}_i \wedge dy, \qquad H^{(5)}_{3,i} = dB^{(5)}_{2,i}, \qquad \mathcal{F}_i = d\mathcal{A}_i. \tag{XII.1.42}$$

A nonchiral six-dimensional two-form would leave two independent fields in this decomposition. To see what the chirality constraint does here, compute the two product stars:

$$*_6 H^{(5)}_{3,i} = (*_5 H^{(5)}_{3,i}) \wedge dy, \qquad *_6(\mathcal{F}_i \wedge dy) = -*_5 \mathcal{F}_i. \tag{XII.1.43}$$

The second sign comes from passing dy through an external form of degree $5-2=3$. Equating the components of $*_6 H_i = -H_i$ gives

$$H^{(5)}_{3,i} = \frac{*_5 \mathcal{F}_i}{L}, \qquad *_5 H^{(5)}_{3,i} = -\frac{\mathcal{F}_i}{L}. \tag{XII.1.44}$$

These relations are consistent because $*_5^2 = -1$ on two-forms in Lorentzian signature. The curvature of $B_{2,i}^{(5)}$ is the three-form dual of $\mathcal{F}_i/L$. Each six-dimensional tensor supplies just one independent vector in five dimensions.

The local equations of motion illustrate what the identification accomplishes. Away from string sources, the zero-mode Bianchi identity $dH_i = 0$ separates into its components with and without dy. At constant L, substituting (XII.1.44) yields

$$d\mathcal{F}_i = 0, \qquad dH_{3,i}^{(5)} = 0 \quad \Longrightarrow \quad d\mathcal{F}_i = 0, \qquad d(*_5\mathcal{F}_i) = 0. \tag{XII.1.45}$$

These are the Bianchi identity and source-free Maxwell equation of the abelian vector. The relation to the three-form supplies its dynamics without introducing a second independent vector. This reasoning uses the linear abelian tensor sector away from charged sources; the nonabelian enhancement at the origin is the sourced circle identification used below.

For a compact charge with components n_i, wrap the string worldsheet on the product of a five-dimensional worldline γ and the circle with oriented winding w. Inserting (XII.1.41) into the coupling (XII.1.22) gives

$$\sum_i n_i \int_{\gamma \times wS^1} \mathcal{B}_i = w \sum_i n_i \int_\gamma \mathcal{A}_i. \tag{XII.1.46}$$

The particle's charge changes sign with the winding orientation. Its rest mass does not.

The normalization by $1/L$ in (XII.1.41) is needed here. On the wrapped worldsheet the integral of dy is wL, so that

$$\frac{1}{L}\int_{wS^1} dy = w. \tag{XII.1.47}$$

For example, reversing a one-winding string on Σ_1 changes the vector coupling from $+\int_\gamma \mathcal{A}_1$ to $-\int_\gamma \mathcal{A}_1$. Changing the radius alone does not change that unit charge. It changes the length whose energy we integrate. For an existing static pure winding state with tension T and no additional excitations,

$$M_{\text{wind}} = |w|LT = 2\pi|w|RT. \tag{XII.1.48}$$

This is the energy of the wrapped length in the lower panel of Figure XII.1.2. A pure momentum mode of a massless six-dimensional parent instead has rest mass

$$M_{\text{KK}} = \frac{|m|}{R}, \qquad m \in \mathbb{Z}. \tag{XII.1.49}$$

The two formulae describe distinct sectors. Shrinking R lowers the energy of a given winding and raises the energy of a nonzero momentum mode. Neither formula gives the dispersion of a general state carrying both charges.

There is a useful independent check of the circumference factor. In the perturbative isometric-circle T-duality dictionary the longitudinal D3 becomes a D2 on the same internal sphere. If the IIB parameters are R, g_s, ℓ_s, the dual IIA parameters are $R' = \ell_s^2/R$ and $g_s' = g_s\ell_s/R$. Then the dual D2 area gives

$$\frac{A_i}{(2\pi)^2 g_s' \ell_s^3} = \frac{RA_i}{(2\pi)^2 g_s \ell_s^4} = (2\pi R)\tau_3 A_i. \tag{XII.1.50}$$

Both expressions measure the same pure wrapping energy. This calculation uses the local brane and circle dictionaries. It does not identify the uncompactified six-dimensional theories.

The untwisted circle of the interacting A_2 theory admits a long-wavelength description by maximally supersymmetric five-dimensional Yang–Mills with algebra $\mathfrak{su}(3)$. The two abelian vectors just found are its Cartan fields on the branch. The charged W multiplets carry the six root charges. The two simple charges have winding masses Lt_1, Lt_2 on our slice. For the sum charge, the circle EFT identifies the W mass with $L|t_1 + t_2|$. This use of the root mass in five dimensions does not require an isolated highest-root string on the aligned six-dimensional branch.

Using $R = 1/(20u)$ and the periods (XII.1.30), the three positive-root masses in the circle description and the first pure KK mass are

$$(M_1, M_2, M_{12}) = u\left(\frac{\pi}{5}, \frac{3\pi}{10}, \frac{\pi}{2}\right), \qquad M_{\mathrm{KK},1} = 20u. \tag{XII.1.51}$$

The largest ratio of a W mass to the first KK scale is $\pi/40$. More generally the dimensionless parameter is $2\pi R^2 \max|Z_\alpha|$. To retain all these particles in a description at energies well below $1/R$, this parameter must be small. At fixed R and the full tensionless origin the three root masses go to zero, while $1/R$ stays finite.

The hierarchy is sensitive to a change of radius even when the charge lattice and branch tensions are unchanged. Increase the radius to $R = 1/(4u)$ with $(t_1, t_2) = (2, 3)u^2$. The same calculation gives

$$(M_1, M_2, M_{12}) = u\left(\pi, \frac{3\pi}{2}, \frac{5\pi}{2}\right), \qquad M_{\mathrm{KK},1} = 4u, \qquad \frac{M_{12}}{M_{\mathrm{KK},1}} = \frac{5\pi}{8} > 1. \tag{XII.1.52}$$

These wrapping energies remain the stated kinematic values in their sectors. They cannot all be treated as particles in a theory restricted to energies well below the first KK scale. Merely obtaining a five-dimensional vector zero mode did not ensure a useful energy interval containing every charged root multiplet.

We can restore that interval by moving toward the origin at the same radius. Set $(t_1, t_2) = \lambda(2, 3)u^2$ as in (XII.1.33). Then

$$\frac{\max M_W}{M_{\mathrm{KK},1}} = \frac{5\pi\lambda}{8}, \qquad \lambda = \frac{1}{100} \implies \frac{\max M_W}{M_{\mathrm{KK},1}} = \frac{\pi}{160}. \tag{XII.1.53}$$

The KK threshold has stayed fixed while the charged particles have become light. The radius and the tensor vacuum control different parts of the hierarchy. This is why both must be specified when using the circle gauge theory away from the origin.

XII.1.7 The gauge coupling remembers the radius

The reduction gave the five-dimensional gauge fields and their charges. How is their gauge coupling normalized? Use the matrix connection convention in which a unit charge couples to the connection without a factor of g_5. With $\mathrm{Tr}_f(T^a T^b) = \delta^{ab}/2$ for

the fundamental trace, write the gauge kinetic term as

$$S_{\rm YM} = -\frac{1}{2g_5^2}\int d^5x\ \mathrm{Tr}_f(F_{\mu\nu}F^{\mu\nu}). \tag{XII.1.54}$$

The connection has mass dimension one, since its line integral is dimensionless. Thus $F_{\mu\nu}$ has mass dimension two and the integral in (XII.1.54) has units of length. At the conformal origin the circle radius is the only length, so the leading gauge coupling has

$$[g_5^2] = \text{length}, \qquad g_5^2 \propto R. \tag{XII.1.55}$$

The direction of the scaling is a useful clue. Reducing an ordinary six-dimensional gauge action with a radius-independent coupling by integrating over the circle would put a factor of R in front of the five-dimensional action. Here the coefficient is proportional to $1/R$. The field that was reduced was a chiral two-form, and its period determines the vector normalization.

The numerical constant can be fixed by comparing an instanton particle with a unit of circle momentum. First determine the classical energy of a static purely magnetic configuration on the spatial $\mathbb{R}^4$. Work at the unbroken origin, or with scalar backgrounds compatible with the configuration and with no additional scalar or electric energy. In the fundamental trace define

$$k = \frac{1}{8\pi^2}\int_{\mathbb{R}^4} \mathrm{Tr}_f\, F\wedge F, \qquad E_{\rm mag} = \frac{1}{g_5^2}\int_{\mathbb{R}^4} \mathrm{Tr}_f\, F\wedge *_4 F. \tag{XII.1.56}$$

Take a smooth finite-energy connection approaching a pure gauge at spatial infinity, with the bundle extending across the point at infinity. Then $k\in\mathbb{Z}$. The star $*_4$ here uses the Euclidean metric on spatial $\mathbb{R}^4$ and squares to $+1$ on two-forms. Expanding a square gives

$$\begin{aligned} E_{\rm mag} &= \frac{1}{2g_5^2}\int_{\mathbb{R}^4} \mathrm{Tr}_f\big((F\mp *_4F)\wedge *_4(F\mp *_4F)\big) \\ &\quad \pm \frac{8\pi^2}{g_5^2}k \ \geq\ \frac{8\pi^2}{g_5^2}|k|, \end{aligned} \tag{XII.1.57}$$

where the sign is chosen to agree with k. Equality holds for the corresponding self-dual or anti-self-dual field strength.

To see what is minimized, decompose the magnetic curvature on spatial $\mathbb{R}^4$ into its Euclidean Hodge eigenspaces. Define $F_\pm = (F\pm *_4F)/2$ and the nonnegative squared norms $N_\pm = \int \mathrm{Tr}_f\, F_\pm\wedge *_4F_\pm$. Orthogonality gives

$$g_5^2 E_{\rm mag} = N_+ + N_-, \qquad 8\pi^2 k = N_+ - N_-. \tag{XII.1.58}$$

At fixed positive k, the second equation fixes the difference of the norms. Any anti-self-dual component adds twice its norm to the energy above the bound:

$$E_{\rm mag} - \frac{8\pi^2 k}{g_5^2} = \frac{2N_-}{g_5^2} \quad (k>0). \tag{XII.1.59}$$

For $k < 0$ the roles of the two eigenspaces interchange. This identifies both the sign of the topological charge and the condition for saturation. It also keeps the Euclidean spatial star used in the energy argument distinct from the Lorentzian stars in the tensor reduction.

The BPS matching identifies the unit instanton charge with one unit of circle momentum in magnitude. Equating the saturating energy for $|k| = 1$ to $1/R$ then gives

$$\frac{8\pi^2}{g_5^2} = \frac{1}{R}, \qquad g_5^2 = 8\pi^2 R. \tag{XII.1.60}$$

The comparison uses a physical identification of protected charges and energies. The momentum state is at the KK scale, outside the strict $E \ll 1/R$ domain of the long-wavelength EFT. The classical square completion by itself does not give a quantum description of the KK tower or a five-dimensional ultraviolet completion.

A factor of two can arise when this formula is quoted in a different trace convention. With the same curvature and fundamental matrix trace, a native coefficient $1/(4g_{\mathrm{n}}^2)$ in front of the component trace gives $R = g_{\mathrm{n}}^2/(4\pi^2)$. Comparing coefficients in the two actions yields

$$\frac{1}{2g_5^2} = \frac{1}{4g_{\mathrm{n}}^2}, \qquad g_5^2 = 2g_{\mathrm{n}}^2. \tag{XII.1.61}$$

This is the same result as (XII.1.60). At the radius $R = 1/(20u)$ used in the A_2 example, $g_5^2 = 2\pi^2/(5u)$ and $8\pi^2/g_5^2 = 20u$. This evaluates the protected first momentum scale for that radius. The pure magnetic instanton calculation uses the unbroken origin or a compatible scalar background, while the three nonzero W masses use the aligned tensor-branch values.

At the changed radius $R = 1/(4u)$, the coupling and protected unit instanton mass are instead

$$g_5^2 = \frac{2\pi^2}{u}, \qquad M_{\mathrm{inst},1} = \frac{8\pi^2}{g_5^2} = 4u. \tag{XII.1.62}$$

The mass has decreased by the same factor of five as the first KK threshold. The root wrapping masses at fixed tensions in (XII.1.52) increased by a factor of five. Their ratio to the KK threshold has therefore increased by a factor of twenty-five. The protected instanton match and the light-W condition test different statements. The first fixes the normalization of the radius coupling; the second selects branch parameters for which the charged particles lie inside the low-energy gauge description.

We can now return to the six-dimensional comparison. The IIA D2 wrapping already gives a particle in six dimensions, and the opposite chirality supercharges permit a $(1, 1)$ gauge multiplet. The light wrapped D2 particles give the six-dimensional gauge enhancement of the IIA construction. In IIB the D3 wrapping leaves an external spatial direction. The massless fields on the generic branch are chiral tensors, and collapse brings in tensionless strings at a $(2, 0)$ fixed point. The extra external circle is what turns the IIB strings into charged particles and the tensors into vectors. Volume XVI develops the compactification of $(2, 0)$ theories further. In the next chapter a different internal cycle will use up one more spatial direction of the D3, yielding a particle without this second wrapping.

XII.1.8 Exercises

Use the area, radius and trace conventions of this chapter. Use `benchmark/tasks.json` to find the question IDs and `benchmark/PROTOCOL.md` for submission. Show your reasoning for every problem. A reader assesses the written explanations and interpretations.

1. **One sphere.** In the A_1 resolution, take the positive area of its exceptional sphere to be $A = (2\pi)^3 g_s \ell_s^4 (4u^2)$, for $u > 0$. Find the geometric self-intersection I, the positive charge Gram C, the unit-period harmonic mode Gram C^{-1} and the tension in units of u^2. Assume a static pure winding configuration with $w = -2$ at $R = 1/(10u)$. Find its rest mass in units of πu. Explain what the negative winding changes.

2. **Which coincidence?** In one aligned direction take $(X_1, X_2, X_3) = (4, 1, 4)u^2$ in the given order. Find X_{cm}/u^2 and the three relative coordinates in units of u^2. Give the signed periods of the two simple charges and their sum, in that order, also in units of u^2. Is this a partial coincidence or the full origin? Explain why adding a freely translating common coordinate does not increase the pure-ALE tensor rank.

3. **Two limits.** Hold E fixed and let (a, b) in (XII.1.35) be $(1, 0)$ and then $(2, 1)$. In each case solve for c that keeps a finite nonzero T_i. Find the exponents of κ_{10}^2, M_s, T_{F1} and T_i in that order. Which limit retains a finite intrinsic string scale? Explain why a vanishing κ_{10}^2 does not by itself select a local SCFT.

4. **Radius and trace.** At $R = 1/(10u)$ assume a static pure winding configuration of a string of tension $3u^2$. Calculate its mass for $w = 2$ in units of πu and, separately, the pure KK mass of a massless parent with $m = -3$ in units of u. Find g_5^2 in units of π^2/u in the house trace. Give the ratio of the one-winding mass to the first KK mass in units of π. Compare the actual dimensionless ratio to 1 and explain what it says about the separation of these scales.

5. **A tensor is not a six-dimensional vector.** Explain why the local six-dimensional IIB branch of A_2 has two tensor multiplets, why a free action for those fields does not describe the conformal origin, and why the IIA and circle-reduced IIB constructions can have light vector multiplets. Include the relation between the two zero-mode field strengths in the circle reduction.

6. **A changed interval.** Keep $(t_1 + t_2) = 5u^2$ on the positive aligned slice and compare $(t_1, t_2) = (2, 3)u^2$ with $(1, 4)u^2$. Draw the three relative positions in each case. At a common radius, explain which positive-root mass is unchanged, which masses change, and why this comparison cannot determine a six-dimensional single-string spectrum.

7. **Choosing an energy window.** At $R = 1/(4u)$ follow $(t_1, t_2) = \lambda(2, 3)u^2$ with all other branch components zero. Derive the condition on λ for every root mass to be below the first KK threshold, and then the stronger condition for a parametric

separation. Explain why the unit instanton mass is still at the KK threshold. This written comparison has no exact-answer companion.

Status and sources

Compact spheres and their pairing. The compact geometry and sign in (XII.1.1)–(XII.1.9) are [MATH], using Volume IV and García Etxebarria et al. 2019, arXiv:1908.08027v2, §2.3, (2.42)–(2.50), physical PDF pp. 15–17. The quadratic form, norm-two enumeration and orientation reversal in (XII.1.6)–(XII.1.8) are additional [MATH] consequences of the same A_2 matrix. The compact D3 charge identification is [GEO-E], using Witten 1995, arXiv:hep-th/9507121v1, §1, and the stated RR reduction.

Wrapped D3 tension and tensor coupling. The calibrated-volume calculation (XII.1.10)–(XII.1.12) is [MATH], using Volume III for DBI/WZ and Witten 1995, §1, (1.4)–(1.5), physical PDF p. 4, for the wrapped-brane and BPS inputs ([GEO-E]). The smooth ALE harmonic modes and unit-period arithmetic (XII.1.13)–(XII.1.18) are [MATH], using Hausel et al. 2004, arXiv:math/0207169v2, §7.1.1, physical PDF p. 39. The explicit dual-basis system, wedge pairing and positive norm in (XII.1.15)–(XII.1.17) and (XII.1.19) are [MATH] consequences of those pairings. The flux-free, linearized RR reduction and coupling (XII.1.20)–(XII.1.22) are [SUGRA]. Compare Witten 1995, §1.1, physical PDF p. 5, with the product sign derived here. The metric and chirality conventions of the preceding volumes and the local DBI/WZ normalization fix the RR conventions.

Tensor vacua and the origin. The local supersymmetry reduction (XII.1.23) is [SUGRA] conditional on the product background. The interacting simply-laced ADE origin and generic abelian tensor branch are [GEO-E], from Witten 2009, arXiv:0905.2720v1, §4, physical PDF pp. 9–10. For the A-series five scalar parameters, period tuning and flat-space BPS tension regime used in the A_2 example, see Aharony et al. 2015, arXiv:1501.02904v2, §1, (1.1)–(1.2), physical PDF p. 5, §2.1, pp. 10–11, and §2.3, (2.9) and the ensuing paragraph, pp. 12–13 ([GEO-E]). The relative-coordinate and root-period arithmetic is [MATH]. This includes the inverse difference map, changed positive tensions and common origin path in (XII.1.27)–(XII.1.28), (XII.1.31) and (XII.1.33). The separate center-of-mass sector is [GEO-E], using the footnote in Aharony 2000, arXiv:hep-th/9911147v1, §1.1, physical PDF p. 2, and García Etxebarria et al. 2019, §5, physical PDF p. 51. The sum-charge example computes an aligned threshold.

Decoupling and the little-string scale. The exponent relations (XII.1.34)–(XII.1.38) are [MATH], with the ten-dimensional Newton normalization of Volume II. The dimensionless ratios and changed scaling in (XII.1.39)–(XII.1.40) are [MATH] at fixed E and branch tensions. The A-series little-string and infrared fixed-point comparison is [GEO-E], as reviewed in Aharony 2000, §1.1, physical PDF pp. 2–3. The localized-sector decoupling used in passing to a non-gravitational theory is [DEC]. Bulk continua are not eliminated by the absence of a normalizable constant graviton.

Circle reduction, particles and coupling. The chiral zero-mode reduction, pure winding and pure KK formulas, and dual mass equality in (XII.1.41)–(XII.1.50) are conditional

[MATH], using Witten 1995, §§1–1.1, physical PDF pp. 3–5, and the Volume III circle dictionary. The source-free Maxwell consequence (XII.1.45), charge normalization (XII.1.47), changed-radius hierarchy (XII.1.52)–(XII.1.53), magnetic eigenspace calculation (XII.1.58)–(XII.1.59) and changed-coupling arithmetic (XII.1.62) are conditional [MATH] within those same reductions. The long-wavelength gauge description and root W identification are [GEO-E], using Witten 2009, §4, physical PDF pp. 9–10, and Aharony et al. 2015, §1, physical PDF p. 5. For the $1/R$ scaling of the action coefficient in (XII.1.55), see Witten 2009, (4.1). The instanton bound and trace conversion are [MATH]. The native trace coefficient is from Lambert et al. 2011, arXiv:1012.2882v3, (2.2), physical PDF p. 4. The protected unit instanton/KK match is [GEO-E], from the same source, (2.18), physical PDF p. 6. The six-dimensional IIA gauge enhancement is [GEO-E], from XI.1 and the local degeneration comparison of Witten 1995, arXiv:hep-th/9507121v1, §1, physical PDF pp. 2–4.

References

Aharony, O. (2000). "A Brief Review of Little String Theories". In: *Class. Quant. Grav.* 17, pp. 929–938. DOI: 10.1088/0264-9381/17/5/302. arXiv: hep-th/9911147.

Aharony, O., M. Berkooz, and S.-J. Rey (2015). "Rigid Holography and Six-Dimensional $\mathcal{N} = (2,0)$ Theories on $AdS_5 \times S^1$". In: *JHEP* 03, p. 121. DOI: 10.1007/JHEP03(2015)121. arXiv: 1501.02904 [hep-th].

García Etxebarria, I., B. Heidenreich, and D. Regalado (2019). "IIB Flux Non-Commutativity and the Global Structure of Field Theories". In: *JHEP* 10, p. 169. DOI: 10.1007/JHEP10(2019)169. arXiv: 1908.08027 [hep-th].

Hausel, T., E. Hunsicker, and R. Mazzeo (2004). "Hodge Cohomology of Gravitational Instantons". In: *Duke Math. J.* 122.3, pp. 485–548. DOI: 10.1215/S0012-7094-04-12233-X. arXiv: math/0207169.

Lambert, N., C. Papageorgakis, and M. Schmidt-Sommerfeld (2011). "M5-Branes, D4-Branes and Quantum 5D Super-Yang–Mills". In: *JHEP* 01, p. 083. DOI: 10.1007/JHEP01(2011)083. arXiv: 1012.2882 [hep-th].

Witten, E. (1995). "Some Comments on String Dynamics". In: arXiv: hep-th/9507121.

Witten, E. (2009). "Geometric Langlands From Six Dimensions". In: arXiv: 0905.2720 [hep-th].

Chapter XII.2

Local threefolds, D3 particles, and the conifold

XII.2.1 A particle at a shrinking sphere

A D3-brane wrapped on a compact three-cycle has only time left in its worldvolume outside the internal space. In four dimensions it is a particle. As the cycle shrinks, the wrapped particle can become light while the other excitations of a string compactification stay heavy. The conifold gives a simple case in which we can calculate the mass coordinate, identify the charge, and see why a description that has integrated out this particle breaks down.

Two features of this example need to be distinguished. The geometry contains a compact sphere and a second integration path that runs out to a chosen endpoint. Only the compact sphere gives the local wrapped particle. Also, the same particle can be charged under a background flavor field in a noncompact space or under a dynamical photon in a compact embedding. To tell the two possibilities apart we will need a kinetic norm as well as a period. We use the basic facts about calibrated branes, the conifold and periods from Volumes III, IV and V, and the four-dimensional central charge from Volume 0.

XII.2.2 The cycles of a smoothed node

Which part of the smoothed conifold can a D3-brane wrap, and what should count as its dual cycle? Start with the family

$$X_s = \{F_s = 0\} \subset \mathbb{C}^4, \qquad F_s = x^2 + y_1^2 + y_2^2 + y_3^2 - s. \tag{XII.2.1}$$

The four derivatives of F_s vanish together only at the origin, which belongs to X_s only when $s = 0$. Thus s smooths an isolated node. First take $s > 0$ real. With $(x, y_1, y_2, y_3) = u + iv$, the real and imaginary parts of the equation are

$$|u|^2 - |v|^2 = s, \qquad u \cdot v = 0. \tag{XII.2.2}$$

Since u cannot vanish, $n = u/|u|$ lies on the unit three-sphere and v is tangent to it at n. Conversely, every such tangent vector gives a point of X_s by

$$(n, v) \longmapsto \sqrt{s + |v|^2}\, n + iv, \qquad |n| = 1, \quad n \cdot v = 0. \tag{XII.2.3}$$

Using the round metric to identify tangent and cotangent fibers gives T^*S^3. Scaling v to zero in this description contracts the cotangent fibers. In particular, the compact class A is the real sphere $v = 0$, with its outward orientation in the ordered real coordinates x, y_1, y_2, y_3. The radius $\sqrt{s}$ is measured in these coordinates. It is not a proper radius in the Calabi–Yau metric. For a nonzero complex s the same argument works after a local phase rotation of all four coordinates.

The map also tells us which topology is compact. At a point of the threefold its inverse reads

$$n = \frac{\operatorname{Re} z}{\sqrt{s + |\operatorname{Im} z|^2}}, \qquad v = \operatorname{Im} z, \qquad z = (x, y_1, y_2, y_3). \tag{XII.2.4}$$

The noncompact directions are the three real components of v tangent to the sphere. A deformation retraction must reduce those components while staying on $F_s = 0$. Multiplying the complex point z by a number less than one would change s, so instead use

$$h_t(n, v) = \sqrt{s + t^2|v|^2}\, n + itv, \qquad 0 \le t \le 1. \tag{XII.2.5}$$

Its squared real length minus its squared imaginary length is always s, and its real and imaginary parts remain orthogonal. At $t = 0$ the image is precisely A. Thus the sphere generates $H_3(X_s; \mathbb{Z})$ primitively: the noncompact fibers have added no new absolute three-cycle. This will distinguish a genuine wrapped particle from a chain whose endpoint must be supplied from outside.

We need a holomorphic three-form to measure these cycles. Use the ordered ambient form $\nu = dx \wedge dy_1 \wedge dy_2 \wedge dy_3$ and define its residue by putting dF_s first:

$$dF_s \wedge \Omega = \nu, \qquad \Omega = \begin{cases} dy_1 \wedge dy_2 \wedge dy_3/(2x) & x \neq 0, \\ -dx \wedge dy_1 \wedge dy_2/(2y_3) & y_3 \neq 0. \end{cases} \tag{XII.2.6}$$

The wedge equation fixes the pullback of the local three-form to X_s. Adding a form with a factor of dF_s does not change that pullback. This explains why the local formulas agree on overlaps and why the minus sign in the second patch is required. The two displayed patches suffice for the integrations below, together with relabelings of the y_i at the patch boundaries.

The apparent pole at $x = 0$ in the first formula is a chart issue. At such a point of a smooth fiber at least one y_i is nonzero; that coordinate can be used as the normal direction instead. A constant change $\widehat{\Omega} = h\Omega$, $h \neq 0$, multiplies every period by h. Changing a cycle orientation instead multiplies the integral over that cycle by -1. We keep these operations separate, because only the latter reverses the oriented wrapped D3.

To find a second integration path, project onto the x-plane. Over the real interval from $-\sqrt{s}$ to $+\sqrt{s}$ the real fiber is a two-sphere of coordinate radius $\sqrt{s - x^2}$. It shrinks

at both endpoints, making A a three-sphere. To continue past $x = +\sqrt{s}$ on the real axis, keep y imaginary so that $\sum_i y_i^2 = s - x^2 < 0$. Choose a fixed real $L > \sqrt{s}$ and take the three-chain

$$B_L : \quad \sqrt{s} \le x \le L, \qquad y = i\sqrt{x^2 - s}\, n, \quad n \in S^2, \qquad \text{orientation } dx \wedge \omega_{S^2}. \tag{XII.2.7}$$

Here ω_{S^2} is the outward area form on the unit two-sphere. The sphere collapses at the left endpoint only. At $x = L$ it is the boundary of B_L, oriented by ω_{S^2}. The actual chain runs in the threefold; Figure XII.2.1 displays its projection and the spheres it carries.

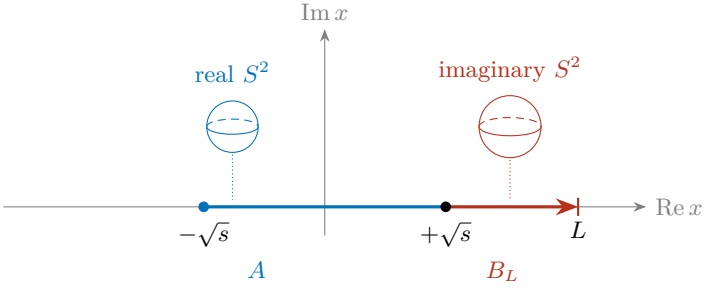


Figure XII.2.1: The cycles projected to the x-plane for real $0 < s < L^2$. The real two-sphere shrinks to a point at each end of the blue interval. Along the red path the imaginary sphere grows from a point and ends on the marked fiber at L. The arrow gives the x orientation of B_L; the orientation of A is that of the real three-sphere.

The marked fiber is $D_{L,s} = \{x = L\}$ inside X_s. For $0 < |s| < L^2$, the equation $\sum y_i^2 = s - L^2$ defines a smooth affine quadric retracting to a two-sphere. Over the whole disk $|s| < L^2$, the branch of $\sqrt{L^2 - s}$ positive at $s = 0$ identifies these marked fibers. For example, dividing y by $i\sqrt{L^2 - s}$ makes the equation $\sum n_i^2 = 1$, independent of s. This fixes the boundary class during a loop about the node. The homology sequence of the pair gives

$$0 \longrightarrow \mathbb{Z}[A] \longrightarrow H_3(X_s, D_{L,s}; \mathbb{Z}) \xrightarrow{\partial} \mathbb{Z}[\partial B_L] \longrightarrow 0. \tag{XII.2.8}$$

Indeed $H_3(D_{L,s}) = H_2(X_s) = 0$, whereas $H_2(D_{L,s})$ is generated by the sphere at L. The chain B_L lifts this generator, and any two lifts differ by an integral multiple of A. The integral of Ω is well defined on these classes: $d\Omega = 0$, and its restriction to the marked complex surface vanishes because it is a holomorphic three-form.

The choice of boundary in this calculation matters. For a disk cotangent bundle K containing the zero section, the *entire* radial boundary is a sphere bundle over S^3. Because S^3 is parallelizable, that bundle is $S^3 \times S^2$, and the inclusion maps a section to the generator of $H_3(K)$. Exactness now gives

$$H_3(\partial K) \xrightarrow{\sim} H_3(K), \qquad H_3(K) \longrightarrow H_3(K, \partial K) \quad \text{zero.} \tag{XII.2.9}$$

The compact class would therefore vanish in the second relative group. The endpoint $x = L$ singles out a smaller subspace, so (XII.2.8) retains the very cycle that can be added to B_L.

There is a local test of the orientation. At the single crossing $x = +\sqrt{s}$, solve for x and use the y_i as complex coordinates. In these coordinates the tangent planes of A and B_L are the real and imaginary y planes, each with its coordinate orientation. The concatenation of three real axes followed by three imaginary axes requires three swaps to give the complex orientation, in which each real axis is followed by its imaginary partner. Thus the raw crossing I and the period pairing we will use have the signs

$$I(A, B_L) = -1, \qquad \langle A, B_L \rangle_{\text{per}} := I(B_L, A) = +1. \tag{XII.2.10}$$

The second sign declares the order for the period pair. It does not give the absolute local group $H_3(X_s)$ a second generator or a nondegenerate pairing. The continuation of the period itself will provide an independent way to fix the sign of the shift.

For comparison, either small resolution of the same singular node has total space $\mathcal{O}(-1)\oplus\mathcal{O}(-1)$ over $\mathbb{P}^1$. It retracts to the exceptional two-sphere, whereas the smoothing retracts to the real three-sphere:

$$H_3(X_s; \mathbb{Z}) = \mathbb{Z}[A], \qquad H_3(X_{\text{res}}; \mathbb{Z}) = 0, \qquad H_2(X_{\text{res}}; \mathbb{Z}) = \mathbb{Z}[\mathbb{P}^1]. \tag{XII.2.11}$$

The size of the exceptional curve is a Kähler parameter of the resolution. It is not the complex parameter s. A D3 wrapped on a two-cycle would leave a spatial worldvolume direction in four dimensions and thus describe a string configuration. We need the three-sphere of the smoothing for a particle.

We can see the exceptional curve without confusing it with a different real slice of X_s. Introduce the matrix of linear coordinates

$$\mathsf{M} = \begin{pmatrix} x + iy_1 & y_2 + iy_3 \\ -y_2 + iy_3 & x - iy_1 \end{pmatrix}, \qquad \det \mathsf{M} = x^2 + y_1^2 + y_2^2 + y_3^2. \tag{XII.2.12}$$

At $s = 0$, a nonzero matrix on the node has rank one and hence a unique kernel line in $\mathbb{C}^2$. One small resolution retains that line even at $\mathsf{M} = 0$:

$$X_{\text{res}} = \{(\mathsf{M}, [a : b]) : \mathsf{M}(a, b)^t = 0\} \longrightarrow \{\det \mathsf{M} = 0\}. \tag{XII.2.13}$$

The map forgets $[a : b]$. Away from the node it is one-to-one; above the node every line is allowed, producing the exceptional $\mathbb{P}^1$. In the chart $a \neq 0$, put $t = b/a$. The incidence equation determines the first column from the second:

$$\mathsf{M} = \begin{pmatrix} -tU & U \\ -tV & V \end{pmatrix}. \tag{XII.2.14}$$

In the other chart put $t' = a/b$ and take the first column as the fiber coordinates (U', V'). On the overlap,

$$t' = t^{-1}, \qquad U' = -tU, \qquad V' = -tV. \tag{XII.2.15}$$

Up to the constant fiber sign these are the transition functions of two copies of $\mathcal{O}(-1)$. Scaling the fiber coordinates to zero leaves its zero section, giving the retraction used in (XII.2.11).

For $s \neq 0$, however, $\det \mathsf{M} = s$ is invertible and has no kernel line. The incidence equations above then have no points. The construction resolves the singular fiber; it does not replace the three-sphere of a smooth fiber by a two-sphere inside that same fiber. Changing the complex equation by s and assigning a Kähler area to the exceptional curve are distinct operations. The D3 dimension count follows directly: three internal spatial directions leave time only, while two leave time and one spatial direction. It does not assert the existence of a stable BPS string on the resolved geometry.

XII.2.3 Period integrals and the cutoff

How much of the dual period measures the degeneration, and how much comes from where we stop the integral? We can separate them by doing the integral at finite L, following the paths in Figure XII.2.1.

In the $y_3 \neq 0$ patch, write $y = \rho(x)n$ on either chain. The terms in $dy_1 \wedge dy_2$ containing dx vanish in (XII.2.6). The outward unit sphere area form is $dn_1 \wedge dn_2/n_3$ in the $n_3 \neq 0$ chart. Substitution gives

$$\Omega\big|_{y=\rho n} = -\frac{\rho}{2}\, dx \wedge \omega_{S^2}. \tag{XII.2.16}$$

The result extends across the equator by using the other sphere charts. On A, the outward orientation is $-dx \wedge \omega_{S^2}$: contracting the ordered real ambient volume with the outward radial vector yields this sign in the interior of the interval. On B_L the orientation is the one in (XII.2.7). Since $\int_{S^2} \omega_{S^2} = 4\pi$,

$$P(s) := \int_A \Omega = 2\pi \int_{-\sqrt{s}}^{+\sqrt{s}} \sqrt{s - x^2}\, dx, \tag{XII.2.17}$$

$$Q(s; L) := \int_{B_L} \Omega = -2\pi i \int_{\sqrt{s}}^{L} \sqrt{x^2 - s}\, dx. \tag{XII.2.18}$$

The signs have different origins: the real cycle uses its outward orientation; the relative cycle uses the positive x direction and an imaginary fiber radius. For P, the integral is the area of a semicircle. Equivalently $x = \sqrt{s}\cos\vartheta$ gives

$$P = 2\pi s \int_0^{\pi} \sin^2\vartheta\, d\vartheta = \pi^2 s. \tag{XII.2.19}$$

A second normalization check uses the radial vector E in $\mathbb{R}^4$. On the real sphere $\Omega = \iota_{\mathsf{E}}\nu/(2s)$, since $dF_s(\mathsf{E}) = 2s$. This gives

$$P = \frac{\mathrm{Vol}_{\mathrm{Eucl}}(S^3_{\sqrt{s}})}{2\sqrt{s}} = \frac{2\pi^2 s^{3/2}}{2\sqrt{s}} = \pi^2 s. \tag{XII.2.20}$$

The Euclidean sphere volume checks the algebraic residue normalization. We will separately normalize the physical calibration.

This integral explains why a coordinate radius does not directly give the mass power. The coordinate sphere has volume proportional to $s^{3/2}$, but the residue includes the inverse normal derivative of the defining equation. On the sphere its factor is $1/(2\sqrt{s})$; the period is therefore proportional to s. The same conclusion follows under a simultaneous dilation of all four coordinates. If $d_\lambda : X_s \to X_{\lambda^2 s}$ sends z to λz, the residue prescription gives

$$d_\lambda^* \Omega_{\lambda^2 s} = \lambda^{4-2} \Omega_s = \lambda^2 \Omega_s, \qquad P(\lambda^2 s) = \lambda^2 P(s). \tag{XII.2.21}$$

The four powers come from the ambient volume form and the two from the quadratic equation. Counting only the three tangent directions would miss the normalization of the residue.

For a changed phase, write $s = \sigma e^{i\phi}$, $\sigma > 0$, and transport the outward sphere by $z = e^{i\phi/2} w$, $w \in A_\sigma$. On this chosen branch,

$$r_\phi^* \Omega_s = e^{i\phi} \Omega_\sigma, \qquad P(s) = e^{i\phi} \pi^2 \sigma. \tag{XII.2.22}$$

For example, at $s = -\sigma$, reached through the upper half-plane, the sphere lies in the imaginary coordinate slice, with its transported orientation; its period is $-\pi^2\sigma$. At $s = i\sigma$ the period is $i\pi^2\sigma$. These are compact cycle integrals with different complex phases. The value of the three-form at a single point would determine neither of them.

For Q, set $x = \sqrt{s}\cosh u$ and $u_L = \operatorname{arcosh}(L/\sqrt{s})$. The square root and dx each contribute a factor $\sqrt{s}\sinh u$, so the primitive and its value are

$$\int_{\sqrt{s}}^{L} \sqrt{x^2 - s}\, dx = s \int_0^{u_L} \sinh^2 u\, du = \frac{s}{4} \sinh(2u_L) - \frac{s}{2} u_L, \tag{XII.2.23}$$

$$Q = -\pi i \left[LD - s \log \frac{L + D}{\sqrt{s}} \right], \qquad D = \sqrt{L^2 - s}. \tag{XII.2.24}$$

The branch starts with real $D > 0$ and a real logarithm in the bracket at the chosen base fiber. For $|s| < L^2$, D extends holomorphically with $D(0) = L$. The only logarithm in (XII.2.24) that is multivalued around zero comes from $\sqrt{s}$. To write it with a dimensionless argument, split the period into

$$Q(s; L) = \frac{P(s)}{2\pi i} \log \frac{s}{4L^2} + H_L(s), \tag{XII.2.25}$$

$$H_L(s) = -\pi i \left[LD - s \log \frac{L + D}{2L} \right]. \tag{XII.2.26}$$

The second logarithm has a branch analytic on the disk and equal to zero at $s = 0$: $L + D$ has no zero there. The initial branch of $\log s$ has its cut along the negative real s-axis. The algebraic units are fixed by $[s] = [x]^2 = [L]^2$, independently of any units for the four-dimensional mass.

Expanding both analytic factors for $|s|/L^2 \ll 1$ gives

$$H_L(s) = -\pi i L^2 + \frac{\pi i}{2} s - \frac{\pi i}{8L^2} s^2 + O(s^3/L^4). \tag{XII.2.27}$$

In this particular split the linear term of H_L does not depend on L. The full analytic part does have a cutoff-dependent linear term if we instead use a fixed reference argument $\log(s/s_\star)$, where $s_\star > 0$ has the same units as s. In that convention the analytic part is

$$H_L(s) + \frac{P(s)}{2\pi i} \log \frac{s_\star}{4L^2}. \tag{XII.2.28}$$

In particular, subtracting only the constant divergence does not produce a cutoff-independent period.

As a check, change the endpoint L to $3L$ at fixed s. The logarithms of s cancel in the difference, but their scales do not. Using (XII.2.27) gives

$$Q(s;3L) - Q(s;L) = \pi i \left[-8L^2 + s\log 3 + \frac{s^2}{9L^2} + O(s^3/L^4) \right]. \tag{XII.2.29}$$

The endpoint derivative provides a check without choosing a logarithmic split:

$$\partial_L Q = -2\pi i \sqrt{L^2 - s}. \tag{XII.2.30}$$

At fixed L, the integral instead goes to zero as $s \uparrow L^2$, because the real path from $\sqrt{s}$ to L has shrunk to length zero. This second endpoint singularity is why the analytic disk in (XII.2.25) has radius L^2. The degeneration of the particle cycle is at $s = 0$.

It is useful to organize changes of input by the ratio of the two algebraic scales. With $\epsilon = s/L^2$, the exact answer becomes

$$\frac{Q}{-\pi i L^2} = \sqrt{1-\epsilon} - \epsilon \log \frac{1+\sqrt{1-\epsilon}}{\sqrt{\epsilon}}, \qquad \frac{P}{\pi^2 L^2} = \epsilon, \quad 0 < \epsilon < 1. \tag{XII.2.31}$$

The small parameter in the earlier expansion is thus ϵ, rather than s without a comparison scale. At fixed s, replacing L by bL, with fixed $b > 0$ and both endpoints larger than $\sqrt{s}$, replaces ϵ by ϵ/b^2. In a common small-s disk we obtain

$$\begin{aligned} Q(s;bL) - Q(s;L) = \pi i \big[&-(b^2-1)L^2 + s\log b \\ &+ \frac{1-b^{-2}}{8L^2} s^2 + O(s^3/L^4) \Big], \end{aligned} \tag{XII.2.32}$$

$$\lim_{s\to 0} \frac{Q(s;bL) - Q(s;L) + \pi i (b^2-1)L^2}{s} = \pi i \log b. \tag{XII.2.33}$$

The first example $b = 3$ recovers (XII.2.29); the last limit isolates exactly what remains after removing the constant term. Changing the endpoint changes the answer even arbitrarily close to the node. It preserves the singular coefficient, because the two logarithms of s cancel in the difference.

The other edge of the interval tests a different approximation. Let $\delta = 1 - s/L^2$ tend to zero through positive values. The logarithm in (XII.2.31) is $\operatorname{arctanh}\sqrt{\delta}$. Expanding it gives

$$Q = -\pi i L^2 \left[\frac{2}{3}\delta^{3/2} + \frac{2}{15}\delta^{5/2} + O(\delta^{7/2}) \right]. \tag{XII.2.34}$$

Here the relative chain collapses, while $P \to \pi^2 L^2 \neq 0$. The $\delta^{3/2}$ behavior comes from integrating a square-root fiber radius over a short interval. This limit cannot describe the light electric particle: its compact cycle has not vanished. It also explains why an expansion around $s = 0$ cannot be used uniformly up to the marked fiber's own degeneration.

XII.2.4 A loop around the node

What does the logarithm do to the cycles when the parameter returns to the same smooth fiber? Fix $0 < s_0 < L^2$ and follow the positive loop

$$s(t) = s_0 e^{2\pi i t}, \qquad 0 \le t \le 1. \tag{XII.2.35}$$

The boundary sphere at L returns with its orientation unchanged, because the marking extends across the disk. The real sphere, transported by the rotation $z \mapsto e^{\pi i t} z$ on its coordinates, returns by the antipodal map on S^3, of degree $+1$. Thus the two possible changes are already constrained:

$$A \longmapsto A, \qquad B_L \longmapsto B_L + kA, \qquad k \in \mathbb{Z}. \tag{XII.2.36}$$

The integer follows by continuing (XII.2.25). The holomorphic term returns to its initial value; the logarithm increases by $2\pi i$. We find

$$(P, Q) \longmapsto (P, Q + P), \qquad B_L \longmapsto B_L + A. \tag{XII.2.37}$$

The second statement uses the injective compact class in (XII.2.8) and the fact that $P(s_0) \neq 0$. It is the Picard–Lefschetz shift for the crossing in (XII.2.10). In raw crossing notation the coefficient is $I(B_L, A) = 1$.

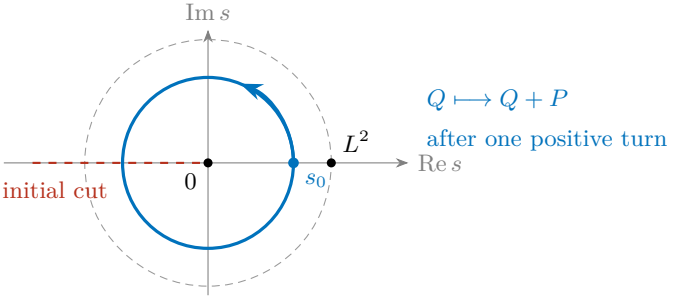


Figure XII.2.2: Positive continuation in the s-plane, starting at the marked base point s_0. The red cut specifies the initial branch; continuation crosses it instead of resetting the logarithm. The dashed circle marks the disk boundary $|s| = L^2$. This cut lives in parameter space, not in the x-plane of Figure XII.2.1.

We can recover the same sign without prescribing a jump to the logarithm. Differentiate with respect to s at fixed L. The lower-endpoint term of the first derivative

vanishes because the integrand is zero there. Differentiating the resulting analytic function yields

$$Q' = \pi i \log \frac{L+D}{\sqrt{s}}, \qquad Q'' = -\frac{\pi i L}{2sD}. \tag{XII.2.38}$$

Here Q'' is single valued on the punctured disk and has residue $-\pi i/2$ at zero. Integrate $Q''\,ds$ and $d(sQ'-Q) = sQ''\,ds$ along the lift of (XII.2.35). The second integrand is analytic through zero, so

$$\Delta Q' = \pi^2, \qquad \Delta Q = s_0 \Delta Q' - \oint sQ''\,ds = \pi^2 s_0 = P(s_0). \tag{XII.2.39}$$

In the opposite direction the residue contributes with the opposite sign and the change is $-P(s_0)$. Changing the cutoff within the disk instead adds the single-valued function in (XII.2.29). It cannot change the winding.

The shift acts on the period column by T. To express a fixed linear functional on this column in the new basis, transform its coefficients contragrediently:

$$\begin{pmatrix} P \\ Q \end{pmatrix} \longmapsto T \begin{pmatrix} P \\ Q \end{pmatrix}, \quad T = \begin{pmatrix} 1 & 0 \\ 1 & 1 \end{pmatrix}, \qquad \begin{pmatrix} n_e \\ n_m \end{pmatrix} \longmapsto T^{-t} \begin{pmatrix} n_e \\ n_m \end{pmatrix}. \tag{XII.2.40}$$

For example, $(2,1)$ becomes $(1,1)$, and $P + (Q+P) = 2P + Q$. This is a calculation with coefficients in the pair. It does not produce a local particle with magnetic charge 1: that would require a compact magnetic cycle. The primitive charge $(1,0)$ is fixed, as expected for the particle on the sphere A.

Two changes let us use this calculation without memorizing a single matrix. First, a loop of winding k adds $2\pi i k$ to the logarithm. Since the nilpotent part of T has square zero,

$$T^k = \begin{pmatrix} 1 & 0 \\ k & 1 \end{pmatrix}, \qquad Q \longmapsto Q + kP, \qquad (n_e, n_m) \longmapsto (n_e - k n_m, n_m). \tag{XII.2.41}$$

For instance a twice-wound positive loop changes the formal coefficient pair $(3,1)$ to $(1,1)$, and its expression $P + (Q+2P)$ still equals $3P+Q$. A negative winding gives the inverse operation. The invariance concerns the value of the linear functional under passive changes of its basis. Following an actual state through a moduli-space path is a separate physical question involving the available spectrum.

Second, we could have chosen a different lift of the same boundary sphere. Let $B_L^{(m)} = B_L + mA$, with $m \in \mathbb{Z}$, and write its period as Q_m. Then

$$Q_m = Q + mP, \qquad (Q_m)_{\text{continued}} - Q_m = P, \qquad B_L^{(m)} \longmapsto B_L^{(m)} + A. \tag{XII.2.42}$$

The analytic piece in (XII.2.25) changes by mP, but the logarithmic coefficient remains fixed. This integral ambiguity differs from a change of endpoint: the latter adds the analytic function (XII.2.32), which need not be an integer multiple of P. It also differs from reversing the loop, which changes the sign of the shift. The boundary marking, the oriented compact generator and the winding together fix which operation is being performed.

XII.2.5 The wrapped D3 and its electric charge

Which period can be the central charge of a particle? In unwarped, fluxless type IIB a D3 can follow a spacetime worldline and wrap a calibrated internal three-cycle. For real $s > 0$ the standard deformed-conifold metric is invariant under complex conjugation. Its fixed real slice is A. Conjugation sends the Kähler form J to $-J$, so the pullback of J to the slice is zero. The pullback of the residue is real and positive in the orientation used above. Choose the constant phase of the metric-normalized form $\Omega_{\rm cal} = c\Omega$ so that its real part calibrates this orientation:

$$J|_A = 0, \qquad \mathrm{Im}\,\Omega_{\rm cal}|_A = 0, \qquad \mathrm{Re}\,\Omega_{\rm cal}|_A = d\,\mathrm{vol}_A\,. \tag{XII.2.43}$$

A local phase rotation relates the description to the sphere at complex s, where the phase of the central charge can vary.

The calibration condition states more than the vanishing of the imaginary part at a point. The phase is constant on the whole cycle, and its real part equals the induced volume form. Using (XII.2.22), let $\beta = \arg(cP)$ on the continued sphere. Its positive volume is measured by

$$\mathrm{Vol}(A_s) = \int_{A_s} \mathrm{Re}(e^{-i\beta}\Omega_{\rm cal}) = \left| c \int_{A_s} \Omega \right|. \tag{XII.2.44}$$

At real positive s we chose $\beta = 0$. Reversing the sphere requires the calibration phase $\beta + \pi$, so its volume stays positive. Rotating s changes the phase of its period; reversing the brane changes its oriented charge. These are distinguishable operations even when both happen to multiply a period by -1.

In the smooth probe calculation, take a constant dilaton and zero gauge-invariant flux on the worldvolume. The string-frame mass from the D3 tension is

$$T_3 = \frac{1}{(2\pi)^3 g_s \alpha'^2}, \qquad M_{\rm D3} = T_3\,\mathrm{Vol}(A) = T_3 \left| \int_A \Omega_{\rm cal} \right| = T_3 |c\,P|. \tag{XII.2.45}$$

Here g_s is the string coupling and α' has units of length squared. The calibration has period units of length cubed in this frame, so the mass has units of inverse length. The constant converting the residue to the calibration is extra metric information; an arbitrary holomorphic normalization of Ω does not give a string-frame mass. For example, within one common local calibration scale, s and $2s$ have compact periods P and $2P$. The predicted mass ratio is then two. The use of the period to follow the light state to a string-scale sphere is the protected wrapped-D3 identification. The smooth Dirac–Born–Infeld calculation alone does not control that regime.

The Ramond–Ramond coupling fixes the electric charge. Take the component of C_4 with one spacetime leg and three internal legs, and normalize the associated connection $\mathcal{A}$ by the unit D3 coupling. For an internal mode η with $\int_A \eta = 1$, reduction of the worldvolume coupling gives

$$\int_{\gamma \times n_e A} \mathcal{A} \wedge \eta = n_e \int_\gamma \mathcal{A}. \tag{XII.2.46}$$

Here γ is the particle worldline; the common D3 charge unit has been absorbed in $\mathcal{A}$. An A-wrapped D3 has charge $+1$; reversing its cycle reverses the coupling while the mass, an absolute value, stays the same. In an ordinary compact conifold degeneration with a primitive surviving A and no other light sector, the light BPS state and its charge conjugate furnish one hypermultiplet. The single hypermultiplet is the wrapped-state input for this simple node. The homology computation by itself does not count one-particle states of all possible wrapping numbers.

To connect this to four-dimensional central charges, suppose the node sits in a compact family with a dual integral cycle that completes B_L through the exterior. In a common local rigid normalization write

$$a = \kappa P, \qquad a_D = \kappa(Q + Q_{\text{ext}}), \qquad Z = n_e a + n_m a_D, \qquad M_{\text{BPS}} = \sqrt{2}\,|Z|. \tag{XII.2.47}$$

Here Q_{ext} accounts for the completion, and the common $\kappa \neq 0$ fixes units and phase in the rigid comparison. The compact supergravity formula in its own units uses projectively normalized periods, with the factor $e^{K/2}$ from the Kähler potential. A constant κ in the rigid comparison is not a substitute for that factor throughout a compact moduli space. For the primitive wrapped state $(n_e, n_m) = (1, 0)$, the rigid formula gives

$$M_{\text{BPS}} = \sqrt{2}\,|\kappa P| = \sqrt{2}\,|\kappa|\pi^2|s|. \tag{XII.2.48}$$

The mass vanishes with s. The dual period does not enter this electric central charge, even if it has a nonzero limit at a fixed cutoff.

To compare the two mass formulas at a smooth point in their common local frame, their constants must obey

$$\sqrt{2}\,|\kappa| = T_3|c|. \tag{XII.2.49}$$

This equation fixes a conversion between conventions. It is not an additional determination of the metric scale. For a constant nonzero h, the replacements

$$\widehat{\Omega} = h\Omega, \qquad (\widehat{P}, \widehat{Q}) = h(P, Q), \qquad \widehat{c} = c/h, \quad \widehat{\kappa} = \kappa/h \tag{XII.2.50}$$

leave Ω_{cal}, a, a_D and the mass unchanged, provided the exterior period uses the same normalization. Rescaling only the compact period would instead destroy the common normalization needed for its comparison with the dual period.

For a concrete phase variation, take $s = \sigma$, $i\sigma$, and $-\sigma$ along the continued family, with a common κ. The primitive central charges are respectively

$$Z = \kappa\pi^2\sigma, \qquad i\kappa\pi^2\sigma, \qquad -\kappa\pi^2\sigma; \qquad M = \sqrt{2}\,|\kappa|\pi^2\sigma. \tag{XII.2.51}$$

Their magnitudes agree. At any one of these points the oppositely oriented brane has central charge $-Z$ and opposite electric charge. This is the charge-conjugate state already included in the hypermultiplet, rather than a second independent hypermultiplet.

Linearity assigns $Z(nA) = na$ to an integral compact class. If a one-particle BPS state in that class exists, its mass is $\sqrt{2}|na|$. For positive n this equals the rest energy of n separated primitive BPS particles:

$$\sqrt{2}|na| = n\sqrt{2}|a|. \tag{XII.2.52}$$

Equality of these numbers supplies no binding energy and no count of one-particle states. The single primitive hyper used here is the ordinary-node physical input stated above. The period integral determines its central charge once that input is made.

Equation (XII.2.46) states how a charged particle couples to a connection. It has made no assertion that $\mathcal{A}$ is integrated over as a dynamical field. That depends on the internal mode that was used to obtain it.

XII.2.6 When the photon becomes dynamical

Why can a compact sphere carry a charged particle without producing a localized photon? The charge samples an integral on A, whereas the photon kinetic term samples the whole threefold. In an unwarped reduction, a four-dimensional gauge kinetic coefficient contains the internal squared norm

$$\|\eta\|^2 = \int_{X_s} \eta \wedge *_6 \overline{\eta}. \tag{XII.2.53}$$

The electric frame of the self-dual C_4 reduction is understood here. We only use the convergence test of this norm, which does not require a formula for the full gauge coupling. If the coefficient is infinite at fixed unit coupling to A, the mode does not provide a normalizable four-dimensional photon on the isolated space.

Write the asymptotic metric as $dr^2 + r^2 g_Y$ to leading order, where r is the proper cone coordinate and Y is the five-dimensional unit link. A tangential three-form pulled back from Y has each of its three orthonormal-frame legs scaled by r^{-1}. The asymptotic volume scales as r^5, so a nonzero such mode has a tail proportional to

$$\int_{r_0}^{R} r^5 (r^{-3})^2 \, dr = \log \frac{R}{r_0}. \tag{XII.2.54}$$

The asymptotic metric need only be uniformly comparable to the cone metric for the divergence test. The proper radius R here is distinct from the algebraic endpoint L of the period. In the usual deformed-conifold metric the squared algebraic radius scales as the cube of the proper cone radius at infinity.

Could another closed representative with the same electric charge decay faster? Use the sphere bundle description near infinity. A section of the unit cotangent sphere bundle gives a three-cycle $A_r \subset Y_r$ that maps to A in the threefold. The cycles at different radii are homologous, so for a closed form η with $\int_A \eta = 1$,

$$\int_{A_r} \eta = 1 \qquad \text{for every sufficiently large } r. \tag{XII.2.55}$$

Pull the tangential restriction of η back to the unit link Y. It is closed and has the same fixed nonzero class there, since Y is diffeomorphic to $S^3 \times S^2$ and the period on the generator is fixed. Its harmonic representative on the compact unit link has a strictly positive squared norm c_Y. Harmonic projection minimizes the norm in its cohomology class. Rescaling the slice and including the radial integration therefore gives the bound

$$\|\eta\|^2_{r_0<r<R} \;\geq\; c \int_{r_0}^{R} \frac{dr}{r}, \qquad c > 0. \tag{XII.2.56}$$

The constant can incorporate the comparison between the actual metric and the cone metric. A radial component cannot cancel the lower bound from the tangential component. Consequently a closed mode that sees A cannot become square integrable by changing representative.

Canonical normalization makes the physical effect of this divergence visible. At a fixed background, let N_R be the regulated coefficient of $F_{\mu\nu}F^{\mu\nu}/4$ in the chosen electric mode. Its norm contribution has a fixed positive conversion factor K_0. The unit worldline coupling and the quadratic kinetic contribution then have the form

$$\frac{N_R}{4}F_{\mu\nu}F^{\mu\nu}, \qquad \int_\gamma \mathcal{A}, \qquad N_R \geq K_0 c \log(R/r_0), \quad K_0 > 0. \tag{XII.2.57}$$

For this comparison all other conversion factors are held fixed. Writing $\mathcal{A}_{\mathrm{can}} = \sqrt{N_R}\mathcal{A}$ would put the kinetic term in canonical form, while the particle's coefficient in the worldline coupling becomes

$$q_{\mathrm{can}}(R) = N_R^{-1/2}, \qquad q_{\mathrm{can}}(R)^2 \leq \frac{1}{K_0 c \log(R/r_0)}. \tag{XII.2.58}$$

For $R = 2^j r_0$, the upper bound is $1/(K_0 c\, j \log 2)$, tending to zero. The integer charge in (XII.2.46) has not changed; the cost of a mode with that fixed period grows without bound. Holding a finite canonical field fluctuation instead makes its value at the charged cycle vanish in this norm comparison. A regulated kinetic coefficient therefore does not supply a normalizable photon after removing the regulator. A compact embedding changes the end of the geometry and the mode problem, rather than just this field normalization.

For comparison, a mode with an orthonormal-frame amplitude proportional to $r^{-\alpha}$ has a tail controlled by

$$\int_{r_0}^{R} r^{5-2\alpha}\, dr = \begin{cases} \dfrac{R^{6-2\alpha} - r_0^{6-2\alpha}}{6-2\alpha}, & \alpha \neq 3, \\ \log(R/r_0), & \alpha = 3. \end{cases} \tag{XII.2.59}$$

Thus $\alpha > 3$ gives convergence at the upper end, while $\alpha = 3$ gives $\log 2$ on each interval $[2^j r_0, 2^{j+1} r_0]$. For $\alpha = 4$, the two intervals $[4, 8]$ and $[8, 16]$, in common radius units, contribute $3/128$ and $3/512$ respectively with the angular norm omitted. This faster decay is a useful comparison but is unavailable to the nonzero-period class.

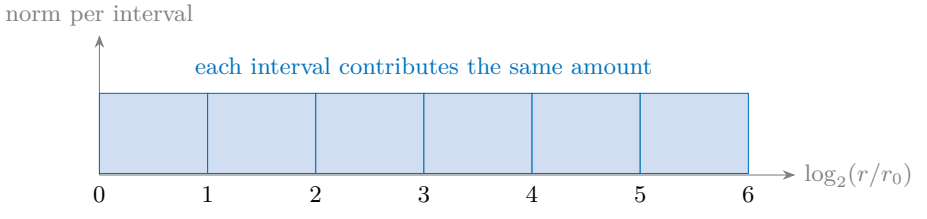


Figure XII.2.3: The contribution per doubling of the radius for an r^{-3} mode on the cone. Each bar has the same height, which represents the contribution of a whole interval, rather than the pointwise field amplitude. The sum over intervals diverges.

There is a parallel distinction for the deformation itself. Transport the residue with its asymptotic normalization fixed. Its s derivative has period $\partial_s P = \pi^2$ on A; an s-dependent rescaling that changes the normalization at infinity would change the deformation problem. For the physical metric variation compare the unwarped metrics at fixed algebraic radius $\widetilde{r}$ and fixed asymptotic angular coordinates $(\theta_1, \phi_1, \theta_2, \phi_2, \psi)$. The leading squared variation scales as $\widetilde{r}^{-4}$ times an angular factor, while the shell measure scales as $\widetilde{r}^3 d\widetilde{r}$. Since $\widetilde{r}^2 \propto r^3$ asymptotically, this is the $r^5 r^{-6} dr$ logarithm in proper cone radius. Thus the selected metric comparison gives an integral proportional to

$$\int^{\widetilde{r}_{\max}} \frac{d\widetilde{r}}{\widetilde{r}}. \tag{XII.2.60}$$

This is the metric-mode computation; the lower bound (XII.2.56) alone does not provide its upper asymptotic estimate or its coefficient.

With the boundary conditions of the complete unwarped local threefold held fixed, a is therefore a background mass. The connection in (XII.2.46) can be a background flavor field, while the charged wrapped particle is retained. A finite-radius regulator does not change this conclusion if it is removed at fixed s. If a smooth fluxless compact compactification instead contains the local region, a primitive nonzero vanishing class can pair with a compact dual cycle. Provided the smoothing is an unstabilized complex-structure deformation and the corresponding field is retained, the associated internal modes on the smooth compact fiber have finite norm. The scalar can then lie in a dynamical vector multiplet. Compact completion also supplies the finite matching terms in (XII.2.47); it is not represented merely by imposing the coordinate endpoint L.

It takes a further limit to use a four-dimensional sector separately from its parent string theory. To see the scale requirement, hold the wrapped mass fixed as $\alpha' \to 0$ at bounded fixed g_s. In the local calibration frame, (XII.2.45) requires

$$|c\, s| \;\propto\; g_s \alpha'^2 \quad \text{at fixed } M_{\mathrm{D3}}. \tag{XII.2.61}$$

This scaling specifies what is held fixed; it does not show that all other couplings vanish. In a noncompact model a gapless bulk continuum can remain even when there is no normalizable four-dimensional graviton. We use the isolated light sector only when its couplings to unwanted bulk modes can be neglected in the limit. In a compact model the comparison to a rigid gauge theory likewise requires a window in which gravity and the other coupled sectors decouple.

An explicit scaling illustrates which part of this limit the period does determine. Introduce a dimensionless $\varepsilon > 0$, fix g_s, and choose

$$\alpha'(\varepsilon) = \varepsilon \alpha'_0, \qquad |cs|(\varepsilon) = \varepsilon^2 |cs|_0. \tag{XII.2.62}$$

Then the calibrated period volume decreases as ε^2 and the tension increases as ε^{-2}. Consequently

$$\frac{M_{\mathrm{D3}}(\varepsilon)}{M_{\mathrm{D3}}(1)} = 1, \qquad \frac{M_s(\varepsilon)}{M_s(1)} = \varepsilon^{-1/2}, \qquad M_s = \alpha'^{-1/2}. \tag{XII.2.63}$$

The calibrated volume in string units scales as

$$\frac{|cP|(\varepsilon)}{\alpha'(\varepsilon)^{3/2}} = \varepsilon^{1/2}\frac{|cP|_0}{(\alpha'_0)^{3/2}}. \tag{XII.2.64}$$

Thus the cycle becomes small in string units. The fixed mass uses the protected period identification already specified for the light wrapped state; the smooth classical DBI approximation does not improve in this limit. For any fixed external energy, its ratio to the string scale tends to zero. Its ratio to the retained particle mass has not changed. This is a fixed-mass field-theory scaling, distinct from taking $s \to 0$ with the string parameters and period conversion fixed, which makes the particle massless. The calculation has separated the wrapped mass from string oscillators. It has not computed a bulk Kaluza–Klein gap, a gravitational coupling or the coupling to a continuum. Those quantities depend on the exterior and the metric limit. They must be controlled separately before either the local free hyper or the compact rigid abelian sector can be used as an isolated four-dimensional system.

XII.2.7 The four-dimensional threshold

What would a four-dimensional observer infer from the logarithm in the dual period? In a compact embedding with a dynamical photon, an observer working well below the mass of the wrapped particle can integrate it out. We will calculate the singular term that this procedure produces, and identify the window where the calculation ceases to apply.

Use a connection $\mathcal{A}$ with unit electric charge and curvature $F = d\mathcal{A}$. On a spin test four-manifold $F/(2\pi)$ has integral periods. The Maxwell action and complex coupling in this frame are

$$S_E = \frac{1}{2e^2}\int F \wedge *F - \frac{i\theta}{8\pi^2}\int F \wedge F, \qquad \tau = \frac{\theta}{2\pi} + \frac{2\pi i}{e^2}. \tag{XII.2.65}$$

The component kinetic term is $F_{\mu\nu}F^{\mu\nu}/(4e^2)$. The θ term is $-i\theta$ times half the square of the integral flux class, an integer on a spin manifold. Thus θ can shift by 2π, the unit shift of τ in this normalization. Rescaling the electric connection to use a different charge unit would change the coefficient used to compare with the primitive period pair.

A charged $\mathcal{N} = 2$ hypermultiplet contributes one Dirac fermion and two complex scalars of the same mass M. Only the square of the electric charge q enters the parity-even threshold. We need the part of the determinant quadratic in a slowly varying external F, in the range $E_{\text{ext}} \ll M \ll \Lambda$, with Λ a matching scale in energy units. It can be read from the flat heat-kernel coefficient of a Laplace-type operator $-D^2 - E$. With $D_\mu = \partial_\mu + iq\mathcal{A}_\mu$ the connection curvature is $\mathcal{R}_{\mu\nu} = iqF_{\mu\nu}$. Up to total derivatives, the local coefficient of the proper-time logarithm is

$$\frac{1}{16\pi^2}\,\mathrm{tr}\left(\frac{E^2}{2} + \frac{\mathcal{R}_{\mu\nu}\mathcal{R}^{\mu\nu}}{12}\right). \tag{XII.2.66}$$

For a minimally coupled scalar $E = 0$. For a Dirac fermion, squaring the Dirac operator gives $E = (iq/2)\gamma^\mu\gamma^\nu F_{\mu\nu}$ in the stated Laplace convention. Put $F^2 = F_{\mu\nu}F^{\mu\nu}$. The Clifford trace and the spin trace give

$$\operatorname{tr}_{\text{spin}} E^2 = 2q^2F^2, \qquad \operatorname{tr}_{\text{spin}} \mathcal{R}^2 = -4q^2F^2. \tag{XII.2.67}$$

For instance, with $F_{12} = B$ the only independent component, $E = iqB\gamma^1\gamma^2$ and $E^2 = q^2B^2\mathbf{1}$. Its trace is $4q^2B^2 = 2q^2F^2$, as required. The coefficients inside $1/(16\pi^2)$ are therefore

$$b_{\text{scalar}} = -\frac{q^2F^2}{12}, \qquad b_{\text{Dirac}} = \frac{2q^2F^2}{3}. \tag{XII.2.68}$$

In a proper-time integral the complex scalar determinant has a minus sign. The fermion gives the opposite sign and a factor $1/2$ because we used the squared Dirac operator. The hypermultiplet coefficient is

$$-2b_{\text{scalar}} + \tfrac{1}{2}b_{\text{Dirac}} = \tfrac{1}{2}q^2F^2. \tag{XII.2.69}$$

Combining this with the logarithmic integral $\int_{\Lambda^{-2}}^{M^{-2}} dt/t = \log(\Lambda^2/M^2)$ gives the singular local term

$$\Delta\mathcal{L}_E = \frac{q^2F^2}{32\pi^2}\log\frac{\Lambda^2}{M^2}, \qquad \Delta \operatorname{Im}\tau = \frac{q^2}{2\pi}\log\frac{\Lambda}{M}. \tag{XII.2.70}$$

The proper-time limits compute the log coefficient, not the finite part of a threshold. In particular the two scalar determinants add; charge conjugation does not make one of them cancel the other.

In rigid $\mathcal{N} = 2$ special geometry the gauge coupling is holomorphic in the period coordinates. With masses proportional to $|a|$, choose a nonzero reference a_0 in the same units as a, and put analytic matching terms in the regular part of the coupling. On one branch, the logarithmic term and its two primitives are

$$\Delta\tau = \frac{\sum_j q_j^2}{2\pi i}\log\frac{a}{a_0}, \tag{XII.2.71}$$

$$\Delta a_D = \frac{\sum_j q_j^2}{2\pi i}\left[a\log\frac{a}{a_0} - a\right], \tag{XII.2.72}$$

$$\Delta\mathcal{F} = \frac{\sum_j q_j^2}{2\pi i}\left[\frac{a^2}{2}\log\frac{a}{a_0} - \frac{3a^2}{4}\right]. \tag{XII.2.73}$$

Here $\mathcal{F}$ is the local rigid prepotential; differentiating it gives a_D, and at fixed spectator moduli the rigid electric patch obeys $\tau = \partial a_D/\partial a$. The one-loop determinant fixes the parity-even logarithmic coefficient. Holomorphy fixes the corresponding mass-phase dependence, up to the stated regular terms. In particular, one charge -2 gives $\sum_j q_j^2 = 4$; the sign of the charge does not affect the parity-even response. The conifold instead has a single primitive state.

For the conifold period pair the same calculation is visible in the derivatives:

$$\frac{Q'}{P'} = \frac{i}{\pi}\log\frac{L+D}{\sqrt{s}} = \frac{1}{2\pi i}\log\frac{s}{4L^2} + O(s/L^2). \tag{XII.2.74}$$

A common conversion $a = \kappa P$ changes the reference argument but preserves the coefficient $1/(2\pi i)$. This matches (XII.2.71) for $q = 1$ and gives a unit shift of τ in the primitive pair. The regular terms from compact completion can change the finite coupling, so this comparison is of singular terms. There is no identification of the geometric L with the energy scale Λ.

The phase dependence now has a direct four-dimensional reading. Write $a/a_0 = \rho e^{i\varphi}$, with $\rho > 0$, and put $C = \sum_j q_j^2$. The real and imaginary parts of the singular coupling are

$$\Delta \operatorname{Re} \tau = \frac{C\varphi}{2\pi}, \qquad \Delta \operatorname{Im} \tau = \frac{C}{2\pi} \log \frac{1}{\rho}. \tag{XII.2.75}$$

Decreasing the mass magnitude increases the inverse squared coupling. A positive loop in its phase shifts the theta angle by $2\pi C$. For the primitive conifold hyper $C = 1$, this is the unit shift already found by continuing the relative integral. The determinant calculation controls the parity-even part; the holomorphic completion is the input that relates this part to the phase response.

Changing the nonzero reference from a_0 to ba_0, with $b > 0$, provides a useful check of what this match can fix. The displayed singular representatives change by

$$\delta\tau = -\frac{C \log b}{2\pi i}, \qquad \delta a_D = -\frac{Ca \log b}{2\pi i}, \qquad \delta\mathcal{F} = -\frac{Ca^2 \log b}{4\pi i}. \tag{XII.2.76}$$

They are a constant, a linear term and a quadratic term, respectively. Differentiation twice relates all three, while none has logarithmic monodromy. The regular matching coupling must change correspondingly if the total physical coupling is held fixed. This is the field-theory counterpart of the cutoff-dependent analytic terms in the period. The agreement of singular coefficients fixes the response of the light charged sector, leaving the finite matching data to its embedding.

At fixed nonzero external energy, the condition $E_{\text{ext}} \ll M$ fails as $s \to 0$. The Wilsonian theory must then keep the hypermultiplet. In the stipulated abelian theory with the massless hyper retained, the one-loop screening term in (XII.2.70) corresponds to

$$\frac{de}{d\log\mu} = \frac{e^3}{8\pi^2}, \qquad \frac{1}{e^2(\mu)} = \frac{1}{e^2(\mu_0)} + \frac{1}{4\pi^2} \log \frac{\mu_0}{\mu}. \tag{XII.2.77}$$

The solution is for this perturbative running in its weakly coupled window. A nonzero hyper mass stops its contribution below the threshold. In the massless limit, the coupling decreases toward the infrared. This is the usual infrared free abelian description of the compact node's light sector. It does not indicate an interacting rank-one fixed point.

For a massive hyper the stopping condition can be made explicit. Take $\mu_0 > M$ and compare scales well below the other thresholds. In the leading-log approximation with matching at M, the contribution of this hyper to the running is

$$\frac{1}{e^2(\mu)} - \frac{1}{e^2(\mu_0)} = \frac{1}{4\pi^2} \begin{cases} \log(\mu_0/\mu), & M < \mu < \mu_0, \\ \log(\mu_0/M), & 0 < \mu < M. \end{cases} \tag{XII.2.78}$$

Finite matching constants are omitted, and the second line refers only to this particle's contribution. The log in an effective action below its mass records modes already

integrated out; it does not mean those massive modes continue screening at arbitrarily low energies.

There is also a controlled way to approach the vanishing mass while keeping an integrated-out expansion. Hold κ fixed, put $|s| = \epsilon|s_0|$, and choose the external energy to tend to zero faster than the mass:

$$M(\epsilon) = \epsilon M_0, \qquad E_{\text{ext}}(\epsilon) = \epsilon^2 E_0, \qquad \frac{E_{\text{ext}}(\epsilon)}{M(\epsilon)} = \epsilon \frac{E_0}{M_0} \longrightarrow 0. \tag{XII.2.79}$$

At a fixed positive matching scale, M/Λ also tends to zero. These two inequalities preserve the domain of the massive threshold calculation at each nonzero ϵ. In contrast, with $E_{\text{ext}} = E_0 > 0$ fixed, E_0/M diverges. The singular effective action and the regular description with an explicit massless hyper address different orders of limits. The distinction is a statement about which degrees of freedom are kept, rather than a divergence in the mass of the wrapped state.

The isolated model also lacks an interacting rank-one fixed point, but its light sector has rank zero: there is no localized vector with the A-period coupling. The compact-embedded abelian sector above instead has rank one and is infrared free. In the isolated construction, with the prescribed decoupling and no additional light sector, the massless limit is a single free hypermultiplet. One check of the mass assignment uses the polynomial itself. The four weights are $1/2$ when the quadratic polynomial has degree one. Its Jacobian ideal contains all four coordinates, so

$$\mathbb{C}[x, y_1, y_2, y_3]/(\partial F_s) = \mathbb{C} \cdot 1, \qquad \text{wt}(\Omega) = 4 \cdot \tfrac{1}{2} - 1 = 1, \qquad [s]_{\text{mass}} = 1. \tag{XII.2.80}$$

The last equality uses the period mass normalization $[\Omega]_{\text{mass}} = 1$ and is a scaling dimension, not the dimensional conversion in (XII.2.45). It is consistent with the single background mass and does not by itself establish the existence of a free sector. In the next chapter this same weight calculation will separate masses from Coulomb-branch coordinates in less elementary threefolds.

Calculation	Limit being probed	Physical use
Internal kinetic norm	$R \to \infty$ at fixed $s \neq 0$	Tests whether the isolated mode defines a dynamical field.
Hyper threshold in the rigid embedded sector	M small at finite matching scale; valid below M	Describes the coupling after the hyper has been integrated out.
Massless embedded sector	$M = 0$, with the hyper retained	The weak abelian coupling decreases toward the infrared.

Table XII.2.1: The logarithms distinguish different limits. The coordinate endpoint L, the metric radius R, and the field-theory matching scale do different jobs.

XII.2.8 Exercises

1. **Reverse the cycles consistently.** Take $A' = -A$ and $B'_L = -B_L$, and keep the same geometric particle. Give the signs of its two basis periods relative to

P, Q. Find the coefficient of A' in the positive-loop shift of B'_L, the electric charge of the same particle in the primed frame, and the shift coefficient for the inverse loop. Explain why its mass is unchanged.

2. **Recover the dual threshold.** Take two hypers with electric charges $1, -2$, with masses proportional to $|a|$. Put the constant terms from the mass factors into regular matching terms. Let $\ell = \log(a/a_0)$, and write

$$\Delta\tau = \frac{C\ell}{2\pi i}, \qquad \Delta a_D = \frac{Ca\ell + Da}{2\pi i}, \qquad \Delta\mathcal{F} = \frac{Ea^2\ell + Ha^2}{2\pi i}.$$

With $\Delta\tau(a_0) = 0$, omit the linear and constant integration terms in $\Delta\mathcal{F}$. Determine C, D, E, H, and explain why the two charges do not cancel the running.

3. **Test a norm at infinity.** On an exact cone, compare the norm contributions on $[8, 16]$ and $[4, 8]$ for amplitudes r^{-3}, $r^{-7/2}$, and $r^{-5/2}$ in an orthonormal frame. Omit the common angular norm for each mode. For each mode divide the contribution of the outer interval by that of the inner interval. How many have finite total norm at the upper end? Explain why finiteness on any one interval does not settle this question.

4. **Change the cutoff.** At fixed s, expand

$$Q(s; 2L) - Q(s; L) = \pi i \left[c_0 L^2 + c_1 s \log 2 + c_2 s^2/L^2 + O(s^3/L^4)\right].$$

Determine c_0, c_1, c_2. Give the change of this difference after one positive loop in units of P. Explain how changing L differs from changing the branch of one period at fixed L.

5. **Explain the absence of an interacting rank-one fixed point.** Contrast the isolated conifold with a compact embedding that retains its primitive photon. Use both the radial norm calculation and the sign of the hypermultiplet threshold. Which step in the embedded argument fails if additional mutually nonlocal particles become light at the same point?

6. **Transport a sphere and compare conventions.** At fixed $\sigma > 0$, continue s from σ to $i\sigma$ through a quarter-turn. Describe the cycle in the four complex coordinates and compute the phase of its compact period from the residue pullback. Compare this with reversing the brane at fixed $s = \sigma$. Which operation changes its electric charge in the chosen local frame? Then replace Ω by $3i\Omega$ and give the compensating changes of c and κ that preserve the physical mass. Explain why this convention change does not create an extra charge-conjugate hypermultiplet. This is written transfer practice, assessed separately from the numerical tasks above.

7. **Choose a limit for a measurement.** A probe has fixed positive energy E_0. Compare three operations: removing the proper-radius regulator at fixed $s \neq 0$; sending $s \to 0$ at fixed string parameters; and the fixed-mass string scaling (XII.2.62). State which ratio or norm determines the conclusion in each case. In

which operation does the integrated-out particle description eventually fail at the probe energy? Construct a changed probe energy that avoids that failure, and explain what observable regime has then been changed. Finally explain why $Q \to 0$ as $s \uparrow L^2$ is unrelated to the vanishing particle mass. All parts are human-assessed.

Status and sources

§ The cycles of a smoothed node. [MATH]. Equations (XII.2.2)–(XII.2.6) give the real-fiber construction and fix the residue sign. The relative sequence and full-boundary contrast are (XII.2.8) and (XII.2.9). The crossing is computed in (XII.2.10). The deformation and resolution topologies reuse Volume IV, Chapter 5; the compact period pairing convention is distinguished from the local absolute group as in Volume V, Chapter 3. Xie and Yau (2015, (2.24)–(2.26), (2.30)) give the residue, compact pairing, and quadratic local model. Equation (XII.2.11) and the wrapped dimension count use only the local smooth spaces and the D3 worldvolume dimension. The explicit retraction (XII.2.5) and the incidence charts (XII.2.12)–(XII.2.15) develop the same ordinary-node topology; they introduce no transition or new string-theory dictionary.

§ Period integrals and the cutoff. [MATH]. Equations (XII.2.17) and (XII.2.18) are evaluated in the stated residue normalization, with a fixed endpoint in the marked fiber. The local exact formula (XII.2.24) and its analytic split are derived here; Strominger (1995, (2.3)–(2.4)) give the simple compact singular term, not the finite-cutoff formula. His vanishing cycle is called B_1 and his dual A^1, so the ordered periods (Z^1, F_1) correspond to our (P, Q). The dilation and phase pullbacks (XII.2.21)–(XII.2.22) are consequences of the same residue. The endpoint variations (XII.2.31)–(XII.2.34) use the exact finite-chain integral, without identifying its endpoint with a proper radius or energy.

§ A loop around the node. [MATH]. Equation (XII.2.37) uses the positive loop and the marked boundary; the residue calculation (XII.2.39) checks the sign. Compare Xie and Yau (2015, (2.28)–(2.30)) in the raw intersection order and Strominger (1995, (2.3)–(2.4)) in period order. Equation (XII.2.40) is the passive change of coefficients, not the assertion of a magnetic state in the local space. Equations (XII.2.41) and (XII.2.42) extend this algebra to arbitrary integer winding and another lift of the same marked boundary.

§ The wrapped D3 and its electric charge. [SUGRA]. The smooth probe calculation (XII.2.45) uses the unwarped metric and the calibrated form, zero gauge-invariant worldvolume flux and constant dilaton. See Strominger (1995, (3.5)–(3.8)), Xie and Yau (2015, sec. 2.5), and the unwarped metric of Klebanov and Strassler (2000, (53)–(59)). [GEO-X]. The protected continuation and the one light hyper of primitive charge use the ordinary compact node input in Strominger (1995, secs. 3.1 and 4). His sec. 4.2 distinguishes the single-particle assumption from a general spectrum calculation. In

(XII.2.47) the rigid mass uses $\sqrt{2}|Z|$, while his compact mass in (3.7) carries $g_5 e^{K/2}$ and a charge sign fixed in his convention. The phase, common normalization and threshold-energy comparisons in (XII.2.44) and (XII.2.49)–(XII.2.52) are consequences within those stated frames; no extra BPS spectrum or existence claim for multiple wrapping follows.

§ When the photon becomes dynamical. [MATH]. The link class and the cone scaling give the lower bound (XII.2.56) for closed representatives. [SUGRA]. The separate metric logarithm (XII.2.60) follows from the unwarped asymptotics of Klebanov and Strassler (2000, (53)–(59)) and the kinetic calculation of Koroteev et al. (2016, (5.12), (5.17)–(5.23)); their vortex/IIA interpretation is not used. [GEO-E]. The fixed local background mass uses Xie and Yau (2015, secs. 2.4–2.5) and the strict deformation criterion of Shapere and Vafa (1999, (2.4)–(2.5)). [GEO-E]. For the compact vector scalar, see Strominger (1995, secs. 3.1 and 4): the vanishing class must survive primitively, and its unstabilized mode must be retained in the fluxless compact reduction. [DEC]. The scale in (XII.2.61) requires gravity and unwanted coupled modes to decouple before using an isolated light sector. The canonical normalization (XII.2.57)–(XII.2.58) interprets the same norm lower bound with a fixed positive reduction prefactor. Equations (XII.2.62)–(XII.2.64) check the wrapped/string mass ratio under the isolation premise; they do not prove bulk decoupling.

§ The four-dimensional threshold. [MATH]. The spin-manifold unit-flux frame of (XII.2.65) uses the Maxwell normalization of Witten (1995, (2.3)–(2.4)) after translating the Euclidean theta sign and kinetic coefficient. The conditional determinant calculation (XII.2.66)–(XII.2.70) uses Vassilevich (2003, (1.20), (4.28)). Rigid holomorphy is an input to the completion; the match in (XII.2.74) is of the log coefficient only, as in Strominger (1995, (4.1)). Equation (XII.2.77) solves the stipulated one-loop ODE and the below-mass inequality fails as $M \to 0$ at fixed external energy. These calculations do not certify a full compact effective theory. The node's weights in (XII.2.80) reuse the degree-one convention of the next chapter. The reference change (XII.2.76), the stopped leading-log solution (XII.2.78), and the soft external-energy scaling (XII.2.79) are conditional algebraic consequences of the same threshold description. The phase split (XII.2.75) uses its already imported holomorphic completion. [GEO-E]. The free hyper interpretation for the isolated, decoupled sector is that of Xie and Yau (2015, sec. 2.6, Example I) and Closset et al. (2021, sec. 5, (5.1)).

Reproducing the calculations. The worked calculations above evaluate the periods, the signed contour jump, and the comparison of the one-loop coefficient with the geometric logarithm. Use `benchmark/tasks.json` to find the question IDs and `benchmark/PROTOCOL.md` for submission.

References

Closset, C., S. Schäfer-Nameki, and Y.-N. Wang (2021). "Coulomb and Higgs branches from canonical singularities. Part 0". In: *JHEP* 02, p. 003. DOI: 10.1007/JHEP02(2021)003. arXiv: 2007.15600 [hep-th].

Klebanov, I. R. and M. J. Strassler (2000). "Supergravity and a confining gauge theory: Duality cascades and chi SB resolution of naked singularities". In: *JHEP* 08, p. 052. DOI: 10.1088/1126-6708/2000/08/052. arXiv: hep-th/0007191.

Koroteev, P., M. Shifman, and A. Yung (2016). "Non-Abelian vortex in four dimensions as a critical string on a conifold". In: *Phys. Rev. D* 94, p. 065002. DOI: 10.1103/PhysRevD.94.065002. arXiv: 1605.08433 [hep-th].

Shapere, A. D. and C. Vafa (1999). "BPS structure of Argyres–Douglas superconformal theories". In: arXiv: hep-th/9910182.

Strominger, A. (1995). "Massless black holes and conifolds in string theory". In: *Nucl. Phys. B* 451, pp. 96–108. DOI: 10.1016/0550-3213(95)00287-3. arXiv: hep-th/9504090.

Vassilevich, D. V. (2003). "Heat kernel expansion: User's manual". In: *Phys. Rept.* 388, pp. 279–360. DOI: 10.1016/j.physrep.2003.09.002. arXiv: hep-th/0306138.

Witten, E. (1995). "On S-duality in Abelian gauge theory". In: *Selecta Math.* 1, pp. 383–410. DOI: 10.1007/BF01671570. arXiv: hep-th/9505186.

Xie, D. and S.-T. Yau (2015). "4d N=2 SCFT and singularity theory Part I: Classification". In: arXiv: 1510.01324 [hep-th].

Chapter XII.3

Hypersurface singularities and the deformation spectrum

XII.3.1 A singularity with two different deformations

A local Calabi–Yau threefold can describe a four-dimensional theory without first presenting a four-dimensional Lagrangian. In the direct type-IIB construction, its complex structure carries the information needed to specify a Seiberg–Witten geometry. The first question is therefore elementary but physically consequential. If we change the equation of the threefold, which changes describe a choice of vacuum, which introduce a mass, and which alter the theory itself?

Consider a hypersurface whose equation is quadratic in three complex coordinates and cubic in the fourth. Two independent perturbations survive: a constant term and a term linear in the fourth coordinate. Call their coefficients u and g. There are exactly two coefficients, yet they have different physical roles. We will first check that this singularity is admissible, then derive why only these two deformations survive coordinate redefinitions. Normalizing the holomorphic three-form will give their dimensions and let us distinguish vacuum data from sources. Comparing nearby examples will show when a mass parameter appears. We will then keep two nonquadratic coordinates and construct complete local rank-four and rank-seven families, separating their vacuum coordinates from the external parameters.

We start directly with a local IIB threefold and ask how its complex-structure deformations are read. The type-IIB ALE construction begins from a six-dimensional $(2, 0)$ SCFT and its tensor branch. The present chapter addresses the four-dimensional local hypersurface construction.

The physical premise is that a suitable isolated singularity admits a decoupled four-dimensional $\mathcal{N} = 2$ sector and that periods of the three-form set particle masses in its Seiberg–Witten description. Our calculations determine the deformation algebra and weighted dimensions conditional on that premise. They do not establish a string decoupling limit for every polynomial. We will test the stated input conditions before assigning any physical role.

XII.3.2 Which singularities enter the construction?

To extract a scale-invariant spectrum, the defining equation must admit a positive scaling of its coordinates. Choose positive rational numbers q_1, q_2, q_3, q_z such that

$$f(\lambda^{q_1}x_1, \lambda^{q_2}x_2, \lambda^{q_3}x_3, \lambda^{q_z}z) = \lambda f(x_1, x_2, x_3, z), \qquad q_i > 0. \tag{XII.3.1}$$

We have normalized the weighted degree of f to one. The weights are algebraic grades. A four-dimensional mass dimension will emerge only after the three-form is normalized by the physical period premise.

Our example is the zero set

$$X_0 = \{f = 0\}, \qquad f = x_1^2 + x_2^2 + x_3^2 + z^3. \tag{XII.3.2}$$

Each monomial must have degree one. Thus

$$2q_1 = 2q_2 = 2q_3 = 3q_z = 1, \qquad (q_1, q_2, q_3, q_z) = \left(\frac{1}{2}, \frac{1}{2}, \frac{1}{2}, \frac{1}{3}\right). \tag{XII.3.3}$$

The sum is $11/6$. The difference $\sum_i q_i - 1 = 5/6$ will be the weight of the residue three-form. In particular, it is positive.

Positive weights alone do not make the local deformation space finite. At the origin, a hypersurface singularity is isolated when the common zero of f and all four first derivatives has no neighboring point. For the flagship equation,

$$(\partial_{x_1}f, \partial_{x_2}f, \partial_{x_3}f, \partial_z f) = (2x_1, 2x_2, 2x_3, 3z^2). \tag{XII.3.4}$$

All derivatives vanish only at the origin. Since $f(0) = 0$, the hypersurface has an isolated critical point there. This is a direct algebraic check, not an inference from the name of the singularity.

It helps to separate the dimension of the threefold from the dimension of its singular locus. A regular point of $f = 0$ satisfies one independent equation in four complex variables. For example, for any small nonzero a,

$$p = (a, \mathrm{i}a, 0, 0), \qquad f(p) = 0, \qquad df(p) = 2a\,dx_1 + 2\mathrm{i}a\,dx_2 \neq 0. \tag{XII.3.5}$$

The tangent space there has complex dimension three. At the origin all first derivatives vanish, so the linearized equation imposes no condition and the Zariski tangent space has dimension four. The hypersurface germ still has dimension three; its enlarged tangent space detects its singularity. Isolation says that the origin is the only such singular point nearby. It does not mean that the hypersurface consists of a single point.

For a weighted-homogeneous polynomial, we can check the singular locus using only the gradient. Differentiating the degree-one scaling relation with respect to the scale gives

$$\frac{d}{d\lambda}f(\lambda^{q_i}x_i)\bigg|_{\lambda=1} = \sum_i q_i x_i \partial_i f = f. \tag{XII.3.6}$$

Hence any common zero of the derivatives is automatically on the central fiber $f = 0$. This fact justifies the gradient test in the present class. It will also explain why multiplication of the equation by a unit introduces no extra deformation relation.

The primary-source prescription for the isolated weighted-homogeneous class also requires

$$Q_\Omega := q_1 + q_2 + q_3 + q_z - 1 > 0. \tag{XII.3.7}$$

The condition makes the subsequent physical normalization possible with positive scale. It is related in the source argument to a finite-distance condition in the string construction. We use it as an input condition. Isolation, positive coordinate weights, and positive Q_Ω are three distinct tests. Passing the first two does not imply the third.

Two examples expose the distinction. First take $f_{\text{line}} = x_1^2 + x_2^2 + z^3$ as a polynomial in the same four ambient variables, leaving x_3 absent. The gradient vanishes whenever $x_1 = x_2 = z = 0$, regardless of x_3. The critical locus is a complex line, and the Jacobi quotient contains all powers of x_3. It is therefore infinite-dimensional. Assigning a finite list of deformations by pretending that x_3 is a spectator would change the problem. The hypersurface as posed fails isolation.

Next consider two isolated diagonal polynomials,

$$f_4 = y_1^4 + y_2^4 + y_3^4 + y_4^4, \qquad f_5 = y_1^5 + y_2^5 + y_3^5 + y_4^5. \tag{XII.3.8}$$

Their coordinate weights are respectively all $1/4$ and all $1/5$, and their gradients vanish only at the origin. Nevertheless

$$Q_\Omega(f_4) = 4\left(\frac{1}{4}\right) - 1 = 0, \qquad Q_\Omega(f_5) = 4\left(\frac{1}{5}\right) - 1 = -\frac{1}{5}. \tag{XII.3.9}$$

For f_4 the normalizing denominator in the dimension formula is literally zero. For f_5 it is nonzero, so one could formally divide, but the result lies outside the positive-residue-weight physical prescription. Neither example fails isolation. These tests prevent a purely algebraic list of rational numbers from being mistaken for a spectrum of an admissible four-dimensional construction.

The missing-variable example fails at an earlier step. Its derivative ideal is (x_1, x_2, z^2), and consequently

$$J(f_{\text{line}}) = \mathbb{C}[x_3, z]/(z^2), \qquad 1, x_3, x_3^2, \dots \text{ are linearly independent classes.} \tag{XII.3.10}$$

The unrestricted powers of x_3 make the quotient infinite, even though the z powers truncate. Dropping x_3 would replace a threefold in $\mathbb{C}^4$ by a surface in $\mathbb{C}^3$. It would also change the degree of the residue form. Thus this proposed repair changes precisely the geometric object whose periods enter the four-dimensional construction.

The quartic and quintic examples demonstrate a different obstruction. Their finite Jacobi dimensions are

$$\mu(f_4) = (4-1)^4 = 81, \qquad \mu(f_5) = (5-1)^4 = 256. \tag{XII.3.11}$$

There is no missing truncation to repair. Instead the conversion from weight to positive physical scale fails. For $Q_\Omega = 0$, no finite scale factor can give Ω dimension one. For $Q_\Omega < 0$, a positive scale factor cannot do so. Isolation controls the finiteness of the deformation problem; residue positivity controls the physical normalization. We must establish both before reading coefficient weights as physical dimensions.

XII.3.3 The Jacobi algebra counts independent deformations

An arbitrary polynomial perturbation of f contains many coefficients that do not change the germ in an independent way. To first order, a coordinate redefinition

$$x_i \longmapsto x_i + \varepsilon v_i(x), \qquad z \longmapsto z + \varepsilon v_z(x) \tag{XII.3.12}$$

changes the equation by

$$f(x + \varepsilon v) = f(x) + \varepsilon \left(\sum_{i=1}^{3} v_i \, \partial_{x_i} f + v_z \, \partial_z f \right) + O(\varepsilon^2). \tag{XII.3.13}$$

Thus a perturbation in the ideal generated by the partial derivatives is tangent to a coordinate change. The quotient by these redundant directions is the Jacobi algebra

$$J(f) = \frac{\mathbb{C}[x_1, x_2, x_3, z]}{(\partial_{x_1} f, \partial_{x_2} f, \partial_{x_3} f, \partial_z f)}. \tag{XII.3.14}$$

For a local hypersurface germ, multiplying the equation by a nonvanishing function also leaves its zero set unchanged. Its tangent direction introduces f itself into the contact-equivalence quotient. In our weighted-homogeneous class, Euler's identity gives

$$f = \sum_{i=1}^{3} q_i x_i \partial_{x_i} f + q_z z \partial_z f. \tag{XII.3.15}$$

Consequently f already lies in the Jacobian ideal. This is why the simpler quotient (XII.3.14) describes the deformation directions here. The same simplification should not be assumed for an arbitrary polynomial without weighted homogeneity.

For the flagship polynomial, the nonzero constants 2 and 3 can be removed from the generators of the ideal, yielding

$$J(f) = \frac{\mathbb{C}[x_1, x_2, x_3, z]}{(x_1, x_2, x_3, z^2)} \simeq \frac{\mathbb{C}[z]}{(z^2)}. \tag{XII.3.16}$$

Every class has a unique representative $a + bz$. The classes of 1 and z form a basis, so

$$\mu := \dim_{\mathbb{C}} J(f) = 2. \tag{XII.3.17}$$

The number μ is the Milnor number. Its immediate use here is as the dimension of the miniversal deformation base. It tells us why (XII.3.21) contains exactly two independent local coefficients. It does not, by itself, label either coefficient as an operator or a coupling.

The calculation extends without new machinery to a diagonal polynomial

$$f_{\boldsymbol{n}} = y_1^{n_1} + y_2^{n_2} + y_3^{n_3} + y_4^{n_4}, \qquad n_i \geq 2. \tag{XII.3.18}$$

Here $q_i = 1/n_i$, and the derivative ideal contains $y_i^{n_i-1}$. A monomial survives precisely when each exponent a_i satisfies $0 \le a_i \le n_i - 2$. Therefore

$$J(f_{\boldsymbol{n}}) = \bigotimes_{i=1}^{4} \frac{\mathbb{C}[y_i]}{(y_i^{n_i-1})}, \qquad \mu = \prod_{i=1}^{4}(n_i - 1). \tag{XII.3.19}$$

This formula can be checked by counting the displayed basis, rather than memorized as a separate singularity invariant. The polynomial has an isolated critical point because every derivative equation forces its corresponding coordinate to vanish. The remaining admissibility test is $\sum_i 1/n_i > 1$.

For any basis ϕ_α of the Jacobi algebra, the local miniversal equation takes the form

$$F = f + \sum_{\alpha=1}^{\mu} \lambda_\alpha \phi_\alpha = 0. \tag{XII.3.20}$$

The basis records infinitesimally independent directions, with the usual analytic interpretation of the miniversal family near the original germ. For the flagship case, $\phi_1 = 1$ and $\phi_2 = z$, so this becomes

$$X_{u,g} = \{F = 0\}, \qquad F = x_1^2 + x_2^2 + x_3^2 + z^3 + u + gz. \tag{XII.3.21}$$

The two surviving monomials now give the two coefficients announced in the opening. Nothing in the quotient alone establishes that the deformed fiber with fixed u, g remains scale invariant. The weights will apply to the whole family when the coefficients scale along with the coordinates.

To use the quotient, let us reduce a perturbation containing both surviving and redundant terms. Keep all perturbations to first order in ε and set

$$f + \varepsilon h, \qquad h = u + gz + Ax_1 z + Bx_2^2 + Cz^2 + Dz^4. \tag{XII.3.22}$$

Terms that contain x_1, x_2, x_3 vanish in the quotient, as do terms divisible by z^2. More explicitly, the difference between h and its representative is

$$h - (u + gz) = \frac{Az}{2}\partial_{x_1} f + \frac{Bx_2}{2}\partial_{x_2} f + \frac{C + Dz^2}{3}\partial_z f. \tag{XII.3.23}$$

Choose the coordinate change with vector field equal to the negative of the displayed coefficients. Substitution into $f + \varepsilon h$ cancels these three terms to first order. The change of h itself contributes only at order ε^2. Thus this six-term perturbation has the same tangent deformation class as $u + gz$.

Neither 1 nor z can be removed by this operation. Every term of the derivative ideal is divisible by at least one of x_1, x_2, x_3, z^2. A polynomial $a + bz$ has none of those factors unless $a = b = 0$. This proves both spanning and independence of the basis. It is also why quotienting by z instead of $\partial_z f = 3z^2$ would lose a genuine deformation. The derivative lowers the exponent by one; it does not eliminate the coordinate itself.

The infinitesimal restriction is essential when translating a finite polynomial into normal form. Consider adding a finite quadratic term in z and write

$$P(z) = z^3 + Az^2 + gz + u, \qquad z = w - \frac{A}{3}. \tag{XII.3.24}$$

Expansion gives a depressed cubic,

$$P(w - A/3) = w^3 + g'w + u', \qquad g' = g - \frac{A^2}{3}, \qquad u' = u - \frac{Ag}{3} + \frac{2A^3}{27}. \quad \text{(XII.3.25)}$$

The coefficient of z^2 is removable, but removing it changes the two remaining coefficients. In a first-order perturbation where A, g, u are all of order ε, these shifts are of higher order and disappear. At finite values, simply erasing Az^2 while keeping u, g fixed would describe a different family member. The Jacobi algebra counts independent local directions; a coordinate choice supplies coordinates on the deformation base.

The same reasoning works for convergent power series near the origin. Any such series can be written as a constant, a multiple of z, and terms divisible by the derivative generators. In this example the quotient therefore has the same two representatives in the analytic germ as in the polynomial calculation. This gives a direct local meaning to the finite algebra used in (XII.3.20).

XII.3.4 The three-form sets the physical unit

The Jacobi algebra answers how many deformation coefficients exist. To assign dimensions, we need to know what a unit of algebraic weight means physically. A smooth fiber of (XII.3.20) carries a holomorphic three-form obtained as the Poincaré residue

$$\Omega = \mathrm{Res}_{F=0} \frac{dx_1 \wedge dx_2 \wedge dx_3 \wedge dz}{F}. \quad \text{(XII.3.26)}$$

On a patch where $\partial_{x_3} F \neq 0$, the same form is represented, up to a sign fixed by the coordinate ordering, by

$$\Omega = \pm \frac{dx_1 \wedge dx_2 \wedge dz}{\partial_{x_3} F}. \quad \text{(XII.3.27)}$$

The denominator in this patch expression is a derivative of F, not an instruction to divide a differential form by the one-form dF. The apparent singularity of this expression where $\partial_{x_3} F = 0$ calls for another coordinate patch when the fiber is smooth.

Under the scaling (XII.3.1), each dx_i has the same weight as x_i. The ambient four-form has weight $\sum_i q_i$. Since the defining equation has weighted degree one, the residue form has weight

$$Q_\Omega = \sum_i q_i - 1. \quad \text{(XII.3.28)}$$

The patch expression checks this without relying on shorthand. For the flagship equation, $\partial_{x_3} F = 2x_3$ and hence

$$Q\left(\frac{dx_1 \wedge dx_2 \wedge dz}{2x_3}\right) = \frac{1}{2} + \frac{1}{2} + \frac{1}{3} - \frac{1}{2} = \frac{5}{6}. \quad \text{(XII.3.29)}$$

The choice of patch changes neither this weight nor the global residue form on the smooth fiber.

We can derive the patch formula by making the normal direction to the fiber explicit. Put $v = F$ and keep x_1, x_2, z as three other local coordinates. On a patch with $\partial_{x_3} F \neq 0$,

the change of variables is nonsingular. In the ambient four-form only the dx_3 term of dF survives the wedge with the other three differentials, so, with the appropriate ordering sign,

$$\frac{dx_1 \wedge dx_2 \wedge dx_3 \wedge dz}{F} = \pm \frac{dv}{v} \wedge \frac{dx_1 \wedge dx_2 \wedge dz}{\partial_{x_3} F}. \tag{XII.3.30}$$

The residue takes the coefficient of dv/v and restricts it to the fiber. This is a three-form because one normal coordinate has been removed. A zero of the chosen derivative signals failure of these local coordinates, rather than a singularity of the smooth fiber's volume form.

The weight can likewise be checked on any patch. If coordinate x_j is eliminated, the numerator retains weight $\sum_{i \neq j} q_i$ and $\partial_j F$ has weight $1 - q_j$ under the combined family scaling. Their difference is

$$Q(\Omega) = \sum_{i \neq j} q_i - (1 - q_j) = \sum_i q_i - 1. \tag{XII.3.31}$$

The cancellation of q_j shows why changing the eliminated coordinate cannot change the physical unit. Keeping only the ambient four-form weight would miss the degree of the defining equation and would normalize every parameter incorrectly.

The physical input is that a suitable type-IIB singularity gives a Seiberg–Witten geometry in which periods of Ω over relevant three-cycles have the units of a four-dimensional central charge or particle mass. We need only the dimension statement

$$Z_\gamma \;\propto\; \int_\gamma \Omega, \qquad [Z_\gamma] = [\Omega] = 1. \tag{XII.3.32}$$

The proportionality absorbs conventions that this local weighted calculation does not fix. We do not import an absolute coefficient from a different Seiberg–Witten curve or a different brane realization. Equation (XII.3.32) is a sourced physical premise; the weights in (XII.3.28) and (XII.3.29) are algebraic results.

Write δ for the four-dimensional mass dimension assigned to one unit of weighted degree. Since $Q_\Omega \delta = 1$, positivity gives

$$\delta = \frac{1}{Q_\Omega} = \frac{1}{\sum_i q_i - 1} > 0. \tag{XII.3.33}$$

Now let a Jacobi-basis monomial ϕ_α have weight Q_α. The term $\lambda_\alpha \phi_\alpha$ must carry the same total weight one as f, so the coefficient has algebraic weight $1 - Q_\alpha$. Thus

$$[\lambda_\alpha] = \delta(1 - Q_\alpha) = \frac{1 - Q_\alpha}{\sum_i q_i - 1}. \tag{XII.3.34}$$

In this statement the scaling acts on both λ_α and the ambient coordinates. A generic fixed-parameter member $F = 0$ is not invariant under the original coordinate-only scaling. The weights describe the family near the singular point and the dimensions of its parameters.

For (XII.3.21), $Q(1) = 0$ and $Q(z) = 1/3$. Combining them with $Q_\Omega = 5/6$ gives

$$[u] = \frac{1 - 0}{5/6} = \frac{6}{5}, \qquad [g] = \frac{1 - 1/3}{5/6} = \frac{4}{5}. \tag{XII.3.35}$$

The two rational numbers share a denominator because both use the same mass unit fixed by the three-form. Their difference arises from the monomial weights. A reader can now repeat the calculation for any other member of the admissible diagonal family without finding a new normalization each time.

For completeness, the variable dimensions inferred from the same normalization are

$$[x_1] = [x_2] = [x_3] = \frac{1/2}{5/6} = \frac{3}{5}, \qquad [z] = \frac{1/3}{5/6} = \frac{2}{5}. \tag{XII.3.36}$$

Every term of F then has dimension $6/5$: $[x_i^2] = 2(3/5) = 6/5$, $[z^3] = 3(2/5) = 6/5$, and $[gz] = 4/5 + 2/5 = 6/5$. This dimensional equality is a useful internal check. It does not add a new independent deformation or alter the coefficient roles.

There are two scales in this calculation, and it is useful to compare them explicitly. Let $s > 0$ be a physical mass rescaling. One unit of algebraic degree has dimension δ, so setting $\lambda = s^\delta$ in the weighted scaling gives

$$x_i \mapsto s^{3/5} x_i, \qquad z \mapsto s^{2/5} z, \qquad u \mapsto s^{6/5} u, \qquad g \mapsto s^{4/5} g. \tag{XII.3.37}$$

Then F scales by $s^{6/5}$ and Ω scales by s. A cycle transported by this coordinate identification between smooth fibers has a period with the same scaling. This statement uses the period's homogeneity; it does not evaluate that cycle integral. In particular, the dimension of z is a coordinate dimension in the geometry. It is not a new local operator dimension in the four-dimensional theory.

On the constant-deformation ray $g = 0$, the same relation has a particularly direct form. For nonzero u in a chosen local branch, set

$$x_i = u^{1/2} X_i, \qquad z = u^{1/3} Z, \qquad F = u\big(X_1^2 + X_2^2 + X_3^2 + Z^3 + 1\big). \tag{XII.3.38}$$

The derivative equations force $x_i = z = 0$, which is not on this fiber when $u \neq 0$, so the fiber is smooth. Let ι_u be the coordinate map in (XII.3.38) from the reference fiber at $u = 1$ to this fiber. Its pullback of the residue is

$$\iota_u^* \Omega_u = u^{3/2+1/3-1} \Omega_1 = u^{5/6} \Omega_1, \qquad [u^{5/6}] = 1. \tag{XII.3.39}$$

This recovers $[u] = 6/5$ from the family itself. Fractional powers require a branch on the nonzero-u slice; this local scaling calculation makes no statement about transport around $u = 0$. It also leaves the numerical period on the reference fiber unevaluated.

XII.3.5 Reading a deformation spectrum

The scaling dimensions of coefficients become a physical spectrum only after we apply the type-IIB deformation dictionary. The source prescription places coefficients above dimension one on the Coulomb branch as expectation values of operators. A coefficient of dimension one is a mass deformation. Coefficients between zero and one are couplings; zero dimension is the candidate scale for an exactly marginal parameter, while negative dimensions correspond to irrelevant deformations. The algebra determines the

dimensions. The identification of a coefficient with a field-theory role is physical input from the geometric construction.

The distinction matters in the flagship example because a Coulomb operator and its coupling appear in the same miniversal equation. Introduce a Coulomb chiral operator $\mathcal{O}$ whose expectation value is represented by u. Then

$$\Delta(\mathcal{O}) = [u] = \frac{6}{5}, \qquad [g] = \frac{4}{5} = 2 - \Delta(\mathcal{O}). \tag{XII.3.40}$$

The second relation is the dimension of its paired $\mathcal{N} = 2$ chiral superspace source. The $4/5$ coefficient is not a second Coulomb operator of dimension $4/5$; it changes the theory, while u selects a vacuum of that theory. Their sum is two because they form the source/expectation-value pair described by the singularity-ring pairing.

The pairing can also be seen directly in the Jacobi algebra. Its two basis elements have weights 0 and $1/3$. The coefficient dimensions from (XII.3.34) add to

$$\frac{1-0}{5/6} + \frac{1-1/3}{5/6} = 2. \tag{XII.3.41}$$

This numerical identity does not by itself tell us which member is the vev. The dimension threshold does: $6/5 > 1$ and $4/5 < 1$. In particular, there is no basis monomial whose coefficient has dimension exactly one, hence no mass parameter in this local model.

Figure XII.3.1 places the flagship and the nearest higher-power example on one coefficient-dimension axis. The threshold at one is a physical classification line, not a singularity of the algebraic formula.

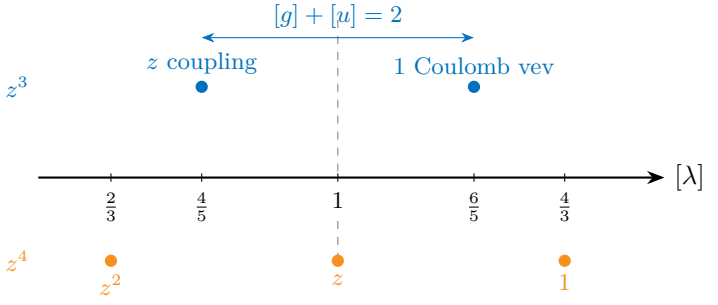


Figure XII.3.1: The ordered coefficient spectra of $x_1^2 + x_2^2 + x_3^2 + z^3$ (blue) and the corresponding z^4 model (orange). The basis label is written at each mark. For the cubic case, g multiplies z and u multiplies 1; their dimensions add to two. The quartic case has an additional dimension-one coefficient multiplying z, so it has a mass deformation. The axis displays coefficient dimensions, not monomial weights.

The z^4 polynomial is

$$f_{(4)} = x_1^2 + x_2^2 + x_3^2 + z^4, \qquad J(f_{(4)}) \simeq \frac{\mathbb{C}[z]}{(z^3)}. \tag{XII.3.42}$$

Its Jacobi basis is $1, z, z^2$, so $\mu = 3$. The three quadratic variables still have weights $1/2$, while $q_z = 1/4$ and

$$Q_\Omega = 3\left(\frac{1}{2}\right) + \frac{1}{4} - 1 = \frac{3}{4}. \tag{XII.3.43}$$

Writing $F_{(4)} = f_{(4)} + u + mz + gz^2$, the coefficient dimensions are

$$[u] = \frac{1}{3/4} = \frac{4}{3}, \qquad [m] = \frac{1 - 1/4}{3/4} = 1, \qquad [g] = \frac{1 - 2/4}{3/4} = \frac{2}{3}. \tag{XII.3.44}$$

Here u is a Coulomb expectation value and g its paired coupling. The middle coefficient m is a mass parameter. Its dimension-one status cannot be inferred merely from its position in the basis; it follows from the same normalized formula used for the other two. The example tests all three positive-dimension roles with one additional monomial.

An even simpler contrast is the ordinary quadratic node

$$f_{(2)} = x_1^2 + x_2^2 + x_3^2 + z^2. \tag{XII.3.45}$$

Its Jacobi algebra is $\mathbb{C}$, with basis 1 and $\mu = 1$. Every coordinate has weight $1/2$, so $Q_\Omega = 1$ and its sole smoothing coefficient m has $[m] = 1$. There is no coefficient above one and therefore no Coulomb expectation value in this local spectrum. The physical identification of this quadratic singularity with a free hypermultiplet is supplied by the primary source. The equality $\mu = 1$ alone would not prove that identification.

The apparent simplicity of these examples should not obscure the distinction between a deformation coefficient and an operator. A deformation equation is a compact way to display both vacuum and source directions. In four-dimensional language, turning on a vev changes the state while holding the defining couplings fixed. Turning on g changes the action. A mass deformation is a dimension-one external parameter. The weighted polynomial keeps these directions in one algebraic family; the role split tells us how to read them physically.

For example, the two paths

$$(u, g) = (u_0 + t, g_0), \qquad (u, g) = (u_0, g_0 + t) \tag{XII.3.46}$$

move through the same two-dimensional deformation base but do different physical jobs. Along the first, the source g_0 is held fixed and the Coulomb expectation value changes. Along the second, the source changes. The tangent parameter t has dimension $6/5$ in the first expression and $4/5$ in the second; these are separate paths, not a single dimensionally identified parameter. Counting both paths as Coulomb moduli would replace a one-dimensional Coulomb branch by the full deformation base and would confuse changes of theory with changes of vacuum.

For the quartic model the distinction can be organized in the same way:

$$F_{(4)} = x_1^2 + x_2^2 + x_3^2 + z^4 + u + mz + gz^2, \qquad \text{fixed sources: } m, g; \quad \text{vacuum coordinate: } u. \tag{XII.3.47}$$

The mass coefficient multiplies a monomial of weight $1/4$, rather than weight one. Its coefficient weight is $3/4$, exactly Q_Ω, so its physical dimension is one. Setting the

monomial weight equal to one would therefore be the wrong way to search for masses. The correct test, obtained by setting (XII.3.34) to one, is

$$[\lambda_\alpha] = 1 \quad \Longleftrightarrow \quad Q_\alpha = 1 - Q_\Omega. \tag{XII.3.48}$$

For the cubic model the right-hand side is $1/6$, absent from its basis weights $0, 1/3$. For the quartic it is $1/4$, present once. This determines the number of mass directions in the local deformation spectrum. A flavor Lie algebra or an absolute mass normalization would require further physical data.

The source pairing also clarifies the boundary at dimension one. For a Coulomb operator of dimension $\Delta > 1$, its chiral source has dimension $2 - \Delta$. Thus the flagship and quartic pairs give

$$\Delta = \frac{6}{5}: \quad 2 - \Delta = \frac{4}{5}, \qquad \Delta = \frac{4}{3}: \quad 2 - \Delta = \frac{2}{3}. \tag{XII.3.49}$$

At dimension one both sides of this arithmetic relation equal one. The mass interpretation at the threshold comes from the sourced dictionary; the numerical symmetry alone would not distinguish a mass from a vacuum coordinate. This is why we use the role thresholds after, rather than before, the weight calculation.

XII.3.6 A reusable family and its limits

We can now carry the whole calculation through the family that contains all three examples above:

$$f_n = x_1^2 + x_2^2 + x_3^2 + z^n, \qquad n \geq 2. \tag{XII.3.50}$$

The gradient criterion and the Jacobi quotient immediately give

$$J(f_n) = \frac{\mathbb{C}[z]}{(z^{n-1})}, \qquad \{1, z, \ldots, z^{n-2}\}, \qquad \mu = n - 1. \tag{XII.3.51}$$

The coordinate weights are $(1/2, 1/2, 1/2, 1/n)$, so

$$Q_\Omega = \frac{3}{2} + \frac{1}{n} - 1 = \frac{1}{2} + \frac{1}{n} = \frac{n+2}{2n} > 0. \tag{XII.3.52}$$

All members satisfy the three input tests of this chapter. For a coefficient λ_k multiplying z^k, where $0 \leq k \leq n-2$, formula (XII.3.34) becomes

$$[\lambda_k] = \frac{1 - k/n}{1/2 + 1/n} = \frac{2(n-k)}{n+2}. \tag{XII.3.53}$$

This one expression reproduces the dimensions in (XII.3.35) and (XII.3.44). It also lets us predict when a mass appears. The equation $[\lambda_k] = 1$ requires $k = (n-2)/2$. Since k is an integer, the family has one dimension-one coefficient when n is even and none when n is odd. Coefficients above one satisfy $k < (n-2)/2$. Under the sourced dictionary their count is $\lfloor (n-1)/2 \rfloor$ for this family. This is a count of Coulomb directions in the stated local construction, not a classification of every four-dimensional $\mathcal{N} = 2$ theory.

The pairing is equally transparent. The basis monomials z^k and z^{n-2-k} have coefficient dimensions

$$[\lambda_k] + [\lambda_{n-2-k}] = \frac{2(n-k)}{n+2} + \frac{2(k+2)}{n+2} = 2. \tag{XII.3.54}$$

For even n, the middle monomial pairs with itself and has dimension one. For odd n, each dimension above one is paired with one below one. The algebraic symmetry of the basis and the source/vev interpretation fit together in this family, while remaining conceptually distinct.

For instance, taking $n = 5$ gives four basis elements and coefficient dimensions

$$\begin{array}{c|cccc} \phi_k & 1 & z & z^2 & z^3 \\ \hline [\lambda_k] & 10/7 & 8/7 & 6/7 & 4/7 \end{array}. \tag{XII.3.55}$$

There are two Coulomb expectation values and two paired couplings, with no mass. Compared with $n = 3$, the extra basis elements change the number of vacuum directions, not the rule that distinguishes a vacuum direction from its source. The pairs are $10/7 + 4/7 = 2$ and $8/7 + 6/7 = 2$.

Changing the exponent once more tests both the role count and the appearance of a mass. For $n = 6$ the derivative $6z^5$ kills powers z^5 and above. The five surviving terms give

$$F_6 = x_1^2 + x_2^2 + x_3^2 + z^6 + u_0 + u_1 z + m z^2 + g_1 z^3 + g_0 z^4. \tag{XII.3.56}$$

Now $q_z = 1/6$, $Q_\Omega = 2/3$ and $\delta = 3/2$. Apply the coefficient rule separately to each power:

$$\begin{array}{c|ccccc} \text{basis} & 1 & z & z^2 & z^3 & z^4 \\ \hline Q(\phi) & 0 & 1/6 & 1/3 & 1/2 & 2/3 \\ \text{coefficient} & u_0 & u_1 & m & g_1 & g_0 \\ [\text{coefficient}] & 3/2 & 5/4 & 1 & 3/4 & 1/2 \end{array}. \tag{XII.3.57}$$

There are two Coulomb directions, two paired sources, and one mass direction. Holding m, g_1, g_0 fixed leaves the vacuum coordinates u_0, u_1. The pairs are (u_0, g_0) and (u_1, g_1), while the middle grade has dimension one. The larger Milnor number counts all five coefficients, not just the two Coulomb directions.

The integer inequalities make the parity effect precise. Write r for the number of Coulomb coefficients and s for the number of mass coefficients in this family. If $n = 2\ell$, the surviving indices split as

$$\begin{array}{c|ccc} k & 0, \ldots, \ell-2 & \ell-1 & \ell, \ldots, 2\ell-2 \\ \hline [\lambda_k] & > 1 & 1 & < 1 \end{array}, \qquad r = \ell - 1, \quad s = 1. \tag{XII.3.58}$$

The two outer ranges have equal size. For $n = 2\ell+1$ there is no integer at the threshold:

$$k = 0, \ldots, \ell-1 : \ [\lambda_k] > 1, \qquad k = \ell, \ldots, 2\ell-1 : \ [\lambda_k] < 1, \qquad r = \ell, \quad s = 0. \tag{XII.3.59}$$

An empty outer range at $n = 2$ is allowed. Together these cases give

$$r = \left\lfloor \frac{n-1}{2} \right\rfloor, \qquad \mu = 2r + s = n - 1. \tag{XII.3.60}$$

Here the identity follows because every coefficient above one has exactly one partner below one, and every unpaired middle entry is a mass. It is a useful check on the enumeration in this family.

There is an algebraic way to locate the partner without first computing either dimension. In $\mathbb{C}[z]/(z^{n-1})$ the highest nonzero monomial is z^{n-2}. Multiplication pairs complementary powers through

$$z^k z^{n-2-k} = z^{n-2} \neq 0, \qquad Q(z^{n-2}) = \frac{n-2}{n} = 2 - 2Q_\Omega. \tag{XII.3.61}$$

The bilinear operation that takes the coefficient of z^{n-2} in a product is nondegenerate: in the ordered monomial basis its matrix has ones on the anti-diagonal and zeros elsewhere. Complementary weights therefore sum to $2 - 2Q_\Omega$. Subtracting them from two and dividing by Q_Ω yields the sum-two coefficient relation. This proves the grading symmetry here without presuming that each basis class is a Coulomb operator.

The single-power family never produces a zero or negative coefficient dimension, because its largest allowed k is $n - 2 < n$. A different admissible polynomial can. Take

$$h = y_1^3 + y_2^3 + y_3^3 + y_4^3. \tag{XII.3.62}$$

Each coordinate has weight $1/3$, so $Q_\Omega = 1/3 > 0$. The Jacobi ring has the sixteen square-free monomials $\prod_{i\in S} y_i$, one for each subset $S \subseteq \{1, 2, 3, 4\}$. A monomial involving k distinct variables has weight $k/3$ and coefficient dimension $3 - k$. The multiplicity is $\binom{4}{k}$:

k	0	1	2	3	4
# monomials	1	4	6	4	1
$\Delta(\lambda)$	3	2	1	0	-1

. (XII.3.63)

The mass entries occupy the middle grade. Four coefficients have zero scaling dimension and one has negative dimension. The source calls the zero-dimension directions exactly marginal; the calculation displayed here establishes their weight, while an assertion about a quantum conformal manifold would require a separate physical analysis. The negative-dimension coefficient is an irrelevant deformation in the source dictionary. The same pairing is visible: dimension three pairs with minus one, the four dimension-two coefficients pair with four zero-dimension coefficients, and the six dimension-one entries pair within their grade. This example demonstrates why the full Jacobi algebra must be retained even when an introductory case has only positive dimensions.

To reconstruct the table, use the derivative ideal $(y_1^2, y_2^2, y_3^2, y_4^2)$. A square of any variable vanishes, but a product of distinct variables survives. For example,

$$y_1^2 y_2 = 0 \text{ in } J(h), \qquad y_1 y_2 \neq 0, \qquad y_1 y_2 y_3 y_4 \neq 0. \tag{XII.3.64}$$

Choosing which variables occur gives one constant, four single variables, six pairs, four triples and one product of all four. Equivalently, the generating polynomial for the ordinary number of variables in a monomial is

$$(1 + t)^4 = 1 + 4t + 6t^2 + 4t^3 + t^4. \tag{XII.3.65}$$

Here t counts a variable, whose weighted degree is $1/3$. For example, the coefficient of y_1y_2 has dimension $(1-2/3)/(1/3)=1$, whereas the coefficient of $y_1y_2y_3$ has dimension zero. Both monomials survive the quotient; their different physical roles arise only after the residue normalization.

The partner of a square-free monomial is its complementary subset. Their product is the highest nonzero monomial:

$$\left(\prod_{i\in S} y_i\right)\left(\prod_{j\notin S} y_j\right) = y_1y_2y_3y_4, \qquad Q(y_1y_2y_3y_4)=\frac{4}{3}. \tag{XII.3.66}$$

This weight equals $2-2Q_\Omega$, as in the single-power family. In particular, y_1y_2 pairs with y_3y_4, not with itself: its square vanishes. There are six mass entries, arranged in three complementary pairs. Pairing within a grade therefore need not mean that every monomial is self-paired.

This example also tests the temptation to discard a coefficient when its dimension is nonpositive. The product $y_1y_2y_3y_4$ is an independent class, and its coefficient dimension is -1. Removing that class would reduce the deformation base from dimension sixteen to fifteen and destroy its complementary pairing with the constant. The algebraic miniversal family retains it. The physical interpretation distinguishes an irrelevant source from the parameters used to describe a relevant deformation near the fixed point; it does not change the Jacobi quotient.

The recipe has a definite stopping point. A finite Jacobi ring, positive rational weights, and a positive residue weight make a well-formed local spectrum calculation. They do not independently prove the existence of a decoupled interacting SCFT, identify a complete set of BPS states, or determine all global properties of a four-dimensional theory. In particular, the spectrum here is a spectrum of deformation *parameters*, with the Coulomb operator dimensions identified through the physical IIB dictionary. It is not a particle mass spectrum. The distinction will matter when later chapters use periods, charges or conformal observables.

XII.3.7 Two active coordinates and a lattice of parameters

The single-power family makes the source–vev distinction transparent, but its Jacobi algebra has only one active coordinate. What changes when a deformation can contain two different powers? We want to construct a local Coulomb family with several vacuum coordinates and identify exactly which coefficients must be held fixed. Consider

$$f_{p,q} = x_1^2 + x_2^2 + x^p + z^q, \qquad p,q\in\mathbb{Z}, \quad p,q\geq 2. \tag{XII.3.67}$$

This is a specialization of the diagonal hypersurfaces already considered. Both quadratic derivatives set their coordinates to zero, and the remaining derivatives are px^{p-1} and qz^{q-1}. Their common zero is the origin. The weights and residue normalization are

$$(q_1,q_2,q_x,q_z)=\left(\frac{1}{2},\frac{1}{2},\frac{1}{p},\frac{1}{q}\right), \qquad Q_\Omega=\frac{1}{p}+\frac{1}{q}>0, \qquad \delta=\frac{pq}{p+q}. \tag{XII.3.68}$$

Thus every finite pair of permitted exponents passes the polynomial tests. The physical interpretation uses the same local IIB and period premises as before. The endpoint $p = q = 2$ is the quadratic node, with its free-hypermultiplet interpretation; the family is not uniformly interacting.

The two quadratic variables disappear from the quotient, leaving a rectangular array of monomials:

$$J(f_{p,q}) = \frac{\mathbb{C}[x,z]}{(x^{p-1}, z^{q-1})}, \qquad \phi_{ij} = x^i z^j, \quad 0 \le i \le p-2, \quad 0 \le j \le q-2. \quad \text{(XII.3.69)}$$

Each monomial has its own coefficient. Even if two monomials have equal weight, the quotient does not identify them. Its dimension and local deformation family are

$$\mu = (p-1)(q-1), \qquad F_{p,q} = f_{p,q} + \sum_{i=0}^{p-2}\sum_{j=0}^{q-2} \lambda_{ij} x^i z^j = 0. \quad \text{(XII.3.70)}$$

The sum describes the miniversal family near the undeformed germ. It supplies local coordinates for the deformation problem, rather than a global completion of a Coulomb branch.

The two-dimensional array retains the physical grading. Substituting the monomial weight $i/p + j/q$ into the coefficient rule gives

$$\Delta_{ij} := [\lambda_{ij}] = \frac{1 - i/p - j/q}{1/p + 1/q} = \frac{pq - qi - pj}{p+q}. \quad \text{(XII.3.71)}$$

A lattice point below the line $qi + pj = pq - p - q$ has $\Delta_{ij} > 1$ and labels a Coulomb coordinate. A point on that line labels a mass. Above it lie sources of dimension below one. A second line, $qi + pj = pq$, separates positive-dimension sources from negative-dimension ones. These tests concern coefficients attached to the lattice points, not the dimensions of the monomials themselves.

Before listing examples, we can determine the mass count exactly. Rewrite the dimension-one condition as

$$\Delta_{ij} = 1 \quad \Longleftrightarrow \quad q(i+1) + p(j+1) = pq. \quad \text{(XII.3.72)}$$

Let $d = \gcd(p,q)$ and write $p = dP$, $q = dQ$, with P, Q coprime. Dividing the equation by d and reducing modulo P shows that $i+1$ is a multiple of P. Reducing modulo Q gives the corresponding statement for $j+1$. Hence all mass positions are

$$i + 1 = Pk, \qquad j + 1 = Q(d-k), \qquad k = 1, \dots, d-1. \quad \text{(XII.3.73)}$$

These values satisfy the basis bounds because $1 \le i+1 \le p-1$ and $1 \le j+1 \le q-1$. Conversely, the bounds exclude $k \le 0$ and $k \ge d$. The list is therefore exhaustive, giving

$$s = d - 1. \quad \text{(XII.3.74)}$$

Coprime exponents have no mass coefficient in this construction. A common divisor creates specific mass monomials; it does not by itself identify a nonabelian flavor algebra.

The remaining count follows from the complement of a lattice point. The highest surviving monomial and its product pairing are

$$x^i z^j \, x^{p-2-i} z^{q-2-j} = x^{p-2} z^{q-2}, \qquad Q(x^{p-2} z^{q-2}) = 2 - 2Q_\Omega. \tag{XII.3.75}$$

Taking the coefficient of this top monomial gives a nondegenerate bilinear pairing. Each basis monomial has precisely one complementary partner. As a result,

$$\Delta_{ij} + \Delta_{p-2-i,q-2-j} = 2. \tag{XII.3.76}$$

The complement pairs every Coulomb coefficient with one source below dimension one and preserves the mass grade. If r denotes the Coulomb count, we obtain

$$\mu = 2r + s, \qquad r = \frac{(p-1)(q-1) - d + 1}{2}. \tag{XII.3.77}$$

This is an integer because it counts paired lattice points. The argument includes zero- and negative-dimension sources, which are needed to pair Coulomb dimensions at or above two.

There is also a direct way to count one row at a time. Exchange x, z if necessary so that $p \le q$. At fixed i, the Coulomb inequality and the number r_i of allowed integers j become

$$j < q - 1 - \frac{q(i+1)}{p}, \qquad r_i = q - 1 - \left\lfloor \frac{q(i+1)}{p} \right\rfloor, \qquad r = \sum_{i=0}^{p-2} r_i. \tag{XII.3.78}$$

The bound on p, q makes r_i nonnegative. Counting the same Coulomb directions by rows and by complements will give independent checks in the examples. The positions of those directions tell us how to write the family with vacuum coordinates and external parameters separated.

XII.3.8 Holding sources fixed in a rank-four construction

Take $p = 3$, $q = 5$. We will specify all local deformation coefficients and then choose which ones remain fixed while the vacuum changes. The quotient, residue weight and coefficient rule are

$$J(f_{3,5}) = \frac{\mathbb{C}[x,z]}{(x^2, z^4)}, \qquad Q_\Omega = \frac{8}{15}, \qquad \Delta_{ij} = \frac{15 - 5i - 3j}{8}. \tag{XII.3.79}$$

For $i = 0$ the monomials are $1, z, z^2, z^3$; for $i = 1$ they are x, xz, xz^2, xz^3. Computing their grades separately gives the complete array

	$j=0$	$j=1$	$j=2$	$j=3$
$i=0$	15/8	3/2	9/8	3/4
$i=1$	5/4	7/8	1/2	1/8

. (XII.3.80)

There are three Coulomb points in the first row and one in the second. There is no dimension-one entry, as expected from $\gcd(3,5)=1$. All four other entries are positive-dimension sources.

Use u_{ij} for coefficients above dimension one and g_{ij} for those below it. The full local family is

$$\begin{aligned} F_{3,5} = x_1^2 + x_2^2 + x^3 + z^5 + u_{00} + u_{01}z + u_{02}z^2 + u_{10}x \\ + g_{03}z^3 + g_{11}xz + g_{12}xz^2 + g_{13}xz^3 = 0. \end{aligned} \tag{XII.3.81}$$

The subscripts retain the monomial positions. For example, u_{10} multiplies x, whereas g_{03} multiplies z^3. The top exponent $(1,3)$ determines their complementary positions: $(1,0)+(0,3)=(1,3)$. Their four source–vev pairs are

Coulomb coefficient	u_{00}	u_{01}	u_{02}	u_{10}
paired source	g_{13}	g_{12}	g_{11}	g_{03}
dimensions	$15/8+1/8$	$3/2+1/2$	$9/8+7/8$	$5/4+3/4$

. (XII.3.82)

Every sum equals two. The different dimensions within each pair tell us why the two coefficients cannot both be coordinates on the Coulomb branch.

Choose numerical values $\boldsymbol{g}$ for the four sources within the local deformation problem. The resulting four-parameter family is

$$X_{\boldsymbol{u};\boldsymbol{g}} = \{F_{3,5}(x_1,x_2,x,z;\boldsymbol{u},\boldsymbol{g})=0\}, \qquad \boldsymbol{u}=(u_{00},u_{01},u_{02},u_{10}), \quad \boldsymbol{g} \text{ fixed.} \tag{XII.3.83}$$

Changing $\boldsymbol{u}$ selects vacua at those source values. Changing a component of $\boldsymbol{g}$ changes the externally specified deformation of the theory. In particular, choosing $\boldsymbol{g}=0$ gives the undeformed SCFT's local Coulomb family, and its conformal vacuum also has $\boldsymbol{u}=0$. A generic nonzero $\boldsymbol{u}$ need not preserve conformal invariance even though the theory whose Coulomb branch we study originated at a conformal point.

The full grading still checks every term. In physical mass dimensions, $[x]=\delta/3=5/8$ and $[z]=\delta/5=3/8$. For two terms in the less familiar second row,

$$[u_{10}x] = \frac{5}{4}+\frac{5}{8}=\frac{15}{8}, \qquad [g_{13}xz^3] = \frac{1}{8}+\frac{5}{8}+3\frac{3}{8}=\frac{15}{8}=[f_{3,5}]. \tag{XII.3.84}$$

The equation is homogeneous when coefficients transform together with coordinates. Holding sources fixed to construct a Coulomb family is a different operation; it need not retain that scaling symmetry at every fiber.

Now change only the last exponent to $q=6$. The Milnor number rises from eight to ten, but the Coulomb rank need not rise. The quotient and normalization become

$$J(f_{3,6}) = \frac{\mathbb{C}[x,z]}{(x^2,z^5)}, \qquad Q_\Omega = \frac{1}{2}, \qquad \Delta_{ij} = 2-\frac{2i}{3}-\frac{j}{3}. \tag{XII.3.85}$$

The complete spectrum is

	$j=0$	$j=1$	$j=2$	$j=3$	$j=4$
$i=0$	2	5/3	4/3	1	2/3
$i=1$	4/3	1	2/3	1/3	0

. (XII.3.86)

The Coulomb points are again $(0,0),(0,1),(0,2),(1,0)$. Two of their coefficients now have the same dimension $4/3$. They remain independent because z^2 and x are distinct classes in $\mathbb{C}[x,z]/(x^2,z^5)$. An equality of dimensions is a degeneracy of the grading, rather than a relation in the deformation space.

The mass equation locates the two new dimension-one directions without guessing a flavor symmetry. Here $d=3$, $P=1$, $Q=2$, so the integer solutions are

$$k=1:\quad (i,j)=(0,3),\qquad k=2:\quad (i,j)=(1,1),\qquad s=2. \tag{XII.3.87}$$

Name these coefficients m_{03} and m_{11}. Name the zero-dimension coefficient τ_{14}, retaining its distinct grading without making a quantum conformal-manifold assertion. The full local equation is

$$\begin{aligned} F_{3,6} = {} & x_1^2+x_2^2+x^3+z^6+u_{00}+u_{01}z+u_{02}z^2+u_{10}x \\ & +m_{03}z^3+m_{11}xz+g_{04}z^4+g_{12}xz^2+g_{13}xz^3+\tau_{14}xz^4=0. \end{aligned} \tag{XII.3.88}$$

The top monomial is now xz^4. It pairs u_{00} with τ_{14}, u_{01} with g_{13}, u_{02} with g_{12}, and u_{10} with g_{04}. The two mass monomials pair with each other. Thus the Coulomb coefficient of dimension two has a source of dimension zero, while the remaining three Coulomb coefficients have positive-dimension sources.

For the local Coulomb family, hold $\boldsymbol{m},\boldsymbol{g},\tau_{14}$ fixed and vary the four u's. Setting all these external parameters to zero selects the undeformed SCFT; its conformal vacuum is again at $\boldsymbol{u}=0$. At sufficiently controlled nearby external parameters the displayed equation supplies the local deformation problem. It does not state that arbitrary finite values of a zero-dimension coefficient preserve an isolated singularity.

Both the integer formula and the row count reproduce the ranks:

(p,q)	μ	s	r_0+r_1	r
$(3,5)$	8	0	$(4-\lfloor 5/3\rfloor)+(4-\lfloor 10/3\rfloor)$	4
$(3,6)$	10	2	$(5-\lfloor 6/3\rfloor)+(5-\lfloor 12/3\rfloor)$	4

. (XII.3.89)

The change in exponent has added two mass directions while keeping the number of Coulomb coordinates fixed. The enlarged Jacobi basis also contains a new zero-dimension source, multiplying xz^4. Consequently the Coulomb rank alone does not determine the deformation content of the local theory. Its full coefficient spectrum records physically different choices of external parameters and different dimensions of vacuum coordinates.

XII.3.9 A rank-seven family with all coefficient roles

The previous construction has no negative-dimension source. We now want an example in which discarding such a coefficient would remove a partner of a genuine Coulomb operator. Take $p=4$, $q=6$. Isolation follows from the derivatives $2x_1, 2x_2, 4x^3, 6z^5$, and the quotient and units are

$$J(f_{4,6})=\frac{\mathbb{C}[x,z]}{(x^3,z^5)},\qquad \mu=15,\quad Q_\Omega=\frac{5}{12},\quad [x]=\frac{3}{5},\quad [z]=\frac{2}{5}. \tag{XII.3.90}$$

There are three rows and five columns. Applying the coefficient formula gives

$$\Delta_{ij} = \frac{24 - 6i - 4j}{10}, \qquad \begin{array}{c|ccccc} & j=0 & j=1 & j=2 & j=3 & j=4 \\ \hline i=0 & 12/5 & 2 & 8/5 & 6/5 & 4/5 \\ i=1 & 9/5 & 7/5 & 1 & 3/5 & 1/5 \\ i=2 & 6/5 & 4/5 & 2/5 & 0 & -2/5 \end{array}. \tag{XII.3.91}$$

The first row contains four Coulomb directions, the second two, and the third one. The two entries with dimension $6/5$ belong to z^3 and x^2, respectively. Their independence is visible in the quotient, just as the two dimension-$4/3$ coefficients were independent in the previous example.

We can locate all threshold entries directly. Since $d = 2$, $P = 2$, $Q = 3$, the mass solution is $i + 1 = 2$, $j + 1 = 3$, giving $(i, j) = (1, 2)$. The zero-dimension equation and its allowed solution are

$$\Delta_{ij} = 0 \quad \Longleftrightarrow \quad 3i + 2j = 12, \qquad (i, j) = (2, 3). \tag{XII.3.92}$$

The first excluded solution $(0, 6)$ lies outside the Jacobi basis. Above the zero-dimension line the only surviving lattice point is $(2, 4)$, where the coefficient dimension is $-2/5$. The gradient quotient, rather than an unrestricted list of monomials, determines which solutions count.

Figure XII.3.2 makes the classification visible. Reflecting a point through the center $(1, 2)$ gives its complementary monomial. For example, $(0, 0)$ reflects to $(2, 4)$ and $(0, 1)$ reflects to $(2, 3)$. Their parameter dimensions therefore sum to two. The mass point is fixed by the reflection in this particular example.

To construct the actual local family, assign separate names to its coefficient roles. The Coulomb part of the perturbation is

$$U(x, z) = u_{00} + u_{01}z + u_{02}z^2 + u_{03}z^3 + u_{10}x + u_{11}xz + u_{20}x^2. \tag{XII.3.93}$$

The seven corresponding dimensions are $12/5, 2, 8/5, 6/5, 9/5, 7/5, 6/5$ in that order. The mass is m_{12} multiplying xz^2. Write the five positive-dimension sources as

$$G_+(x, z) = g_{04}z^4 + g_{13}xz^3 + g_{14}xz^4 + g_{21}x^2z + g_{22}x^2z^2, \tag{XII.3.94}$$

with dimensions $4/5, 3/5, 1/5, 4/5, 2/5$. Finally let τ_{23} multiply x^2z^3 and h_{24} multiply x^2z^4. Then the full local miniversal equation is

$$F_{4,6} = x_1^2 + x_2^2 + x^4 + z^6 + U(x, z) + m_{12}xz^2 + G_+(x, z) + \tau_{23}x^2z^3 + h_{24}x^2z^4 = 0. \tag{XII.3.95}$$

Every one of the fifteen Jacobi classes is represented once. This explicit split allows us to choose external parameters without losing a vacuum coordinate or treating a source as an additional modulus.

The pairings check both the names and the dimensions. The top monomial is x^2z^4. Its seven pairs away from the mass grade are

$$\begin{array}{c|ccccccc} \text{Coulomb} & u_{00} & u_{01} & u_{02} & u_{03} & u_{10} & u_{11} & u_{20} \\ \text{source} & h_{24} & \tau_{23} & g_{22} & g_{21} & g_{14} & g_{13} & g_{04} \end{array}. \tag{XII.3.96}$$

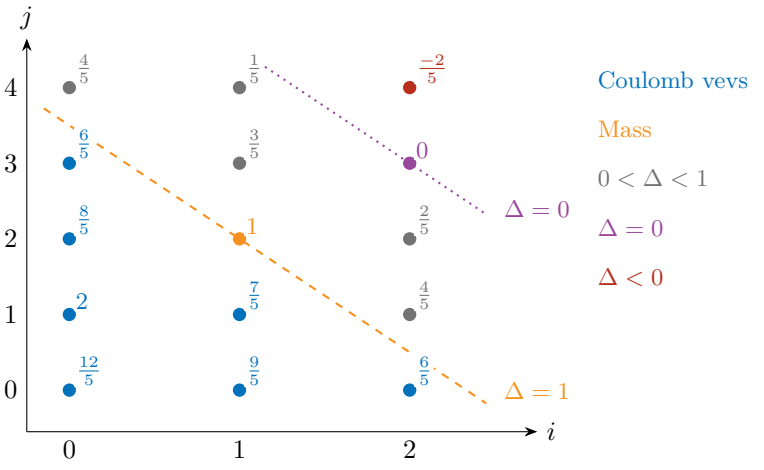


Figure XII.3.2: The Jacobi monomials $x^i z^j$ of $f_{4,6}$ form a 3×5 array. Each point is labeled by its coefficient dimension Δ_{ij}. Blue points label Coulomb vevs, the orange point a mass, gray points positive-dimension sources, the purple point a zero-dimension source, and the red point a negative-dimension source. The dashed orange line is $3i+2j = 7$, where $\Delta = 1$; the dotted purple line is $3i+2j = 12$, where $\Delta = 0$. Reflection about $(1, 2)$ pairs dimensions whose sum is two.

For the first two pairs the sum-two rule reads

$$\frac{12}{5} + \left(-\frac{2}{5}\right) = 2, \qquad 2 + 0 = 2. \tag{XII.3.97}$$

Deleting the negative-dimension source would leave the constant Coulomb deformation without its complementary class. Deleting both nonpositive-dimension sources would shrink the miniversal base from fifteen directions to thirteen. Neither deletion is an operation on the Jacobi quotient.

The physical distinction is between retaining a local deformation coefficient and choosing a particular theory to study. For the undeformed SCFT, set all sources and the mass to zero. Its local Coulomb family then has the particularly simple form

$$X_{\boldsymbol{u};0} = \{x_1^2 + x_2^2 + x^4 + z^6 + U(x, z) = 0\}, \qquad \boldsymbol{u} = (u_{00}, u_{01}, u_{02}, u_{03}, u_{10}, u_{11}, u_{20}). \tag{XII.3.98}$$

The conformal vacuum is $\boldsymbol{u} = 0$. Nonzero values move along seven Coulomb directions. More generally, masses and permitted sources can be fixed within the local deformation problem before the u's vary. Retaining h_{24} in that algebraic problem does not establish a continuum theory at arbitrary finite irrelevant coupling. Such a claim would require additional ultraviolet information.

A dimensional check explains why its negative grade is required. Here $[f_{4,6}] = 12/5$. The top monomial by itself has dimension $2[x] + 4[z] = 14/5$, so its coefficient must

carry the deficit:

$$[h_{24}x^2z^4] = -\frac{2}{5} + 2\frac{3}{5} + 4\frac{2}{5} = \frac{12}{5}, \qquad [\tau_{23}x^2z^3] = 0 + 2\frac{3}{5} + 3\frac{2}{5} = \frac{12}{5}. \tag{XII.3.99}$$

A negative coefficient dimension is therefore consistent with the combined scaling of the family. It is a statement about how an external source scales near the fixed point, not a negative-dimension Coulomb operator.

The qualification that the family is local matters even for the zero-dimension coefficient. Set all other deformations, including $\boldsymbol{u}$, to zero and write $\tau = \tau_{23}$. At the finite value $\tau = 2$ the active polynomial factors:

$$\begin{aligned} H_2 &= x^4 + z^6 + 2x^2z^3 = (x^2 + z^3)^2, \\ \partial_x H_2 &= 4x(x^2 + z^3), \qquad \partial_z H_2 = 6z^2(x^2 + z^3). \end{aligned} \tag{XII.3.100}$$

Together with $x_1 = x_2 = 0$, the curve $x^2 + z^3 = 0$ is now a critical locus on the central fiber. Isolation has failed. Thus a dimension-zero coefficient is not a license to extend the isolated construction to every finite value. Nor does its grading alone identify a quantum conformal manifold. The original isolated germ and its local miniversal deformation remain the objects whose parameter roles we have calculated.

Finally, both counting methods give seven Coulomb directions. The common divisor gives $s = 1$, so

$$r = \frac{15 - 1}{2} = 7, \qquad \sum_{k=1}^{3} \left(5 - \left\lfloor \frac{6k}{4} \right\rfloor\right) = (5-1) + (5-3) + (5-4) = 7. \tag{XII.3.101}$$

The mass coefficient and seven paired sources account for the other eight directions. Starting from the polynomial, we have therefore specified a local rank-seven Coulomb family, the dimensions of its coordinates, and the external coefficients to hold fixed. Periods and charge data would be needed to develop its further low-energy physics. No conformal anomaly or particle spectrum has entered this construction.

XII.3.10 Exercises

For each problem, show the derivative or weight calculation and explain the physical interpretation. Use `benchmark/tasks.json` for the JSON fields and `benchmark/PROTOCOL.md` for submission. Written explanations remain part of the exercise.

1. For $f = x_1^2 + x_2^2 + x_3^2 + z^4$, compute the coordinate weights, residue weight, Jacobi basis and Milnor number. Order the coefficient dimensions by the basis $1, z, z^2$ and classify each as a Coulomb vev, mass or coupling. Submit the residue weight, Milnor number, ordered dimension array and role array as E1. Explain why the middle coefficient is a mass rather than a second Coulomb operator.

2. Regard $f = x_1^2 + x_2^2 + z^3$ as a polynomial in (x_1, x_2, x_3, z), with x_3 present in the ambient space but absent from the equation. Compute its critical locus and decide whether the Jacobi quotient has finite dimension. Submit the isolation flag, variables fixed to zero, free variables and finite/infinite Jacobi status as E2. Explain why dropping the unused coordinate from the ambient space would answer a different question.

3. Compare the two isolated polynomials $f_4 = \sum_{i=1}^{4} y_i^4$ and $f_5 = \sum_{i=1}^{4} y_i^5$. Compute each residue weight and decide whether the normalized physical spectrum prescription used here applies. Submit both weights, both applicability flags and the two distinct reason tokens as E3. Explain the difference between division by zero in the first case and exclusion by the positive residue-weight condition in the second. Check isolation separately so that it is not confused with either failure.

4. Return to $f = x_1^2 + x_2^2 + x_3^2 + z^3$. Identify which coefficient in $f + u + gz$ represents the Coulomb expectation value and which is a source. Compute the associated operator and coupling dimensions and their sum. Submit those three numbers and the two corresponding basis monomials as E4. Explain why the number $4/5$ should not be reported as the dimension of a second Coulomb operator.

The following written problems practice transfer of the method. They are separate from the numerical submissions E1–E4.

1. Reduce the perturbation in (XII.3.22) by an explicit coordinate change, keeping terms through first order in ε. Explain why the same cancellation cannot simply erase a finite quadratic coefficient without shifting the constant and linear coefficients. Verify the shifted coefficients in (XII.3.25) by direct expansion.

2. Change the single-power example to z^7. Determine its basis, residue weight, ordered coefficient dimensions, Coulomb count and mass count. Pair the basis monomials through the highest surviving power. Explain which coefficients should be held fixed while moving through the Coulomb vacua.

3. In the four-cubic example, list the six mass monomials and their three complementary pairs. Then identify the partner of y_1 and compute both coefficient dimensions. Explain why the square of $y_1 y_2$ can vanish while the pairing of its grade remains nondegenerate.

4. For $f_{4,7} = x_1^2 + x_2^2 + x^4 + z^7$, calculate the complete 3×6 array of coefficient dimensions. Determine the Coulomb and mass counts first from the integer formulas and then directly from the array. Identify every nonpositive-dimension source and its complementary Coulomb coefficient. Write the local family with all sources set to zero, keeping a separate coefficient for each Coulomb monomial even when dimensions coincide.

5. For $f_{4,6}$, multiply the mass monomial by itself in the Jacobi algebra and compare with the highest surviving monomial. Explain why its mass grade is self-paired here, whereas the two mass monomials of $f_{3,6}$ pair with each other. Verify the critical curve in (XII.3.100) and explain why it restricts an interpretation of arbitrary finite zero-dimension sources.

Take-home message of this chapter

For a weighted-homogeneous isolated hypersurface $f = 0$ in four complex variables, normalized to degree one, compute the Jacobi algebra $J(f)$ and a basis $\{\phi_\alpha\}$. If $Q_\Omega = \sum_i q_i - 1 > 0$, the coefficient of ϕ_α has dimension

$$[\lambda_\alpha] = \frac{1 - Q(\phi_\alpha)}{Q_\Omega}.$$

The physical IIB dictionary distinguishes Coulomb expectation values above dimension one, masses at one, and couplings below one. It is the coefficient dimension, rather than the monomial degree alone, that determines this role.

Status and sources

Scope and physical input. This chapter treats the isolated weighted-homogeneous hypersurface class of the direct type-IIB construction. The admissibility conditions and geometry-to-four-dimensional interpretation are taken from Xie and Yau (2015), arXiv:1510.01324v1, physical PDF pages 6–7, §§2.1–2.2, equations (2.2)–(2.8). The string decoupling limit is an explicit premise [DEC]; the geometry-to-theory and deformation-role dictionary is a sourced extrapolated geometric argument [GEO-E]. These physical inputs are distinct from the exact polynomial calculations below. The six-dimensional ALE type-IIB starting theory is the $(2, 0)$ SCFT. This label specifies its chirality without a separate spinor-sign calculation.

§§3.2–3.3. Admissibility and deformation algebra. The isolation, weighted Euler, Jacobi quotient and basis calculations in (XII.3.4)–(XII.3.19) are conditional algebraic results [MATH]. The source's Jacobi and miniversal formulas are Xie and Yau (2015), physical PDF page 7, (2.4)–(2.5), and the Milnor-number product is on physical PDF page 8, (2.12). The missing-variable critical line and four-quartic/four-quintic counterexamples are direct computations in their explicitly stated ambient spaces. Positive coordinate weights and positive residue weight are separate requirements. The contact-equivalence statement uses Euler's identity for a degree-one weighted-homogeneous polynomial; it is not asserted for a general nonhomogeneous germ.

§3.4. Residue and dimensions. The residue expression and source-normalized coefficient formula are in Xie and Yau (2015), physical PDF page 7, (2.6)–(2.8), and Shapere and Vafa (1999), arXiv:hep-th/9910182v2, physical PDF pages 5–7, (2.4)–(2.5) and the unnumbered source/vev pairing in §2.2. The weighted form and fractional arithmetic are [MATH]; assigning mass dimension one to its periods and identifying physical roles are [GEO-E]. The displayed proportionality in (XII.3.32) does not fix an absolute Seiberg–Witten differential normalization. The deformed family scales when both coordinates and parameters scale, not when generic parameters are held fixed.

§§3.5–3.6. Roles and examples. The role thresholds and coefficient pairing are stated in Xie and Yau (2015), physical PDF pages 8–9, (2.14)–(2.17), and Shapere and Vafa (1999), physical PDF page 7, §2.2. The A2 and A3 values, the f_n formula and the four-cubics table are exact calculations [MATH] within that physical dictionary [GEO-E]. The quadratic node's free-hypermultiplet identification is explicitly given in Xie and Yau (2015), physical PDF page 18, §2.6 Example I; it is not derived from its Jacobi dimension alone. The source describes dimension-zero deformations as exactly marginal. Here the computed result is their zero dimension; no quantum conformal-manifold statement is established by the algebra. Conformal anomaly calculations belong to the planned atlas of four-dimensional SCFTs.

Physical boundary. The explicit normal-form reduction and finite cubic translation, the residue patch and constant-ray scaling, and the $n = 6$ and complementary-monomial calculations are algebraic consequences [MATH] of the same polynomial families and normalization. They introduce no new geometry-to-theory premise. The constant-ray formula transports forms between smooth fibers on a chosen branch; it neither evaluates a period nor determines monodromy.

§§3.7–3.9. Two-exponent local families. The physical class with two quadratic variables is explicitly treated in Shapere and Vafa (1999), physical PDF page 6, §2.2, (2.6), and is the $(2, 2, p, q)$ specialization of Type I in Xie and Yau (2015), physical PDF pages 25–27, §3.1, (3.6) and Table 2. The DEC and GEO-E premises remain those stated above. The rectangular quotient, dimension array, complementary monomials, integer mass count and rank formula, the full $(3, 5)$, $(3, 6)$ and $(4, 6)$ local families, and the finite-parameter nonisolation example are direct calculations [MATH] within the sourced role dictionary [GEO-E]. The derivative quotient for arbitrary diagonal exponents is given in Xie and Yau (2015), physical PDF page 10, (2.19)–(2.20); the source–vev relation and role thresholds are on physical PDF pages 8–9, (2.14)–(2.16), and Shapere and Vafa (1999), physical PDF page 7, §2.2. Equal coefficient grades are not identifications of Jacobi classes. The mass count supplies no flavor Lie-algebra identification. Zero dimension alone supplies no quantum conformal-manifold conclusion, and retaining irrelevant coefficients algebraically supplies no finite-irrelevant-coupling ultraviolet completion. These statements specify local families only; arbitrary finite zero-dimension sources can fail isolation. No named two-index SCFT classification is required for the examples.

The local deformation algebra does not itself establish the IIB decoupling limit or the existence of a four-dimensional SCFT. Those are the physical premises under which its coefficient dimensions are interpreted. The geometric spectrum is also distinct

from a complete particle spectrum. Neither the polynomial calculation nor the listed examples classify all $\mathcal{N} = 2$ theories.

References

Shapere, A. D. and C. Vafa (1999). "BPS structure of Argyres–Douglas superconformal theories". In: arXiv: `hep-th/9910182`.

Xie, D. and S.-T. Yau (2015). "4d N=2 SCFT and singularity theory Part I: Classification". In: arXiv: `1510.01324 [hep-th]`.

Chapter XII.4

Vanishing cycles, charge pairings, and a controlled BPS chamber

XII.4.1 Which charges disappear?

A D3-brane wrapped on a shrinking three-sphere can become a light particle. The conifold has one such compact cycle. A more informative example has two cycles shrinking in the same limit. The question is whether their charges can both be called electric. If their intersection is nonzero, they cannot. Then an effective description in which one light charge is electric has a magnetic component for the other. Knowing the two charge classes still leaves another question. Is their sum the charge of a single BPS particle, or merely the total charge of two particles?

We will answer both questions for the cubic singularity of the previous chapter. First we separate the singularity into two ordinary nodes. Paths to the nodes tell us which spheres shrink. Their oriented intersection determines how the charges mix when we circle the nodes. At a smooth reference point we can then compute the two periods, use their phases to test binding, and see why a change of cycles and a change of BPS chamber are different operations. We use the 4D $\mathcal{N} = 2$ central charge and the residue description of the preceding chapters. We develop the required cycle transport and quiver stability here. We then retain a third matching sphere in the quartic example. Its null charge has a computable period, and the two-map representation problem will let us test all positive charges without truncating their coefficients.

XII.4.2 Distinguished paths and matching spheres

How does the cubic collision separate into two elementary collapses? At the singular point the polynomial is $x^3 + \sum_{i=1}^{3} y_i^2$. We deform the linear term and look at a family

of level sets. Fix a small real $a > 0$, and put

$$f_a(x,y) = x^3 - 3a^2x + \sum_{i=1}^{3} y_i^2, \qquad X_t = \{f_a = t\}, \qquad P_t(x) = t - x^3 + 3a^2x. \tag{XII.4.1}$$

Take the levels and cycles inside a local Milnor neighborhood, that is, inside a small ball about the original singular point with smooth fibers transverse to its boundary at the levels in use. The limit $a = t = 0$ recovers the (A_1, A_2) singularity. We keep a fixed in the following motion in t. In the period units of the previous chapter, t has dimension $6/5$ and the coefficient $-3a^2$ has dimension $4/5$. The latter is a relevant coupling, not a dimension-one mass.

The singular fibers occur at critical values of f_a. The critical point equations and Hessian are

$$y_i = 0, \qquad x^2 = a^2, \qquad \operatorname{Hess} f_a = \operatorname{diag}(6x, 2, 2, 2). \tag{XII.4.2}$$

The Hessian is invertible at both critical points. Thus each critical fiber has an ordinary node. A deformation of the original collision into separate nondegenerate critical points is called a morsification. Here the correspondence between levels and points is

$$t_L = +2a^3 \quad (x = -a), \qquad t_R = -2a^3 \quad (x = +a). \tag{XII.4.3}$$

The sign of the level need not match the sign of the critical x. The polynomial in the fiber coordinates gives a second way to check the labels. The two singular values are precisely the zeroes of its discriminant, and at those values the polynomial factors as

$$\operatorname{disc}_x P_t = 27(4a^6 - t^2), \tag{XII.4.4}$$

$$P_{t_L}(x) = -(x+a)^2(x-2a), \qquad P_{t_R}(x) = -(x-a)^2(x+2a). \tag{XII.4.5}$$

At the reference level $t = 0$ the roots are $-b, 0, b$, where $b = \sqrt{3}\,a$. For real t between the critical values the three roots remain distinct and real. As t increases from zero to t_L, the two left roots meet. As t decreases to t_R, the two right roots meet. Their order cannot change before a collision. The factorizations therefore fix which pair collapses at each end.

We can follow the roots without solving the cubic at every level. If $x_j(t)$ is a simple root, implicit differentiation gives

$$\frac{dx_j}{dt} = \frac{1}{3(x_j^2 - a^2)}, \qquad \left(\frac{dx_1}{dt}, \frac{dx_2}{dt}, \frac{dx_3}{dt}\right)\Big|_{t=0} = \frac{1}{a^2}\left(\frac{1}{6}, -\frac{1}{3}, \frac{1}{6}\right). \tag{XII.4.6}$$

Initially the left and middle roots approach one another as t increases. The right root moves farther right. Near the left node put $h = 2a^3 - t$ and $x = -a + z$. The equation for the two colliding roots is

$$0 = -h + 3az^2 - z^3, \qquad z_\pm = \pm\sqrt{\frac{h}{3a}} + O(h), \qquad x_2 - x_1 = 2\sqrt{\frac{h}{3a}} + O(h). \tag{XII.4.7}$$

The square-root separation is the local geometry of an ordinary node. The derivative in (XII.4.6) diverges at the collision because the root is no longer a smooth function of the

level. The matching sphere itself has a smooth interior until it collapses; the singular derivative of a root does not signal an earlier singular fiber.

The two straight paths in the t-plane have disjoint interiors and a common base point $t = 0$. We take them as a distinguished pair and order the resulting cycles as (L, R). These paths vary the level of the entire fiber. Inside the reference fiber a different pair of paths appears, namely the intervals $[-b, 0]$ and $[0, b]$ in the x-plane. Each interval supports a sphere. To construct it, choose a square root $s_t(x)$ of $P_t(x)$ along the interval and set

$$y = s_t(x)n, \qquad n \in S^2 \subset \mathbb{R}^3, \qquad s_t(x) = \begin{cases} i\sqrt{-P_t(x)} & \text{left interval,} \\ \sqrt{P_t(x)} & \text{right interval.} \end{cases} \tag{XII.4.8}$$

At a simple root x_*, write $s_t = r$ or ir with $r \geq 0$. Since $P_t'(x_*) \neq 0$, the equation $P_t(x) = \pm r^2$ determines x smoothly in r^2. The real vector rn then supplies a smooth coordinate through the pole where the two-sphere has collapsed. There is one such cap at each end. A cylinder of two-spheres closed with these two caps is a three-sphere. Orient the interior by increasing x followed by the outward orientation of the unit two-sphere. This convention also determines the orientation at each cap.

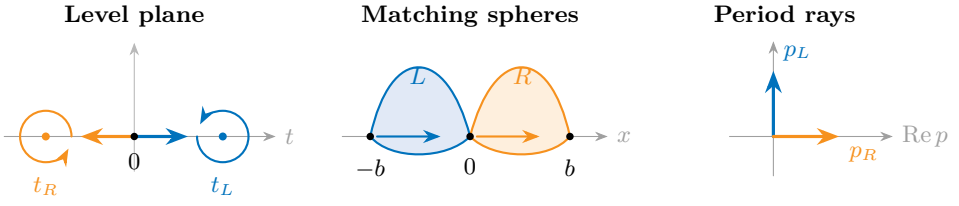


Figure XII.4.1: The vanishing paths and the matching intervals. The left panel is the t-plane. The real stems connect the reference level to the two critical values, and the curved arrows show positive meridians. The middle panel is inside the $t = 0$ fiber. Over the two colored intervals the two-spheres lie in $i\mathbb{R}^3$ and $\mathbb{R}^3$, respectively. Their sizes go to zero at the roots; L and R share the middle cap. The interval arrows specify increasing x. The right panel previews their period rays, derived in §XII.4.4.

The topological construction is the suspension of the two-sphere,

$$\frac{[x_j, x_{j+1}] \times S^2}{\{x_j\} \times S^2 \text{ collapsed}, \ \{x_{j+1}\} \times S^2 \text{ collapsed}} \simeq \Sigma S^2 \simeq S^3. \tag{XII.4.9}$$

The cap charts establish that this quotient is a smooth embedded sphere. Its orientation still needs the interval direction and sphere orientation. At the middle root the two collapsed fibers occupy the same point, but their real and imaginary tangent planes differ. We must therefore calculate an intersection sign even though their common locus is only one point.

Figure XII.4.1 keeps the two projections separate. To follow L, for example, move along the positive real stem in t, and in every smooth fiber take the interval between the two left roots. The union sweeps out a *thimble*, whose sphere in the reference fiber is its

boundary. At the endpoint both the interval and its fiber spheres collapse. Following the other stem shrinks R. One cannot obtain this information by drawing only the three roots at $t = 0$.

The distinguished cycle theorem identifies the spheres of a morsification as a basis of the middle integral homology of the local smooth fiber. The rank in this example can be read off independently. At the original collision the Jacobi algebra is

$$\frac{\mathbb{C}[x, y_1, y_2, y_3]}{(3x^2, 2y_1, 2y_2, 2y_3)} \simeq \mathbb{C}[x]/(x^2), \qquad \mu = 2, \qquad H_3(X_0, \mathbb{Z})_{\text{local}} = \mathbb{Z}L \oplus \mathbb{Z}R. \tag{XII.4.10}$$

Here X_0 denotes the smooth reference level at nonzero a. We will also see directly that the two explicit classes generate integrally, rather than just over $\mathbb{Q}$. For that we need the sign and magnitude of the intersection at the common cap.

XII.4.3 The intersection of two three-spheres

Can both cycles supply electric charges in the same frame? The geometric calculation begins at the single point where the two spheres meet, namely $x = 0,\ y = 0$. At that point $P_0'(0) = 3a^2 > 0$, so the y_i are local holomorphic coordinates on the hypersurface. The raw intersection $I(L, R)$ compares the oriented tangent basis of L followed by that of R with the complex orientation of this chart. A transverse intersection has sign $+1$ or -1 according to this comparison.

There are two signs to track. The left sphere near its right pole has tangent plane $i\mathbb{R}^3$; the right sphere near its left pole has tangent plane $\mathbb{R}^3$. The local radius r decreases with increasing x as we approach the left sphere's right pole. It increases with x as we leave the right sphere's left pole. More explicitly, the leading terms of the cap charts are

$$x_L(r) = -\frac{r^2}{3a^2} + O(r^4), \qquad x_R(r) = +\frac{r^2}{3a^2} + O(r^4), \qquad r \longrightarrow 0. \tag{XII.4.11}$$

An outward radial vector followed by the outward angular frame would orient each $\mathbb{R}^3$ of real parameters positively. The left orientation, with x increasing, reverses that radial vector. With e_i a unit vector in the i-th real coordinate direction, we can use the frames

$$\mathcal{F}_L = (-ie_1, ie_2, ie_3), \qquad \mathcal{F}_R = (e_1, e_2, e_3), \qquad \mathcal{F}_{\mathbb{C}} = (e_1, ie_1, e_2, ie_2, e_3, ie_3). \tag{XII.4.12}$$

With the minus sign omitted, the concatenated frame has positions $(2, 4, 6, 1, 3, 5)$ in $\mathcal{F}_{\mathbb{C}}$, a permutation with six inversions. Restoring the radial sign gives a negative determinant. There are no intersections away from the common cap.

The sign in Figure XII.4.2 would change if we reversed one sphere. It also changes when we exchange the two spheres. In fact, exchanging two tangent frames of dimension three contributes $(-1)^{3\cdot 3} = -1$. With both diagonal entries zero, the full integral form is

$$J = \begin{pmatrix} I(L,L) & I(L,R) \\ I(R,L) & I(R,R) \end{pmatrix} = \begin{pmatrix} 0 & -1 \\ 1 & 0 \end{pmatrix}, \qquad I(v, w) = v^{\mathsf{T}} J w, \qquad \det J = 1. \tag{XII.4.13}$$

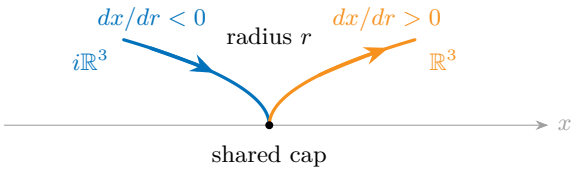


Figure XII.4.2: Orientations at a shared cap, shown in radial profiles. On the left interval the radius decreases along the positive x direction. On the right it increases. The ordered tangent frame at the shared point therefore uses a reversed radial vector in the imaginary tangent plane and an outward one in the real plane. The angular directions of each S^2 are suppressed.

Here v, w denote charge columns in the ordered basis (L, R). The intersection matrix of these three-cycles is skew, even though the adjacency of the two spheres can be drawn as an A_2 diagram. It is not the symmetric A_2 Cartan matrix. As an integral check, if the sublattice generated by L, R had index d in the full free rank-two homology, its intersection determinant would be d^2 times that of the full integral form. Since the determinant is one, the index must be one.

In the local wrapped D3 charge dictionary, the Dirac pairing is this intersection up to a fixed sign convention. We will use the charge pairing $B = -J$. The sign matters for the direction of a quiver map. The nonzero pairing itself is independent of which sign convention we use. Purely electric charges lie in an isotropic sublattice, so L, R cannot both be purely electric in a single polarization. This statement concerns their mutual locality. It makes no choice of the genuine line operators of the theory.

For two general charge columns, the geometric and physical signs now have a concrete meaning. If $v = (m, n)^{\mathsf{T}}$ and $w = (r, s)^{\mathsf{T}}$, then

$$I(v, w) = nr - ms, \qquad B(v, w) = ms - nr. \tag{XII.4.14}$$

For example, $v = 2L - R$ and $w = L + 3R$ have $I(v, w) = -7$ and $B(v, w) = 7$. These are pairings of classes; neither example assumes a particle of either charge. The number is preserved when both vectors are expressed in any other integral basis and the matrix is transformed with that basis. Reversing just the orientation assigned to L changes its coordinate representative and the displayed matrix together. It cannot turn a nonzero physical pairing into zero.

For comparison, a single compact node cycle spans a rank-one lattice and its skew form vanishes. Adding a third matching interval can give a null direction even with nonzero intersections. Take the quartic smoothing

$$P(x) = -(x^2 - a^2)(x^2 - 9a^2), \qquad x_1 = -3a, \quad x_2 = -a, \quad x_3 = a, \quad x_4 = 3a. \tag{XII.4.15}$$

The three intervals have signs $(+, -, +)$ for P and make the adjacent matching basis. The Jacobi algebra at the quartic collision is $\mathbb{C}[x]/(x^3)$, of dimension three. At the first common cap the order of the planes is real then imaginary. In that order the unsigned frame has three inversions, and the left radial reversal contributes another minus. The

first pairing is $+1$. At the second cap the order is imaginary then real and the pairing is -1, as in (XII.4.13). The outer cycles are disjoint. Thus

$$J_3 = \begin{pmatrix} 0 & 1 & 0 \\ -1 & 0 & -1 \\ 0 & 1 & 0 \end{pmatrix}, \qquad J_3 v = 0 \iff v_2 = 0,\ v_1 + v_3 = 0. \tag{XII.4.16}$$

A 2×2 minor has determinant one, so J_3 has rank two and the primitive integral null direction is $(1, 0, -1)^{\mathsf{T}}$. A null class pairs trivially with every compact cycle. This calculation neither identifies a flavor group nor says whether that class is occupied by a particle. Back in the two-cycle problem, even the nondegenerate pairing does not tell us how a candidate bound state is positioned in the complex central charge plane. For that we compute the periods.

XII.4.4 Periods and the rays at the real-root point

Which relative phase does the geometry give the two charges? For $F = f_a - t$, choose the residue Ω with dF wedged first in the ordered ambient form $dy_1 \wedge dy_2 \wedge dy_3 \wedge dx$. On the patch $y_3 \neq 0$ the residue and its fiber form are

$$\Omega = dx \wedge \omega, \qquad \omega = \frac{dy_1 \wedge dy_2}{2y_3}, \qquad dF \wedge \Omega = dy_1 \wedge dy_2 \wedge dy_3 \wedge dx. \tag{XII.4.17}$$

The last equality uses the indicated local extension. On a fixed x fiber with $P_t(x) \neq 0$, one can avoid singling out the patch. Write $Y = \sum_i y_i \partial_{y_i}$. The contraction form

$$\omega = \left. \frac{\iota_Y (dy_1 \wedge dy_2 \wedge dy_3)}{2P_t(x)} \right|_{\sum y_i^2 = P_t(x)} \tag{XII.4.18}$$

gives the same form on tangent vectors. Indeed, $d_y F(Y) = 2P_t(x)$, so contraction divided by this normal derivative produces the residue of the fiber quadric.

In $y = s_t(x) n$, hold x fixed while integrating over n. The numerator of (XII.4.18) supplies a factor s_t^3 and the denominator a factor $2s_t^2$. It follows that

$$\omega|_{S^2} = \frac{s_t(x)}{2}\, d\mathrm{area}_{S^2}, \qquad \int_{S^2} \omega = 2\pi s_t(x). \tag{XII.4.19}$$

In the three-sphere integral the x-dependent part of dy_i does not contribute because Ω already contains dx. Thus the chosen branches and interval directions give the oriented periods directly. At the real-root reference point the radicand is $P_0(x) = x(b^2 - x^2)$. In particular $P_0(-x) = -P_0(x)$. The equal positive magnitudes and relative factor of i follow from

$$p_L = \int_L \Omega = 2\pi i \int_{-b}^{0} \sqrt{-P_0(x)}\, dx = iA, \tag{XII.4.20}$$

$$p_R = \int_R \Omega = 2\pi \int_0^b \sqrt{P_0(x)}\, dx = A. \tag{XII.4.21}$$

To evaluate A, put $x = b\sqrt{u}$. The square root contributes $b^{3/2}u^{1/4}(1-u)^{1/2}$ and the differential contributes $b\,du/(2\sqrt{u})$. Hence

$$A = \pi b^{5/2}\int_0^1 u^{-1/4}(1-u)^{1/2}\,du = \pi b^{5/2}\mathrm{B}\left(\tfrac{3}{4},\tfrac{3}{2}\right) > 0. \tag{XII.4.22}$$

The scaling $A \propto a^{5/2}$ agrees with the physical period dimension one since $[a] = 2/5$. At fixed nonzero a, the two periods at $t = 0$ are finite. Going to that level by itself does not recover the singular limit.

A changed real level tests which features depended on the symmetric reference point. Write $x = au$ and $t = a^3\tau$. Then

$$P_t(au) = a^3(\tau - u^3 + 3u), \qquad p_L = 2\pi i a^{5/2}\mathcal{A}_L(\tau), \qquad p_R = 2\pi a^{5/2}\mathcal{A}_R(\tau), \tag{XII.4.23}$$

where, with $u_1 < u_2 < u_3$ the three real roots,

$$\begin{aligned}\mathcal{A}_L(\tau) &= \int_{u_1}^{u_2}\sqrt{u^3 - 3u - \tau}\,du > 0,\\ \mathcal{A}_R(\tau) &= \int_{u_2}^{u_3}\sqrt{\tau - u^3 + 3u}\,du > 0, \qquad -2 < \tau < 2.\end{aligned} \tag{XII.4.24}$$

Both integrals are finite; a simple endpoint contributes a square-root zero. Their equality at $\tau = 0$ used the odd symmetry of the radicand. That equality is lost away from the center, while the relative phase remains $\pi/2$ in this transported real-interval frame. For an explicit unequal input, at $\tau = 1$ the roots are

$$(u_1,u_2,u_3) = \left(2\cos\frac{7\pi}{9}, 2\cos\frac{13\pi}{9}, 2\cos\frac{\pi}{9}\right), \qquad (\mathcal{A}_L,\mathcal{A}_R) \simeq (0.924260, 2.929132). \tag{XII.4.25}$$

Here $u^3 - 3u = 2\cos 3\theta$ for $u = 2\cos\theta$, so the stated angles solve the root equation. Numerical integration can be done without singular moving endpoints by putting $u = u_j + (u_{j+1} - u_j)v$. In either interval the positive magnitude is

$$(u_{j+1} - u_j)^2\int_0^1 \sqrt{v(1-v)\,|u_j + (u_{j+1} - u_j)v - u_k|}\,dv, \qquad k \neq j, j+1. \tag{XII.4.26}$$

This expresses the answer using a fixed interval and the distance to the third root. It also explains the different magnitudes: the two intervals have different lengths and different distances from the third root. Holding τ fixed while halving a multiplies both periods by $2^{-5/2}$. Holding a fixed while varying τ changes their ratio. A common rescaling and a change of relative periods are therefore distinct operations in this same family.

To interpret these periods as central charges, consider the local Type IIB light sector with the compact wrapped D3 charges retained. We assume that gravity and any coupled bulk or string excitations are removed or uncoupled while the retained masses are held finite. The hypersurface alone does not establish this decoupling. In this sector the common conversion $C \neq 0$ from the periods to the central charge gives

$$Z(n_L L + n_R R) = C(n_L p_L + n_R p_R), \qquad M_{\mathrm{BPS}} = |Z|, \qquad Z = \sqrt{2}\,Z_{\mathrm{SW}}. \tag{XII.4.27}$$

The last equality states the translation from the convention with mass $\sqrt{2}|Z_{\mathrm{SW}}|$; it does not fix the absolute conversion C. The mass equation applies when the state is BPS. The linear period, in contrast, is defined for the charge class whether or not it is populated. In particular we can form $Z(L+R)$ before asking if there is a particle at that charge.

Remove the common phase of C when choosing the origin for phase angles. With this choice, the rays of Z_L, Z_R in Figure XII.4.3 are at $\pi/2$ and 0. One open half-plane that contains both is

$$H = \{Z \neq 0 \mid -\pi/4 < \arg Z < 3\pi/4\}. \tag{XII.4.28}$$

Within this region the angle has a continuous branch, so that a strict phase ordering has an unambiguous meaning. Before using that order to test stability, we use the same residue integrals for a second purpose. Their local behavior near each node fixes the sign of the charge transport.

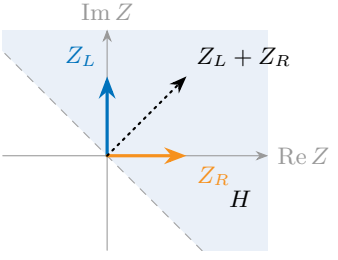


Figure XII.4.3: The period rays of the two spheres at $t = 0$, with their common scale removed. The dashed line bounds the open half-plane H; its shaded side contains the rays of L and R. The dotted ray represents the candidate charge $L + R$, not a claim of a bound state. The colors match the matching intervals in Figure XII.4.1.

XII.4.5 Two elementary monodromies

What happens to the charge labels when we go around one of the nodes? The loop goes in along its real stem, encircles the critical value counterclockwise, and returns along the stem. Such a based loop is a positive meridian. Its vanishing cycle δ returns to itself, but another cycle can pick up a copy of δ. For an ordinary node of a complex threefold, the Picard–Lefschetz action in our intersection convention is

$$T_\delta(v) = v + I(v,\delta)\delta, \qquad M_\delta = \mathbf{1} + \delta(J\delta)^{\mathsf{T}}. \tag{XII.4.29}$$

The order $I(v,\delta)$ fixes the sign. The matrix acts on active charge columns, so its j-th column records the transported j-th basis cycle in the original coordinates.

From $I(R,L) = 1$ and $I(L,R) = -1$ we obtain

$$T_L(L) = L, \qquad T_L(R) = R + L, \qquad M_L = \begin{pmatrix} 1 & 1 \\ 0 & 1 \end{pmatrix}. \tag{XII.4.30}$$

At the right node the sign is reversed because the spectator is now L.

$$T_R(L) = L - R, \qquad T_R(R) = R, \qquad M_R = \begin{pmatrix} 1 & 0 \\ -1 & 1 \end{pmatrix}. \tag{XII.4.31}$$

In the pairing of two transported columns the term quadratic in δ vanishes by $I(\delta, \delta) = 0$. The two terms linear in δ cancel by antisymmetry. Thus $M_\delta^{\mathsf{T}} J M_\delta = J$. Either inverse also preserves J. Pairing preservation alone cannot decide which matrix belongs to a counterclockwise loop.

The based loop around both values starts along the positive imaginary t-axis. On the counterclockwise outer circle the upper access reaches the $t_R < 0$ side first, so the meridians are traversed in the order R, L. As the rightmost matrix acts first, the total action and its characteristic polynomial are

$$M = M_L M_R = \begin{pmatrix} 0 & 1 \\ -1 & 1 \end{pmatrix}, \qquad \det(\lambda \mathbf{1} - M) = \lambda^2 - \lambda + 1. \tag{XII.4.32}$$

In particular $M^2 = M - \mathbf{1}$ and $M^3 = -\mathbf{1}$, so M has order six. The weights of $1, x$ in the Jacobi algebra supply a check of the eigenvalues. In the weighted monodromy formula the exponent for x^m is $(m+1)/3 + 3/2 - 1$, giving $5/6$ and $7/6$. The two phases $\exp(2\pi i \cdot 5/6)$ and $\exp(2\pi i \cdot 7/6)$ give the same characteristic polynomial. They cannot check the based word. $M_R M_L$ is a different matrix with the same eigenvalues.

The ordered period column $p = (p_L, p_R)^{\mathsf{T}}$ is evaluated on the transported cycles. For example, under the L meridian the second period acquires the first. In general,

$$p_{\mathrm{cont}} = M^{\mathsf{T}} p, \qquad n_{\mathrm{comp}} = M^{-1} n, \qquad n_{\mathrm{comp}}^{\mathsf{T}} p_{\mathrm{cont}} = n^{\mathsf{T}} p. \tag{XII.4.33}$$

Here M can denote either elementary action or their product. The compensating charge coordinates keep the evaluated class fixed while its period basis has changed. They are different from the active monodromy of a transported cycle.

For a concrete active transport, take the class $v = 2L - R$. The two meridians act differently on its coefficients:

$$M_L \begin{pmatrix} 2 \\ -1 \end{pmatrix} = \begin{pmatrix} 1 \\ -1 \end{pmatrix}, \qquad M_R \begin{pmatrix} 2 \\ -1 \end{pmatrix} = \begin{pmatrix} 2 \\ -3 \end{pmatrix}. \tag{XII.4.34}$$

In the first case its continued period is $p_L - p_R$, because $2p_L - (p_R + p_L) = p_L - p_R$. If instead the physical class is held fixed while the continued period basis is used, the compensating coordinates are $M_L^{-1} v = (3, -1)^{\mathsf{T}}$; evaluating those on $(p_L, p_R + p_L)$ recovers $2p_L - p_R$. The first operation moves a cycle. The second rewrites the evaluation of the original class.

We can decide the sign of each shear directly from the periods. Omit the common factor 2π in both integrals temporarily. Near the left node set $h = t_L - t > 0$ and $k = \sqrt{3a}$. With $z = x + a$ one has $P_t = -h + k^2 z^2 - z^3$. A real analytic Morse coordinate $u = z + O(z^2)$ absorbs the cubic correction into $k^2 u^2$. The left interval shrinks to the section $-\sqrt{h}/k \le u \le \sqrt{h}/k$; its branch is imaginary. The leading shrinking period comes from the area under a semicircle,

$$\widetilde{p}_L = i \int_{-\sqrt{h}/k}^{\sqrt{h}/k} \sqrt{h - k^2 u^2}\,(1 + O(u))\, du = \frac{i\pi}{2k}\, h + O(h^2). \tag{XII.4.35}$$

The odd part of the analytic Jacobian integrates to zero on this symmetric interval. The first even correction starts at u^2 and gives $O(h^2)$.

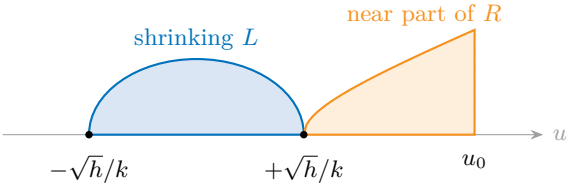


Figure XII.4.4: The two integrals near t_L in the local Morse coordinate. L shrinks over the imaginary branch between the colliding roots. The right spectator period includes the real branch from the common root $+\sqrt{h}/k$ to a fixed cut $u_0 > 0$. The far end of the full spectator interval is outside the diagram.

The right interval does not collapse. Its lower endpoint meets the shrinking interval at $u = \sqrt{h}/k$. In the part up to a fixed cut u_0, shown in Figure XII.4.4, the integrand on the real branch is $\sqrt{k^2u^2 - h}$ times the analytic Jacobian. The elementary antiderivative at unit Jacobian is

$$G(u; h) = \frac{u}{2}\sqrt{k^2u^2 - h} - \frac{h}{2k}\log\Big(ku + \sqrt{k^2u^2 - h}\Big). \tag{XII.4.36}$$

At the lower endpoint $G(\sqrt{h}/k; h) = -h\log h/(4k)$. The upper endpoint is analytic near $h = 0$ on the chosen branch. A nonconstant term in the Jacobian does not contribute to the coefficient of $h\log h$. For example, away from the shrinking endpoint the order-h term in the square root is $-h/(2ku)$. Multiplying by the constant in the Jacobian gives the $1/u$ term whose integral is a logarithm. Multiplying by its part $O(u)$ removes that pole at this order. The remaining, distant part of the spectator integral does not affect this local logarithm. The left node therefore yields

$$[h\log h]\widetilde{p}_R = \frac{1}{4k}, \qquad \lim_{h\to 0}\frac{\Delta\widetilde{p}_R}{\widetilde{p}_L} = \frac{2\pi i/(4k)}{i\pi/(2k)} = +1. \tag{XII.4.37}$$

The bracket denotes the coefficient, and Δ is the jump from $\log h \mapsto \log h + 2\pi i$. Multiplication by -1 in $h = t_L - t$ changes the starting direction, not the positive winding of a loop.

It is useful to restore the common fiber factor and state what this logarithm has measured. Up to terms that do not change the leading jump, the left-node periods have the form

$$p_L = \frac{i\pi^2}{k}h + O(h^2), \qquad p_R = p_R^{\mathrm{reg}}(h) + \frac{\pi}{2k}h\log h + O(h^2\log h). \tag{XII.4.38}$$

The function denoted by p_R^{reg} is single-valued and analytic locally. A positive circuit adds $2\pi i$ to the logarithm and hence adds $i\pi^2 h/k + O(h^2)$ to the spectator. Its ratio to the shrinking period approaches one. Multiplying the residue by any common nonzero constant multiplies the two coefficients together and leaves this ratio unchanged. The

integer coefficient is a charge shear, whereas the individual period coefficient depends on the chosen holomorphic form. The local Picard–Lefschetz theorem supplies the restriction to an integer multiple of the shrinking cycle; the integral determines which integer and which sign occur.

For the right node take $h = t - t_R > 0$. Now the small interval is on the real branch, with leading period $\pi h/(2k)$. The spectator is on the left and runs with increasing x toward the left root of the small interval. Replacing u by $-u$ brings that spectator integral to the same ordered real interval as in (XII.4.36), with the branch factor i. Consequently

$$[h \log h]\widetilde{p}_L = \frac{i}{4k}, \qquad \lim_{h\to 0} \frac{\Delta\widetilde{p}_L}{\widetilde{p}_R} = \frac{2\pi i\, i/(4k)}{\pi/(2k)} = -1. \tag{XII.4.39}$$

The local transvection restricts the spectator jump to an integer multiple of the vanishing period. The leading coefficients are therefore enough to fix that integer exactly. They do not determine the entire spectator period.

With only one compact node cycle A_0, the compact pairing is zero and $T_{A_0}(A_0) = A_0$. The conifold spectator in the earlier chapter was a relative cycle, so it could still acquire a logarithm. Here a second *compact* sphere provides the spectator. We have now computed the two compact charges, their pairings and their transport. To turn this information into a particle spectrum, we next specify which objects the charge basis represents.

XII.4.6 From a charge basis to a stable spectrum

Which of the positive charge vectors in H describe a single light BPS particle? The geometry supplies candidate charge classes and periods. A BPS quiver needs more. In the chosen half-plane its nodes must be elementary hypermultiplets that form a positive integral basis for the light particle charges. If $\mathcal{Q}_H$ is the set of charges carried by those particles, positivity means

$$\mathcal{Q}_H \subseteq \sum_i \mathbb{Z}_{\geq 0}\gamma_i, \qquad \gamma_i \in \mathcal{Q}_H. \tag{XII.4.40}$$

The inclusion does not make every sum a particle. The existence of an integral homology basis does not even guarantee this inclusion or the population of the basis charges.

For the cubic with three collinear roots we have a separate physical input. In the local wrapped D3 analysis, a supersymmetric matching path has constant phase for the projected one-form $s_0(x)\,dx$, up to a common normalization. For a path $x(\sigma)$ this means that some fixed ϑ gives

$$e^{-i\vartheta} s_0(x(\sigma))\,\frac{dx}{d\sigma} > 0 \tag{XII.4.41}$$

on its oriented interior. The two adjacent real intervals satisfy this with $\vartheta = \pi/2$ and 0, respectively. The result for this collinear configuration supplies one light hypermultiplet on each adjacent sphere and no other stable light particles in the local sector. The

exclusion of a further path uses the uniqueness of a trajectory joining a given pair of roots and reflection across the real line. An off-axis trajectory joining the outer roots would have a distinct reflected partner. A real path joining them would instead run into the middle root. This is a statement of the local D3 trajectory analysis, with its supersymmetry and light-sector assumptions. It is not an inference from the matrix J. The rays computed in (XII.4.20) and (XII.4.21) place both of the resulting hypermultiplets in H.

We can now apply the BPS quiver quantum mechanics for this positive basis. In the representation convention, $B_{ij} > 0$ gives B_{ij} maps from node j to node i. Because $B = -J$, $B_{LR} = +1$, and the representation of dimension (n_L, n_R) is a single map

$$f : V_R \longrightarrow V_L, \qquad V_L = \mathbb{C}^{n_L}, \quad V_R = \mathbb{C}^{n_R}, \qquad f \longmapsto g_L f g_R^{-1}. \tag{XII.4.42}$$

In the matrix arrow notation used elsewhere in the book, the field $X_{LR} = f$ is drawn as $L \to R$. The arrow labels the fundamental and antifundamental indices; the actual map is $R \to L$. In either drawing convention the subobject test uses (XII.4.42). There is no cycle in the quiver and hence no nonconstant invariant superpotential of this one map. For example, a scalar change of basis of V_L rescales f while leaving V_R fixed, so a holomorphic invariant of positive degree in f cannot occur. The quiver describes the particle quantum mechanics, not a new 4D quiver gauge theory.

The central charge of a representation is the charge of its dimension vector $n = (n_L, n_R)$,

$$Z(n) = n_L Z_L + n_R Z_R. \tag{XII.4.43}$$

A subrepresentation is a pair of subspaces preserved by the map. Strict phase stability requires

$$U_L \subseteq V_L, \qquad U_R \subseteq V_R, \qquad f(U_R) \subseteq U_L, \tag{XII.4.44}$$

$$\arg Z(\dim U_L, \dim U_R) < \arg Z(n_L, n_R) \quad \text{for every nonzero proper subrepresentation.} \tag{XII.4.45}$$

An allowed subobject of higher phase destabilizes the total charge in this quantum mechanics. At equal phases the strict inequality fails as well. The open half-plane ensures that sums of nonzero positive charges have well-defined phases in the same branch.

There is an elementary way to test every dimension vector. Let $r = \operatorname{rank} f$. Split V_R into its kernel and a complement, and V_L into the image and a complement. The map identifies the two r-dimensional spaces, so one can choose bases in which this part is the identity. Define S_L, S_R as the two simple representations supported at one node, and E as the representation with a copy of $\mathbb{C}$ at each node and $f = 1$. Then any representation has the direct-sum form

$$(V_L, V_R; f) \simeq S_L^{\oplus(n_L - r)} \oplus S_R^{\oplus(n_R - r)} \oplus E^{\oplus r}. \tag{XII.4.46}$$

A sum of two or more nonzero summands cannot be strictly stable. At least one summand has phase greater than or equal to the phase of the total, since the phase of a sum in H lies between the extreme summand phases. This makes that summand a

destabilizing subrepresentation or an equality case. The simples have no proper nonzero subrepresentations and are stable.

To see the reduction on a map with a nontrivial kernel, take $V_L = \mathbb{C}^2$, $V_R = \mathbb{C}^3$, and

$$f = \begin{pmatrix} 1 & 1 & 0 \\ 0 & 0 & 1 \end{pmatrix}. \tag{XII.4.47}$$

Its image is all of V_L, and its kernel is spanned by $-e_1 + e_2$. Use $e_1, e_3, -e_1 + e_2$ as the source basis and retain the original target basis. The column change and the reduced matrix are

$$S = \begin{pmatrix} 1 & 0 & -1 \\ 0 & 0 & 1 \\ 0 & 1 & 0 \end{pmatrix}, \qquad fS = \begin{pmatrix} 1 & 0 & 0 \\ 0 & 1 & 0 \end{pmatrix}, \qquad (V_L, V_R; f) \simeq E \oplus E \oplus S_R. \tag{XII.4.48}$$

In the transformation rule (XII.4.42) this is $g_L = 1$, $g_R^{-1} = S$. Each of the first two source vectors maps isomorphically onto its own target line; the last maps to zero. Thus the summands are actual subrepresentations in these bases, not merely a decomposition of the dimension vector. At the marked normalized periods $(Z_L, Z_R) = (i, 1)$, the total central charge and one summand charge are

$$Z(2,3) = 3 + 2i, \qquad Z(E) = 1 + i, \qquad \arg(3 + 2i) < \frac{\pi}{4} = \arg Z(E). \tag{XII.4.49}$$

Either identity-block summand already violates strict stability. At the abstract assignment $(1, i)$, where each E will be stable, the entire direct sum is still unstable: its S_R summand has phase $\pi/2$, above that of $2 + 3i$. Stability of constituents does not make their direct sum a stable bound state.

It remains to check the identity block E. If $U_R = \mathbb{C}$ then $f(U_R) = \mathbb{C}$, so a proper subrepresentation must have $U_R = 0$. The only nonzero possibility is $U_L = \mathbb{C}$, which is S_L. The zero map has no such constraint. The two lists of proper nonzero subobjects in dimension $(1, 1)$ are

$$f \neq 0 : \ \{S_L\}, \qquad f = 0 : \ \{S_L, S_R\}. \tag{XII.4.50}$$

The latter object is split. For $f \neq 0$ in dimension $(1, 1)$, all maps lie in a single orbit under $\mathrm{GL}(1, \mathbb{C})^2$. When E is stable, its space of inequivalent stable representations is a point. The phase of $Z_L + Z_R$ lies between the two node phases, so its stability is exactly

$$\arg Z_L < \arg(Z_L + Z_R) \iff \arg Z_L < \arg Z_R \iff \mathrm{Im}(\overline{Z_L} Z_R) > 0. \tag{XII.4.51}$$

The last sign test uses that the two phases are in the same open half-plane. In particular it is the *target* of f that must have the lower phase. Reading the direction of the drawn matrix arrow as the map would reverse this condition.

The phase test also separates binding from the mass inequality. Remove a common phase, and allow arbitrary positive magnitudes q, m with a relative phase $-\pi < \theta < \pi$:

$$Z_L = q, \qquad Z_R = m e^{i\theta}, \qquad \mathrm{Im}(\overline{Z_L} Z_R) = qm \sin\theta, \tag{XII.4.52}$$

$$|Z_L + Z_R|^2 = q^2 + m^2 + 2qm \cos\theta. \tag{XII.4.53}$$

For $0 < \theta < \pi$, the identity block is stable in this representation category. For $-\pi < \theta < 0$, the target is the subobject of higher phase and the block is unstable. Changing q/m moves the ray of the sum between the node rays without changing either conclusion. The strict triangle inequality holds for both signs of nonzero θ; it is therefore insufficient to decide if a BPS particle occupies the sum charge. At $\theta = 0$ the mass bound becomes the threshold equality

$$|Z_L + Z_R| = |Z_L| + |Z_R|, \qquad \arg Z_L = \arg(Z_L + Z_R) = \arg Z_R. \tag{XII.4.54}$$

The target subobject has equal phase, so the nonzero map is semistable and fails strict stability. An antiparallel alignment at $\theta = \pi$ is outside the common open half-plane assumed here. It cannot be included by replacing the strict test with an absolute value of the determinant.

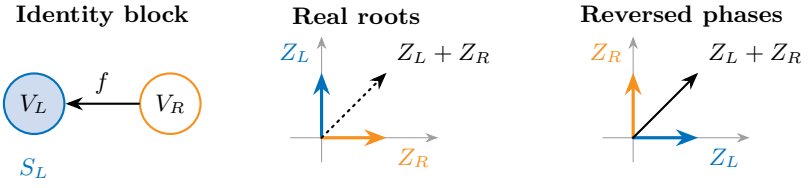


Figure XII.4.5: The subobject responsible for stability and the order of the central charges. The left panel shows the identity block. The shaded target node is its only proper nonzero subobject. In the middle of the figure the real-root ray of this subobject lies above the sum in phase and destabilizes it. The right panel uses the abstract reversed phase assignment, for which the sum is stable in the same representation category.

At the geometric point $Z_L = i|C|A$, $Z_R = |C|A$, so the determinant in (XII.4.51) is $-|C|^2A^2$. The bound-state candidate fails the test. Within the applicable quiver mechanics a point of the stable moduli space gives one hypermultiplet. The two simples give one point each, hence one hypermultiplet of each of the charges L, R in H. Their opposite charges lie in the opposite half-plane and are their CPT partners. The decomposition (XII.4.46) excludes any further strictly stable dimension vector. This recovers the independent real-root result.

The unequal real-root example in (XII.4.25) gives the same instability test with a different mass ratio. In the continuous interval basis of (XII.4.23),

$$\mathrm{Im}(\overline{Z_L} Z_R) = -|C|^2(2\pi)^2 a^5 \mathcal{A}_L(\tau)\mathcal{A}_R(\tau) < 0, \qquad -2 < \tau < 2. \tag{XII.4.55}$$

Under the same local light-sector and quiver premises, changing the real level in this interval changes the two masses while keeping their phase order. At either endpoint one period vanishes and the smooth fiber calculation ends. Reaching the abstract stable order requires a change beyond this real-interval calculation; no value of complex t or of another geometric deformation realizing that order has been computed here.

Figure XII.4.5 also compares two phase orders at fixed quiver. Let $\mathcal{S}(Z_L, Z_R)$ be the set of strict stable dimension vectors. The marked periods give $(i, 1)$ after removing

their common positive magnitude. For contrast, abstract assignments $(1, i)$ and $(1, 2)$ give determinants $+1$ and 0, respectively. The three results are

$$\mathcal{S}(Z_L, Z_R) = \begin{cases} \{(1,0),(0,1)\} & (Z_L, Z_R) = (i, 1), \\ \{(1,0),(0,1),(1,1)\} & (Z_L, Z_R) = (1, i), \\ \{(1,0),(0,1)\} & (Z_L, Z_R) = (1, 2). \end{cases} \tag{XII.4.56}$$

In the second case E is strictly stable. In the third case it is strictly semistable, meaning it satisfies the weak phase inequality but not the strict one. The last two assignments are tests in the representation category, with no identification here of their values with points in the cubic family. They show directly why an intersection matrix, even supplemented by this arrow and potential, is insufficient to determine stability. We next separate a change of basis in geometry from a change of half-plane in this particle description.

XII.4.7 Changing the paths and rotating the half-plane

Which changes relabel the compact lattice, and which change the choice of particle representatives? The meridians of a distinguished system remember the order in which we go around the two critical values. To exchange their paths without changing the based outer loop, we must conjugate one meridian. Let ℓ_L, ℓ_R be the original loops and compose paths right to left, as for their matrices. The Hurwitz exchange takes the ordered pair to

$$(\ell_1', \ell_2') = (\ell_L \ell_R \ell_L^{-1}, \ell_L), \qquad \ell_1' \ell_2' = \ell_L \ell_R. \tag{XII.4.57}$$

This exchange takes place in the t-plane. The first new cycle is the old R transported once around the left meridian. The second new cycle is the old L. Using (XII.4.30) gives the new basis matrix D, whose columns are in the original basis,

$$(\delta_1', \delta_2') = (L + R, L), \qquad D = \begin{pmatrix} 1 & 1 \\ 1 & 0 \end{pmatrix}. \tag{XII.4.58}$$

In the old coordinates the first new twist is the conjugate $M_L M_R M_L^{-1}$, and the second is M_L. Their product is indeed $M_L M_R$. A mere swap would give $M_R M_L$, which we already found to be a different based action.

For this or any integral change of basis, the transformations of the matrix, period column and charge coordinates are

$$J' = D^{\mathsf{T}} J D, \qquad p' = D^{\mathsf{T}} p, \qquad n' = D^{-1} n, \qquad (n')^{\mathsf{T}} p' = n^{\mathsf{T}} p. \tag{XII.4.59}$$

The formula distinguishes changing the labels of the same charge from physically transporting the charge around a loop. In the new distinguished basis both $p_1' = A(1+i)$ and $p_2' = iA$ lie in the original H, once the common phase is removed. Yet

$$J' = -J, \qquad R = \delta_1' - \delta_2', \qquad n_R' = \begin{pmatrix} 1 \\ -1 \end{pmatrix}. \tag{XII.4.60}$$

One of the known particles now has a negative coefficient. Moreover δ_1' is the unstable composite of the preceding section. Neither the fact that the basis is distinguished nor the locations of the two period rays in H make this a positive BPS basis.

We can check the coordinate rules on the mixed class used above. The inverse basis matrix and its action give

$$D^{-1} = \begin{pmatrix} 0 & 1 \\ 1 & -1 \end{pmatrix}, \qquad D^{-1} \begin{pmatrix} 2 \\ -1 \end{pmatrix} = \begin{pmatrix} -1 \\ 3 \end{pmatrix}, \qquad -(p_L + p_R) + 3p_L = 2p_L - p_R. \tag{XII.4.61}$$

This equality uses the transformed periods, not a new period integral. A linear operator on the lattice must also be rewritten in the new coordinates. For the original meridians, and for their based product,

$$D^{-1} M_L D = \begin{pmatrix} 1 & 0 \\ 1 & 1 \end{pmatrix}, \qquad D^{-1} M_R D = \begin{pmatrix} 0 & -1 \\ 1 & 2 \end{pmatrix}, \qquad D^{-1} M D = \begin{pmatrix} 0 & -1 \\ 1 & 1 \end{pmatrix}. \tag{XII.4.62}$$

These are the same original loops in new cycle coordinates. The Hurwitz operation in (XII.4.57) also changes the loops themselves. First conjugating a loop in the old coordinates and then changing its coordinates is different from only rewriting the original loop. Keeping those two operations explicit prevents an apparent conflict between product preservation and the changed matrix entries.

Reversing one cycle orientation is another basis change. For $(-L, R)$ the matrix of the change is $U = \mathrm{diag}(-1, 1)$, and the sign of the off-diagonal intersection changes. The abstract twist is unchanged because the sign of the cycle enters twice:

$$T_{-L}(v) = v + I(v, -L)(-L) = T_L(v). \tag{XII.4.63}$$

If the physical half-plane remains fixed, the particle L has first coordinate -1 in this basis. Reversing a loop instead would invert its monodromy.

Now keep the geometry at $t = 0$ and rotate the particle half-plane clockwise through $\pi/3$. Its new range and the selected charge representatives are

$$H' = \{Z \neq 0 \mid -7\pi/12 < \arg Z < 5\pi/12\}, \qquad (L', R') = (-L, R). \tag{XII.4.64}$$

This time the phase of L at $\pi/2$ is outside H' and the phase of $-L$ at $-\pi/2$ is inside. The ray of R at 0 has stayed inside. Figure XII.4.6 shows the boundary passing the L ray and the antiparticle ray at the same time. No central charge is transported. The full set $\{\pm L, \pm R\}$ is unchanged, but the new particle basis is $(-L, R)$, now with both charges actually represented by particles in the chosen half-plane.

The change of quiver basis is a mutation. Here one can obtain it from the charges directly. The clockwise mutation rule gives the same result. At the exiting node L it replaces the charge by $-L$; the R update adds $\max(B_{RL}, 0)L$, which is zero because $B_{RL} = -1$. In the new basis the pairing reverses the map, so the source of the single map is $-L$ at phase $-\pi/2$ and the target is R at phase 0. The target again has the higher phase, and the candidate sum is again unstable. This is the same stability test in a different positive basis.

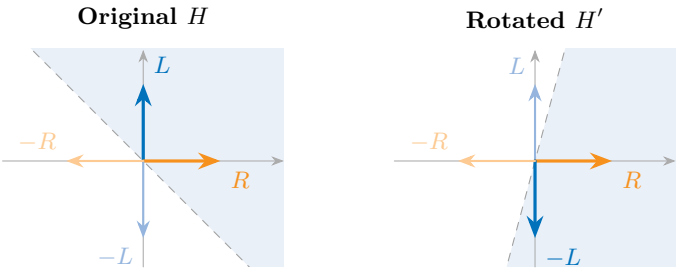


Figure XII.4.6: The particle half-plane at fixed geometry before and after the clockwise rotation by $\pi/3$. The shaded open half-planes select L, R on the left and $-L, R$ on the right. Faded arrows denote the CPT partners outside the chosen half-plane. None of the rays moves.

The reversed map can be checked without a mutation formula. Set $\widetilde{L} = -L$, $\widetilde{R} = R$. Then

$$\widetilde{J} = U^{\mathsf{T}} J U = -J, \qquad (Z_{\widetilde{L}}, Z_{\widetilde{R}}) = (-i|C|A, |C|A), \qquad f' : V_{\widetilde{L}} \longrightarrow V_{\widetilde{R}}. \tag{XII.4.65}$$

The nonzero identity block now has only the target subobject $S_{\widetilde{R}}$. Its total phase is $-\pi/4$, whereas that subobject has phase zero. It is again destabilized. The candidate charge is $R - L$, rather than $L + R$, because positivity is being tested with different particle representatives. The two simple charges and their opposites still reconstruct the same four physical charges. Neither candidate composite has been turned into a state by the change of half-plane.

A marginal stability wall concerns the phases of physical charges at varying moduli. For example, the composite test (XII.4.51) changes when the two node rays align with the same orientation and exchange order. By contrast, the rotation in (XII.4.64) only moves the boundary that separates particles from antiparticles. The Hurwitz exchange moves the geometric paths and can give a basis that fails the particle criterion altogether. These three operations act on different choices. The compact lattice and its marked transport remain useful without any BPS basis. A BPS spectrum additionally requires a physical light sector and a stability condition. The general theory of changes of that spectrum belongs to the later treatment of wall crossing.

XII.4.8 Three spheres and a measurable null period

What does the null direction of (XII.4.16) measure? We now carry that quartic example through the period and binding calculations. The extra cycle introduces a charge which pairs trivially with every compact charge. Its period can vary even though its pairings stay zero. To see this directly, keep the same quadratic suspension and add a real odd

coefficient m:

$$F = x^4 - 10a^2x^2 + mx + 9a^4 + \sum_{j=1}^{3} y_j^2 = 0, \qquad P_m(x) = -(x^2 - a^2)(x^2 - 9a^2) - mx. \tag{XII.4.66}$$

Here $a > 0$ is small and $m = \eta a^3$. We will use the controlled real slice $|\eta| < 1$. In the dimensionless coordinate $u = x/a$, the radicand is

$$P_m(au) = a^4 Q_\eta(u), \qquad Q_\eta(u) = -(u^2 - 1)(u^2 - 9) - \eta u. \tag{XII.4.67}$$

The values of Q_η at $-4, -2, 0, 2, 4$ have signs $(-, +, -, +, -)$. For example the two interior positive values are $15 + 2\eta$ and $15 - 2\eta$, while $Q_\eta(0) = -9$. There is a root in each successive interval between these five points. Since the polynomial has degree four, these exhaust its roots and are simple. We can therefore label them continuously by

$$r_1 < r_2 < r_3 < r_4, \qquad (r_1, r_2, r_3, r_4)\big|_{m=0} = (-3a, -a, a, 3a). \tag{XII.4.68}$$

This gives a smooth real-root family on which to compare periods, without crossing a root collision.

Take the three adjacent matching paths $[r_1, r_2]$, $[r_2, r_3]$, $[r_3, r_4]$ in the x-plane. The same cap construction used for the cubic gives three spheres $\delta_1, \delta_2, \delta_3$, with sheet choices

$$y = s_j(x)n, \qquad n \in S^2, \qquad (s_1, s_2, s_3) = \big(\sqrt{P_m},\ i\sqrt{-P_m},\ \sqrt{P_m}\big). \tag{XII.4.69}$$

Each interval is oriented towards increasing x, followed by the outward orientation of S^2. A simple root supplies a smooth cap at each end. At $m = 0$ the local real and imaginary tangent planes at the shared caps reproduce exactly J_3 in (XII.4.16). Their integral null class is

$$\rho = \delta_1 - \delta_3, \qquad I(\rho, \delta_j) = 0 \quad (j = 1, 2, 3). \tag{XII.4.70}$$

The middle sphere meets both outer spheres, with opposite signs; the outer spheres are disjoint. The matching paths are drawn in Figure XII.4.7. They are paths inside the reference fiber construction. In particular, they need not correspond to three separate meridians of a chosen level-plane diagram. At $m = 0$, the two outer critical points of the quartic have equal critical values. A small generic m separates those values while the three real matching intervals remain available.

The residue normalization is unchanged. Integrating the fiber first again gives $2\pi s_j(x)\,dx$. Define three positive magnitudes by

$$\begin{aligned} A_L(m) &= 2\pi \int_{r_1}^{r_2} \sqrt{P_m(x)}\,dx, \qquad A_R(m) = 2\pi \int_{r_3}^{r_4} \sqrt{P_m(x)}\,dx, \\ B(m) &= 2\pi \int_{r_2}^{r_3} \sqrt{-P_m(x)}\,dx. \end{aligned} \tag{XII.4.71}$$

Thus the actual ordered period column and the null period are

$$p = \begin{pmatrix} A_L \\ iB \\ A_R \end{pmatrix}, \qquad p_\rho = A_L - A_R. \tag{XII.4.72}$$

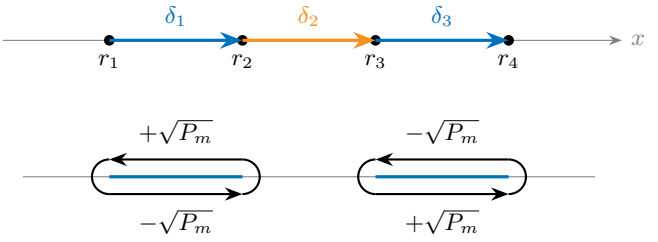


Figure XII.4.7: The three real matching intervals in the quartic suspension. The outer spheres use real fiber coordinates, while the middle sphere uses imaginary ones. The lower panel depicts the two outer branch cuts for the analytic branch with $\sqrt{P_m} \sim ix^2$ at infinity. The upper-lip square roots are positive on the left cut and negative on the right cut; a counterclockwise contour runs right to left on each upper lip. These signs determine the null-period difference.

At the symmetric point, the two outer intervals are reflected copies, so $A_L = A_R = A$. Scaling $x = au$ makes the three periods explicit:

$$\begin{aligned} A &= 2\pi a^3 \int_1^3 \sqrt{(u^2-1)(9-u^2)}\, du, \\ B &= 2\pi a^3 \int_{-1}^1 \sqrt{(1-u^2)(9-u^2)}\, du. \end{aligned} \tag{XII.4.73}$$

The dimensionless coefficients are $A/a^3 \simeq 38.20277168$ and $B/a^3 \simeq 29.19165955$. The real slice has two outer rays at phase zero and one middle ray at phase $\pi/2$, independent of these unequal magnitudes. This is actual period data for the quartic, with the same common physical calibration $Z = Cp$ as before.

The weights also explain why an odd coefficient is useful here. For the quartic collision the normalized residue weight is

$$q_x = \frac{1}{4}, \qquad q_{y_j} = \frac{1}{2}, \qquad q_\Omega = \frac{1}{4} + \frac{3}{2} - 1 = \frac{3}{4}. \tag{XII.4.74}$$

Dividing polynomial weights by q_Ω gives $[x] = [a] = 1/3$. The coefficient of x has weight $3/4$, whereas the constant coefficient has weight one. Consequently

$$[m] = 1, \qquad [a^2] = \frac{2}{3}, \qquad [a^4] = \frac{4}{3}, \qquad [p_j] = [a^3] = 1. \tag{XII.4.75}$$

The dimension-one deformation will change the null central charge. We can measure its coefficient without evaluating either outer elliptic integral separately.

Choose the analytic square root outside the two outer cuts by $\sqrt{P_m(x)} \sim ix^2$ at infinity. Its expansion is

$$\sqrt{P_m(x)} = ix^2\sqrt{1 - \frac{10a^2}{x^2} + \frac{m}{x^3} + \frac{9a^4}{x^4}} = i\left(x^2 - 5a^2 + \frac{m}{2x} + O(x^{-2})\right). \tag{XII.4.76}$$

Only the $1/x$ coefficient contributes to a large counterclockwise contour $\mathcal{C}$ enclosing both cuts:

$$\oint_{\mathcal{C}} \sqrt{P_m(x)}\,dx = 2\pi i\,\frac{im}{2} = -\pi m. \tag{XII.4.77}$$

On the upper lip of the right cut this branch is the negative real square root. On the upper lip of the left cut it is positive. The lower lips have the opposite signs. Shrinking the counterclockwise contour, whose upper portions run towards decreasing x, therefore gives

$$\oint_{\mathcal{C}} \sqrt{P_m}\,dx = 2\left(\int_{r_3}^{r_4} \sqrt{P_m}\,dx - \int_{r_1}^{r_2} \sqrt{P_m}\,dx\right) = \frac{A_R - A_L}{\pi}. \tag{XII.4.78}$$

Combining the two evaluations fixes the sign as well as the magnitude:

$$p_\rho = \pi^2 m, \qquad Z_\rho = C\pi^2 m. \tag{XII.4.79}$$

Thus the pairing radical has a nontrivial central-charge function. Its vanishing at $m = 0$ reflects the even polynomial, while its first derivative measures the odd perturbation.

There is a useful local check of this contour argument. Differentiating the two outer periods at $m = 0$, the moving endpoints contribute nothing because their square roots vanish. Reflection of the left interval then yields

$$\left.\frac{d(A_L - A_R)}{dm}\right|_{m=0} = 2\pi \int_a^{3a} \frac{x\,dx}{\sqrt{(x^2 - a^2)(9a^2 - x^2)}}. \tag{XII.4.80}$$

Put $v = x^2 = 5a^2 - 4a^2\cos\theta$, with $0 \le \theta \le \pi$. The two factors under the square root and the Jacobian give

$$\sqrt{(v - a^2)(9a^2 - v)} = 4a^2 \sin\theta, \qquad x\,dx = \frac{dv}{2} = 2a^2 \sin\theta\,d\theta. \tag{XII.4.81}$$

The derivative is $2\pi \int_0^\pi d\theta/2 = \pi^2$, in agreement with (XII.4.79). This also distinguishes the sign convention for ρ from the equally primitive generator $-\rho$. The local null direction and its dimension-one parameter are the charge data needed below. They do not determine a global flavor group. We next ask which positive combinations of the three cycles are occupied by particles.

XII.4.9 Two maps and six indecomposable charges

How can we test all positive charges without imposing an arbitrary upper bound on their coefficients? The cubic needed the rank of one map. With three nodes there are two maps, and the overlap of their images becomes a new invariant. It will supply a complete decomposition of every representation into six elementary possibilities.

We first specify the physical input that allows a representation calculation. For this local quadratic suspension with four collinear roots, use the adjacent-interval result: there are three light hypermultiplets, carried by the adjacent matching spheres. Under the same local decoupling and wrapped-D3 dictionary as in the cubic, these

three charges form the positive elementary hypermultiplet basis in the half-plane H of (XII.4.28). Their periods are (A_L, iB, A_R). This is a supplied physical identification of this real-root sector, before the binding calculation. It supplies the positive basis needed for the applicable BPS quiver quantum mechanics.

Write $z_j = Z_{\delta_j}$, and continue the convention $B = -J_3$. The positive entries $B_{21} = B_{23} = 1$ give the representation maps

$$f : V_1 \longrightarrow V_2, \qquad g : V_3 \longrightarrow V_2, \qquad W = 0. \tag{XII.4.82}$$

These are map directions: both arrows end at node 2. In the book's matrix-arrow notation they denote X_{21} and X_{23}, respectively. As in the cubic, explicitly specifying the maps avoids reversing a subobject test when using the alternative drawn-arrow convention. There is no directed cycle and hence no nonconstant holomorphic gauge-invariant potential in this reduced model. We use the same strict phase stability condition and the same interpretation of a stable point quotient as one hypermultiplet. The nodes here label particle charges, rather than four-dimensional gauge factors.

For a representation with dimensions (n_1, n_2, n_3), define

$$U = \operatorname{im} f, \qquad V = \operatorname{im} g, \qquad r_1 = \dim U, \quad r_3 = \dim V, \quad c = \dim(U \cap V). \tag{XII.4.83}$$

To split the representation, first choose a basis of $U \cap V$. Extend it to bases of U and V, then extend their union to a basis of V_2. Denote the added target subspaces by U_0, V_0, T_0. The target has the direct decomposition

$$\begin{aligned} V_2 &= (U \cap V) \oplus U_0 \oplus V_0 \oplus T_0, \\ (\dim U_0, \dim V_0, \dim T_0) &= (r_1 - c, r_3 - c, n_2 - r_1 - r_3 + c). \end{aligned} \tag{XII.4.84}$$

Lift the chosen bases of U and V to V_1 and V_3, respectively, and append bases of $\ker f$ and $\ker g$. In these bases each image basis vector is reached by an identity map from its chosen lift. The resulting blocks are the six representations

R	S_1	S_2	S_3	E_{12}	E_{23}	E_{123}
$\dim R$	$(1,0,0)$	$(0,1,0)$	$(0,0,1)$	$(1,1,0)$	$(0,1,1)$	$(1,1,1)$

(XII.4.85)

For E_{12} or E_{23} the one supported map is the identity. For E_{123} both source lines map identically onto the same central line. The common image is the essential feature of this last block. In particular,

$$E_{123} = (\mathbb{C} \xrightarrow{1} \mathbb{C} \xleftarrow{1} \mathbb{C}), \qquad \dim(E_{12} \oplus E_{23}) = (1,2,1) \neq (1,1,1). \tag{XII.4.86}$$

Thus adding the two edge blocks does not replace the triple block. Every nonzero map in the latter ties its source to the same target, so no nontrivial direct decomposition can split its support. The same argument shows that the two edge blocks are indecomposable; the simples are indecomposable by definition.

The numbers of these blocks follow directly from the basis construction:

$$\begin{aligned} R \simeq\ & S_1^{\oplus(n_1 - r_1)} \oplus S_2^{\oplus(n_2 - r_1 - r_3 + c)} \oplus S_3^{\oplus(n_3 - r_3)} \\ & \oplus E_{12}^{\oplus(r_1 - c)} \oplus E_{23}^{\oplus(r_3 - c)} \oplus E_{123}^{\oplus c}. \end{aligned} \tag{XII.4.87}$$

All multiplicities are nonnegative: the first and third are kernel dimensions, the second is the unused target dimension, and the last three count the two separate image complements and their intersection. The construction applies to every pair of finite-dimensional maps. It therefore establishes the full list of indecomposables, rather than testing a finite set of dimension vectors.

For a concrete larger example take $V_1 = \mathbb{C}^3$ and $V_2 = V_3 = \mathbb{C}^4$, with the matrices

$$f = \begin{pmatrix} 1 & 0 & 0 \\ 0 & 1 & 0 \\ 0 & 0 & 0 \\ 0 & 0 & 0 \end{pmatrix}, \qquad g = \begin{pmatrix} 0 & 0 & 0 & 0 \\ 1 & 0 & 0 & 0 \\ 0 & 1 & 0 & 0 \\ 0 & 0 & 0 & 0 \end{pmatrix}. \tag{XII.4.88}$$

Their images are $\langle e_1, e_2 \rangle$ and $\langle e_2, e_3 \rangle$, so $(r_1, r_3, c) = (2, 2, 1)$. The first source's third vector and the second source's last two vectors supply kernels. In the target, e_2 supplies the common image, e_1, e_3 the separate images, and e_4 the unused line. Thus

$$R \simeq S_1 \oplus S_2 \oplus S_3^{\oplus 2} \oplus E_{12} \oplus E_{23} \oplus E_{123}. \tag{XII.4.89}$$

Adding its dimension vectors gives $(3, 4, 4)$, as required. This is the two-map counterpart of the rectangular single-map example.

Individual map ranks do not determine this answer. Keeping the same source and target dimensions, replace only g by

$$g_0 = \begin{pmatrix} 0 & 0 & 0 & 0 \\ 0 & 0 & 0 & 0 \\ 1 & 0 & 0 & 0 \\ 0 & 1 & 0 & 0 \end{pmatrix}. \tag{XII.4.90}$$

Now $\operatorname{im} g_0 = \langle e_3, e_4 \rangle$, still of rank two, but $c = 0$. The decomposition becomes

$$R_0 \simeq S_1 \oplus S_3^{\oplus 2} \oplus E_{12}^{\oplus 2} \oplus E_{23}^{\oplus 2}. \tag{XII.4.91}$$

The triple and unused-target blocks have disappeared. The source kernels have not changed. This example isolates exactly what the image intersection adds to the information carried by two ranks.

Finally, a strictly stable object must occur among the six blocks. For if $R = R' \oplus R''$ is nontrivial, the total central charge has phase between those of its two summands in a common open half-plane. One summand has phase at least that of R, and is a proper subobject. This contradicts strict stability, including when the phases coincide. For each thin block with both maps nonzero, independent changes of basis at the nodes set those maps to one. The corresponding isomorphism class is a point. The remaining problem is to decide when each of these points passes all its subobject tests.

XII.4.10 Which interval representations bind?

Can two edge bound states exist while their three-node extension is unstable? The answer depends on more than comparing the sink with the total charge. The triple has

edge subobjects as well, and one of these can destabilize it even after the simple sink passes.

The maps in (XII.4.82) determine which subspaces are allowed. Since each supported space in a thin interval is a line, a subobject either retains or removes it. Retaining source 1 or 3 requires retaining its image at node 2. Thus the two edge objects have the sole proper nonzero subobject S_2. The triple has exactly

$$\mathrm{Sub}_{\neq 0,\neq R}(E_{123}) = \{S_2, E_{12}, E_{23}\}. \tag{XII.4.92}$$

For example, support $(1, 0, 1)$ is not a subobject: both nonzero maps would leave it. Figure XII.4.8 displays these three possible proper supports. A representation containing both sources can only omit the central line by turning off maps; that would be a different, decomposable representation.

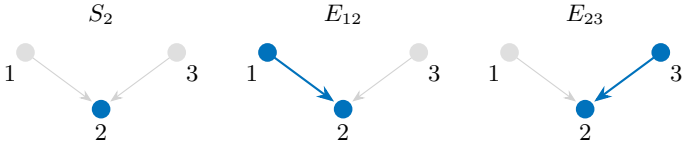


Figure XII.4.8: All proper nonzero subobjects of the triple identity representation. Filled nodes are retained lines and faded nodes are zero subspaces. Each retained source forces the central target to be retained. The corresponding subobject charges are z_2, $z_1 + z_2$, and $z_2 + z_3$. Testing only the first omits two possible decays. Arrows here show the actual representation maps.

Keep all node charges in one open half-plane, so their positive sums have an unambiguous continuous phase. Write $D(v, w) = \mathrm{Im}(\overline{v}w)$. The two edge stability conditions are

$$E_{12} \text{ stable} \iff D(z_2, z_1) > 0, \qquad E_{23} \text{ stable} \iff D(z_2, z_3) > 0. \tag{XII.4.93}$$

For the triple, put $z_T = z_1 + z_2 + z_3$. Its complete test is

$$\begin{aligned} D(z_2, z_T) &> 0, \\ D(z_1 + z_2, z_T) &> 0, \\ D(z_2 + z_3, z_T) &> 0. \end{aligned} \tag{XII.4.94}$$

Each inequality compares the total phase with one actual subobject in (XII.4.92). The simple objects always pass, as they have no proper nonzero subobject. Together with the complete decomposition, these tests determine every strictly stable charge.

First apply them to the actual quartic periods. Remove only the common phase of C, and denote the positive calibrated magnitudes again by A_L, B, A_R. The node charges then have the form

$$(z_1, z_2, z_3) = (A_L, iB, A_R), \qquad A_L, B, A_R > 0. \tag{XII.4.95}$$

For each edge the sink is at the higher phase:

$$D(iB, A_L) = -BA_L < 0, \qquad D(iB, A_R) = -BA_R < 0. \tag{XII.4.96}$$

For the triple, even its first test already fails,

$$D(iB, A_L + iB + A_R) = -B(A_L + A_R) < 0. \tag{XII.4.97}$$

Only S_1, S_2, S_3 are strictly stable. Under the stated local D3 and quiver premises, these three point quotients give the three light hypermultiplets of the real-root chamber. The classification has recovered the supplied geometric result by checking all positive representations. Varying m within the controlled real-root region changes the magnitudes and Z_ρ, but leaves these strict signs unchanged.

There is no contradiction between the vanishing of Z_ρ at $m = 0$ and the absence of an extra massless hypermultiplet here. The particle cone in this half-plane is $\mathbb{Z}_{\geq 0}\delta_1 + \mathbb{Z}_{\geq 0}\delta_2 + \mathbb{Z}_{\geq 0}\delta_3$. For a null charge to lie in that cone,

$$k\rho = (k, 0, -k) \in \mathbb{Z}^3_{\geq 0} \quad \Longrightarrow \quad k \geq 0,\ -k \geq 0 \quad \Longrightarrow \quad k = 0. \tag{XII.4.98}$$

The null direction is a legitimate charge direction whose period is measured by m; no nonzero pure null charge is a particle in this chamber. A central charge that vanishes on an unoccupied lattice site does not create a BPS state.

To see the extra binding information in the same category, we now vary an explicitly assigned central charge, without identifying it with a point of the quartic geometric family. Set

$$(z_1, z_2, z_3) = (i, 1, u + i), \qquad -2 \leq u \leq 0, \qquad H_* : \ -\frac{\pi}{8} < \arg z < \frac{7\pi}{8}. \tag{XII.4.99}$$

The node rays lie strictly inside H_* throughout this interval; so do their positive sums. The edges are stable everywhere because

$$D(1, i) = 1, \qquad D(1, u + i) = 1. \tag{XII.4.100}$$

For the triple $z_T = 1 + u + 2i$, its three tests reduce to

$$D(1, z_T) = 2, \qquad D(1 + i, z_T) = 1 - u, \qquad D(1 + u + i, z_T) = 1 + u. \tag{XII.4.101}$$

The sink and the first edge subobject pass throughout the interval. The second edge subobject changes the result at $u = -1$. Consequently the strict stable supports at its two ends are

$$\begin{aligned} \mathcal{S}_{u=0} &= \{S_1, S_2, S_3, E_{12}, E_{23}, E_{123}\}, \\ \mathcal{S}_{u=-2} &= \{S_1, S_2, S_3, E_{12}, E_{23}\}. \end{aligned} \tag{XII.4.102}$$

All listed stable quotients are points. This is a six-versus-five comparison of strict stable representations for assigned central charges in the same category of representations. The physical real-root chamber was instead computed from its own periods and has three simples.

The lost triple can be diagnosed without an overall phase plot. At $u = -2$, the total charge is $-1+2i$. The subobject E_{23} has charge $-1+i$, and lies above it in phase, since

$$D(z_2, z_T) = 2 > 0, \qquad D(z_2 + z_3, z_T) = D(-1+i, -1+2i) = -1 < 0. \quad \text{(XII.4.103)}$$

Testing just the sink would give the wrong stability answer. The new obstruction is a composite subobject already bound along the second edge, rather than an elementary node. It is precisely the kind of decay channel that appears once a third cycle is retained.

At $u = -1$, the same subobject and its quotient align. The representation maps give an exact sequence

$$0 \longrightarrow E_{23} \longrightarrow E_{123} \longrightarrow S_1 \longrightarrow 0, \qquad (z_{23}, z_1, z_T) = (i, i, 2i). \quad \text{(XII.4.104)}$$

The quotient removes the central and third-node lines, leaving the first source line. The extension is nonsplit, since its map from that source into the central line is nonzero. At alignment it is semistable but fails the strict inequality for E_{23}. Its charge lies at threshold,

$$|z_T| = |z_{23}| + |z_1| = 2. \quad \text{(XII.4.105)}$$

On the six-state side $-1 < u \leq 0$, the two factor rays separate and $|z_T| < |z_{23}| + |z_1|$; all three subobject inequalities hold. On the other side the extension remains a representation, but its E_{23} subobject violates strict stability. These calculations locate a wall in the specified space of stability conditions. A physical wall in the quartic coefficient space would additionally require computing its period map and transporting the positive heart. The actual real-root calculation and the assigned-ray comparison have supplied different parts of that problem: geometric periods in one physical chamber, and a complete test of binding for every object in the selected representation category.

XII.4.11 Exercises

Use column coordinates for the charges. In the computational parts, matrices are given by rows and a set of charges can be listed in any order. The written explanations are a separate part of each exercise.

1. **Reorient a cycle without moving a ray.** Keep the physical half-plane H and the positive loops fixed. Change the coordinate basis to $(-L, R)$. Compute the raw intersection matrix, the active matrix of the original positive L loop in the new basis, and the coordinate vectors of the two physical particles in H. Explain why this exercise does not select the same particles as the half-plane rotation.

2. **Exchange distinguished paths.** Take the first new path to be the old R path transported by the positive L meridian, and take the second new path to be the old L path. Give the new basis columns and both new positive monodromy matrices in the *old* coordinates. Give the coordinates of the old R in the *new* basis. Compare the product to the original based word. Explain why having both new period rays in H does not make this a positive BPS basis.

3. **Find a primitive null charge.** For $P(x) = -(x^2 - a^2)(x^2 - 9a^2)$, use the three adjacent intervals oriented with increasing x, followed by the outward two-sphere. Compute the rank of their raw intersection form and give a primitive generator of its integral radical. Obtain the two off-diagonal signs by writing the oriented tangent frames at the common caps. What does the resulting vector say about the pairing, and what does it leave undetermined about the spectrum?

4. **Separate stability from the skew form.** For the single map $V_R \to V_L$, find the complete strict stable charge support for the three assignments $(Z_L, Z_R) = (i, 1), (1, i), (1, 2)$ in the open half-plane $-\pi/4 < \arg Z < 3\pi/4$. In dimension $(1, 1)$, list the nonzero proper subobjects separately for the zero and nonzero maps. Explain why equality of phases does not count as strict stability, and why keeping the same intersection matrix does not make the three supports equal.

5. **Transfer the construction to unequal intervals.** Use the real level $t = a^3$ and the roots in (XII.4.25). Explain which two roots collapse as the level approaches each critical value. Use (XII.4.26) to compare the two period magnitudes, and determine their phase order without a numerical phase fit. Would a change of their positive magnitudes alone stabilize the nonzero identity block? Explain why this exercise does not locate a wall in the complex parameter plane.

6. **Find a destabilizing subrepresentation before taking a quotient.** Reduce the map (XII.4.47) to rank normal form with the explicit source basis in (XII.4.48). At each assignment $(i, 1)$ and $(1, i)$, exhibit a proper subrepresentation that violates strict stability. Explain why a point quotient for each identity block does not make the direct sum stable. These two transfer exercises are written practice; their explanations are assessed separately from the four numerical submissions above.

7. **Measure an odd deformation by a null period.** For the quartic family (XII.4.66), reverse the orientation of the null generator to $-\rho$. Recompute its period from the signed cut contour, and verify its first derivative by the substitution in (XII.4.81). Explain why the zero period at $m = 0$ does not add a particle to this positive cone.

8. **Retain every composite subobject.** For the maps (XII.4.88), identify explicit source lifts for the common image line and for each separate image. Recover (XII.4.89), then repeat for g_0. For the thin triple at $u = -2$ in (XII.4.99), compute all three subobject determinants. Which would be omitted by checking only the simple sink? These two quartic exercises are written extensions; the original four numerical submission contracts are unchanged.

Status and sources

§XII.4.2. The critical values, matching spheres and middle homology in (XII.4.1)–(XII.4.10) are [MATH]. The distinguished basis and morsification are imported from Xie and Yau (2015, arXiv v1, §2.5, eqs. (2.30)–(2.35)); the interval construction uses Shapere and Vafa (1999,

arXiv v2, §4, pp. 8–9). The coefficient dimensions use the local residue scaling of the preceding chapter. The root motion and square-root separation in (XII.4.6)–(XII.4.7) are algebraic consequences of the same family, and (XII.4.9) explains the cap construction. The source's linear coefficient is the dimension-4/5 coupling in these conventions.

§XII.4.3. The raw compact signs and rank calculations in (XII.4.13) and (XII.4.16) are [MATH]; the chain basis follows Shapere and Vafa (1999, arXiv v2, §4, pp. 8–9). The local charge-pairing identification is [GEO-E], with $B = -J$ in the declared oriented frame. See Alim et al. (2013, arXiv v2, §3.2, p. 20) on the charge pairing and signed shared endpoints. No statement about a flavor group or an absolute line lattice follows.

§XII.4.4. The residue integral and beta evaluation (XII.4.17)–(XII.4.22) are [MATH]. Shapere and Vafa (1999, arXiv v2, §4, eqs. (4.2)–(4.4)) uses the reduced integral with a common normalization absorbed. The isolation of the local sector is [DEC]; the common conversion and compact charge assignment in (XII.4.27) are [GEO-E]. The period formula is additive on the charge lattice (Xie and Yau 2015, arXiv v1, §2.5, eqs. (2.38)–(2.39)). Its evaluation does not assert a representative or a stable state. The scaled integrals and unequal real-root input in (XII.4.23)–(XII.4.26) are further residue-period evaluations in the same family.

§XII.4.5. The Picard–Lefschetz and weighted monodromy formulas are from Xie and Yau (2015, arXiv v1, §2.5, eqs. (2.28)–(2.34)). The action on active columns, based product, nodal logarithms and compact one-node check are [MATH]. The matrix labels printed in the source's eq. (2.40) cannot be read as active columns with the stated pairing in eq. (2.28) without specifying the action convention. The signs here are fixed independently by (XII.4.37) and (XII.4.39).

§XII.4.6. The positive hypermultiplet basis at the real-root point is [GEO-E], using Shapere and Vafa (1999, arXiv v2, §5.1, pp. 16–18). Quiver applicability and the point-to-hypermultiplet interpretation are [GEO-E]. The arrow-to-map rule, quotient and strict phase condition follow Alim et al. (2013, arXiv v2, §§2.2–2.4, eqs. (2.2)–(2.7)). The rank classification and phase test (XII.4.46)–(XII.4.51) are [MATH]. For the direction of the phase comparison use the explicit target-supported subobject in Alim et al. (2013, arXiv v2, §4.2, p. 36) rather than the shorthand comparison in its §4.1. The exact phase tests outside the marked point are mathematical comparisons. The rectangular map reduction, arbitrary positive magnitudes and threshold equations are explicit consequences of the representation and stability calculations. The real-interval sign in (XII.4.55) uses the same isolation, compact charge and local BPS premises; it does not identify a new geometric chamber.

§XII.4.7. The path exchange and basis transformations are [MATH]; see Xie and Yau (2015, arXiv v1, §2.5, eqs. (2.36)–(2.37)). The mutation after rotation is [GEO-E], under the same local quiver hypotheses, with the clockwise convention of Alim et al. (2013, arXiv v2, §2.5, eqs. (2.8)–(2.11)). No general singularity-to-quiver identification or wall-crossing formula is used here.

§XII.4.8. The quartic continuation uses the same matching-cycle basis [MATH]. Equations (XII.4.71)–(XII.4.81) compute the actual real-root periods, their signed null combination and the dimension-one coefficient. The root and sheet restrictions are local. The null central charge does not specify a global flavor group or line lattice.

§XII.4.9. The adjacent real-root three-hyper basis is [GEO-E], from Shapere and Vafa (1999, arXiv v2, §4 and §5.1, especially p. 18). It is used under the local-isolation [DEC] and common compact D3 charge/period premises. The scoped three-node quiver quantum mechanics is [GEO-E]; its positive-basis, map, potential, stability and point-quotient rules use Alim et al. (2013, arXiv v2, §§2.2–2.4). The ADE identification in its §4.1, p. 34, is consistent with this case; no arbitrary assigned-ray realization theorem is imported. The image/kernel splitting and explicit rectangular examples are [MATH].

§XII.4.10. The complete subobject tests and assigned-ray six/five comparison are [MATH]. The physical three-simple interpretation retains the adjacent real-root hypermultiplet basis and its quiver stability prescription; the comparison along (XII.4.99) is in the fixed representation category, with no quartic coefficient point computed for those assignments. The radical-cone exclusion is [MATH]. The calculation is local; no global spectrum or flavor-group conclusion follows.

References

Alim, M. et al. (2013). "BPS Quivers and Spectra of Complete $\mathcal{N} = 2$ Quantum Field Theories". In: *Commun. Math. Phys.* 323.3, pp. 1185–1227. DOI: 10.1007/s00220-013-1789-8. arXiv: 1109.4941 [hep-th].

Shapere, A. D. and C. Vafa (1999). *BPS Structure of Argyres–Douglas Superconformal Theories*. DOI: 10.48550/arXiv.hep-th/9910182. arXiv: hep-th/9910182.

Xie, D. and S.-T. Yau (2015). *4d $\mathcal{N} = 2$ SCFT and singularity theory Part I: Classification*. DOI: 10.48550/arXiv.1510.01324. arXiv: 1510.01324 [hep-th].

Chapter XII.5

Gauge sectors from ALE fibrations

XII.5.1 How an ALE fiber produces four-dimensional periods

How can a weakly coupled four-dimensional gauge theory arise directly in Type IIB? An A_1 ALE (asymptotically locally Euclidean) surface has a two-sphere that can collapse. Let the surface vary over a complex curve. The sphere now sweeps out three-cycles, and a D3-brane on such a cycle can give a four-dimensional particle. For a calibrated D3, a period of the holomorphic three-form gives the size and phase of its central charge. The new step is to do the sphere integral first. Its two endpoints in a fiber select the two values of a one-form on a double cover of the base.

We will carry out the construction over a sphere with four marked ends. Keeping those ends fixed leaves one Coulomb parameter. Moving the ends changes the complex structure of the base and can create a long tube. The tube produces the large imaginary period ratio characteristic of weak coupling. Its two sides also tell us which matter becomes charged under the weak gauge factor. We then send one fundamental mass to infinity while tuning the end separation and the interior coefficient. The resulting irregular end retains a three-flavor gauge sector, whose finite compact periods we will follow explicitly. The starting points are the Type IIB ALE construction of the six-dimensional $(2, 0)$ theory, the D3 central charge of Chapter 2, and the matching spheres of Chapter 4. We use elementary complex curves and the four-dimensional $\mathcal{N} = 2$ period description; we develop the required covering and degeneration calculations here.

XII.5.2 The threefold over the punctured sphere

What makes the same ALE surface equation meaningful in different base charts? To compare two fibers we first need to say what their coordinates are. Put three of the

ordered marks at $0, 1, \infty$ and the fourth at q, with $q \neq 0, 1$. Write

$$\bar{C} = \mathbb{P}^1, \qquad D = 0 + q + 1 + \infty, \qquad C = \bar{C} \setminus D, \qquad K = K_{\bar{C}}|_C. \tag{XII.5.1}$$

We use the cotangent line K for each of the three fiber directions. The deformation of the ALE fiber is then a quadratic differential:

$$E = K \oplus K \oplus K, \qquad Q \in H^0(\bar{C}, K_{\bar{C}}^2(2D)), \qquad X_Q = \{uv + x^2 = Q\} \subset \mathrm{Tot}(E). \tag{XII.5.2}$$

Here the equation takes values in the pullback of K^2. Allowing at most double poles at D supplies the ordinary end data; we will identify those data with masses after computing the periods.

In the frame dz, use u_z, v_z, x_z for the coefficients of the three fiber coordinates and write $Q = \phi_z\, dz^2$. If $\zeta = f(z)$ and $J = f'(z) \neq 0$, a covector has coefficient $x_\zeta = x_z/J$. The same law for u, v gives

$$(u_\zeta, v_\zeta, x_\zeta) = J^{-1}(u_z, v_z, x_z), \qquad \phi_\zeta = J^{-2}\phi_z, \tag{XII.5.3}$$

$$F_z = u_z v_z + x_z^2 - \phi_z, \qquad F_\zeta = J^{-2} F_z. \tag{XII.5.4}$$

For example, inversion $\zeta = 1/z$ gives $J = -z^{-2}$. The fiber coefficients multiply by $-z^2$ while $\phi_\zeta = z^4 \phi_z$. The sign has disappeared from the quadratic equation, but it will matter for the one-form measured by a period.

The coordinates in (XII.5.3) are coefficients of covectors. For example, the same point of a cotangent fiber has the two representations

$$x_z\, dz = x_\zeta\, d\zeta, \qquad u_z v_z\, dz^2 = u_\zeta v_\zeta\, d\zeta^2. \tag{XII.5.5}$$

This explains why the product of two fiber coordinates can be compared with a quadratic differential on the base. If the three fiber coefficients were instead kept unchanged under inversion, the term x^2 would be a scalar while ϕ_z would acquire a factor z^4. The equations in the two charts would describe different fibers. The bundle assignment is therefore part of the geometry that allows a sphere transported through several charts to remain the same sphere.

To compute that period we also need a global three-form. In each frame we take the residue with dF_z first, suppressing the subscript on the fiber coordinates:

$$dF_z \wedge \Omega = dv \wedge du \wedge dx \wedge dz. \tag{XII.5.6}$$

This equation defines the restriction of the residue form on the smooth hypersurface. Each transformed fiber differential contributes J^{-1} in the wedge product; terms containing dJ vanish because they already contain dz. The new base differential contributes J. Thus the four-form and $dF_z|_{F_z=0}$ as an ambient covector both transform with J^{-2}. Their factors cancel in the residue. Solving (XII.5.6) with a different nonzero partial derivative in each chart gives

$$\Omega = \frac{du}{u} \wedge dx \wedge dz = -\frac{dv}{v} \wedge dx \wedge dz = \frac{dv \wedge du \wedge dz}{2x} = \frac{dv \wedge du \wedge dx}{\partial_z \phi_z}. \tag{XII.5.7}$$

For example, in the last chart only the term $-\partial_z\phi_z\,dz$ of dF_z contributes, and moving dz through the three fiber differentials cancels its minus sign. Each expression applies where its denominator is nonzero. Together they give a nowhere vanishing three-form on the smooth locus.

One can see the cancellation directly in the u-chart, without choosing a constant Jacobian. On the overlap,

$$\frac{du_\zeta}{u_\zeta} = \frac{du_z}{u_z} - \frac{dJ}{J}, \qquad dx_\zeta = \frac{dx_z}{J} - \frac{x_z\,dJ}{J^2}, \qquad d\zeta = J\,dz. \tag{XII.5.8}$$

Here $dJ = J'(z)dz$. Every added term has a factor dz, so it vanishes when wedged with the last factor. The remaining product is precisely $du_z/u_z \wedge dx_z \wedge dz$. In particular, the global three-form does not require a preferred coordinate on the four-marked sphere. The same cancellation will make the reduced one-form a coordinate-independent object.

The last chart also explains how a sphere can collapse in a smooth threefold. At an interior zero of ϕ_z, the fiber has an A_1 point at $u = v = x = 0$. For a simple zero z_0, the equation solves locally for z as a function of u, v, x, and the last expression in (XII.5.7) is regular. In contrast, the full gradient vanishes at the origin of the fiber precisely when

$$u = v = x = 0, \qquad \phi_z = \partial_z\phi_z = 0. \tag{XII.5.9}$$

For instance, $\phi_z = z - z_0$ gives a smooth total space and $\phi_z = (z - z_0)^2$ gives a singular total space at the center. If $Q = 0$ everywhere, every point of the zero section is singular. In the undeformed local model the gradient quotient is

$$\mathbb{C}\{u, v, x, z - z_0\}/(v, u, 2x, 0) \simeq \mathbb{C}\{z - z_0\}. \tag{XII.5.10}$$

Powers of the base coordinate survive to all orders. The finite local Jacobi count for an isolated point in Chapter 3 does not count the deformations of this locus. We will use the allowed poles and the global base to select a finite set of parameters instead.

Near a removed mark let t be a coordinate vanishing at the mark. The logarithmic frame dt/t of $K_{\bar{C}}(D)$ rewrites $x_t\,dt$ with coefficient $\widetilde{x} = tx_t$, and likewise for u, v. It gives

$$\widetilde{u}\widetilde{v} + \widetilde{x}^2 = t^2\phi_t, \qquad \Omega = \frac{d\widetilde{u}}{\widetilde{u}} \wedge d\widetilde{x} \wedge \frac{dt}{t}. \tag{XII.5.11}$$

The equation coefficient on the right is regular at the mark. This frame records end data and does not add the end fiber to X_Q.

For clarity, the apparent logarithmic factor follows by substituting rather than adding a boundary condition to the residue:

$$\frac{du}{u} = \frac{d\widetilde{u}}{\widetilde{u}} - \frac{dt}{t}, \qquad dx = \frac{d\widetilde{x}}{t} - \frac{\widetilde{x}}{t^2}\,dt, \qquad \frac{du}{u} \wedge dx \wedge dt = \frac{d\widetilde{u}}{\widetilde{u}} \wedge d\widetilde{x} \wedge \frac{dt}{t}. \tag{XII.5.12}$$

The regular coefficient $t^2\phi_t$ specifies what the ALE fiber approaches at the removed end. Its regularity does not make dt/t a regular differential on a filled base. The distinction between an interior cap and a removed end will reappear as the distinction between a compact gauge period and a flavor residue. At an interior simple zero, by contrast, the collapsing sphere is part of the threefold. Figure XII.5.1 uses two such interior zeros as caps of a compact cycle.

XII.5.3 From a wrapped sphere to a spectral period

What one-form remains when we integrate out the sphere? At a smooth fiber choose a root $s^2 = \phi_z$, $s \neq 0$. The coordinate x runs along the segment between $-s$ and $+s$. Above an interior point of this segment the equation $uv = s^2 - x^2$ allows a circle. A real two-sphere in the fiber is parametrized by

$$x = ts, \quad u = s\sqrt{1-t^2}\, e^{i\theta}, \quad v = s\sqrt{1-t^2}\, e^{-i\theta}, \quad -1 \le t \le 1, \quad 0 \le \theta < 2\pi. \tag{XII.5.13}$$

The circle contracts at the two endpoints. Orient the sphere by $d\theta \wedge dt$. At fixed z its relative form is $du/u \wedge dx$. The derivative of the latitude radius contributes only a dt term and drops out:

$$\frac{du}{u} \wedge dx\Big|_{S^2_z} = \left(i\, d\theta - \frac{t\, dt}{1-t^2} \right) \wedge s\, dt = is\, d\theta \wedge dt, \tag{XII.5.14}$$

$$\int_{S^2_z} \frac{du}{u} \wedge dx = 4\pi i s. \tag{XII.5.15}$$

Although the u-chart omits the poles of the sphere, the pulled back area form has a finite integral over both caps.

The same calculation applies when the sphere moves along a base path. Parametrize that path by a real variable σ, so that both s and z depend on σ. In the interior of the sphere,

$$\frac{du}{u} = i\, d\theta - \frac{t\, dt}{1-t^2} + \frac{ds}{s}, \qquad dx = s\, dt + t\, ds, \qquad dz = z'(\sigma) d\sigma. \tag{XII.5.16}$$

Every term containing ds is proportional to $d\sigma$ and vanishes after wedging with dz. Thus the threefold integrand on the sweep is

$$\Omega|_{\Gamma_\gamma} = is\, d\theta \wedge dt \wedge dz. \tag{XII.5.17}$$

Integrating the two fiber variables first is justified on a smooth segment of the path. Taking a limit at a simple-zero cap then closes the cycle. There is no additional term from the rate at which the sphere shrinks.

A real sphere supplies a separate check of the factor and sign. For $s > 0$ write $u = b + ic$ and $v = b - ic$ with real b, c. Then $b^2 + c^2 + x^2 = s^2$, and $dv \wedge du = 2i\, db \wedge dc$. The outward orientation of the sphere in (b, c, x) is $d\theta \wedge dt$. The real residue divides its area form by the gradient length $2s$:

$$2i\, \frac{\mathrm{Area}(S^2_s)}{2s} = 2i\, \frac{4\pi s^2}{2s} = 4\pi i s. \tag{XII.5.18}$$

In particular the raw fiber integral is linear in s, rather than in the area s^2. The inverse power of s from the residue is essential.

To transport the oriented sphere, continue the root along a base path γ. A single circuit of an interior simple zero sends s to $-s$, taking (θ, t) to $(\theta + \pi, -t)$ in (XII.5.13).

Thus the sphere comes back with its orientation reversed. A way to record the continuation is the spectral cover and its tautological one-form:

$$\Sigma:\ x_z^2 = \phi_z, \qquad \lambda = x_z\, dz, \qquad \iota(x_z) = -x_z, \qquad \iota^*\lambda = -\lambda. \tag{XII.5.19}$$

The cotangent transition in (XII.5.3) makes λ independent of the coordinate. On the two lifts γ_+, γ_- of the same oriented path, its values are $+s\, dz$ and $-s\, dz$.

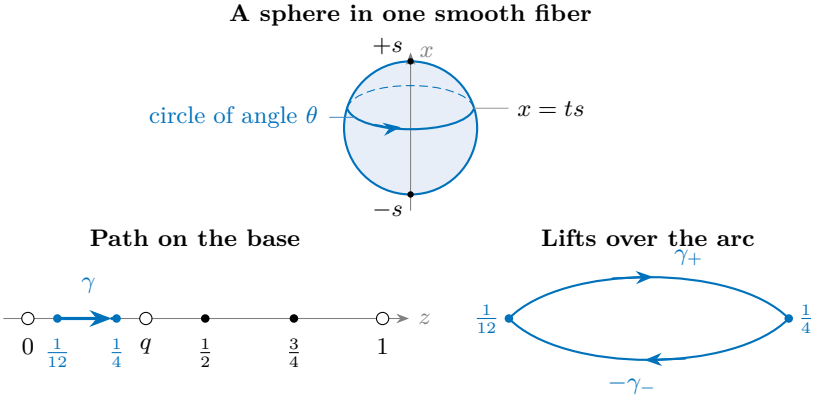


Figure XII.5.1: Fiber and spectral pictures of a compact sweep. Top: the circle over an interior latitude of the fiber sphere contracts at the points $x = \pm s$. Bottom left: in the real $q = 1/3$ example of (XII.5.34), filled dots are the four interior zeros and open circles are marked ends. The ∞ mark is outside this affine chart. The sphere collapses at both ends of the highlighted arc from $1/12$ to $1/4$. Bottom right: the lifts join at these two branch points. The arrows show the orientation of the difference chain: forward on the $+$ lift and backward on the $-$ lift.

If γ joins two interior simple zeros and contains no other zero or end, the spheres collapse at both endpoints. The sweep Γ_γ is topologically a three-sphere, the suspension of the two-sphere. An example is the arc $[1/12, 1/4]$ of Figure XII.5.1. Both lifts are oriented as γ before taking their difference; their endpoints coincide, so the difference is a closed cycle. Integrating (XII.5.15) along the base gives

$$\frac{1}{2\pi i}\int_{\Gamma_\gamma} \Omega = 2\int_\gamma s\, dz = \int_{\gamma_+ - \gamma_-} \lambda. \tag{XII.5.20}$$

The normalized sweep measures the difference of the sheets. A closed base loop for which s returns also closes the sweep, now as a product $S^2 \times S^1$ in the parametrization above. Its normalized period is twice the period of its single returning lift. A one-branch meridian, with its orientation reversal, does not give this oriented product.

A local collision makes the vanishing of this period explicit. Write $h = z - z_*$ and retain the exact quadratic local model

$$\phi_z = c(h^2 - \delta), \qquad c > 0, \quad \delta > 0, \qquad \gamma = [-\sqrt{\delta}, \sqrt{\delta}]. \tag{XII.5.21}$$

This is a local model near two colliding interior zeros; the expression is not being imposed as the global four-ended differential. Choose on the forward lift $s = i\sqrt{c}\sqrt{\delta - h^2}$. With the orientation of (XII.5.20), the compact sweep has normalized period

$$\begin{aligned}\Pi_{\mathrm{loc}} &= 2i\sqrt{c}\int_{-\sqrt{\delta}}^{\sqrt{\delta}} \sqrt{\delta - h^2}\, dh \\ &= 2i\sqrt{c}\,\delta \int_{-\pi/2}^{\pi/2} \cos^2\vartheta\, d\vartheta = i\pi\sqrt{c}\,\delta. \end{aligned} \tag{XII.5.22}$$

The branch points approach each other with separation $2\sqrt{\delta}$, while the period vanishes linearly in δ. Both the length of the interval and the value of the fiber integral shrink. Reversing the cycle reverses the period, and using only the forward lift would lose a factor of two. At $\delta = 0$ the total-space gradient vanishes at the fiber center, as predicted by (XII.5.9). The integral gives the local period associated with this geometric degeneration; the existence and stability of a particle of that charge require the physical conditions in the next paragraph.

In the ordinary zero-flux local sector of Type IIB, the wrapped-D3 dictionary identifies the period with a central charge when a retained charge has a calibrated representative. We use one common conversion c_{cal} from the geometric normalization to the house normalization:

$$Z_\Gamma = c_{\mathrm{cal}} \int_\Gamma \frac{\Omega}{2\pi i}, \qquad M_{\mathrm{BPS}} = \sqrt{2}\,|Z_\Gamma|. \tag{XII.5.23}$$

This is a protected charge formula under the local-limit assumptions given below. A closed sweep alone gives neither a calibrated representative nor a stable particle at a chosen vacuum. We next use the differential itself to separate boundary periods from the periods that vary when the ends are held fixed.

XII.5.4 Four masses and one interior coefficient

Which parameters belong to the ends, and which can vary with the ends fixed? Near a mark p, use a regular coordinate t vanishing there. An ordinary nonzero-mass end has a double pole of Q. If its leading coefficient is m_p^2, the two lifted one-forms and their small counterclockwise loop integrals are

$$\phi_t = \frac{m_p^2}{t^2} + O(t^{-1}), \qquad \lambda_\pm = \pm m_p \frac{dt}{t} + O(1)\, dt, \qquad \oint \lambda_\pm = \pm 2\pi i m_p. \tag{XII.5.24}$$

These loops measure flavor data even though they vanish on filling the punctures of the spectral curve. The threefold sweep about the same end measures their difference, $4\pi i m_p$ in the normalization of (XII.5.20). The sign of m_p specifies a sheet, whereas m_p^2 is invariant. These parameters are masses in common relative period units.

An ordinary mark need not carry a nonzero mass. If the double pole coefficient vanishes, there may still be a simple pole. For a simple pole and for a third-order

pole, the coordinate on the local normalized cover is $t = r^2$. With $c \neq 0$, the leading behaviors are

$$Q \sim c\,\frac{dt^2}{t} \quad \Longrightarrow \quad \lambda \sim 2\sqrt{c}\,dr, \tag{XII.5.25}$$

$$Q \sim c\,\frac{dt^2}{t^3} \quad \Longrightarrow \quad \lambda \sim 2\sqrt{c}\,\frac{dr}{r^2}. \tag{XII.5.26}$$

A massless ordinary mark can therefore be a branch point where λ has no pole. A third-order pole produces a different end condition even on the cover. It cannot be removed by a regular change of base coordinate and is excluded by (XII.5.2).

To construct ϕ_z, first subtract the three double poles at $0, q, 1$. The remainder has at most simple poles there and must be $O(z^{-2})$ at infinity, since

$$t = 1/z: \qquad \phi_t(t) = t^{-4}\phi_z(1/t). \tag{XII.5.27}$$

Put $P = z(z-q)(z-1)$. Multiplying the remainder by P gives a polynomial of degree at most one. The coefficient of z^{-2} of the entire differential must be m_∞^2, so the remainder is $[M(z-q)+U]/P$, where M is the difference between the desired infinity coefficient and the sum of the three finite squares. We arrive at

$$\phi_z = \frac{m_0^2}{z^2} + \frac{m_q^2}{(z-q)^2} + \frac{m_1^2}{(z-1)^2} + \frac{M}{z(z-1)} + \frac{U}{P}, \tag{XII.5.28}$$

$$M = m_\infty^2 - m_0^2 - m_q^2 - m_1^2. \tag{XII.5.29}$$

Indeed U/P falls as z^{-3}; it does not change the double pole at infinity or at any finite mark. Thus U is an affine coordinate at fixed end data.

The numerator also counts the coefficients without using the partial fractions. Set $N = P^2\phi_z$. A differential with the allowed poles corresponds to a polynomial N of degree at most four, because $\phi_z = O(z^{-2})$. The four evaluations of the squared masses are

$$m_p^2 = \frac{N(p)}{P'(p)^2} \quad (p = 0, q, 1), \qquad m_\infty^2 = [z^4]N. \tag{XII.5.30}$$

The kernel has degree at most three and vanishes at $0, q, 1$. It is exactly $\mathbb{C}P$. The map from the five polynomial coefficients to the four end squares therefore has rank four.

For a concrete change of base parameter, take $q = 1/2$ and write $N = \sum_{k=0}^{4} n_k z^k$. The evaluation map is then a small linear system:

$$\begin{pmatrix} m_0^2 \\ m_q^2 \\ m_1^2 \\ m_\infty^2 \end{pmatrix} = \begin{pmatrix} 4 & 0 & 0 & 0 & 0 \\ 16 & 8 & 4 & 2 & 1 \\ 4 & 4 & 4 & 4 & 4 \\ 0 & 0 & 0 & 0 & 1 \end{pmatrix} \begin{pmatrix} n_0 \\ n_1 \\ n_2 \\ n_3 \\ n_4 \end{pmatrix}. \tag{XII.5.31}$$

The last row extracts the infinity coefficient; it is independent of the three finite evaluations. The kernel vector gives

$$(\delta n_0, \delta n_1, \delta n_2, \delta n_3, \delta n_4) = \delta U\,(0, 1/2, -3/2, 1, 0), \qquad \delta N = \delta U\, z(z-1/2)(z-1). \tag{XII.5.32}$$

This calculation makes the word affine precise. Choosing the four masses picks one solution N_0, and every other solution is $N_0 + UP$. A different origin for U shifts N_0 by a multiple of P, without changing the number of independent vacuum parameters. We use the origin fixed by (XII.5.28) throughout. In line-bundle language the degrees give the same count:

$$K_{\bar{C}}^2(2D) \simeq \mathcal{O}(4), \qquad K_{\bar{C}}^2(D) \simeq \mathcal{O}(0), \qquad h^0\big(\mathcal{O}(4)\big) = 5, \quad h^0\big(\mathcal{O}(0)\big) = 1. \tag{XII.5.33}$$

Here the second space describes differences at fixed leading poles. There is one further complex parameter in the ordered marked base: the three Möbius parameters fix the three chosen marks, leaving q free. Changing q moves the puncture; it does not change a coefficient at fixed base. This distinction will allow us to pinch the tube at fixed U.

For a worked example at $q = 1/3$, start from the real branch locations in Figure XII.5.1 and take

$$N = (z - 1/12)(z - 1/4)(z - 1/2)(z - 3/4). \tag{XII.5.34}$$

The three values of P' at the finite ends are $1/3, -2/9, 2/3$. For instance, $N(0) = 1/128$, and the first square is $(1/128)/(1/9) = 9/128$. The other evaluations and the leading coefficient give

$$(m_0^2, m_q^2, m_1^2, m_\infty^2) = \left(\frac{9}{128}, \frac{15}{512}, \frac{99}{512}, 1\right). \tag{XII.5.35}$$

To recover U, let N_0 be the numerator of (XII.5.28) at those squares and $U = 0$. Its degree-four coefficient agrees with that of N, and the three finite evaluations agree as well. So $N - N_0 = UP$. Since P is monic, subtracting the cubic coefficients gives

$$[z^3]N = -\frac{19}{12}, \qquad [z^3]N_0 = -\frac{1193}{768}, \qquad U = -\frac{23}{768}. \tag{XII.5.36}$$

The mass squares, although fixed by this example, do not determine the branch locations of every member of its affine family. Adding UP moves the branch locations without changing the leading end behavior.

The motion can also be read locally without solving the quartic. If $r_j(U)$ is a simple zero away from the marks, differentiate its vanishing condition with masses and q fixed:

$$N(r_j(U), U) = 0 \quad \Longrightarrow \quad \frac{dr_j}{dU} = -\frac{P(r_j)}{\partial_z N(r_j)}. \tag{XII.5.37}$$

The numerator is nonzero away from the marked ends. Therefore a simple interior branch point generally moves even though all four leading poles stay fixed. The denominator signals where this description fails: when two roots collide, one must use a local smoothing coordinate instead of a differentiable choice of individual roots. The quadratic model (XII.5.21) shows this explicitly through the two square-root root positions. In period units $[\lambda] = 1$, the base coordinates z, q have dimension zero, $[m_p] = 1$ and $[U] = 2$, consistently with $\lambda^2 = \phi_z\, dz^2$. The next calculation explains why the fixed-end variation is the rank-one Coulomb direction.

XII.5.5 The rank and the finite kinetic variation

Why does the fixed-end coefficient give a single Coulomb direction? The compact part of the spectral period problem is particularly useful for answering this question. Extend the bundle on the base to $K_{\bar{C}}(D)$ and use the square of this bundle for Q. The compact spectral cover $\bar{\Sigma}$ is defined by

$$\eta^2 = Q, \qquad \eta \in K_{\bar{C}}(D), \qquad y = Px_z, \qquad y^2 = N(z) \tag{XII.5.38}$$

where the last two equations are in the finite z-chart. The cover now includes points above the marks. This compactification is a device for computing the compact gauge periods; the ends of X_Q are still removed. Small loops surrounding the preimages of the marks carry the boundary periods of (XII.5.24) and disappear in the compact homology.

The branch points of the cover are the simple zeros of the homogeneous quartic corresponding to N. For the massive example (XII.5.34), there are four distinct finite branch points and none at infinity. The two lifts of an interval ending at a branch point join there, as in Figure XII.5.1. Riemann–Hurwitz for this degree-two cover gives

$$2g(\bar{\Sigma}) - 2 = 2\big(2g(\bar{C}) - 2\big) + 4 = 0. \tag{XII.5.39}$$

At zero masses with $U \neq 0$, $N = UP$ has degree three. The missing fourth root is a simple root at infinity: the quartic in the other chart has leading behavior $t^4 N(1/t) = Ut + O(t^2)$. All four marked points are then branch points on the compact curve, and the same formula still gives genus one. In either smooth case there is one compact period pair.

To see what the periods measure as U varies, transport the cycles in the smooth family at fixed ends. A contour can be chosen locally away from the moving branch points and projected onto fixed base paths. The derivative at fixed z of the one-form on those paths is

$$2x_z \partial_U x_z = \frac{1}{P}, \qquad \omega_U := \partial_U \lambda = \frac{dz}{2Px_z} = \frac{dz}{2y}. \tag{XII.5.40}$$

It has no pole at an ordinary branch point: in a coordinate $z - z_* = r^2$, y vanishes linearly in r while $dz = 2r\,dr$. At infinity in the massive quartic, $y \sim \pm m_\infty z^2$, so dz/y is regular in $1/z$. In the massless cubic, take $z = r^{-2}$ near infinity on the cover. Then

$$y \sim \sqrt{U}\, r^{-3}, \qquad dz = -2r^{-3}\, dr, \qquad \omega_U \sim -\frac{dr}{\sqrt{U}}. \tag{XII.5.41}$$

Thus ω_U spans the holomorphic one-forms of the compact genus-one curve.

A changed mass assignment illustrates both the smooth-family condition and its failure. Set $q = 1/2$ and all four signed end masses equal to 1, in the relative units used here. The fixed-end family is

$$N_U(z) = z^4 + (U-2)z^3 + \left(2 - \frac{3}{2}U\right) z^2 + \left(\frac{U}{2} - 1\right) z + \frac{1}{4}. \tag{XII.5.42}$$

At $z = 0, 1/2, 1$, its values are $1/4, 1/16, 1/4$, and its leading coefficient is 1. These are independent of U and reproduce the four unit mass squares by (XII.5.30). Nevertheless the branch geometry changes. The quartic discriminant is

$$\operatorname{disc}_z N_U = \frac{1}{16} U^2 (U-2)^2 (U+2)^2. \tag{XII.5.43}$$

For example $U = 1$ and $U = 3$ give four distinct branch points and a smooth compact genus-one curve, while the three exceptional values yield

$$N_{-2} = \tfrac{1}{4}(2z^2 - 4z + 1)^2, \quad N_0 = \tfrac{1}{4}(2z^2 - 2z + 1)^2, \quad N_2 = \tfrac{1}{4}(2z^2 - 1)^2. \tag{XII.5.44}$$

All repeated roots here remain away from the marks. In a neighborhood of any such root, $P \neq 0$, so $\phi_z = N_U/P^2$ has a double zero. The corresponding fiber center is a total-space singularity. On the spectral side $y^2 = N_U$ has intersecting components at these points rather than a smooth torus. Its holomorphic differential must be studied on the degeneration, not by blindly applying the smooth-curve statement above. The especially symmetric mass assignment makes two root collisions occur together. Neither the order of a factor in the discriminant nor the number of these intersections counts stable BPS particles.

This experiment changes U at fixed q, so it changes the vacuum within one end problem. The weak tube below changes q instead. Both operations can make a spectral curve degenerate, but they hold different physical parameters fixed. Keeping track of which coefficients are controlled is necessary before interpreting a vanishing period or a divergent coupling.

Compare a variation of a nonzero mass at fixed q. On a given sheet the leading term of $\delta\lambda$ is now $\pm\delta m_p\, dt/t$. For a one-form α the reduced spectral norm is $(i/2)\int \alpha \wedge \overline{\alpha}$. On an annulus $\epsilon < |t| < R$ the mass variation on one sheet contributes

$$\frac{i}{2}\int \delta\lambda \wedge \overline{\delta\lambda} = 2\pi|\delta m_p|^2 \int_\epsilon^R \frac{dr}{r} + O(1) = 2\pi|\delta m_p|^2 \log(R/\epsilon) + O(1). \tag{XII.5.45}$$

The integrand is positive, so opposite residues do not cancel this divergence between the sheets. For $\delta U\, \omega_U$ the integrand is locally a bounded multiple of the area element even at the filled points; its spectral norm is finite.

This is a norm of a variation, not a norm of the original meromorphic λ. The latter already has the fixed mass poles even when only U is varied. Holding a residue fixed removes its singular part from the variation:

$$\lambda_\pm = \pm m_p \frac{dt}{t} + a_{\pm,0}(U)dt + O(t)dt \quad \Longrightarrow \quad \partial_U \lambda_\pm = (\partial_U a_{\pm,0})dt + O(t)dt. \tag{XII.5.46}$$

For nonzero m_p, this expansion is on the two unbranched sheets above the end. The explicit global expression $dz/(2y)$ also handles the massless branch-point limits. By contrast, on the two unbranched sheets a varied residue contributes

$$2\pi\big(|\delta m_p|^2 + |-\delta m_p|^2\big)\log(R/\epsilon) = 4\pi|\delta m_p|^2 \log(R/\epsilon). \tag{XII.5.47}$$

The signs that cancel in a sum of residues add in a positive kinetic norm. This is why the boundary parameters are held fixed when constructing the finite Coulomb variation.

In the reduced spectral description with fixed ordinary ends, this is the kinetic distinction between the dynamical Coulomb variation and the background mass data. The integral above concerns one-forms on a curve; it does not compute an L^2 norm in the full threefold metric. Moving q changes the marked boundary problem itself. We can study that change by following the periods with U and the masses fixed, without assigning a metric kinetic norm to q.

XII.5.6 Pinching a weak gauge tube

Which motion of the marks makes a gauge interaction weak? Let $q \to 0$ at fixed masses and fixed U. The marks $0, q$ move close together in the original coordinate. To resolve them, keep $w = z/q$ fixed in an inner region. The old coordinate z resolves the other two marks in an outer region. Since $x_w = q x_z$, the inner coefficient is $q^2 \phi_z(qw)$. The differential is a tensor, and the factor q^2 is needed even though q is constant in each base chart.

The two coordinates answer different limiting questions. A point $z = z_0 \neq 0$ stays at finite distance in the outer coordinate and moves to $w = z_0/q \to \infty$ in the inner one. A point $z = q w_0$, with w_0 finite, stays among the two colliding marks in the inner coordinate and approaches the node in the outer one. The overlap is described by

$$|q| \ll |z| \ll 1, \qquad 1 \ll |w| \ll |q|^{-1}, \qquad \xi = w^{-1}, \qquad z\xi = q. \tag{XII.5.48}$$

Thus the small separation of marked points has become a gluing parameter between two component spheres. Their common node is not an extra independent mass parameter: both limiting differentials must inherit the same coefficient from the original family.

For the outer limit use $1/[z^2(z-1)] = -1/z^2 + 1/[z(z-1)]$. In the inner limit the U term becomes $U/[w(w-1)(qw-1)]$. The terms proportional to m_1^2 and M in (XII.5.28) vanish after multiplication by q^2: the first is $O(q^2)$ and the second is $O(q)$ at fixed w away from the marks. Thus

$$\phi_{\mathrm{out}}(z) = \frac{m_0^2 + m_q^2 - U}{z^2} + \frac{m_1^2}{(z-1)^2} + \frac{M+U}{z(z-1)}, \tag{XII.5.49}$$

$$\phi_{\mathrm{in}}(w) = \frac{m_0^2}{w^2} + \frac{m_q^2}{(w-1)^2} - \frac{U}{w(w-1)}. \tag{XII.5.50}$$

Each is a differential on a three-marked sphere, also called a trinion. To see their common form, define

$$S(t; b, c, d) = \frac{b^2}{t^2} + \frac{c^2}{(t-1)^2} + \frac{d^2 - b^2 - c^2}{t(t-1)}, \qquad a^2 = m_0^2 + m_q^2 - U. \tag{XII.5.51}$$

The end squares at $(0, 1, \infty)$ are (b^2, c^2, d^2). We have $\phi_{\mathrm{out}} = S(z; a, m_1, m_\infty)$ and $\phi_{\mathrm{in}} = S(w; m_0, m_q, a)$. Their node is the outer $z = 0$ and inner $w = \infty$. The node residues on a matched sheet are opposite: if $\xi = 1/w$, then $z\xi = q$ and

$$a\,\frac{dz}{z} = -a\,\frac{d\xi}{\xi}. \tag{XII.5.52}$$

The a here is a limiting eigenvalue. It need not be the special coordinate at finite q. Setting $q = 0$ only in the old chart would keep (XII.5.49) and lose the two inner marks.

The matching of residues can be checked directly at the level of the one-form. Near the outer node take the chosen sheet with $\lambda \sim a\,dz/z$. On the inner sphere the same sheet has $\lambda \sim a\,dw/w$ at large w, which becomes $-a\,d\xi/\xi$ in a coordinate that vanishes at its node. Consequently the two local residues at a node sum to zero. There is a common square a^2, but there is no common sign in the two coordinates that vanish at the node. Matching only the squared equations would hide this orientation information.

For example, take $(m_0, m_q, m_1, m_\infty) = (1, 2, 3, 5)$ and $U = 3$. The shared square is $a^2 = 2$. Multiplying the inner and outer coefficients by $t^2(t-1)^2$ in their respective charts gives

$$N_{\mathrm{in}}(w) = (w-1)^2 + 4w^2 - 3w(w-1) = 2w^2 + w + 1, \tag{XII.5.53}$$

$$N_{\mathrm{out}}(z) = 2(z-1)^2 + 9z^2 + 14z(z-1) = 25z^2 - 18z + 2. \tag{XII.5.54}$$

Both quadratics have two simple roots and neither vanishes at its marked points. Their leading and constant coefficients, respectively, exhibit the inner and outer values of the same node square. This example lies in the regime used next: all external masses and a nonzero, and smooth component covers with branch points away from the marks.

For small nonzero q, choose a small fixed $\rho > 0$. The neck on the base is the annulus $|q|/\rho < |z| < \rho$. In it, multiply (XII.5.28) by z^2 and expand in z and q/z:

$$z^2\phi_z = a^2 + O(|z| + |q/z|), \tag{XII.5.55}$$

$$\lambda_+ = \big[a + O(|z| + |q/z|)\big]\frac{dz}{z}, \qquad \lambda_- = -\lambda_+. \tag{XII.5.56}$$

The nonzero constant lets us choose a root of $z^2\phi_z$ on the whole annulus. There are two lifts of the neck, with no branch points between its rims.

For each smooth limiting trinion the quadratic numerator has two simple roots, and its double cover has genus zero by Riemann–Hurwitz. Each node has two unbranched preimages because $a \neq 0$. Gluing the two component covers therefore requires two annuli. The first annulus joins the two spheres; the second gives one independent handle. This explains geometrically why a single base tube yields the one compact period pair of the nearby torus. It also explains the role of the smooth-component hypothesis. If a component branch point reaches the node or collides with another branch point, its contribution need no longer stay bounded while we stretch the tube. On the compact curve orient A counterclockwise around the upper lift, and B inward along the upper lift and outward along the lower one. A path from an outer to an inner branch point and its opposite lift gives such a B. Its crossing of A has $A \cdot B = +1$: the counterclockwise tangent followed by the inward radial tangent orients the complex annulus.

On the circle $|z| = \sqrt{|q|}$, the error in the square brackets in (XII.5.56) is $O(\sqrt{|q|})$; thus $\oint_A \lambda \to 2\pi i a$.

The middle radius balances the two sources of error. More generally, at $|z| = |q|^\alpha$ with $0 < \alpha < 1$, they have sizes

$$O(|z| + |q/z|) = O\big(|q|^\alpha + |q|^{1-\alpha}\big). \tag{XII.5.57}$$

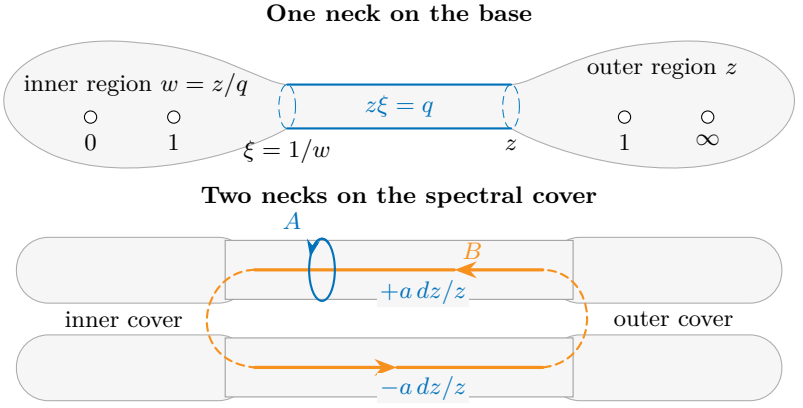


Figure XII.5.2: The tube over the pinching four-marked sphere. Top: the inner and outer regions meet through one annulus with $z\xi = q$, $\xi = 1/w$. The external marks remain on their respective sides. Bottom: the two lifts of the annulus, labeled by $\lambda \simeq \pm a\,dz/z$, connect the same two component covers. The arrow on A is counterclockwise in z on the upper annulus. The B contour goes inward in $|z|$ on the upper lift and outward on the lower lift, closing through the two component covers. Its neck contributions add because both the sheet sign and the direction reverse.

The larger error decays fastest when $\alpha = 1/2$. This is a choice of contour inside a branch-free annulus; it does not move a branch point or change the homology class of A. In a logarithmic coordinate the radial length of the annulus is

$$L = \log \frac{\rho}{|q|/\rho} = \log \frac{\rho^2}{|q|}. \tag{XII.5.58}$$

An A contour travels around its angular direction and has a finite limiting period. The radial contour travels a distance that increases like $-\log|q|$. The two opposite-sheet radial traversals are what produce the growing dual period. To find the effective period ratio use ω_U, the variation of λ at fixed ends. Here $P = -z^2[1 + O(|z| + |q/z|)]$ and $x_z = [a + O(|z| + |q/z|)]/z$ on the upper lift. Consequently,

$$\omega_{U,+} = \big[\beta + O(|z| + |q/z|)\big]\frac{dz}{z}, \qquad \omega_{U,-} = -\omega_{U,+}, \qquad \beta = -\frac{1}{2a}. \tag{XII.5.59}$$

On the upper lift the inward integral of dz/z is $\log q + O(1)$ in a fixed sector of $\log q$. On the lower lift the outward integral has the opposite sign and the form itself also has the opposite sign. The errors remain bounded: their radial absolute integral is controlled by

$$\int_{|q|/\rho}^{\rho} \left(r + \frac{|q|}{r}\right)\frac{dr}{r} = 2\left(\rho - \frac{|q|}{\rho}\right). \tag{XII.5.60}$$

At fixed rims the connections through the smooth component covers contribute bounded

terms. It follows that

$$\oint_A \omega_U = 2\pi i\beta + O(\sqrt{|q|}), \qquad \oint_B \omega_U = 2\beta \log q + O(1), \tag{XII.5.61}$$

$$\tau_{\mathrm{per}} = \frac{\partial_U \oint_B \lambda}{\partial_U \oint_A \lambda} = \frac{\log q}{\pi i} + O(1). \tag{XII.5.62}$$

The correction to the denominator times $\log q$ vanishes. In particular $\operatorname{Im} \tau_{\mathrm{per}} \to +\infty$. Write $\mathfrak{a} = \oint_A \lambda$ and $\mathfrak{a}_D = \oint_B \lambda$ for the two spectral periods, distinct from the limiting node eigenvalue a in (XII.5.51). At fixed ends and fixed q, the chain rule gives $d\mathfrak{a}_D/d\mathfrak{a} = (\partial_U \mathfrak{a}_D)/(\partial_U \mathfrak{a}) = \tau_{\mathrm{per}}$. In a compatible low-energy period frame, the imaginary part of this derivative controls the inverse squared effective abelian coupling. Its divergence is the weak-coupling signal.

This calculation uses the compact spectral basis and a ratio of derivatives. The corresponding A sweep has twice the single-sheet period, while the B sweep over the branch-to-branch arc has the period on its full two-sheet lift. The logarithm in (XII.5.62) fixes neither a primitive D3 basis nor a microscopic coupling convention.

The massless curve supplies an independent check that does not require the massive annulus hypotheses. For $U \neq 0$, rescale $y = \sqrt{U}\, Y$ in (XII.5.38). The result is the Legendre curve $Y^2 = z(z-q)(z-1)$. With $z = Z + (1+q)/3$, the cubic is $Z^3 + pZ + r$, where

$$p = -\frac{1 - q + q^2}{3}, \qquad r = -\frac{2(1+q)^3}{27} + \frac{q(1+q)}{3}. \tag{XII.5.63}$$

The cubic discriminant is $-4p^3 - 27r^2 = q^2(1-q)^2$, the product of the squared root differences. Thus

$$j = 1728\, \frac{4p^3}{4p^3 + 27r^2} = 256\, \frac{(1 - q + q^2)^3}{q^2(1-q)^2}. \tag{XII.5.64}$$

The double pole of j agrees with the two-neck coefficient: $j(\tau)$ begins with $e^{-2\pi i\tau}$ at the cusp.

On the real slice $0 < q < 1$, use intervals $[0, q]$ and $[q, 1]$ for the two period contours. The first has positive P along its interior, and the second has negative P. Define the elliptic integral with parameter m by

$$K(m) = \int_0^{\pi/2} \frac{d\theta}{\sqrt{1 - m \sin^2 \theta}}. \tag{XII.5.65}$$

The changes of variable $z = q \sin^2 \theta$ on the first interval and $z = q/[1 - (1-q)\sin^2 \theta]$ on the second yield

$$\int_0^q \frac{dz}{\sqrt{P}} = 2K(q), \qquad \int_q^1 \frac{dz}{\sqrt{-P}} = 2K(1-q). \tag{XII.5.66}$$

The contour doubles and the common constant in ω_U cancel in their ratio. Choose the second sheet phase and cycle orientation so $A \cdot B = +1$; then

$$\tau_{\mathrm{per}} = i\, \frac{K(1-q)}{K(q)}. \tag{XII.5.67}$$

For example, $q = 1/2$ gives $\tau_{\mathrm{per}} = i$. Even at zero masses the marked-base coordinate q and the compact spectral modulus are different descriptions of the family. A choice of microscopic ultraviolet coupling would require a further convention. At nonzero masses the spectral modulus also varies with the mass data and U. The logarithm identifies where a weak description can appear; the two components determine its matter content.

The massless family also separates an overall period scale from a change in the interaction. At fixed q, choose a local branch of $\sqrt{U}$ and transport a compact cycle γ while varying nonzero U. Its period and derivative are

$$\Pi_\gamma(U,q) = \sqrt{U}\oint_\gamma \frac{dz}{\sqrt{P}}, \qquad \partial_U \Pi_\gamma = \frac{1}{2\sqrt{U}}\oint_\gamma \frac{dz}{\sqrt{P}}. \tag{XII.5.68}$$

The common factor cancels in the ratio of derivatives. Changing U from 1 to 7, for example, multiplies both periods by $\sqrt{7}$, while leaving their ratio fixed. Changing q instead changes the ratio. The exact elliptic expression gives the following values on the stated real slice:

q	0.1	0.01	0.001
$\operatorname{Im}\tau_{\mathrm{per}}$	1.598875	2.346816	3.081190
$\pi^{-1}\log(1/q)$	0.732936	1.465871	2.198807

(XII.5.69)

The two rows differ by a bounded contribution; the logarithm controls the growing part. A finite small value of q need not allow the bounded term to be discarded numerically. At $q = 1/2$ the two elliptic integrals coincide, while reducing q lengthens the tube and increases the imaginary period ratio. This compares an exact period calculation with the asymptotic geometric argument.

XII.5.7 The weak vector and its four fundamentals

What becomes charged under the weak gauge factor? The branch points on a limiting trinion can collide at special values of its node residue. We can compute those values and compare them with the masses of weakly coupled doublets.

For the differential $S(t; b, c, d)$ of (XII.5.51), multiply by $t^2(t-1)^2$ to get the polynomial whose zeros are the branch points:

$$\begin{aligned} N_S(t) &= b^2(t-1)^2 + c^2t^2 + (d^2 - b^2 - c^2)t(t-1) \\ &= d^2t^2 + (c^2 - b^2 - d^2)t + b^2. \end{aligned} \tag{XII.5.70}$$

With nonzero end masses, its zeros avoid the three marks. Its discriminant is symmetric in the three squares. In a form adapted to an infinity node it reads

$$\begin{aligned} \operatorname{disc} N_S &= (c^2 - b^2 - d^2)^2 - 4b^2d^2 \\ &= (d^2 - b^2 - c^2)^2 - 4b^2c^2 = [d^2 - (b+c)^2][d^2 - (b-c)^2]. \end{aligned} \tag{XII.5.71}$$

The inner node is at infinity and the outer node is at zero. Using the symmetry of the discriminant to put the shared square a^2 in the same slot in each formula, the two pairs of collision thresholds are

$$\text{inner: } a^2 = (m_0 \pm m_q)^2, \qquad \text{outer: } a^2 = (m_1 \pm m_\infty)^2. \tag{XII.5.72}$$

For the two component polynomials (XII.5.53) and (XII.5.54) the pairs are $1, 9$ and $4, 64$, respectively. The chosen value $a^2 = 2$ is away from each pair: the discriminants there are $(2-1)(2-9) = -7$ and $(2-4)(2-64) = 124$, in agreement with the two explicit quadratics. These are branch collision tests. By themselves they do not count the multiplets at the thresholds.

For the physical interpretation we use the ordinary rank-two puncture dictionary in the retained zero-flux Type IIB sector, under the isolation conditions below. A trinion supplies a half hypermultiplet in $(\mathbf{2}, \mathbf{2}, \mathbf{2})$ of its three $SU(2)$ factors. Gluing through the long tube gauges the diagonal of the two factors at the node and adds one vector multiplet. The factors on the external marks in Figure XII.5.2 remain flavor factors. With respect to the weak gauge factor, the two external doublet indices give four copies of a half doublet. In the count of full fundamental hypermultiplets, this is

$$\tfrac{1}{2}(\mathbf{2}, \mathbf{2}, \mathbf{2}) \quad \longrightarrow \quad 4 \text{ half doublets} = 2 \text{ full fundamentals} \quad \text{per trinion.} \tag{XII.5.73}$$

The two blocks give the weak $SU(2)$ presentation with four full fundamentals. Here the presentation specifies the gauge algebra and the matter representations; the compact spectral curve has not fixed an absolute line lattice.

The counting can be followed directly through the three doublet indices. Label a weight by $(\epsilon_a, \epsilon_b, \epsilon_c)$, with each sign equal to ± 1. Its Cartan evaluation is

$$\epsilon_a a + \epsilon_b b + \epsilon_c c. \tag{XII.5.74}$$

For fixed (ϵ_b, ϵ_c), the two choices of ϵ_a form a doublet of the node factor. There are four choices of the external pair, so the half hyper contains four half doublets with respect to that factor. Pairing an external pair with its negative organizes them into two full doublets. The associated external Cartan evaluations are

$$\{b + c, b - c, -b + c, -b - c\} = \{\pm(b + c), \pm(b - c)\}. \tag{XII.5.75}$$

This recovers the two full-hyper masses using the sourced representation, before comparing with the geometric discriminant. The dimension of a representation supplies the multiplicity here; the polynomial discriminant supplies the loci where a gauge-weight-shifted evaluation $\pm a \pm b \pm c$ vanishes.

In a doublet the two weights of a Cartan eigenvalue a are $\pm a$. In the inner trinion the three doublet indices give weight evaluations $\pm a \pm m_0 \pm m_q$. The outer trinion gives $\pm a \pm m_1 \pm m_\infty$. Pairing evaluations that differ by an overall sign gives, up to signs, the full-hyper mass pairs

$$(m_0 + m_q,\ m_0 - m_q), \qquad (m_1 + m_\infty,\ m_1 - m_\infty). \tag{XII.5.76}$$

A gauge weight shifted by either mass can vanish exactly at the corresponding square in (XII.5.72). The geometry thus tests the relative masses of the sourced matter description.

Changing the external masses changes the threshold pattern in a predictable way. If $b = c = \mu \neq 0$ on a trinion, the two full-hyper masses become 2μ and 0, and the discriminant reduces to

$$[a^2 - (b + c)^2][a^2 - (b - c)^2] = a^2(a^2 - 4\mu^2). \tag{XII.5.77}$$

In particular, the threshold at $a^2 = 0$ lies outside the nonzero-node hypothesis used to derive the two branch-free annuli. One should use the trinion polynomial to discuss that collision, rather than extend the logarithmic annulus estimate through it. If the second trinion has the same pair of masses, its two threshold values coincide with those of the first. This coincidence does not alter the representation count: each block still supplies two full fundamentals. It changes which signed masses vanish at the same limiting value of a. In the standard $\mathcal{N} = 2$ one-loop normalization with one unit per full fundamental,

$$b_0 = 2h^\vee_{\mathfrak{su}(2)} - N_f = 4 - 4 = 0. \tag{XII.5.78}$$

The identification of q as an exactly marginal coordinate at zero masses uses the massless conformal family of this puncture construction. It is stronger than the arithmetic cancellation in (XII.5.78).

The weak tube limit varies the marked complex structure within the protected period geometry. There is a separate question of obtaining that geometry as an isolated local sector of Type IIB. At fixed q, the algebraic contraction rescales the fibers and quadratic differential:

$$(u, v, x) \longmapsto \varepsilon(u, v, x), \qquad Q \longmapsto \varepsilon^2 Q, \qquad \Omega \longmapsto \varepsilon\Omega. \tag{XII.5.79}$$

The last scaling follows from $du/u \wedge dx \wedge dz$. The periods on transported cycles scale linearly; the rescaled periods can stay finite as the zero section becomes an A_1 locus. This is a statement about an algebraic scale and does not yet say how many modes survive in calibrated mass units.

In the ordinary zero-flux branch, take $\ell_s \to 0$ at fixed weak string coupling g_s. The D3 tension and the calibrated volume of a retained wrapped D3 have to scale together:

$$T_3 = \frac{1}{(2\pi)^3 g_s \ell_s^4}, \qquad T_3 \left| \int_\Gamma \Omega_{\mathrm{cal}} \right| \text{ finite on retained calibrated cycles.} \tag{XII.5.80}$$

The geometric form in (XII.5.79) and the calibrated form Ω_{cal} are related by the choice of metric scale; the residue computation does not determine it. We stipulate a tuned degeneration with fixed ends in the retained mass units. The string oscillators become heavy and gravity is suppressed in the limit. Isolation also requires unwanted Kaluza–Klein modes to decouple and any gapless bulk or end continuum to factorize, with no extra dynamical sector from a completion. These requirements are independent of the weakening $q \to 0$. The algebraic model has no end metric from which to prove them.

The distinction can be written as two separate sets of conditions. Under the algebraic rescaling at fixed base,

$$m_p \mapsto \varepsilon m_p, \qquad U \mapsto \varepsilon^2 U, \qquad q \mapsto q, \qquad \frac{\partial_U \Pi_B}{\partial_U \Pi_A} \mapsto \frac{\partial_U \Pi_B}{\partial_U \Pi_A}, \tag{XII.5.81}$$

where the derivatives on the rescaled side use the rescaled coordinate. Both derivatives acquire the same inverse power of ε. This operation shrinks the central-charge scale without stretching the tube. The physical isolation condition instead compares unwanted excitation scales to a retained particle mass M_{ret}:

$$\frac{\ell_s^{-1}}{M_{\mathrm{ret}}} \longrightarrow \infty, \qquad \frac{M_{\mathrm{KK}}}{M_{\mathrm{ret}}} \longrightarrow \infty, \qquad T_3 \left| \int_\Gamma \Omega_{\mathrm{cal}} \right| = O(M_{\mathrm{ret}}). \tag{XII.5.82}$$

These ratios state which sectors the local field theory retains. They are requirements on a physical degeneration, with a separate factorization requirement if a bulk or end continuum remains gapless. The residue alone fixes neither M_{KK} nor the relation between its coordinate scale and calibrated volumes. Once this local sector has been chosen, varying q changes its weak-gauge description within the protected geometry.

There is a useful comparison with the Class S description. For a traceless two-by-two Higgs field $\Phi = \Phi_z\, dz$ with $\phi_z = \frac{1}{2}\operatorname{tr}\Phi_z^2$, its characteristic polynomial and tautological form are

$$\det(x_z\mathbf{1} - \Phi_z) = x_z^2 - \phi_z, \qquad \lambda = x_z\, dz. \tag{XII.5.83}$$

For example, write a local coefficient matrix as

$$\Phi_z = \begin{pmatrix} A & B \\ C & -A \end{pmatrix}, \qquad \tfrac{1}{2}\operatorname{tr}\Phi_z^2 = A^2 + BC, \qquad \det(x_z\mathbf{1} - \Phi_z) = x_z^2 - (A^2 + BC). \tag{XII.5.84}$$

The eigenvalues are the two sheet coordinates. The one-form λ assigns their eigenvalue times dz, and the swept ALE sphere measures their difference. This identifies the common spectral calculation without solving for a Higgs field metric or deriving a full equivalence of the two physical constructions. For example, in the massless family the coordinate inversion $w = 1/z$ changes the displayed order of the marks by exchanging the roles of zero and infinity. In that new ordering,

$$\phi_w(w) = w^{-4}\frac{U}{P(1/w)} = \frac{U/q}{w(w-1)(w-1/q)}, \qquad x_w = -z^2 x_z. \tag{XII.5.85}$$

The free mark in the new order is $1/q$; the cross-ratio of the original ordered marks is unchanged by the coordinate transformation itself. The cotangent sign in (XII.5.85) ensures $x_w\, dw = x_z\, dz$, beyond what the squared equation alone would establish. The shared objects are the spectral equation and one-form with their periods. Volume XVI takes up the Hitchin system and general puncture rules. The direct IIB calculation here obtains those periods by integrating a threefold form over the ALE spheres.

XII.5.8 Sending one flavor mass to infinity

How can the four-flavor construction leave an interacting gauge sector when one fundamental becomes arbitrarily heavy? Its mass is a sum or difference of end residues, rather than an individual end residue. This gives a precise way to choose the limit. Keep three full-hyper masses finite and send the fourth to a large positive value H. Using the pairs in (XII.5.76), set

$$m_0 = \frac{H+m}{2}, \qquad m_q = \frac{m-H}{2}, \qquad m_1 = b, \qquad m_\infty = c. \tag{XII.5.86}$$

The two residues near the approaching ends have large opposite parts. Their sum stays finite. The four fundamental masses become

$$(m_0 + m_q, m_0 - m_q, m_1 + m_\infty, m_1 - m_\infty) = (m, H, b+c, b-c). \tag{XII.5.87}$$

Thus only the second flavor is removed at energies small compared with H. Sending just m_0 to infinity with m_q fixed would instead make both masses of that pair large.

The end separation must shrink at the same time. Define a nonzero finite geometric scale Λ and take

$$q = \frac{\Lambda}{H}, \qquad H \gg \max\bigl(|m|, |b|, |c|, |\widehat{U}|^{1/2}, |\Lambda|\bigr). \tag{XII.5.88}$$

Here $\widehat{U}$ will be the finite Coulomb coefficient. The three remaining masses, Λ and $\widehat{U}$ are fixed as H grows. The original U must be chosen as a function of H; holding it fixed does not retain the same finite region of the Coulomb family. To determine that function, write the sum of the two large residue squares as S_H and choose

$$S_H = m_0^2 + m_q^2 = \frac{H^2 + m^2}{2}, \qquad U(H) = (1-q)S_H - \widehat{U}, \tag{XII.5.89}$$

$$U(H) = \frac{H^2}{2} - \frac{\Lambda H}{2} + \frac{m^2}{2} - \widehat{U} - \frac{\Lambda m^2}{2H}. \tag{XII.5.90}$$

The finite subtraction defines an origin for $\widehat{U}$. It is a coefficient of the limiting differential, rather than an exact special coordinate. We can verify the tuning directly before interpreting the result.

Substitute (XII.5.89) into (XII.5.28). The terms proportional to S_H first combine by the elementary identity

$$-\frac{S_H}{z(z-1)} + \frac{(1-q)S_H}{z(z-q)(z-1)} = -\frac{S_H}{z(z-q)}. \tag{XII.5.91}$$

Combining this with the two double poles gives

$$\begin{aligned} \frac{m_0^2}{z^2} + \frac{m_q^2}{(z-q)^2} - \frac{S_H}{z(z-q)} &= \frac{qz(m_q^2 - m_0^2) + q^2 m_0^2}{z^2(z-q)^2} \\ &= \frac{\Lambda^2(1+m/H)^2/4 - \Lambda m z}{z^2(z-\Lambda/H)^2}. \end{aligned} \tag{XII.5.92}$$

In the last line we used $m_q^2 - m_0^2 = -Hm$. The apparent H^2 terms have disappeared. The complete finite H expression is

$$\begin{aligned} \phi_H(z) = \frac{\Lambda^2(1+m/H)^2/4 - \Lambda m z}{z^2(z-\Lambda/H)^2} + \frac{b^2}{(z-1)^2} + \frac{c^2 - b^2}{z(z-1)} \\ - \frac{\widehat{U}}{z(z-\Lambda/H)(z-1)}. \end{aligned} \tag{XII.5.93}$$

Every coefficient now has a finite limit at a fixed base point away from the ends. Taking that limit and decomposing the last term into its double and simple pole parts gives

$$\begin{aligned} Q_3 &= \phi_3(z)\, dz^2, \\ \phi_3(z) &= \frac{\Lambda^2}{4z^4} - \frac{\Lambda m}{z^3} + \frac{\widehat{U}}{z^2} + \frac{b^2}{(z-1)^2} - \frac{b^2 - c^2 + \widehat{U}}{z(z-1)}. \end{aligned} \tag{XII.5.94}$$

The two ordinary ends at $0, q$ have produced a fourth-order pole at 0. The ordinary ends at $1, \infty$ remain. The allowed pole orders are $(4, 2, 2)$; the last two poles are exactly double when $b, c \neq 0$, as we assume on the smooth interior-root locus below.

The linear subtraction in H is as necessary as the quadratic one. For example, use $U = S_H - \widehat{U}$, omitting only the term $-qS_H$. The resulting differential differs from (XII.5.93) by qS_H/P. At a fixed point away from the limiting ends,

$$\frac{\phi_{\text{wrong}}}{H} \longrightarrow \frac{\Lambda}{2z^2(z-1)} \neq 0. \tag{XII.5.95}$$

It has no finite limit there. This failed subtraction explains why the finite Coulomb direction must be followed while the end masses change. The fixed-mass neck expansion in (XII.5.55) held a different set of parameters fixed and cannot be applied along this path of diverging masses.

We can identify the resulting family by comparing the whole differential, including its finite coefficient, with the usual three-flavor curve. Put $t = 1/z$, so $x_t = -z^2 x_z$ and $x_t dt = x_z dz$. Introduce the translated parameters

$$\Lambda_G = \frac{\Lambda}{2}, \qquad m_G = -m, \qquad u_G = 2(b^2 + c^2 - \widehat{U}) - \Lambda m, \qquad m_+ = c, \quad m_- = b. \tag{XII.5.96}$$

Substitution in $\phi_t = t^{-4}\phi_3(1/t)$ gives

$$\phi_t(t) = \frac{m_+^2}{t^2} + \frac{m_-^2}{(t-1)^2} + \frac{2\Lambda_G m_G + u_G}{2t} + \frac{2\Lambda_G m_G - u_G}{2(t-1)} + \Lambda_G^2. \tag{XII.5.97}$$

This is the standard $SU(2)$, $N_f = 3$ differential in the convention with its irregular end at infinity. In the direct IIB construction it supplies the protected three-flavor period geometry. The equality uses the tensor factor t^{-4}, the cotangent sign and the displayed shift of the Coulomb coefficient. It is a comparison of complete one-form families, extending the pole-order test to the actual gauge-theory curve. The geometric definition $\Lambda = qH$ fixes our scale convention; it does not specify an exact microscopic instanton coordinate for the parent.

XII.5.9 The irregular end and its finite Coulomb variation

Which data must now be held fixed at the new end? The answer is visible in the one-form that measures the wrapped-sphere period. The limiting base is $C_3 = \mathbb{P}^1 \setminus \{0, 1, \infty\}$, and the enlarged allowed space is

$$Q_3 \in H^0\big(\mathbb{P}^1, K_{\mathbb{P}^1}^2(4[0] + 2[1] + 2[\infty])\big), \qquad K_{\mathbb{P}^1}^2(4[0]+2[1]+2[\infty]) \simeq \mathcal{O}(4). \tag{XII.5.98}$$

There are still five differential coefficients before fixing the end data. The larger allowance at zero replaces two ordinary ends. On C_3 the covector bundle and residue

calculation are the same as before; the ALE equation is $uv + x^2 = \phi_3$ in a local frame. The change is the prescribed asymptotic behavior at the removed point, which is called an irregular end.

To determine that behavior, write the root near zero as $x = A/z^2 + B/z + C + O(z)$. Matching the first three powers of $x^2 = \phi_3$ gives

$$A^2 = \frac{\Lambda^2}{4}, \qquad 2AB = -\Lambda m, \qquad B^2 + 2AC = \widehat{U}. \tag{XII.5.99}$$

Choose the sheet with $A = \Lambda/2$. The other coefficients then follow without a further sign choice:

$$B = -m, \qquad C = \frac{\widehat{U} - m^2}{\Lambda}, \qquad \lambda_+ = \left[\frac{\Lambda}{2z^2} - \frac{m}{z} + \frac{\widehat{U} - m^2}{\Lambda} + O(z)\right] dz. \tag{XII.5.100}$$

The other sheet has $\lambda_- = -\lambda_+$. The leading pole in the one-form has order two, while its residue is $-m$. Only the residue contributes to a small loop:

$$\frac{\Lambda}{2z^2}\, dz = d\!\left(-\frac{\Lambda}{2z}\right), \qquad \oint_{0,+} \lambda = -2\pi i m. \tag{XII.5.101}$$

The stronger pole is locally exact, but it still fixes the asymptotic fiber behavior. Its absence from a loop integral does not make Λ an interior parameter.

For example, take $\Lambda = 2$, $m = 3$ and $\widehat{U} = 11$, with nonzero b, c held fixed. The first three root coefficients are $(1, -3, 1)$, and indeed

$$\left(\frac{1}{z^2} - \frac{3}{z} + 1\right)^2 = \frac{1}{z^4} - \frac{6}{z^3} + \frac{11}{z^2} - \frac{6}{z} + 1. \tag{XII.5.102}$$

The simple-pole and regular terms of $x^2 = \phi_3$ also involve higher coefficients in the expansion of x; the three leading equations already determine the fixed polar part of λ. Raising $\widehat{U}$ to 13 changes the constant root coefficient to 2 while preserving both poles of λ. Thus changing the vacuum can leave the irregular end fixed.

At an irregular end the boundary prescription fixes this polar part of λ, so both Λ and m are fixed. In terms of Q_3, these are its coefficients of z^{-4} and z^{-3}. The ordinary-end residues at $1, \infty$ fix b, c up to the sheet signs. In particular, the old logarithmic end frame cannot make this new equation regular:

$$z^2\phi_3(z) = \frac{\Lambda^2}{4z^2} - \frac{\Lambda m}{z} + \widehat{U} + O(z). \tag{XII.5.103}$$

Since $\Lambda \neq 0$, its leading divergence remains in that frame. A regular invertible change of base coordinate preserves the fourth-order pole of Q_3. The confluence changes the boundary problem, although the interior residue construction continues to apply.

We can count the finite Coulomb direction explicitly. Set $Y = z^2(z-1)x$. The compact spectral equation and its polynomial are

$$\begin{aligned} Y^2 = N_3(z), \qquad N_3(z) &= c^2 z^4 + (b^2 - c^2 - \Lambda m - \widehat{U}) z^3 \\ &\quad + \left(\frac{\Lambda^2}{4} + 2\Lambda m + \widehat{U}\right) z^2 - \left(\frac{\Lambda^2}{2} + \Lambda m\right) z + \frac{\Lambda^2}{4}. \end{aligned} \tag{XII.5.104}$$

Its degree is at most four and is exactly four for $c \neq 0$. Writing $N_3 = \sum_{j=0}^{4} n_j z^j$, the fixed end conditions are

$$n_0 = \frac{\Lambda^2}{4}, \qquad n_1 = -\frac{\Lambda^2}{2} - \Lambda m, \qquad \sum_{j=0}^{4} n_j = b^2, \qquad n_4 = c^2. \tag{XII.5.105}$$

The first, second and fourth constraints fix three separate coefficients. The third fixes the sum of the two that remain. They have rank four on the five polynomial coefficients, leaving one direction:

$$\partial_{\widehat{U}} N_3 = z^2 - z^3 = -z^2(z-1), \qquad \partial_{\widehat{U}} \lambda = -\frac{dz}{2Y}. \tag{XII.5.106}$$

On the locus with four simple roots away from $0, 1, \infty$, the compact double cover has genus one. Three marked base positions have no remaining complex modulus after Möbius transformations. The new family instead carries the fixed dimensionful scale Λ, with

$$[\Lambda] = [m] = [b] = [c] = 1, \qquad [\widehat{U}] = 2. \tag{XII.5.107}$$

The variation in (XII.5.106) is regular at every point of the compact curve. On the selected sheet at zero, $Y \to -\Lambda/2$. At the ordinary ends, with compatible local sheet choices, $Y(1) = b$ and $Y \sim cz^2$ near infinity. Therefore

$$\partial_{\widehat{U}} \lambda \sim \frac{dz}{\Lambda} \quad (z \to 0), \qquad \partial_{\widehat{U}} \lambda \sim -\frac{dz}{2b} \quad (z \to 1), \qquad \partial_{\widehat{U}} \lambda \sim \frac{dt}{2c} \quad (t = 1/z \to 0). \tag{XII.5.108}$$

At a simple branch point the coordinate $z - r = s^2$ cancels the simple zero of Y against $dz = 2s\,ds$, as in the four-ended case. Hence this variation is the single holomorphic one-form of the compact genus-one curve.

Changing the polar part gives a different kinetic behavior. A variation of m at fixed Λ has leading form $-\delta m\, dz/z$; a variation of Λ at fixed m has leading form $\delta\Lambda\, dz/(2z^2)$. For the reduced norm on one sheet of an annulus $\epsilon < |z| < R$, their respective leading polar contributions are

$$\|\delta_m \lambda\|^2_{\text{polar}} = 2\pi |\delta m|^2 \int_\epsilon^R \frac{dr}{r} = 2\pi |\delta m|^2 \log(R/\epsilon), \tag{XII.5.109}$$

$$\|\delta_\Lambda \lambda\|^2_{\text{polar}} = \frac{\pi}{2} |\delta\Lambda|^2 \int_\epsilon^R \frac{dr}{r^3} = \frac{\pi}{4} |\delta\Lambda|^2 (\epsilon^{-2} - R^{-2}). \tag{XII.5.110}$$

The opposite sheet adds the same positive divergences. By holding these polar coefficients fixed, the $\widehat{U}$ variation removes both singular terms and has finite reduced norm. This identifies the finite variation within the spectral period problem; a full threefold metric norm remains a separate question.

XII.5.10 Compact periods that survive the confluence

Where are the finite wrapped-sphere periods after the two ends coalesce? We can follow compact cycles whose caps remain at simple interior zeros. Introduce the finite H

polynomial using the same denominator as the original four-ended curve:

$$P_H = z(z - \Lambda/H)(z - 1), \qquad N_H = P_H^2 \phi_H, \qquad \lambda_H = \frac{\sqrt{N_H}}{P_H}\, dz. \tag{XII.5.111}$$

Multiplying (XII.5.93) out gives

$$\begin{aligned} N_H = {} & \left[\frac{\Lambda^2}{4}(1 + m/H)^2 - \Lambda m z\right](z - 1)^2 + b^2 z^2 (z - \Lambda/H)^2 \\ & + (c^2 - b^2) z (z - \Lambda/H)^2 (z - 1) - \widehat{U} z (z - \Lambda/H)(z - 1). \end{aligned} \tag{XII.5.112}$$

It has degree at most four, and every coefficient converges to the corresponding coefficient of N_3 at rate $O(H^{-1})$. In a neighborhood of any simple root r_j of N_3, the nonzero derivative $N_3'(r_j)$ ensures a unique nearby root $r_j(H)$ for sufficiently large H. Thus

$$r_j(H) = r_j + O(H^{-1}), \qquad \lambda_H \longrightarrow \lambda_3 = \frac{\sqrt{N_3}}{z^2(z - 1)}\, dz \tag{XII.5.113}$$

away from the ends and branch points, with a consistently chosen sheet. This excludes a collision of roots or a root reaching an end, where a different local limit would be required.

Choose a closed spectral contour around a pair of roots, avoiding the ends, and transport it while H increases. Its projected contour can remain a fixed positive distance from every branch point. On that contour the convergence in (XII.5.113) is uniform, including the chosen square root. Consequently its compact period satisfies

$$\Pi_\gamma(H) = \oint_{\gamma(H)} \lambda_H = \oint_{\gamma(\infty)} \lambda_3 + O(H^{-1}). \tag{XII.5.114}$$

The same homology class can be represented by the two lifts of an arc joining the chosen zeros. The collapsing ALE spheres cap the arc at both ends, giving the compact three-cycle of (XII.5.20). The period limit therefore has a direct threefold interpretation. The heavy-mass operation needs no additional common rescaling of these periods.

An explicit example shows both the moving caps and the finite integrals. Take

$$\Lambda = 1, \qquad m = \frac{10}{3}, \qquad \widehat{U} = \frac{47}{4}, \qquad b^2 = \frac{7}{4}, \qquad c^2 = \frac{64}{3}. \tag{XII.5.115}$$

The two residue signs can be chosen as $b = \sqrt{7}/2$, $c = 8/\sqrt{3}$; they do not affect the branch locations. Substitution in (XII.5.104) gives

$$\begin{aligned} N_3(z) &= \frac{64}{3} z^4 - \frac{104}{3} z^3 + \frac{56}{3} z^2 - \frac{23}{6} z + \frac{1}{4} \\ &= \frac{64}{3}(z - 1/8)(z - 1/4)(z - 1/2)(z - 3/4). \end{aligned} \tag{XII.5.116}$$

All four roots are simple interior points, distinct from the limiting ends. Also $N_3(0) = 1/4$, $N_3(1) = 7/4$ and its leading coefficient is $64/3$, so the limiting end conditions agree

with the chosen parameters. At $H = 1000$, the actual finite H roots of (XII.5.112) are approximately

$$(r_1(H), r_2(H), r_3(H), r_4(H)) = (0.12583455,\ 0.24846882,\ 0.50387068,\ 0.74882595). \tag{XII.5.117}$$

The ordinary mark $q = 0.001$ lies well to their left. The two chosen arcs stay in the interior as their endpoints approach the limiting positions in Figure XII.5.3.

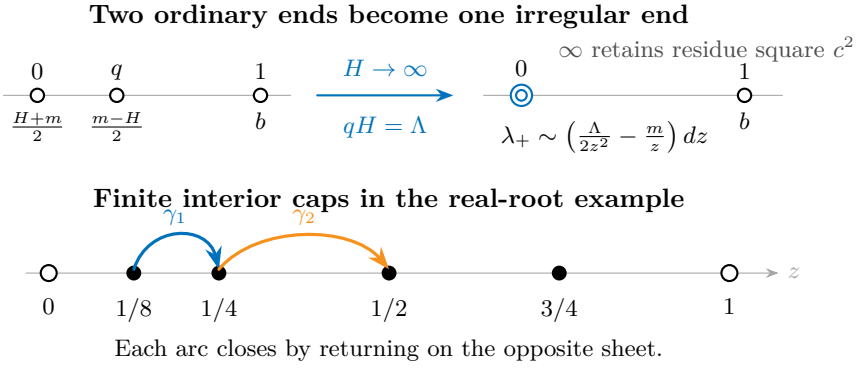


Figure XII.5.3: End confluence and retained compact arcs. Top: the ordinary marks at $0, q$, with signed mass parameters $(H + m)/2$ and $(m - H)/2$, approach each other as $q = \Lambda/H$. Their limit has a fourth-order pole of Q_3, with fixed one-form polar coefficients $\Lambda/2$ and $-m$. The ordinary ends at $1, \infty$ remain. Bottom: for (XII.5.115), the four filled points are the limiting simple zeros. The highlighted arcs join $1/8$ to $1/4$, and $1/4$ to $1/2$. Each arc represents a cycle by going forward on one spectral sheet and backward on the other; the ALE sphere caps it at both endpoints. The open circles are removed ends.

The interval signs determine useful phase choices for a direct integral. The real polynomial N_3 is negative between $1/8, 1/4$, and positive between $1/4, 1/2$. On these intervals choose $\sqrt{N_3} = i\sqrt{-N_3}$ and $\sqrt{N_3} = \sqrt{N_3}_{\,\text{positive}}$, respectively. For the forward arc and backward opposite lift, the doubled periods are

$$\Pi_1 = 2i \int_{1/8}^{1/4} \frac{\sqrt{-N_3(z)}}{z^2(z-1)}\, dz, \tag{XII.5.118}$$

$$\Pi_2 = 2 \int_{1/4}^{1/2} \frac{\sqrt{N_3(z)}_{\,\text{positive}}}{z^2(z-1)}\, dz. \tag{XII.5.119}$$

The denominator is negative on both intervals. Hence Π_1 has negative imaginary part and Π_2 is negative real. These signs specify the two cycle phases; they do not assign a primitive electric and magnetic basis. The factor two measures the sheet difference and agrees with the normalized threefold integral.

These definite integrals can be evaluated without endpoint singularities. On either

interval $[r_j, r_{j+1}]$ put

$$z = r_j + (r_{j+1} - r_j)\sin^2\theta, \qquad dz = 2(r_{j+1} - r_j)\sin\theta\cos\theta\, d\theta, \qquad 0 \le \theta \le \frac{\pi}{2}. \tag{XII.5.120}$$

The root vanishes linearly in $\sin\theta$ or $\cos\theta$ at an endpoint; the Jacobian supplies another such factor. There is no denominator zero on the interval. The result in the relative period units of this chapter is

$$\Pi_1 = -0.9189595852702201\, i, \qquad \Pi_2 = -0.8127760063238480. \tag{XII.5.121}$$

Repeating the integral with the four real roots of N_H, the denominator P_H and the transported phases gives

H	$\Pi_1(H)/i$	$\Pi_2(H)$	$\max_j \lvert\Pi_j(H) - \Pi_j\rvert$
10^3	-0.894660812	-0.845678969	0.032902963
10^4	-0.916523500	-0.816056722	0.003280716
10^5	-0.918715914	-0.813103983	0.000327977

(XII.5.122)

The errors decrease by about ten when H increases by ten, as the coefficient estimate predicts. Both limiting periods are nonzero. The compact contours and the simple-root condition explain this limit; the numerical integrals show its size for a changed set of masses, beyond the massless elliptic example.

End loops behave differently along this operation. At each finite H, a single-sheet loop about zero still measures $\pm 2\pi i m_0$, and a loop about q measures $\pm 2\pi i m_q$. Their leading terms are

$$\oint_{0,\pm} \lambda_H \sim \pm\pi i H, \qquad \oint_{q,\pm} \lambda_H \sim \mp\pi i H. \tag{XII.5.123}$$

They are outside the finite compact-period sector just followed. The finite residue $-m$ of the new end records a remaining flavor parameter. The compact calculation need not classify every linear combination of end charges to retain its selected period pair.

With the sourced matter interpretation, the low-energy theory has the three finite full-hyper masses $m, b+c, b-c$. In the normalization of (XII.5.78), its one-loop coefficient is

$$b_0 = 2h^\vee_{\mathfrak{su}(2)} - 3 = 4 - 3 = 1. \tag{XII.5.124}$$

This is the asymptotically free gauge sector associated with the limiting differential. A dimensionful end scale has replaced the parent's marginal marked-base parameter. To realize these finite periods as an isolated IIB field theory, the string, Kaluza–Klein and bulk conditions in (XII.5.82) must also hold for the limiting end sector. The rational-function limit establishes the protected geometry and its finite cycles; the assumed physical isolation and common D3 conversion relate those periods to retained particle central charges.

XII.5.11 Exercises

For each problem, explain the geometry or derivation in addition to giving the requested data. Polynomial coefficient vectors are ordered from constant term to leading coefficient.

1. **Separate boundary and interior coefficients.**
   In (XII.5.28) set $q = 1/2$, $U = 7$, and use the masses $(m_0, m_q, m_1, m_\infty) = (1, 2, 3, 4)$. Compute all five coefficients of $N = P^2\phi_z$ and the dimensions of the fixed-mass affine family and the ordered marked-base moduli. Explain why the leading coefficient is independent of the finite end data and why adding a multiple of P preserves all four squares.

2. **Keep both components of the weak limit.** Take $(m_0, m_q, m_1, m_\infty) = (2, 5, 4, 9)$ and $U = 7$, and pinch $q \to 0$. Give the shared square and the three numerator coefficients for each trinion in its own coordinate after multiplication by $t^2(t-1)^2$. Then hold the external masses fixed and vary the node square to find each pair of thresholds. Explain why the node residues have opposite signs on a matched sheet.

3. **Diagnose a pole.** At a marked end $t = 0$, compare three quadratic differentials with nonzero leading coefficients of pole orders two, one, and three. Give the order of λ as a one-form on the smooth sheet or local normalization, using t in the even case and $t = r^2$ in the odd cases. Use a negative order for a pole. Explain which odd case can arise as the zero-mass limit of an ordinary mark and why.

4. **Compare equivalent presentations.** Take zero masses, $q = 1/3$, and $U = 6$. Under $w = 1/z$ rewrite the differential as $U'dw^2/[w(w-1)(w-q')]$, where q' is the free mark after re-normalizing the order to $(0, q', 1, \infty)$ with the roles of old zero and infinity exchanged. Give q', U', and the same-sheet ratio x_w/x_z at $z = 2$. Explain why the cotangent transformation preserves the spectral and tautological descriptions and what that comparison leaves undetermined about the charge lattice.

The following two written problems extend the method. They are assessed through the derivation rather than the numerical submissions above.

5. **A singular vacuum at fixed ends.** Set $q = 1/2$ and all four masses equal to 1. Starting from (XII.5.28), reconstruct (XII.5.42) and factor it at $U = -2, 0, 2$. Check that the four end squares stay fixed. Explain why these degenerations are obtained by changing a vacuum parameter, whereas the weak tube changes the marked base. Identify the smooth-family hypothesis that fails at the three exceptional values. State what the discriminant cannot determine about stable particles.

6. **A local collision period.** Use the oriented local model (XII.5.21), with the forward sheet $s = i\sqrt{c}\sqrt{\delta - h^2}$. Derive the normalized sweep period and its response to $\delta \mapsto 4\delta$ and to an orientation reversal. Compare this change with the branch-point separation. Explain why the integral by itself does not establish a stable wrapped-D3 particle.

Status and sources

§XII.5.2. The transitions and residue charts (XII.5.2)–(XII.5.7) are [MATH]. The bundle and threefold are those of Alim et al. (2013, arXiv v2, §3, eqs. (3.1)–(3.5)) with the sign of v reversed to match our equation and the base coordinate renamed z. The singularity and gradient quotient (XII.5.9) and (XII.5.10) are [MATH]; see Xie and Yau (2015, arXiv v1, §4.4, eqs. (4.23)–(4.25)) for the nonisolated ALE setting. The global fixture here uses the bundle transitions rather than the polynomial in that overview.

§XII.5.3. The oriented integral and signed difference (XII.5.15)–(XII.5.20) are [MATH]. The local quadratic collision (XII.5.21)–(XII.5.22) is a further oriented integral within that local model; no stable-particle count is assigned. See Klemm et al. (1996, arXiv v3, §§2, 3.1, eqs. (2.13)–(2.15) and (3.2)–(3.4)) and Gaiotto et al. (2009, arXiv v2, §3.3, printed pp. 57–58). We display the two-sheet difference with the raw residue normalization explicit; in Alim et al. (2013, arXiv v2, eq. (3.6)) the reduced form is written as a one-sheet differential with a normalization choice. The physical wrapped-D3 dictionary in (XII.5.23) is [GEO-E]; see Alim et al. (2013, arXiv v2, eqs. (3.7)–(3.9)). The common conversion accommodates the house $\sqrt{2}$ central-charge convention.

§XII.5.4. The regular-end expansions, quartic evaluation and ordered base count (XII.5.24)–(XII.5.33) are [MATH]. The explicit evaluation map (XII.5.31) and simple-root motion (XII.5.37) are consequences of the same fixed-end family. The four-pole input is Gaiotto (2009b, arXiv v1, §2.2, eq. (2.18)) in a chart with one mark at infinity; see also Gaiotto et al. (2009, arXiv v2, §4.1, eqs. (4.1)–(4.4)) on boundary conditions. The affine coordinate U uses (XII.5.28), without importing the intermediate completed square of Gaiotto's eq. (2.17).

§XII.5.5. The compact genus and fixed-end variation in (XII.5.39)–(XII.5.45) are [MATH]. The equal-mass family, its discriminant and perfect-square degenerations (XII.5.42)–(XII.5.44) are additional algebraic consequences at fixed $q = 1/2$; they carry no claim about BPS multiplicity. The assignment of the reduced finite variation and fixed masses to the IIB sector is [GEO-E]; see Alim et al. (2013, arXiv v2, §3, eqs. (3.3)–(3.6)) and Gaiotto et al. (2009, arXiv v2, §3.1.5, eqs. (3.20)–(3.23) and §10.7, eq. (10.21)). The norm in the former section of the latter source is part of its M5 description. Here the norm calculation is on the spectral curve, with no full threefold metric claim.

§XII.5.6. The two scaled charts, neck periods and Legendre control (XII.5.49)–(XII.5.67) are [MATH]. Compare Gaiotto (2009b, arXiv v1, §2.2, eqs. (2.3)–(2.12) and the degeneration following eq. (2.20)). The coefficient in (XII.5.62) refers to the compact spectral frame only. The balanced-radius estimate and massless changes of scale in (XII.5.57)–(XII.5.58) and (XII.5.68)–(XII.5.69) are consequences of those formulas.

§XII.5.7. The threshold factorization is [MATH]. The weak ordinary-end matter and diagonal gauging in (XII.5.73)–(XII.5.76) are [GEO-E], from Alim et al. (2013, arXiv v2, §§3.4.2, 4.5–4.5.1, printed pp. 30 and 42) and Gaiotto (2009b, arXiv v1, §2.1 and eq. (2.21)). The one-loop arithmetic is [MATH], conditional on that matter content. The physical marginal-coordinate assignment at zero masses is [GEO-E]; see Gaiotto, eqs. (2.10)–(2.12), and Gaiotto et al. (2009, arXiv v2, eq. (10.21)). The algebraic period scaling (XII.5.79) is [MATH]; isolation in (XII.5.80) is [DEC], with the scaling premise of Gaiotto et al. (2009, arXiv v2, §3.3, printed pp. 57–58). The characteristic polynomial and same-sheet inversion (XII.5.83)–(XII.5.85) are [MATH]; compare Gaiotto (2009b, arXiv v1, eqs. (2.12), (2.18) and §2.3).

§XII.5.8. The heavy-mass tuning, exact finite-H identity and differential limit (XII.5.86)–(XII.5.95) are [MATH]. The fixed finite coefficient $\widehat{U}$ is distinct from the ALE fiber coordinate. The complete source translation (XII.5.96)–(XII.5.97) is an equality of differential families

with Gaiotto et al. (2009, arXiv v2, §10.6, eq. (10.19), printed p. 134). Its $SU(2)$, $N_f = 3$ interpretation is [GEO-E], using the direct IIB construction of the same source's §3.3. The heavy-flavor confluence is also described in Gaiotto (2009a, arXiv v1, introduction and §6, eq. (6.1)). No exact parent instanton coordinate or absolute strong-scale normalization is inferred. Allowed pole orders are bounded by $(4, 2, 2)$, with ordinary double poles for nonzero b, c.

§XII.5.9. The root expansion, fixed-end polynomial constraints, compact rank and reduced norms (XII.5.99)–(XII.5.110) are [MATH] on the stated loci. The boundary prescription of fixing the polar part of $\sqrt{\phi}$ is sourced from Gaiotto (2009a, arXiv v1, §7, printed p. 6). The numerator has degree at most four; the smooth four-interior-root locus used for compact transport has $b, c \neq 0$. Spectral norm finiteness remains distinct from a complete threefold L^2 statement.

§XII.5.10. Coefficientwise convergence, smooth compact-cycle transport and the explicit signed periods (XII.5.111)–(XII.5.123) are [MATH]. The finite-H identity, three-coefficient square-root calculation, end constraints and norm integrals are checked symbolically. Direct quadrature checks both signed limiting periods and three finite values of H, including sheet-factor and phase controls. The three surviving full-hyper masses and the conditional one-loop arithmetic (XII.5.124) are algebraic consequences using the sourced matter dictionary. The $N_f = 3$ physical interpretation is [GEO-E], while isolation of the limiting local sector remains [DEC]. Neither primitive charge lattices, a complete end-charge classification nor a BPS stability chamber is supplied by these compact periods. The inspected source anchors are the actual versioned PDF pages specified above; the conformal-block and WKB spectrum results of those papers are outside this chapter's construction.

References

Alim, M. et al. (2013). "BPS Quivers and Spectra of Complete $\mathcal{N} = 2$ Quantum Field Theories". In: *Commun. Math. Phys.* 323.3, pp. 1185–1227. DOI: 10.1007/s00220-013-1789-8. arXiv: 1109.4941 [hep-th].

Gaiotto, D. (2009a). *Asymptotically free $\mathcal{N} = 2$ theories and irregular conformal blocks*. arXiv: 0908.0307 [hep-th].

Gaiotto, D. (2009b). "N=2 Dualities". In: arXiv: 0904.2715 [hep-th].

Gaiotto, D., G. W. Moore, and A. Neitzke (2009). *Wall-crossing, Hitchin Systems, and the WKB Approximation*. arXiv: 0907.3987 [hep-th].

Klemm, A. et al. (1996). "Self-dual strings and $\mathcal{N} = 2$ supersymmetric field theory". In: *Nucl. Phys. B* 477, pp. 746–766. arXiv: hep-th/9604034.

Xie, D. and S.-T. Yau (2015). *4d $\mathcal{N} = 2$ SCFT and singularity theory Part I: Classification*. DOI: 10.48550/arXiv.1510.01324. arXiv: 1510.01324 [hep-th].

Chapter XII.6

Marginal families, discriminants, and local RG limits

XII.6.1 Two ways to change a singularity

In the hypersurface construction of Chapter 3, the Jacobi algebra tells us what can be varied in the equation. The residue of the threefold tells us which variations introduce a scale. Here we use both tools on a suspension of a binary quartic. Its mixed quartic term has the same weight as its two pure quartic terms. We can therefore move its coefficient while keeping the same scaling action. The first problem is to find where this family of isolated singularities breaks down, and to count the independent deformations elsewhere.

A mass deformation changes the problem. We now choose a fiber of the deformed equation, locate a singular point on that fiber, and scale about it. In the example below one quartic variable acquires a quadratic term and the other does not. The resulting local geometry has a new scaling action and a smaller deformation space. Tracking the coefficient of the surviving quadratic monomial through the two calculations will show why its ultraviolet and infrared dimensions differ.

The reader should be able to start with a permitted value of the quartic coefficient, compute its deformation dimensions, and then repeat the local calculation at a fixed nonzero mass coefficient. The tools needed are the Jacobi quotient and period normalization of Chapter 3, and the distinction between a singular central fiber and nearby smooth fibers from Chapter 4. The main new step is to keep track of three choices in order: the fiber, the point on that fiber, and the scaling used to resolve its neighborhood.

We then compare a second mass with a relevant cubic coupling. Their critical fibers and compact periods connect a D_5 principal sector to the A_3 germ and its finer node limit.

XII.6.2 The isolated part of the quartic family

When does the origin stop being an isolated singular point? We take complex coordinates (x, y, z, w), work at finite $\lambda \in \mathbb{C}$, and use the zero fiber of the polynomial

$$f_\lambda = x^2 + y^2 + g_\lambda(z, w), \qquad g_\lambda(z, w) = z^4 + \lambda z^2 w^2 + w^4. \tag{XII.6.1}$$

The quadratic variables are spectators in the isolation test: their derivatives force $x = y = 0$. The weights $q = (1/2, 1/2, 1/4, 1/4)$ give f_λ degree one at fixed λ. With $D_q = \sum_{v=x,y,z,w} q_v v\partial_v$, the weighted Euler identity reads

$$D_q f_\lambda = f_\lambda. \tag{XII.6.2}$$

Thus every critical point is on the central fiber. We will need to check the fiber condition again once the equation contains terms of different weights.

The remaining derivative equations are

$$z(2z^2 + \lambda w^2) = 0, \qquad w(2w^2 + \lambda z^2) = 0. \tag{XII.6.3}$$

If either variable is zero, the other equation forces the other variable to be zero. A nonzero critical point must then give a nonzero solution for the squared coordinates:

$$\begin{pmatrix} 2 & \lambda \\ \lambda & 2 \end{pmatrix} \begin{pmatrix} z^2 \\ w^2 \end{pmatrix} = 0, \qquad \det = 4 - \lambda^2. \tag{XII.6.4}$$

At $\lambda = 0$ the equations are just $z^3 = w^3 = 0$, so the Fermat quartic is an isolated example. At the two exceptional values the binary form becomes a square:

$$\begin{aligned} g_{-2} &= (z^2 - w^2)^2, \quad z = \pm w, \\ g_2 &= (z^2 + w^2)^2, \quad z = \pm iw. \end{aligned} \tag{XII.6.5}$$

Each indicated direction gives a whole line of singular points with $x = y = 0$, including arbitrarily small points. These lines explain the loss of isolation.

To see the same event in the projective directions of the (z, w)-plane, use $t = z/w$. The direction $w = 0$ is not a root, since $g_\lambda(z, 0) = z^4$. The binary form in the remaining chart becomes the monic polynomial

$$P_\lambda(t) = t^4 + \lambda t^2 + 1, \qquad P'_\lambda(t) = 4t(t^2 + \lambda/2). \tag{XII.6.6}$$

A repeated root means a binary direction at which the derivative also vanishes. In a resultant, we can evaluate P_λ at the three roots of its derivative, counted with multiplicity. At $t = 0$ its value is one. At either root of $t^2 = -\lambda/2$, it is $1 - \lambda^2/4$. The leading coefficient of the derivative contributes 4^4. The sign of the resultant under exchanging the two polynomials is $(-1)^{4\cdot 3} = 1$, and the discriminant sign for a monic quartic is $(-1)^6 = 1$. Hence

$$\operatorname{disc}(P_\lambda) = \operatorname{Res}_t(P_\lambda, P'_\lambda) = 4^4 \left(1 - \frac{\lambda^2}{4}\right)^2 = 16(\lambda^2 - 4)^2. \tag{XII.6.7}$$

There is a useful way to follow the roots before they collide. Set $v = t^2$. The four roots of P_λ come from two roots of a quadratic, followed by taking both square roots:

$$v_\pm = \frac{-\lambda \pm \sqrt{\lambda^2 - 4}}{2}, \qquad v_+ v_- = 1, \qquad t = \pm\sqrt{v_+},\ \pm\sqrt{v_-}. \tag{XII.6.8}$$

For finite λ, neither $v_\pm$ is zero. The only possible collision is therefore $v_+ = v_-$. Each of the two square roots then becomes double, which accounts for the square of $\lambda^2 - 4$ in the quartic discriminant. Choosing a branch of the square root in this expression only orders the roots; it does not change their set.

For a changed isolated input, take $\lambda = 1$. The quadratic roots are the two nontrivial cube roots of unity, so the four binary directions are

$$v_\pm = e^{\pm 2\pi i/3}, \qquad \{t : P_1(t) = 0\} = \{e^{i\pi/3}, e^{2i\pi/3}, e^{4i\pi/3}, e^{5i\pi/3}\}, \qquad \operatorname{disc}(P_1) = 144. \tag{XII.6.9}$$

All four roots are distinct. A root of the binary form is a direction on the quartic zero set; it becomes a singular direction only when the derivative vanishes there as well. This explains why following the roots is a convenient picture of the isolation test, while counting roots of P_λ alone is insufficient.

This calculation also holds at $\lambda = 0$, when all three derivative roots coincide at zero. Figure XII.6.1 compares that isolated example with the two collisions. The threefold central fiber already has a singularity at the origin for every λ. The binary discriminant detects the values at which it acquires singular lines.

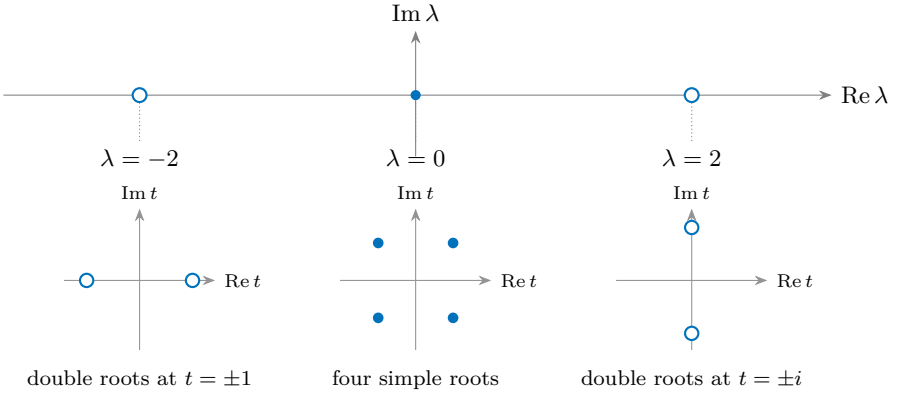


Figure XII.6.1: The finite parameter plane (top) and the binary root chart $t = z/w$ at three selected parameters (bottom). Filled dots mark simple roots and rings mark double roots. The double roots give the slopes of the two singular lines in each exceptional fiber.

We restrict the next calculation to $\lambda^2 \neq 4$. Within this locus the two cubics in (XII.6.3) vanish together only at the origin. This fact both limits the degree of the independent deformations and lets us count them without choosing a different basis at each point of the family.

The exceptional lines also explain why a finite Jacobi count requires isolation. At $\lambda = -2$, evaluation on the line $z = w$ kills both derivative relations. It therefore defines a surjection

$$\frac{\mathbb{C}[z,w]}{\big(z(z^2-w^2),\, w(w^2-z^2)\big)} \longrightarrow \mathbb{C}[w], \qquad [h(z,w)] \longmapsto h(w,w). \tag{XII.6.10}$$

The target has independent powers of w of arbitrarily high degree. The source quotient must thus be infinite-dimensional. The same relation that obstructs an isolated singularity prevents the finite deformation count used below.

XII.6.3 Which deformations carry a scale?

How many independent deformations remain, and which preserve the degree-one scaling? An infinitesimal coordinate change adds a combination of the first derivatives of the equation. Multiplication of the equation by a unit adds a multiple of the equation itself. By (XII.6.2) the latter contributes no extra relation at the homogeneous base point. The first derivatives of $x^2 + y^2$ eliminate x, y from the Jacobi algebra. For the remaining variables we obtain

$$J_\lambda = \mathbb{C}[z,w]/(R_z, R_w), \qquad R_z = z^3 + \tfrac{\lambda}{2} z w^2, \qquad R_w = w^3 + \tfrac{\lambda}{2} z^2 w. \tag{XII.6.11}$$

The quotient is graded by the ordinary total degree $d = i + j$ of $z^i w^j$. Its cubic relations replace the pure cubes with mixed cubics. To see what happens one degree higher, write in the quotient

$$z^3 w = -\tfrac{\lambda}{2} z w^3 = \tfrac{\lambda^2}{4} z^3 w, \qquad z w^3 = -\tfrac{\lambda}{2} z^3 w. \tag{XII.6.12}$$

Since $1 - \lambda^2/4 \neq 0$, both monomials vanish. The pure fourth powers obey

$$z^4 = w^4 = -\tfrac{\lambda}{2} z^2 w^2, \qquad z(z^2 w^2) = w(z^2 w^2) = 0. \tag{XII.6.13}$$

In the last equality the two products are multiples of $z^3 w$ and $z w^3$, respectively. Thus $z^2 w^2$ spans degree four, and all monomials of higher degree vanish. Together with the relations in degree three this proves that the nine monomials $z^i w^j$, $0 \le i, j \le 2$, span the quotient.

For independence, the cubics R_z, R_w have no common factor: over $\mathbb{C}$ a common homogeneous factor would give a common zero on a line. In particular, after quotienting by R_z, multiplication by R_w has no kernel. To see this, if R_z divides $R_w h$ for a polynomial h, coprimality forces R_z to divide h. Each quotient by one of the cubics subtracts a degree-three shift of the Hilbert series of the preceding ring. With s the counting variable for total degree, this gives

$$H_{J_\lambda}(s) = \frac{(1-s^3)^2}{(1-s)^2} = (1+s+s^2)^2 = 1 + 2s + 3s^2 + 2s^3 + s^4. \tag{XII.6.14}$$

The sum of the coefficients is the Milnor number $\mu = 9$. It equals the number of spanning monomials, which therefore form a basis. At the Fermat point this can be

seen without a Hilbert series:

$$J_0 = \mathbb{C}[z]/(z^3) \otimes_{\mathbb{C}} \mathbb{C}[w]/(w^3). \tag{XII.6.15}$$

Here the two mixed cubics survive while both pure cubes are zero. Keeping the mixed cubics in the basis avoids losing these two directions at $\lambda = 0$.

The basis describes classes of perturbations rather than a ban on writing other monomials in the equation. For instance, at $\lambda = 1$ consider the quartic perturbation $h = z^4 + zw^3$. Reducing it gives

$$[z^4] = -\tfrac{1}{2}[z^2w^2], \qquad [zw^3] = 0, \qquad [h] = -\tfrac{1}{2}[z^2w^2] \quad \text{in } J_1. \tag{XII.6.16}$$

Thus an infinitesimal term ηh has the same first-order class as a shift $\delta\lambda = -\eta/2$. The removed terms are generated by infinitesimal coordinate changes. This is a statement about tangent directions at the chosen base equation; it does not identify finite polynomial families term by term.

Degree three illustrates why the choice of representatives matters. The relations give

$$\begin{pmatrix} [z^3] \\ [w^3] \end{pmatrix} = -\frac{\lambda}{2}\begin{pmatrix} 0 & 1 \\ 1 & 0 \end{pmatrix}\begin{pmatrix} [z^2w] \\ [zw^2] \end{pmatrix}, \qquad \det\left[-\frac{\lambda}{2}\begin{pmatrix} 0 & 1 \\ 1 & 0 \end{pmatrix}\right] = -\frac{\lambda^2}{4}. \tag{XII.6.17}$$

For $\lambda \neq 0$, either pair spans degree three on the isolated locus. At $\lambda = 0$, the pure cubes both vanish, while the mixed cubics remain independent. The degree-three space has not lost a dimension; the proposed pure-cube coordinates have ceased to describe it. Keeping the nine representatives in Table XII.6.1 avoids this coordinate failure.

Let u_{ij} multiply the representative z^iw^j in a deformation of (XII.6.1). Rescale the coordinates by $v \mapsto \rho^{q_v}v$, where ρ is the degree-one scaling parameter. If the varied polynomial is to transform with degree one under a combined action on coordinates and coefficients, the coefficient of z^iw^j must transform as

$$u_{ij} \longmapsto \rho^{1-(i+j)/4}u_{ij}. \tag{XII.6.18}$$

The residue $\Omega_F = \mathrm{Res}(dx\wedge dy\wedge dz\wedge dw/F)$ on the smooth locus scales by the coordinate volume factor divided by the equation's scaling factor. Here its geometric weight is

$$Q_\Omega = q_x + q_y + q_z + q_w - 1 = \tfrac{1}{2}. \tag{XII.6.19}$$

In the local IIB period prescription of Chapter 3, the periods of Ω_F set the mass scale, so $[\Omega_F] = 1$. One unit of geometric weight therefore counts as two units of mass dimension, and

$$[u_{ij}]_{\mathrm{UV}} = \frac{1-(i+j)/4}{Q_\Omega} = 2 - \frac{i+j}{2}. \tag{XII.6.20}$$

Jacobi representatives	d	$1-d/4$	$[u_{ij}]_{\mathrm{UV}}$	Local IIB role
1	0	1	2	Coulomb vev
z, w	1	$3/4$	$3/2$	Coulomb vevs
z^2, zw, w^2	2	$1/2$	1	Mass parameters
z^2w, zw^2	3	$1/4$	$1/2$	Relevant couplings
z^2w^2	4	0	0	Dimensionless parameter

Table XII.6.1: The nine deformations at any isolated finite member of the quartic family. The weight and dimension columns refer to the coefficients of the displayed representatives. The role column uses the local IIB parameter dictionary.

The dimension is that of the coefficient, not that of the monomial considered as a field-theory operator. Applying the local IIB role map gives three Coulomb expectation value coordinates above dimension one, three masses at dimension one, and two relevant coupling coefficients between zero and one. There is one dimensionless geometric direction. At a chosen base point its coordinate is u_{22}, which shifts λ rather than adding a second direction. We will use $a = u_{20}$, one of the dimension-one coefficients, to change the quadratic part of the local equation.

XII.6.4 From geometric parameters to physical couplings

A dimensionless coefficient changes the shape of a homogeneous equation without introducing a scale in that equation. Even as a coordinate on geometries it need not distinguish isomorphic members. Let $T(x, y, z, w) = (x, y, iz, w)$. Since $i^4 = 1$ and $i^2 = -1$, the pullbacks are

$$T^* f_\lambda = f_{-\lambda}, \qquad T^* \Omega_{f_\lambda} = i\, \Omega_{f_{-\lambda}}. \tag{XII.6.21}$$

The residue factor follows from the factor i in $d(iz)$. The two polynomials thus describe the same germ after a coordinate change. If one instead compactifies the *binary pencil*, one writes

$$[s : t] \longmapsto s(z^4 + w^4) + tz^2w^2, \qquad \lambda = t/s \quad (s \neq 0). \tag{XII.6.22}$$

The binary form at $s = 0$ has double roots on the two coordinate axes. This uses a different normalization of the pencil at its boundary; the coefficient of z^2w^2 in (XII.6.1) does not have a finite limit there with the other coefficients unchanged.

The residue factor in (XII.6.21) contains information beyond equality of the polynomial zero sets. If a compact cycle is transported by T between corresponding smooth local fibers, then the change-of-variables formula gives

$$\int_{T(\Gamma)} \Omega_{f_\lambda} = i \int_{\Gamma} \Omega_{f_{-\lambda}}. \tag{XII.6.23}$$

All periods compared in this way receive the same factor, so their ratios with nonzero denominator are unchanged and their complex phases rotate together. Determining a physical identification still requires the relevant charge and coupling information. This simple coordinate calculation only tells us how the local forms and their transported integrals transform.

A physical exactly marginal coupling parametrizes fixed points: the beta functions must continue to vanish as it varies. To describe a conformal manifold one must also establish which coupling values label the same physical theory. A weak gauge limit requires further information, such as a period calculation that identifies a gauge sector with a small coupling and specifies the matter to which it couples. The zero weight in Table XII.6.1, the coordinate change (XII.6.21), and the collisions of the binary roots answer geometric questions. The physical fixed-point and duality analyses belong to the planned atlas of four-dimensional SCFTs and the planned treatment of Class S duality webs. To obtain a different scaling geometry here, we hold λ fixed and turn on a.

XII.6.5 Zooming in on the tuned origin

Which singularity remains on the zero fiber after the chosen mass deformation? Fix finite λ with $\lambda^2 \neq 4$ and a nonzero complex a. Keep only the coefficient $a = u_{20}$ besides λ and set the constant deformation to zero:

$$F_a = f_\lambda + az^2, \qquad F_a = 0. \tag{XII.6.24}$$

Here a is a mass coefficient in the UV period frame. The zero level in (XII.6.24) selects the fiber on which we want to find the local geometry. Stationarity determines a point and its *critical value*, the value of F_a there. A stationary point is singular on the selected fiber only if that value is zero.

The new term has UV geometric weight $1/2$ with a held fixed. Applying the same Euler operator as before gives

$$D_q F_a = F_a - \tfrac{a}{2} z^2 \quad \Longrightarrow \quad F_a\big|_{dF_a=0} = \tfrac{a}{2} z^2. \tag{XII.6.25}$$

On the zero fiber this forces $z = 0$. The remaining gradient equations then give $x = y = w = 0$. To see where the other stationary points went, the nontrivial equations at $x = y = 0$ are

$$z(2z^2 + \lambda w^2 + a) = 0, \qquad w(2w^2 + \lambda z^2) = 0. \tag{XII.6.26}$$

If $w = 0$ and $z \neq 0$, the first equation gives $z^2 = -a/2$. If $zw \neq 0$, the second gives $w^2 = -\lambda z^2/2$; substitution in the first yields $(2 - \lambda^2/2)z^2 = -a$. The critical values now follow from (XII.6.25):

	z^2	w^2	F_a
$w = 0,\ z \neq 0$	$-a/2$	0	$-a^2/4$
$zw \neq 0$	$-2a/(4-\lambda^2)$	$\lambda a/(4-\lambda^2)$	$-a^2/(4-\lambda^2)$

(XII.6.27)

The second row is a separate branch only for $\lambda \neq 0$. At the Fermat point it reduces to the first. Either nonzero critical value could occur on another level set, but neither

is on the tuned zero fiber. This is why solving the gradient alone, as we did for the homogeneous family, would now give too many points.

For example, choose $a = 2$ and $\lambda = 1$. The axis branch has $z = \pm i, w = 0$; the mixed branch has $z = \pm 2i/\sqrt{3}$, $w = \pm\sqrt{2/3}$, with independent signs. Their critical values are

$$F_2(0, 0, \pm i, 0) = -1, \qquad F_2\left(0, 0, \pm\frac{2i}{\sqrt{3}}, \pm\sqrt{\frac{2}{3}}\right) = -\frac{4}{3}. \tag{XII.6.28}$$

Both sets solve the derivative equations. Neither lies on $F_2 = 0$. Adding a constant $c = 1$ or $c = 4/3$ to the polynomial would move the corresponding critical value to zero; the origin would then have value c and leave that fiber. The constant deformation selects a level of the same function, so it changes which stationary points are singularities of the chosen hypersurface.

Near the origin az^2 is quadratic along with x^2 and y^2, while the first pure w-term is still quartic. In the order x, y, z, w the Hessian is

$$\operatorname{Hess}_0 F_a = \operatorname{diag}(2, 2, 2a, 0). \tag{XII.6.29}$$

Its rank is three, compared with two for the UV equation. The missing quadratic direction accounts for the single fourth power in the local model. To balance these four terms at order $a^2\epsilon^4$, let the quadratic variables shrink with ϵ^2 and the quartic variable with ϵ. Fix a branch of $\sqrt{a}$ and define the map Ψ_ϵ by

$$x = a\epsilon^2 X, \qquad y = a\epsilon^2 Y, \qquad z = \sqrt{a}\,\epsilon^2 Z, \qquad w = \sqrt{a}\,\epsilon W. \tag{XII.6.30}$$

The powers of ϵ can be recovered without guessing Ψ_ϵ. Suppose w scales as ϵ, and require all terms in the retained polynomial to have the same power. Since w^4 has power four and a is fixed, the conditions are

$$2\nu_x = 2\nu_y = 2\nu_z = 4\nu_w = 4, \qquad (\nu_x, \nu_y, \nu_z, \nu_w) = (2, 2, 2, 1). \tag{XII.6.31}$$

The mixed quartic then has power $2\nu_z + 2\nu_w = 6$, and the pure z^4 term has power eight. Their suppression follows from this balance. A uniform shrink of all four coordinates would instead lose w^4 relative to the quadratic terms and fail to retain the singularity we want to study.

The factors of a put the four leading coefficients on the same footing. For instance, $az^2 = a^2\epsilon^4 Z^2$, whereas $z^2w^2 = a^2\epsilon^6 Z^2 W^2$. Division by the common leading factor gives

$$\begin{aligned} G_\epsilon &= \frac{F_a \circ \Psi_\epsilon}{a^2\epsilon^4} \\ &= X^2 + Y^2 + Z^2 + W^4 + \lambda\epsilon^2 Z^2 W^2 + \epsilon^4 Z^4. \end{aligned} \tag{XII.6.32}$$

With a, λ fixed, $\epsilon \to 0$ keeps the first four terms on bounded sets of the scaled coordinates. This convergence has a precise local domain. On a scaled patch with $|Z|, |W| \le R$, the omitted terms obey

$$|G_\epsilon - (X^2 + Y^2 + Z^2 + W^4)| \le R^4\big(|\lambda|\,|\epsilon|^2 + |\epsilon|^4\big). \tag{XII.6.33}$$

For $\lambda = 1$, $\epsilon = 1/10$ and $R = 1$, the bound is $101/10000$. At $Z = W = 1$ it is attained for these real positive choices. Reducing ϵ by a factor two reduces the mixed correction by four and the pure quartic correction by sixteen. The bound requires fixed R and fixed finite λ; allowing the patch or λ to grow with ϵ^{-1} would be a different limit.

Figure XII.6.2 shows the different shrinking rates. Setting $a = 0$ first removes the quadratic term used for the balance and makes Ψ_ϵ singular. In that case the quartic UV scaling is the one appropriate to the origin.

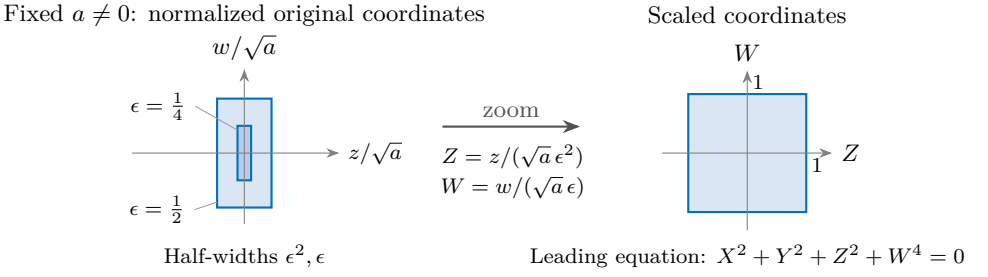


Figure XII.6.2: The fixed-a scaling viewed in a real two-dimensional coordinate slice. The rectangle of unit half-widths in (Z, W) maps to half-widths proportional to ϵ^2 in z and ϵ in w. The omitted x, y directions also scale as ϵ^2. The rectangles mark coordinate patches, not sections of the hypersurface.

The limiting polynomial is the standard A_3 suspension. One can also exhibit this germ at fixed a without a limit. On a neighborhood where the holomorphic square root can be chosen, take

$$Z_{\mathrm{loc}} = z\sqrt{a + z^2 + \lambda w^2}, \qquad F_a = x^2 + y^2 + Z_{\mathrm{loc}}^2 + w^4. \tag{XII.6.34}$$

Since $\partial Z_{\mathrm{loc}}/\partial z|_0 = \sqrt{a} \neq 0$, this is an invertible local coordinate change. The exact change identifies the germ; the scaling in (XII.6.30) also tells us how the residue changes. The four coordinate differentials contribute $a^3\epsilon^7$ in the given wedge order, and the equation contributes $a^2\epsilon^4$ in the denominator. On the smooth locus, for $\epsilon \neq 0$,

$$\Psi_\epsilon^* \Omega_{F_a} = \frac{a^3\epsilon^7}{a^2\epsilon^4}\,\Omega_{G_\epsilon} = a\epsilon^3 \Omega_{G_\epsilon}. \tag{XII.6.35}$$

Nonzero vanishing-cycle periods are read on nearby smooth fibers of the locally deformed family introduced in Section XII.6.6. The same residue scaling applies to the corresponding deformed polynomials. If Γ_ϵ is a compact cycle in a smooth bounded scaled patch, its image in the original coordinates has period

$$\int_{\Psi_\epsilon(\Gamma_\epsilon)} \Omega_{F_a} = a\epsilon^3 \int_{\Gamma_\epsilon} \Omega_{G_\epsilon}. \tag{XII.6.36}$$

For cycles whose scaled integral tends to a finite, nonzero limit, this gives a period of order $a\epsilon^3$. Relative to the fixed scale set by a, this period goes to zero. For the limiting

equation itself the degree-one weights and residue weight are

$$q^{\mathrm{IR}} = (\tfrac{1}{2}, \tfrac{1}{2}, \tfrac{1}{2}, \tfrac{1}{4}), \qquad Q_\Omega^{\mathrm{IR}} = \tfrac{3}{4}. \tag{XII.6.37}$$

The factor ϵ^3 in (XII.6.35) agrees with this weight: the degree-one scaling parameter for the limiting equation is $\rho = \epsilon^4$.

It is useful to check the scale in the same mass units used in the UV. Dividing the coordinate weights by $Q_\Omega = 1/2$ gives the ambient coordinate scaling dimensions. The powers of a in (XII.6.30) then have exactly the required dimensions:

$$[x]_{\mathrm{UV}} = [y]_{\mathrm{UV}} = 1, \qquad [z]_{\mathrm{UV}} = [w]_{\mathrm{UV}} = \tfrac{1}{2}, \qquad [a]_{\mathrm{UV}} = 1, \qquad [\epsilon] = 0. \tag{XII.6.38}$$

These are scaling assignments of geometric coordinates, not additional local field-theory operators. The rescaled coordinates are dimensionless with respect to this fixed reference scale. The new IR weights describe how they scale when the leading local polynomial is considered in its own period frame. A period with a finite nonzero limiting integral therefore has both the correct UV mass unit, supplied by a, and the small relative factor ϵ^3. The Jacobian calculation does not give the limiting integral itself.

To interpret this limit as a four-dimensional sector, we assume the direct IIB low-energy limit in which the normalizable local sector decouples from gravity and bulk and string modes. At energies small compared with the fixed mass scale we retain the sector of the selected germ. With the local IIB identification, the A_3 geometry gives the (A_1, A_3) sector. The coordinate calculation does not establish decoupling or identify the full infrared theory. We can, however, determine which deformations of the original polynomial enter the new local geometry and what their dimensions are.

XII.6.6 Parameters that survive the local limit

What can be varied independently in the surviving local geometry? Start with the nine representatives of J_λ and vary their coefficients about the deformed point F_a. To first order we must now divide out coordinate changes of the *new* germ. Work in the ring $\mathbb{C}\{x, y, z, w\}$ of holomorphic germs at the origin. In this ring

$$\partial_z F_a = 2z(a + 2z^2 + \lambda w^2), \qquad \partial_w F_a = 4w^3 + 2\lambda z^2 w. \tag{XII.6.39}$$

The first factor in parentheses is a unit because its constant term is $a \neq 0$. It follows that z itself belongs to the local Jacobi ideal. The other derivatives put x, y in the ideal and reduce $\partial_w F_a$ to $4w^3$. Conversely all four derivatives lie in (x, y, z, w^3), so

$$(\partial F_a) = (x, y, z, w^3), \qquad J_{a,0} = \mathbb{C}\{x, y, z, w\}/(\partial F_a) \simeq \mathbb{C}[w]/(w^3). \tag{XII.6.40}$$

Also $F_a \in (\partial F_a)$, so allowing multiplication of the equation by a unit gives the same quotient. The three independent classes give the local Milnor number $\mu = 3$. The map on the chosen representatives is particularly simple:

$$z^i w^j \longmapsto \begin{cases} w^j & i = 0, \\ 0 & i > 0 \end{cases} \qquad (0 \leq i, j \leq 2). \tag{XII.6.41}$$

In this slice the projection even descends from the UV Jacobi quotient: the only derivative that changed differs from its UV value by $2az$, already in the local ideal. A zero image means that the first-order change can be removed at the selected germ. It gives no general rule for finite changes of the coefficients or for other regions of the fiber.

Localization is doing physical work in this count: we have chosen the origin before asking which perturbations remain there. The factor $a + 2z^2 + \lambda w^2$ can be inverted as a holomorphic germ near the origin. It cannot be inverted at every point of the global polynomial critical scheme, since it vanishes at some off-origin stationary points. The quotient (XII.6.40) therefore counts the selected local singularity, rather than all stationary points in the polynomial chart.

A short calculation shows how a class with zero tangent image can still affect the equation beyond first order. Set $\lambda = 0$ and add hz to F_a, keeping $a \neq 0$. The stationary point near the origin has $x = y = w = 0$. The equation for its z coordinate and its solution to leading order are

$$4z_*^3 + 2az_* + h = 0, \qquad z_*(h) = -\frac{h}{2a} + O(h^3), \qquad (F_a + hz)(z_*) = -\frac{h^2}{4a} + O(h^4). \tag{XII.6.42}$$

The analytic solution exists for sufficiently small h because the derivative of the left-hand side with respect to z_* is $2a \neq 0$ at $h = z_* = 0$. The linear perturbation moves the point, and the critical value changes at second order. To keep this moving point on the zero fiber one must also tune the constant coefficient by

$$u_{00}(h) = \frac{h^2}{4a} + O(h^4). \tag{XII.6.43}$$

The vanishing class $[z] = 0$ correctly says that there is no new first-order deformation of the chosen germ. It does not say that a finite hz can be added while holding the point and fiber fixed. Here the induced constant shift is invisible to the linear tangent projection.

The quotient tells us which directions to keep; the scaling tells us how to keep them. To find the size of a term after the zoom in Figure XII.6.2, substitute (XII.6.30) and divide by $a^2\epsilon^4$:

$$\frac{u_{ij} z^i w^j}{a^2\epsilon^4} = u_{ij} a^{(i+j)/2-2} \epsilon^{2i+j-4} Z^i W^j. \tag{XII.6.44}$$

For each surviving representative the power of ϵ is negative, so a fixed nonzero coefficient would overwhelm the leading polynomial. Set the other perturbations to zero, hold a, λ fixed, and tune the three coefficients as

$$u_{0j} = a^{2-j/2} \epsilon^{4-j} U_j, \qquad j = 0, 1, 2. \tag{XII.6.45}$$

For a concrete tuning, take $a = 4$, choose $\sqrt{a} = 2$, and let $(U_0, U_1, U_2) = (1, -1, 2)$. Then

$$(u_{00}, u_{01}, u_{02}) = (16\epsilon^4, -8\epsilon^3, 8\epsilon^2), \qquad \frac{u_{00} + u_{01} w + u_{02} w^2}{16\epsilon^4} = 1 - W + 2W^2. \tag{XII.6.46}$$

All three UV perturbations approach zero, at different rates, yet each contributes a finite term after magnification. If instead u_{02} were held fixed and nonzero, its coefficient

in the normalized equation would grow like ϵ^{-2}. Thus the finite U_j family describes a specified correlated approach to the deformed point.

The U_j remain finite. Their dimensions in the new local period frame are determined by (XII.6.37):

$$[U_j]_{\mathrm{IR}} = \frac{1 - j/4}{3/4} = \frac{4 - j}{3}. \tag{XII.6.47}$$

In particular the same surviving quadratic monomial has coefficient dimension one in the UV frame and 2/3 in the IR frame. It is a UV mass direction and an IR relevant coupling direction under the respective local IIB role maps. The weight of the monomial itself has not changed; it is the geometric weight of the residue that has changed. A fixed mass dimension of one for the residue then gives a different conversion factor.

Representative	$[u_{0j}]_{\mathrm{UV}}$	Power of ϵ in u_{0j}	$[U_j]_{\mathrm{IR}}$
1	2	4	4/3
w	3/2	3	1
w^2	1	2	2/3

Table XII.6.2: The three tangent directions that survive in the selected germ. The tuning column uses fixed nonzero a; the last column normalizes the residue of the leading local family.

We can now ask which fibers of the leading local family are singular. The tuned parameters give the equation

$$X^2 + Y^2 + Z^2 + p(W) = 0, \qquad p(W) = W^4 + U_2 W^2 + U_1 W + U_0. \tag{XII.6.48}$$

The three quadratic derivatives force $X = Y = Z = 0$; stationarity in W requires $p'(r) = 0$ and the fiber condition requires $p(r) = 0$. First solve the derivative equation for U_1, then substitute it in the fiber equation:

$$\begin{aligned} U_1 &= -4r^3 - 2U_2 r, \\ 0 &= r^4 + U_2 r^2 + (-4r^3 - 2U_2 r)r + U_0 = -3r^4 - U_2 r^2 + U_0. \end{aligned} \tag{XII.6.49}$$

For $U_1 = 0$ the derivative condition splits into $r = 0$ and $r^2 = -U_2/2$. The two branches of the singular-fiber discriminant are

Stationary root condition	Fiber condition	$p(W)$
$r = 0$	$U_0 = 0$	$W^2(W^2 + U_2)$
$r^2 = -U_2/2$	$U_0 = U_2^2/4$	$(W^2 + U_2/2)^2$

(XII.6.50)

For example, at $U_2 = 2$ the first branch gives a double root at zero and two simple roots. The second gives two double roots at $W = \pm i$. At $U_2 = 0$ the two branches meet at the quartic root at zero.

The repeated-root parametrization also works away from the even slice. For instance, retain $U_2 = 2$ and choose the repeated root $r = 1$. Equation (XII.6.49) fixes $U_1 = -8$ and $U_0 = 5$, and the polynomial factors as

$$p(W) = W^4 + 2W^2 - 8W + 5 = (W-1)^2(W^2 + 2W + 5). \tag{XII.6.51}$$

The other two roots are $-1 \pm 2i$, both simple. Near the repeated root set $W = 1 + \xi$. Since $p''(1) = 16$, the local equation begins as

$$X^2 + Y^2 + Z^2 + 8\xi^2 + 4\xi^3 + \xi^4 = 0. \tag{XII.6.52}$$

Its quadratic part has rank four. The higher terms can be removed locally by the holomorphic Morse lemma, giving an ordinary quadratic node at this fiber. This is a calculation of a local geometric type; a spectrum is not determined by counting its repeated roots.

A small constant change $U_0 = 5 + \delta$, with U_1, U_2 fixed, changes the repeated-root equation to

$$\delta + 8\xi^2 + 4\xi^3 + \xi^4 = 0, \qquad \xi_\pm = \pm\sqrt{-\delta/8} + O(\delta). \tag{XII.6.53}$$

Thus the double root separates with a square-root scale. The critical point near $W = 1$ is still a stationary point of the quartic, but its value is now δ, so it no longer gives a singularity on the zero fiber. This repeats, in the leading local family, the distinction between stationarity and a tuned singular fiber that controlled the mass deformation. This discriminant locates singular fibers of the leading deformation (XII.6.48). The UV binary discriminant (XII.6.7) instead locates loss of isolation in a family whose central fiber is always singular. In the exercises we use both tests, and change the quadratic perturbation itself to see how much of the argument depends on its rank.

XII.6.7 Two masses and the choice of a critical fiber

The single mass a left one quartic direction at the origin. What happens if that direction also receives a mass? We can follow the answer on the same quartic, including the stationary points that do not lie on the original zero fiber. Choose the Fermat member $\lambda = 0$ and introduce a second mass coefficient b and a constant c:

$$H_{a,b,c} = x^2 + y^2 + V_a(z) + V_b(w) + c, \qquad V_a(z) = z^4 + az^2, \qquad V_b(w) = w^4 + bw^2. \tag{XII.6.54}$$

Both a and b have UV dimension one, while c has dimension two. Holding a, b fixed and varying c selects a Coulomb fiber. We first take $ab \neq 0$. The two derivative problems separate:

$$V_a'(z) = 2z(2z^2 + a) = 0, \qquad V_b'(w) = 2w(2w^2 + b) = 0. \tag{XII.6.55}$$

There are three choices for each coordinate, with independent square-root signs. The coordinate values and function values before adding c are

z^2	w^2	$H_{a,b,0}$	Number of points
0	0	0	1
$-a/2$	0	$-a^2/4$	2
0	$-b/2$	$-b^2/4$	2
$-a/2$	$-b/2$	$-(a^2+b^2)/4$	4

(XII.6.56)

For example, substituting $z^2 = -a/2$ gives $z^4 + az^2 = a^2/4 - a^2/2 = -a^2/4$. Thus the singular fibers occur when c cancels one of the four values. This also illustrates why the constant coefficient is physically useful: it selects which local degenerations are reached while the two mass parameters remain fixed.

The type of each degeneration follows from its Hessian, rather than from its multiplicity in the table. At a critical point $p = (0, 0, z_*, w_*)$,

$$\operatorname{Hess}_p H_{a,b,c} = \operatorname{diag}\big(2, 2, 12z_*^2 + 2a, 12w_*^2 + 2b\big), \qquad 12z_*^2 + 2a = \begin{cases} 2a & z_* = 0, \\ -4a & z_*^2 = -a/2. \end{cases} \tag{XII.6.57}$$

The analogous w entry is $2b$ or $-4b$. All four entries are nonzero for $ab \neq 0$. On its tuned fiber every point in the table is therefore an ordinary quadratic node. Each has local Milnor number one. The number of distinct points on a fiber and the local Milnor number at one point answer different questions.

A concrete comparison keeps the fiber choices visible. For $a = 2, b = 4$, the values of c that give singular fibers are

c	0	1	4	5
Number of nodes	1	2	2	4

(XII.6.58)

At $c = 1$, for instance, the two singular points are $(z, w) = (i, 0), (-i, 0)$. At $c = 4$, they are $(0, i\sqrt{2}), (0, -i\sqrt{2})$. All four combinations $(\pm i, \pm i\sqrt{2})$ occur at $c = 5$. These are points of three different hypersurfaces in the family.

Now tune the masses so that $a^2 = b^2 \neq 0$. The two axis critical values in (XII.6.56) agree. Taking $a = b = 2$ gives

c	0	1	2
Number of nodes	1	4	4

, $\qquad \operatorname{Sing}(H_{2,2,1} = 0) = \{(0, 0, \pm i, 0), (0, 0, 0, \pm i)\}.$ (XII.6.59)

Four nodes now lie on the same fiber. Their positions remain distinct, and their Hessians remain nonsingular. Tuning a critical *value* to coincide with another value has not made the corresponding critical *points* collide. The same equality occurs at $b = -a$; it is the squares of the mass coefficients that enter the fiber levels.

Complex masses allow another coincidence in the same table. At $b = \pm ia$ the mixed critical value is zero, so

$$\operatorname{Sing}(H_{a,\pm ia,0} = 0) = \{(0, 0, 0, 0)\} \cup \{(0, 0, z, w) : z^2 = -a/2,\ w^2 = \mp ia/2\}. \tag{XII.6.60}$$

There are five distinct nodes. Their Hessians remain nonsingular because both masses are nonzero. The two coincidences, $b^2 = a^2$ and $b^2 = -a^2$, identify different pairs of critical values without changing any local node type.

There is a separate way to make points collide: let $b \to 0$ at fixed $a \neq 0$. The three stationary w coordinates approach zero. For each of the three stationary z coordinates, a group of three points approaches a single point. Expanding at $z = z_* + \zeta$ gives

$$V_a(z_* + \zeta) - V_a(z_*) = \begin{cases} a\zeta^2 + \zeta^4, & z_* = 0, \\ -2a\zeta^2 + 4z_*\zeta^3 + \zeta^4, & z_*^2 = -a/2, \end{cases} \qquad V_0(w) = w^4. \tag{XII.6.61}$$

The ζ direction remains quadratic in each neighborhood. Removing its higher powers by a local holomorphic coordinate change leaves an A_3 suspension at each point, on the fiber that cancels its own critical value. Thus the origin has an A_3 germ at $c = 0$, and the two off-origin points have A_3 germs at $c = a^2/4$. Locally, three Morse points have merged into one germ of Milnor number three. Across these three neighborhoods the geometric counts read

$$9 = 1 + 2 + 2 + 4 = 3 + 3 + 3. \tag{XII.6.62}$$

This organizes the deformation geometry. To compare physical sectors one must also specify the chosen fiber and the local low-energy limit, as in the preceding sections. The count alone supplies neither a product decomposition of the theory nor its spectrum.

XII.6.8 From quartic scaling to a node

The mass b makes the origin a node for every nonzero value, yet the $b = 0$ limit has an A_3 germ. How does the vanishing-period scale change between them? Introduce a small nonzero constant smoothing $c = \delta$, and keep $a \neq 0$ fixed. We use a simply connected sector of the δ-plane so that the required roots are chosen consistently.

First hold $b \neq 0$ fixed. Balancing the four quadratic terms against δ suggests the coordinates

$$x = \delta^{1/2} X, \qquad y = \delta^{1/2} Y, \qquad z = \frac{\delta^{1/2}}{\sqrt{a}} Z, \qquad w = \frac{\delta^{1/2}}{\sqrt{b}} W. \tag{XII.6.63}$$

The normalized equation is

$$\frac{H_{a,b,\delta}}{\delta} = X^2 + Y^2 + Z^2 + W^2 + 1 + \frac{\delta}{a^2} Z^4 + \frac{\delta}{b^2} W^4. \tag{XII.6.64}$$

Both quartics disappear on bounded scaled patches when $|\delta| \ll |a|^2, |b|^2$. The coordinate Jacobian is $\delta^2/\sqrt{ab}$, while the equation contributes δ to the residue denominator. For a transported compact cycle whose normalized period tends to a finite nonzero constant C_{n},

$$\Omega_H = \frac{\delta}{\sqrt{ab}} \Omega_{\mathrm{n},\delta}, \qquad \Pi_{\mathrm{n}}(\delta) = \frac{\delta}{\sqrt{ab}} \big(C_{\mathrm{n}} + o(1)\big). \tag{XII.6.65}$$

Here and below equalities of forms mean pullbacks by the displayed coordinate map. The period has UV dimension one, since $[\delta] = 2$ and $[a] = [b] = 1$. The dimensionless constant is a period of a specified cycle; its value is not fixed by homogeneity.

For the quartic regime we instead retain w^4. Use

$$x = \delta^{1/2} X, \qquad y = \delta^{1/2} Y, \qquad z = \frac{\delta^{1/2}}{\sqrt{a}} Z, \qquad w = \delta^{1/4} W. \tag{XII.6.66}$$

Now the family and residue become

$$\begin{aligned} \frac{H_{a,b,\delta}}{\delta} &= X^2 + Y^2 + Z^2 + W^4 + 1 + \frac{\delta}{a^2} Z^4 + \beta W^2, \qquad \beta = \frac{b}{\delta^{1/2}}, \\ \Omega_H &= \frac{\delta^{3/4}}{\sqrt{a}} \Omega_{\mathrm{A},\delta,\beta}. \end{aligned} \tag{XII.6.67}$$

The first correction is small if $|\delta| \ll |a|^2$. For $|\beta| \ll 1$, the second mass is also a small perturbation of the smoothed A_3 geometry. Its compact periods with finite nonzero limiting normalized integrals obey

$$\Pi_{\mathrm{A}}(\delta) = \frac{\delta^{3/4}}{\sqrt{a}} \big(C_{\mathrm{A}} + o(1) \big), \qquad |b|^2 \ll |\delta| \ll |a|^2. \tag{XII.6.68}$$

The $3/4$ exponent is the A_3 residue weight. This window exists when the two mass coefficients are separated, $|b| \ll |a|$. At fixed nonzero b, taking δ still closer to zero eventually leaves the window and resolves the node instead.

The interpolation also remembers the other critical fibers. For the leading quartic $P_\beta(W) = W^4 + \beta W^2 + 1$,

$$P_\beta = P'_\beta = 0 \quad \Longleftrightarrow \quad \beta = \pm 2, \qquad W^2 = -\beta/2. \tag{XII.6.69}$$

At those values the smoothing is singular at the off-origin stationary points. A comparison of transported cycles must use a complex parameter path avoiding these values. For positive real masses, reducing positive real δ crosses the critical fiber $\delta = b^2/4$; it cannot define a smooth transport through that value.

The dimensionless quantity β allows a direct comparison of the two local descriptions. In the leading family in (XII.6.67), for large $|\beta|$ the neighborhood of the central stationary point has $W = \beta^{-1/2} V$. Substitution gives

$$W^4 + \beta W^2 + 1 = \beta^{-2} V^4 + V^2 + 1, \qquad \Omega_{\mathrm{A},\beta} = \beta^{-1/2} \Omega_{\mathrm{n},\beta}. \tag{XII.6.70}$$

Consequently its prefactor matches the node result:

$$\frac{\delta^{3/4}}{\sqrt{a}} \, \beta^{-1/2} = \frac{\delta}{\sqrt{ab}}. \tag{XII.6.71}$$

The powers agree because the node scaling is a further zoom inside the quartic scaling patch. This comparison concerns cycles in the central neighborhood, transported on smooth fibers along an admissible path. The two other stationary points can lie outside that further zoom.

For a numerical hierarchy, take $a = 1$, $b = 10^{-4}$. A smoothing with $\delta = 10^{-4}$ has $\delta/a^2 = 10^{-4}$ and $\beta = 10^{-2}$, so the quartic patch is controlled. At $\delta = 10^{-12}$, the node patch has quartic corrections 10^{-12} and 10^{-4}. The switch is governed by $|\delta|$ relative to $|b|^2$, not by whether b is numerically small in isolation. Equivalently, in period mass units the crossover is of order

$$M_{\text{cross}} \sim \frac{|b|^{3/2}}{|a|^{1/2}}, \qquad M_{\text{cross}} \ll |a| \quad \text{when } |b| \ll |a|. \tag{XII.6.72}$$

The estimate suppresses the dimensionless cycle period. Under the same local IIB premise as before, these shrinking periods set local particle central-charge scales. Thus a small second UV mass can leave an intermediate range governed by the quartic sector, while the closest neighborhood of the final tuned singularity has quadratic scaling.

XII.6.9 Turning on a relevant coupling

A mass made one of the quartic variables quadratic. A relevant coupling can instead leave both variables in the leading singularity, with a different balance between them. Turn off the mass coefficients for the moment and choose the mixed cubic representative z^2w. At fixed finite $\lambda^2 \neq 4$, consider the zero fiber

$$F_h = x^2 + y^2 + z^4 + w^4 + \lambda z^2 w^2 + h z^2 w, \qquad h \neq 0, \qquad [h]_{\text{UV}} = \tfrac{1}{2}. \tag{XII.6.73}$$

Unlike a, this coefficient is a relevant coupling already in the UV period frame. The corresponding mass unit is h^2. We again select the origin before taking a local limit. The Hessian there has rank two, so replacing the cubic by a quadratic mass would change the leading problem.

The first balance to try keeps w^4 and hz^2w together. With h fixed, give w dilation power two. The cubic then fixes the power of z, and the quadratic variables fix those of x, y:

$$4\nu_w = 2\nu_z + \nu_w = 2\nu_x = 2\nu_y = 8, \qquad (\nu_x, \nu_y, \nu_z, \nu_w) = (4, 4, 3, 2). \tag{XII.6.74}$$

The UV mass units supply the remaining powers of h. Define the map Θ_ϵ by

$$x = h^2\epsilon^4 X, \qquad y = h^2\epsilon^4 Y, \qquad z = h\epsilon^3 Z, \qquad w = h\epsilon^2 W. \tag{XII.6.75}$$

All four retained terms are then of order $h^4\epsilon^8$. The normalized polynomial is

$$\begin{aligned} K_\epsilon = \frac{F_h \circ \Theta_\epsilon}{h^4\epsilon^8} &= D + \lambda\epsilon^2 Z^2 W^2 + \epsilon^4 Z^4, \\ D &= X^2 + Y^2 + Z^2 W + W^4. \end{aligned} \tag{XII.6.76}$$

On a bounded scaled patch the two omitted terms vanish. The principal polynomial is the D_5 suspension. Its critical equations force $X = Y = 0$, $ZW = 0$, and $Z^2 + 4W^3 = 0$, so its origin is isolated. Its degree-one weights and residue weight follow from the retained terms:

$$q_D = (\tfrac{1}{2}, \tfrac{1}{2}, \tfrac{3}{8}, \tfrac{1}{4}), \qquad 2q_Z + q_W = 4q_W = 1, \qquad Q_D = \sum q_D - 1 = \tfrac{5}{8}. \tag{XII.6.77}$$

The discarded monomials have weights 5/4 and 3/2. Thus the scale change has been derived from the equation, rather than obtained by dropping whichever terms have higher ordinary polynomial degree.

The residue distinguishes this limit from the mass limit. The four-coordinate Jacobian in (XII.6.75) is $h^6\epsilon^{13}$, giving

$$\Theta_\epsilon^*\Omega_{F_h} = h^2\epsilon^5\Omega_{K_\epsilon}, \qquad \int_{\Theta_\epsilon(\Gamma_\epsilon)} \Omega_{F_h} = h^2\epsilon^5 \int_{\Gamma_\epsilon} \Omega_{K_\epsilon}. \tag{XII.6.78}$$

As before, the cycles are compact cycles of nearby smooth, locally deformed fibers. For a bounded scaled cycle with finite nonzero limiting normalized integral, its period is of order $h^2\epsilon^5$, small compared with h^2. The factor ϵ^5 agrees with degree-one scaling parameter $\rho = \epsilon^8$ and residue weight 5/8. Using the same direct IIB local-sector prescription and decoupling premise, this principal scaling describes a selected D_5 Argyres–Douglas sector. The conclusion is about that sector; the polynomial and its principal weights do not establish a complete IR theory or an exact analytic equivalence of the full F_h germ to D.

It remains necessary to check the chosen fiber. The quadratic derivatives set $x = y = 0$. At $\lambda = 0$ the remaining stationary equations are

$$2z(2z^2 + hw) = 0, \qquad 4w^3 + hz^2 = 0. \tag{XII.6.79}$$

The branch $z = 0$ gives the origin. On the other branch, $z^2 = -hw/2$, so the second equation becomes $w(4w^2 - h^2/2) = 0$. The off-origin solutions and their critical values are

$$w = \pm\frac{h}{2\sqrt{2}}, \qquad z = \pm\sqrt{-\frac{hw}{2}}, \qquad F_h = -\frac{h^4}{64}, \qquad \det \mathrm{Hess}\, F_h = -16h^3 w \neq 0. \tag{XII.6.80}$$

The two signs of z are independent for each choice of w. There are four distinct Morse points, all on another critical level. A constant $c = h^4/64$ brings them onto the zero fiber of $F_h + c$; the origin then leaves that fiber. For $h = 2$, for example, their coordinates satisfy $w = \pm 1/\sqrt{2}$, $z^2 = \mp 1/\sqrt{2}$, and the required constant is $c = 1/4$. The $c = 0$ scaling above has selected the origin, not these four points.

One can see the separation directly in the critical algebra. At $\lambda = 0, h = 1$, let $g = z^4 + w^4 + z^2 w$. The derivative relations imply

$$\frac{1}{2}g_z - 2zg_w = zw(1 - 8w^2), \qquad g_w = z^2 + 4w^3. \tag{XII.6.81}$$

The factor $1 - 8w^2$ is a unit at the origin but vanishes at the four remote points. Inverting it gives the origin component. In that local algebra, $zw = 0$; multiplying $z^2 + 4w^3 = 0$ by w gives $w^4 = 0$. The global and localized quotients consequently have different sizes:

$$\begin{aligned} J_{\text{global}}: &\quad z^2 + 4w^3 = 0, \quad 8zw^3 - zw = 0, \quad 8w^6 - w^4 = 0, \quad \dim J_{\text{global}} = 9, \\ J_{\text{origin}}: &\quad zw = 0, \quad z^2 + 4w^3 = 0, \quad w^4 = 0, \quad \dim J_{\text{origin}} = 5. \end{aligned} \tag{XII.6.82}$$

For example, the global leading monomials in lexicographic order are z^2, zw^3, w^6, leaving $1, w, \dots, w^5$ and z, zw, zw^2. Locally only $1, w, w^2, w^3, z$ remain. The geometric decomposition is five at the origin and one at each remote Morse point. Localization, not a count of physical states, is what has reduced nine to five. We now track those five local directions through the original polynomial family.

XII.6.10 Parameters of the local sector

Which of the original perturbations can independently deform the selected D_5 sector? The limiting derivative ideal eliminates X, Y. For the remaining variables,

$$\partial_Z D = 2ZW, \qquad \partial_W D = Z^2 + 4W^3, \qquad J_D = \frac{\mathbb{C}[Z,W]}{(ZW, Z^2+4W^3)}. \tag{XII.6.83}$$

Multiplying the second relation by W and using the first sets W^4 to zero. Multiplying it by Z sets Z^3 to zero. Thus powers of W reduce at degree four, and any mixed monomial containing both Z, W vanishes. A basis and its geometric weights are

$$\begin{array}{c|ccccc} \phi & 1 & W & W^2 & W^3 & Z \\ \hline Q(\phi) & 0 & 1/4 & 1/2 & 3/4 & 3/8 \end{array}. \tag{XII.6.84}$$

Independence also follows by taking the leading monomials Z^2, ZW, W^4 of the derivative ideal. Exactly those five monomials avoid its multiples. In the local period frame, the parameter multiplying ϕ has dimension

$$\Delta(t_\phi) = \frac{1-Q(\phi)}{5/8}, \qquad (\Delta(t_1), \Delta(t_W), \Delta(t_{W^2}), \Delta(t_{W^3}), \Delta(t_Z)) = \left(\frac{8}{5}, \frac{6}{5}, \frac{4}{5}, \frac{2}{5}, 1\right). \tag{XII.6.85}$$

Under the local IIB dictionary, this gives two Coulomb coordinates, two relevant coupling directions, and one mass direction. The dimensions pair as $8/5 + 2/5 = 2$ and $6/5 + 4/5 = 2$, with the mass at dimension one. There is no dimensionless parameter in this local basis. The original λ remains in the suppressed term of (XII.6.76).

We now express these five variations using the original chosen UV representatives. At the D_5 scale keep the coefficients of $1, w, w^2, z, z^2$. To obtain finite normalized variations, set

$$\begin{aligned} &u_{00} = h^4\epsilon^8 T_0, \quad u_{01} = h^3\epsilon^6 T_1, \quad u_{02} = h^2\epsilon^4 T_2, \\ &u_{10} = h^3\epsilon^5 S, \quad u_{20} = h^2\epsilon^2 A. \end{aligned} \tag{XII.6.86}$$

All other perturbations are set to zero while h, λ remain fixed. For example, the quadratic coefficient gives

$$\frac{u_{20} z^2}{h^4\epsilon^8} = AZ^2 \tag{XII.6.87}$$

under (XII.6.75). The finite limiting family in these coordinates is

$$D + T_0 + T_1 W + T_2 W^2 + SZ + AZ^2. \tag{XII.6.88}$$

At first order its last variation represents $-4AW^3$ in J_D. This supplies the fifth independent tangent direction without introducing a UV w^3 parameter.

This last observation exposes a limitation of reducing in the UV quotient first. At the Fermat point its relation is $[w^3]_{\mathrm{UV}} = 0$, whereas $[W^3]_D \neq 0$. Hence there is no map obtained by sending every UV polynomial class to its identically named D_5 class:

$$w^3 \in (\partial f_0), \qquad W^3 \notin (\partial D), \qquad [Z^2]_D = -4[W^3]_D \neq 0. \tag{XII.6.89}$$

What we have tracked is the derivative of the chosen polynomial family, followed by local reduction at the new point and scaling. The descent from the old quotient that happened for az^2 was a property of that particular slice. It is not an extra step that can be assumed for every deformation.

The role changes can be compared without identifying the UV and IR scaling actions. With the above choices they read

UV representative	Δ_{UV}	Local class	Δ_D
1	2	1	$8/5$
w	$3/2$	W	$6/5$
z	$3/2$	Z	1
w^2	1	W^2	$4/5$
z^2	1	$-4W^3$	$2/5$

(XII.6.90)

The mass coefficient u_{20}, in particular, is a relevant coupling in the selected D_5 frame. A UV Coulomb coordinate u_{10} supplies its local mass direction. These statements compare roles of coefficients in two local descriptions; they do not equate operators with different dimensions in a single fixed-point theory.

It also matters that tangent reduction is infinitesimal. Suppose $A \neq 0$ is held fixed and consider just the last term in (XII.6.88). Near the origin,

$$D + AZ^2 = X^2 + Y^2 + Z^2(W + A) + W^4 = X^2 + Y^2 + \left(Z\sqrt{W + A}\right)^2 + W^4. \tag{XII.6.91}$$

The square-root change is invertible since its derivative in Z at the origin is $\sqrt{A} \neq 0$. The resulting A_3 germ has local Milnor number three. Replacing the finite perturbation AZ^2 by $-4AW^3$ would instead give

$$\widetilde{D} = X^2 + Y^2 + Z^2W + W^4 - 4AW^3, \qquad J_{\widetilde{D},0} = \frac{\mathbb{C}\{Z, W\}}{(ZW, Z^2 + 4W^3 - 12AW^2)}. \tag{XII.6.92}$$

Multiplying the second relation by W yields $4W^3(W - 3A) = 0$. The last factor is a local unit for $A \neq 0$, so $W^3 = 0$ and $Z^2 = 12AW^2$. The basis is $1, W, W^2, Z$, of length four. Thus two infinitesimally equivalent representatives give different finite germs when the higher induced coefficient changes are omitted. For a finite deformation one must retain the actual polynomial, as we do in the next scaling.

XII.6.11 Nested scales and the surviving local sector

The direct mass deformation and the relevant-coupling deformation now meet in one equation. After first resolving the D_5 scale, fix $A \neq 0$ and zoom further into (XII.6.91).

Introduce a second small parameter η and coordinates $(\xi, \upsilon, \zeta, \omega)$ by

$$X = \eta^2 \xi, \qquad Y = \eta^2 \upsilon, \qquad Z = \frac{\eta^2}{\sqrt{A}} \zeta, \qquad W = \eta \omega. \tag{XII.6.93}$$

The new leading polynomial and relative residue are

$$\begin{aligned} \frac{(D + AZ^2) \circ \Upsilon_\eta}{\eta^4} &= \xi^2 + \upsilon^2 + \zeta^2 + \omega^4 + \frac{\eta}{A} \zeta^2 \omega, \\ \Upsilon_\eta^* \Omega_{D + AZ^2} &= \frac{\eta^3}{\sqrt{A}} \Omega_{\mathrm{nested}, \eta}. \end{aligned} \tag{XII.6.94}$$

The cubic interaction becomes a higher-weight correction at this finer scale. Uniform scaling of all four coordinates would give quadratic terms proportional to η^{-2} after division by η^4. The anisotropic zoom is needed to retain the quartic direction together with the three quadratic directions.

The comparison survives in the full UV polynomial, rather than only in its principal part. Set the UV mass coefficient to $a = h^2 \epsilon^2 A$, as in (XII.6.86), and compose the two maps. Division by $h^4 \epsilon^8 \eta^4$ yields

$$\begin{aligned} \mathcal{G}_{\epsilon, \eta} &= \xi^2 + \upsilon^2 + \zeta^2 + \omega^4 + \frac{\eta}{A} \zeta^2 \omega \\ &\quad + \frac{\lambda \epsilon^2 \eta^2}{A} \zeta^2 \omega^2 + \frac{\epsilon^4 \eta^4}{A^2} \zeta^4, \\ (\Theta_\epsilon \circ \Upsilon_\eta)^* \Omega &= \frac{h^2 \epsilon^5 \eta^3}{\sqrt{A}} \Omega_{\mathcal{G}_{\epsilon, \eta}}. \end{aligned} \tag{XII.6.95}$$

At fixed $h, A \neq 0$ and fixed finite λ, the suppressed terms vanish on bounded patches. This equation makes the order of choices explicit. A fixed nonzero UV a would make $A = a/(h^2 \epsilon^2)$ grow as the D_5 zoom proceeds. Tuning a along with ϵ is what keeps a finite deformation of that intermediate sector.

There is also a useful way to see both scales in a single smoothed UV family. Take $\lambda = 0$, fix $h \neq 0$, and assume a smaller mass coefficient, $|a| \ll |h|^2$. Write

$$\mathcal{F} = x^2 + y^2 + z^4 + w^4 + h z^2 w + a z^2 + \delta, \qquad \delta \neq 0. \tag{XII.6.96}$$

The D_5 balance with the smoothing term uses $x, y = \delta^{1/2}(X, Y)$, $z = \delta^{3/8} Z / \sqrt{h}$, and $w = \delta^{1/4} W$. It gives

$$\begin{aligned} \frac{\mathcal{F}}{\delta} &= X^2 + Y^2 + Z^2 W + W^4 + 1 + \frac{\delta^{1/2}}{h^2} Z^4 + \frac{a}{h \delta^{1/4}} Z^2, \\ \Omega_{\mathcal{F}} &= \frac{\delta^{5/8}}{\sqrt{h}} \Omega_{D, \delta, a}. \end{aligned} \tag{XII.6.97}$$

The quartic correction and the quadratic perturbation are both small in the intermediate window

$$\left| \frac{a}{h} \right|^4 \ll |\delta| \ll |h|^4. \tag{XII.6.98}$$

It exists precisely when the smaller mass does not already remove the relevant-coupling scaling range. Compact cycles with finite nonzero normalized limiting periods then have period scale $\delta^{5/8}/\sqrt{h}$.

Closer to the tuned fiber, balance az^2 against the smoothing and keep w^4. The A_3 coordinates of (XII.6.66) give

$$\begin{aligned}\frac{\mathcal{F}}{\delta} &= X^2 + Y^2 + Z^2 + W^4 + 1 + \frac{\delta}{a^2}Z^4 + \frac{h\delta^{1/4}}{a}Z^2W,\\ \Omega_{\mathcal{F}} &= \frac{\delta^{3/4}}{\sqrt{a}}\Omega_{A,\delta,h}.\end{aligned} \tag{XII.6.99}$$

Both corrections are small when

$$|\delta| \ll \left|\frac{a}{h}\right|^4, \qquad |a| \ll |h|^2. \tag{XII.6.100}$$

The second inequality ensures that this also implies $|\delta| \ll |a|^2$. The local model has changed because the same fixed az^2 term that was small in (XII.6.97) now dominates the coefficient of z^2. Figure XII.6.3 places this crossover beside the two-mass example.

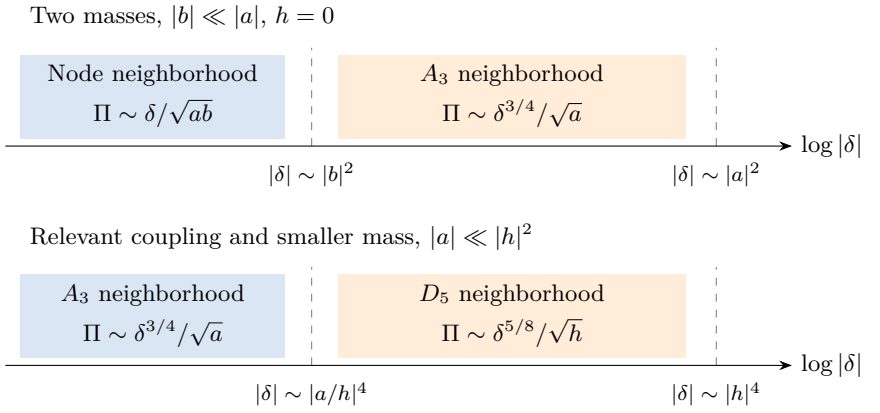


Figure XII.6.3: Two local period crossovers in smoothed quartic families. The horizontal coordinate is $\log|\delta|$, increasing to the right; positions are schematic. Each shaded interval is a regime where the displayed normalized equation has small corrections. The transition bands do not carry a single asymptotic power. The diagrams describe scales of selected compact periods, along paths avoiding singular fibers, rather than a complete QFT flow.

At the boundary of the two windows, the prefactors have the same parametric size. With consistent local root choices,

$$\left.\frac{\delta^{5/8}}{\sqrt{h}}\right|_{\delta=(a/h)^4} = \left.\frac{\delta^{3/4}}{\sqrt{a}}\right|_{\delta=(a/h)^4} = \frac{a^{5/2}}{h^3}, \qquad M_{D\to A} \sim \frac{|a|^{5/2}}{|h|^3} \ll |h|^2. \tag{XII.6.101}$$

This matches scale estimates, not the two dimensionless limiting cycle integrals. Roots and cycles are chosen locally and transported along smooth complex fibers avoiding the discriminant. The singular values between asymptotic regimes can produce monodromy under continuation, so this comparison alone does not specify one global period function.

These calculations join the local limits in a useful sequence. The UV relevant coefficient h exposes the D_5 principal sector. The smaller UV mass a is relevant with dimension $2/5$ in that sector and leaves an A_3 germ at the origin. A further coefficient of w^2 is relevant with dimension $2/3$ in the A_3 frame and yields the node regime derived above. Each step follows a chosen point and fiber and uses a new period normalization. Thus deformation roles and scales can change even though we have followed explicit coefficients of one UV polynomial. The conditional physical interpretation is a sequence of retained local sectors; additional sectors and global couplings require information beyond these local normal forms.

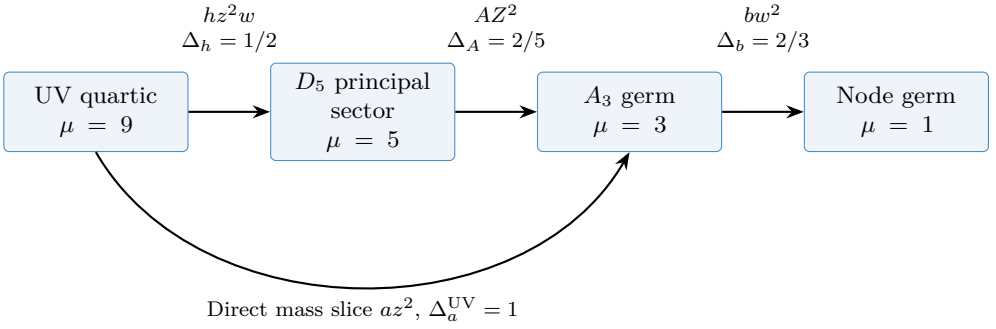


Figure XII.6.4: Selected local limits and the dimensions of the coefficients at the starting sector of each arrow. The lower arrow is the direct mass slice. Here μ is a local Milnor number; the arrows retain a local sector under the stated IIB premise and do not count physical states or identify the complete endpoint. The coefficient called b on the last arrow is written in the local A_3 frame.

XII.6.12 Exercises

Explain the calculation in each problem. Use `benchmark/tasks.json` to find the question IDs and `benchmark/PROTOCOL.md` for submission.

1. **Find the exceptional directions.** For finite λ, give the exceptional values and the value of $(z/w)^2$ at each, for nonzero singular points. Use the two gradient equations and explain why the chart $w = 0$ supplies no other finite exception.

2. **Interpret the zero weight.** Find the coefficient dimensions of all nine representatives $z^i w^j$, $0 \le i, j \le 2$, in the UV period frame. What does the zero weight show about the geometry? Explain what it leaves open about beta functions, physical identifications of coupling values, and a weak gauge limit.

3. **Change the rank of the quadratic part.** At finite $\lambda^2 \neq 4$, replace az^2 by bzw and consider the germ at the origin on the zero fiber. Find the determinant and rank of the full Hessian at $b = 2$, its rank at $b = 0$, and the local Milnor number at $b = 2$. Use the holomorphic Morse lemma to explain the change of local type relative to the az^2 deformation. Recall its implication: a holomorphic critical point with a nonsingular Hessian has a local nondegenerate quadratic normal form.

4. **Track the surviving coefficients.** With $a \neq 0$ fixed, reduce all nine UV representatives at the tuned origin. Give the surviving pairs (i, j), the powers of ϵ on the corresponding u_{ij} that retain finite coefficients, and the resulting IR coefficient dimensions. Order the powers and dimensions by increasing j. Explain the change in role for the coefficient of w^2 and why a zero tangent image does not settle the effect of a finite deformation.

5. **Test both branches of the local discriminant.** In the leading family take $U_1 = 0$ and $U_2 = -2$. List the repeated roots of p for each of $U_0 = 0, 1, 2$, giving an empty list if there are none. Derive the two branches and explain how their interpretation differs from that of the exceptional points in the UV λ-plane.

For written transfer practice, keep the same models and explain the role of each tuning. These tasks supplement the bounded submissions above.

1. At $\lambda = 1$, reduce $z^4 + zw^3$ in the UV Jacobi quotient. Explain why its first-order effect is a change of λ, and why the pure cubes cease to be useful coordinates at the Fermat point.

2. In the leading local family take $r = 1$, $U_2 = -1$. Determine U_1, U_0, factor the resulting polynomial, and locate its singular point on the zero fiber. Add a small constant δ and derive the leading separation of the colliding roots. State which of the fixed-point, fiber and coefficient choices has changed.

3. In the two-mass family set $a = 2$, $b = 2i$. Determine all singular points on the zero fiber and the full Hessian determinant at each. Explain why five nodes on this fiber do not make a germ of Milnor number five at the origin. Then compare this situation with the length-five origin of the relevant-coupling slice at $h = 1$, identifying which localization is needed.

Status and sources

§XII.6.2. The Euler identity, isolation test, and finite discriminant in (XII.6.2)–(XII.6.7) are [MATH]. The weighted hypersurface frame is Xie and Yau (2015, arXiv v1, §2.1, eqs. (2.2)–(2.8)). The quartic presentation also appears in Buican et al. (2015, arXiv v2, §3.2, eqs. (3.7)–(3.8)), with x, z, q there corresponding to z, w, λ here. The line, resultant, squared-root and exceptional-quotient calculations are derived above within the same binary-quartic family.

§XII.6.3. The Jacobi reduction, Hilbert series and combined weights in (XII.6.11)–(XII.6.19) are [MATH]. For the graded method see Xie and Yau (2015, arXiv v1, §2.2, eqs. (2.11)–(2.13)).

The normalization of the dimensions and assignment of parameter roles in (XII.6.20) and Table XII.6.1 are [GEO-E], using Xie and Yau (2015, arXiv v1, §§2.1–2.2, eqs. (2.6)–(2.16)) and Shapere and Vafa (1999, arXiv v2, §2.2 and eqs. (2.4)–(2.6)). The concrete perturbation reduction and cubic-coordinate comparison in (XII.6.16)–(XII.6.17) are algebraic consequences of the displayed polynomial normal form [MATH]. The period and coefficient conventions are those of Chapter 3.

§XII.6.4. The pullback (XII.6.21) and the binary pencil (XII.6.22) and the transported-period identity (XII.6.23) are [MATH]. Xie and Yau (2015, arXiv v1, §2.7) discusses geometric equivalences; the worked example there uses a different polynomial. For a separate period and scaling analysis of limits of this quartic, see Buican et al. (2015, arXiv v2, §3.2, eqs. (3.9)–(3.13), (3.19)–(3.23)). No physical exact marginality, conformal-manifold quotient, or weak-cusp identification is inferred here.

§XII.6.5. The selected fiber, coordinate scaling, residue factor and IR weights in (XII.6.25)–(XII.6.37) are [MATH]. Compare Xie and Yau (2015, arXiv v1, §2.8, eqs. (2.58)–(2.60)) for principal-part scaling. The worked flow in that source uses a different deformation; here a has UV dimension one. The balance, bounded remainder estimate and concrete critical-value example are algebraic consequences of the scaling calculation [MATH]. The mass-unit assignment in (XII.6.38) uses [GEO-E]. The conditional (A_1, A_3) sector identification is [GEO-E]; see Xie and Yau (2015, arXiv v1, §2.2, eqs. (2.17)–(2.18)). The decoupling and retention of the local sector are [DEC], a premise of the IIB application, not independently established by the residue calculation; compare Xie and Yau (2015, arXiv v1, §§2.1 and 2.8) and Shapere and Vafa (1999, arXiv v2, §2.2).

§XII.6.6. The local quotient, tuning and leading singular-fiber discriminant in (XII.6.39)–(XII.6.50) are [MATH], apart from the period-normalized dimensions and the comparison of IIB roles, [GEO-E]. For the repeated-root method compare Xie and Yau (2015, arXiv v1, §2.3, eqs. (2.22)–(2.23)). The alternative Hessian calculation in Exercise 3 is [MATH]. The moving-point expansion, explicit coefficient tuning, non-even repeated-root example and its local splitting are algebraic consequences of the displayed local polynomial calculations [MATH]. The fixed-a calculation concerns the chosen local sector only; it yields neither a complete IR spectrum nor a global charge lattice.

§XII.6.7–§XII.6.8. The separated critical equations, coincident values and colliding points, and local node/A_3 smoothing maps are [MATH]. The two masses use the stated UV family and its coefficient-role assignment. All period estimates retain the displayed bounded-cycle, smooth-transport and finite nonzero normalized-period conditions. Their interpretation as local central-charge scales uses the same [GEO-E] dictionary and [DEC] premise as above; compare Shapere and Vafa (1999, arXiv v2, §2 and §2.2).

§XII.6.9. The relevant-coupling balance, full normalized polynomial, relative residue, four remote points, and global versus localized critical algebras are [MATH]. The D_5 principal normal form and its conditional local IIB interpretation are [GEO-E], using Xie and Yau (2015, arXiv v1, eq. (2.18) and §2.8, eqs. (2.58)–(2.60)). Source z_2, z_3 there are W, Z here. That source does not print this specific quartic-plus-cubic example. Its use here retains [DEC], the assumed decoupling of the selected local sector, rather than a derivation of bulk decoupling or a full IR endpoint.

§XII.6.10–§XII.6.11. The five local directions, chosen-representative tunings, failure of UV quotient descent, finite-deformation comparison, composed full UV scaling and smoothing windows are [MATH]. The conditional coefficient-role comparisons use the local IIB interpretation [GEO-E], the residue normalization in Xie and Yau (2015, arXiv v1, eqs. (2.4)–(2.8), (2.18)) and Shapere and Vafa (1999, arXiv v2, eqs. (2.4)–(2.6) and §2.2). The crossover scales match

parametric powers for the selected local periods. They supply no absolute period integral, global spectrum, conformal-manifold identification or complete QFT trajectory. Decoupling remains [DEC] for each retained sector.

References

Buican, M. et al. (2015). "Argyres-Douglas Theories and S-Duality". In: *JHEP* 02, p. 185. DOI: 10.1007/JHEP02(2015)185. arXiv: 1411.6026 [hep-th].

Shapere, A. D. and C. Vafa (1999). "BPS Structure of Argyres-Douglas Superconformal Theories". In: arXiv: hep-th/9910182.

Xie, D. and S.-T. Yau (2015). "4d $\mathcal{N} = 2$ SCFT and singularity theory Part I: Classification". In: arXiv: 1510.01324 [hep-th].

Chapter XII.7

Beyond hypersurfaces: complete intersections

XII.7.1 Two equations for the same physical question

The deformation of a local threefold separates choices of vacuum from changes of mass and coupling in the four-dimensional theory. For a hypersurface, Chapter 3 made this distinction in two steps. First the Jacobi algebra removed changes of coordinates from the polynomial perturbations. Then the holomorphic three-form, through its periods, converted geometric weights to mass dimensions.

A threefold in five complex coordinates can require two equations. Perturbing the first equation and perturbing the second now give different directions, but the same coordinate change acts on both. There is also freedom to change the generators of the pair of equations without changing their common zero set. We will keep these freedoms together and compute the resulting space of deformations for two quadrics. The answer has two independent constant terms, a feature that a scalar Jacobi algebra would miss. Following a mass deformation will let us eliminate one coordinate, track its residue and tune a local quartic singularity. Replacing one square by a cube will then show how even the mass count can change. We use the residue and period conventions of Chapter 3; the new ingredients are the rank test and the deformation module.

XII.7.2 Finding the isolated threefold

We begin with the germ at the origin of the common zero set in $\mathbb{C}^5$. Is it smooth away from the origin, so that the deformation problem is localized there? To keep the comparison visible, write both examples in one notation:

$$\begin{aligned} &X_0 = \{f_1 = f_2 = 0\}, \qquad f_1 = \sum_{i=1}^{5} h_i, \qquad f_2 = \sum_{i=1}^{5} i h_i, \\ &h_i = x_i^{m_i}, \qquad (m_1, \dots, m_5) = (2, 2, 2, 2, n). \end{aligned} \tag{XII.7.1}$$

Here i in the sum is an integer and $n = 2$ or 3. When $n = 2$ the equations are a pair of diagonal quadrics. Their independence as polynomials is not by itself a dimension count. For these examples, the first nonzero ordinary homogeneous part of f_1 is a quadric of rank five or four. An analytic factorization into nonunits would factor this part into two linear forms, giving rank at most two. Thus f_1 is irreducible in the regular local ring of the ambient space. This ring is factorial, so f_1 is prime. The leading quadratic coefficients of f_2 are not proportional to those of f_1, so f_2 is nonzero modulo (f_1). The two equations form a regular sequence, and

$$\dim_{\mathbb{C}} X_0 = 5 - 2 = 3. \tag{XII.7.2}$$

At a regular point the differentials of the equations are independent: they impose two independent linear restrictions on a tangent vector. The ith column of the Jacobian Df and the minor from columns $i < j$ are

$$\frac{\partial f}{\partial x_i} = m_i x_i^{m_i - 1} \begin{pmatrix} 1 \\ i \end{pmatrix}, \qquad \Delta_{ij} = m_i m_j (j - i) x_i^{m_i - 1} x_j^{m_j - 1}. \tag{XII.7.3}$$

The factor $j - i$ matters: two nonzero coordinates in different columns suffice for rank two. The rank drops precisely where at most one coordinate is nonzero, so the ambient critical locus consists of the five axes. We must intersect it with the fiber. If only x_i can be nonzero, $f_1 = 0$ reduces to $x_i^{m_i} = 0$. Thus no point of these axes except the origin is singular on X_0. We have an isolated complete-intersection singularity (ICIS). For a direct check, the point

$$p_0 = (1, \mathrm{i}\sqrt{2}, 1, 0, 0), \qquad f(p_0) = \begin{pmatrix} 1 - 2 + 1 \\ 1 - 4 + 3 \end{pmatrix} = \begin{pmatrix} 0 \\ 0 \end{pmatrix} \tag{XII.7.4}$$

has nonzero minor Δ_{13}. Scaling its first three coordinates together places such regular points arbitrarily close to the origin.

The argument detects a concrete failure. Change the coefficient of x_2^2 in f_2 from 2 to 1, leaving all other coefficients fixed. On

$$x = (a, \mathrm{i}a, 0, 0, 0), \qquad a \neq 0, \tag{XII.7.5}$$

both equations vanish and the first two nonzero Jacobian columns are parallel. The rank is one, and a singular line now passes through the origin. This particular collision is between two square terms; the form of the singular locus need not be a line for a different collision involving the cube.

For the original distinct slopes, the same minors describe a useful constant slice of the family. Let X_s denote the fiber $f(x) = s$, where $s = (s_1, s_2)^T$. The derivatives do not change when we change s. Restricting f to the ith axis gives

$$(s_1, s_2) = (x_i^{m_i}, i x_i^{m_i}), \qquad \text{critical values:} \quad s_2 = i s_1, \quad i = 1, \ldots, 5. \tag{XII.7.6}$$

Each full line occurs locally over $\mathbb{C}$, since the power map has local roots. Away from these lines a nonempty fiber is smooth. For instance, in the quadratic case $p = (1, 1, 2, 0, 0)$ lies in $X_{(6,15)}$, whose slope $15/6 = 5/2$ lies between 2 and 3. Multiplying p by ε puts

the example in an arbitrarily small smoothing fiber with $s = \varepsilon^2(6, 15)$. Figure XII.7.1 shows the critical-value lines in this constant slice. Allowing other coefficients later will give a larger base, whose discriminant is a different problem.

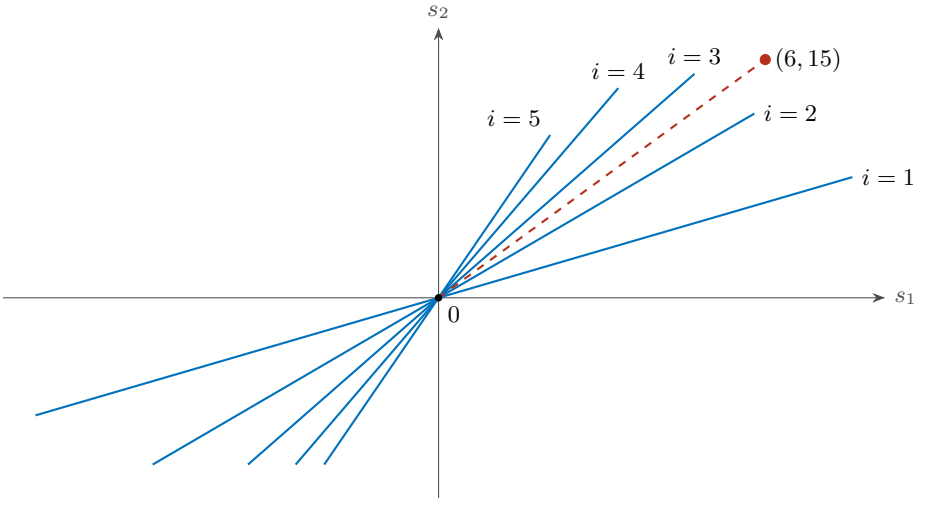


Figure XII.7.1: The real plane in the complex constant-value slice $f = s$. The five solid lines are the real parts of $s_2 = is_1$; the dashed ray reaches the smooth example at $(6, 15)$. The opposite half of each critical line is also present. This figure describes the constant slice, not the discriminant of the full deformation family.

The rank calculation has involved three different spaces. It is useful to trace a single point through them before constructing the larger deformation family. Let $q_i(a)$ be the point whose only nonzero coordinate is $x_i = a$. For $a \neq 0$ its Jacobian has rank one, while its value is

$$q_i(a) \in \mathbb{C}^5, \qquad f(q_i(a)) = (a^{m_i}, ia^{m_i}), \qquad q_i(a) \in X_s \iff s = (a^{m_i}, ia^{m_i}). \tag{XII.7.7}$$

The ambient critical locus is the union of the axes containing these points. Its image lies in the two-dimensional space of constants s. A singular point of X_s must both be critical and lie over that particular s. At $s = 0$ these conditions require $a = 0$. At a nonzero value on the ith line, the equation $a^{m_i} = s_1$ has finitely many nearby solutions; for a square there are two, and for the cube there are three. Thus a whole critical axis does not become a singular axis in each fiber. Most of its points belong to other fibers.

The word isolated refers to the central fiber near its singular point. It does not say that the ambient map $f\colon \mathbb{C}^5 \to \mathbb{C}^2$ has an isolated critical point. Nor does it say that the central value is isolated among critical values. The five critical-value lines accumulate at zero, precisely as needed for singular nearby fibers. The constant slice still contains regular nearby values, such as multiples of $(6, 15)$, because the union of five lines does not fill the two-dimensional value space.

One can also check the distinction on the central fiber itself. At the point p_0 in

(XII.7.4), the nonzero x_1 and x_3 columns have different slopes, and explicitly

$$\Delta_{13}(p_0) = 4(3-1)x_1x_3\big|_{p_0} = 8 \neq 0, \qquad \dim_{\mathbb{C}} \ker Df(p_0) = 5-2 = 3. \tag{XII.7.8}$$

The dimension of this tangent space agrees with the dimension of the complete intersection. At the origin both derivative rows vanish, so the Zariski tangent space has dimension five even though the germ has dimension three. This excess tangent dimension detects the singularity. The calculation concerns geometry on a specified fiber, which is also where the residue three-form will live.

XII.7.3 Independent changes of the defining equations

Which infinitesimal changes of the pair change the threefold? Let $R = \mathbb{C}\{x_1, \dots, x_5\}$ be the ring of convergent power series at the origin, let $I = (f_1, f_2)$, and let $A = R/I$ be the ring on X_0. An equation perturbation is a column $v = v_1e_1 + v_2e_2 \in R^2$, where e_1, e_2 denote the first and second equation slots. Use a formal parameter ϵ with $\epsilon^2 = 0$ and write

$$F(x) = f(x) + \epsilon v(x), \qquad x \longmapsto x + \epsilon b(x), \qquad F \longmapsto (1 + \epsilon C(x))F. \tag{XII.7.9}$$

The last operation is invertible to first order. Each new equation is a combination of the old ones, so the common zero set is unchanged. The coordinate change gives another description of the same germ. Expanding both operations gives

$$(1+\epsilon C)F(x+\epsilon b) = f(x) + \epsilon\big(v(x) + Df(x)b(x) + C(x)f(x)\big). \tag{XII.7.10}$$

To see the coordinate operation without suppressing its coefficients, specialize temporarily to the quadratic pair and translate only x_2. Put $b = (0, c, 0, 0, 0)^T$, where c is constant. Since $\epsilon^2 = 0$, the two terms involving x_2 expand as

$$(x_2 + \epsilon c)^2 = x_2^2 + 2\epsilon c x_2, \qquad 2(x_2 + \epsilon c)^2 = 2x_2^2 + 4\epsilon c x_2. \tag{XII.7.11}$$

Consequently the perturbation $2cx_2e_1 + 4cx_2e_2$ is a coordinate translation. Its two entries cannot be chosen independently. Choosing $c = 1/2$ gives the relation $[x_2e_1] = -2[x_2e_2]$, and leaves one linear direction rather than killing both. The same operation works with a holomorphic function in place of c; terms involving a derivative of that function would be of order ϵ^2 and disappear here.

Equation changes have a different origin. Let E_{12} denote the matrix with its only nonzero entry, equal to one, in row one and column two. Then

$$(1 + \epsilon a E_{12}) \begin{pmatrix} f_1 \\ f_2 \end{pmatrix} = \begin{pmatrix} f_1 + \epsilon a f_2 \\ f_2 \end{pmatrix}, \qquad (1 + \epsilon a E_{12})^{-1} = 1 - \epsilon a E_{12}. \tag{XII.7.12}$$

Here $a = a(x)$ may again be a convergent power series. If the second equation vanishes, the added term in the first vanishes as well. This change therefore preserves the ideal and the common zero set. It accounts for all multiples of f_2e_1. Choosing the other

three matrix entries separately accounts for f_1e_1, f_1e_2, f_2e_2. In a single equation these operations are multiplication by a unit. With two equations they also mix the equation slots.

For each coordinate there is one function b_i, which multiplies the whole ith column of Df. For the equation changes each entry of C is independent: the possible Cf generate all four vectors f_ke_j. We obtain the tangent space to deformations of the germ in the form of an A-module,

$$T^1 = \frac{R^2}{\operatorname{im}_R Df + IR^2} = \frac{A^2}{\operatorname{im}_A Df}. \tag{XII.7.13}$$

This is a deformation of the germ without a marked point required to stay on every fiber. In particular, a constant term can change the value of an equation at the ambient origin. The second form first restricts coefficients to the threefold, then divides by coordinate changes. The first form makes both redundancies explicit in the ambient ring. For an isolated complete-intersection germ, the semiuniversal deformation theorem says that representatives of a basis of T^1 can be inserted in $f + \sum_\alpha \lambda_\alpha v_\alpha$ to obtain a miniversal family. The first-order argument identifies which directions should enter that theorem; it does not prove the theorem itself.

The quotient can be pictured as a calculation with two simultaneous output entries. Coordinate changes enter along columns, while equation changes enter through the defining ideal in each slot:

$$\begin{aligned} R^5 \oplus \operatorname{Mat}_{2\times 2}(R) &\longrightarrow R^2 \longrightarrow T^1 \longrightarrow 0, \\ (b, C) &\longmapsto Df\, b + Cf. \end{aligned} \tag{XII.7.14}$$

The cokernel retains precisely the output vectors that these operations cannot produce. This notation does not require a choice of a basis of T^1; that basis comes from solving the relations. The five inputs in b refer to ambient coordinates, while the two outputs refer to equations. Confusing those roles is the source of the incorrect scalar quotient.

For example, the ideal of all partial derivatives of the quadratic pair contains $2x_i$ for every i. Its scalar quotient would be

$$R/(\partial_i f_1, \partial_i f_2)_{i=1}^5 = R/(x_1, \dots, x_5) \simeq \mathbb{C}. \tag{XII.7.15}$$

It retains just one constant and no linear monomials. But changing the constant in f_1 and changing it in f_2 are two independent perturbations. Every generator of $\operatorname{im} Df + IR^2$ vanishes at the origin, so no nonzero constant vector belongs to that submodule. Already in grade zero the correct quotient must retain both e_1 and e_2. This gives a quick diagnostic before doing any longer reduction.

In the single-equation calculation, weighted Euler places the entire defining ideal in the derivative ideal. For coordinate weights w_i and common equation degree $d = d_1 = d_2$, the equal-degree pair also satisfies an Euler equation. It is now a vector equation,

$$\sum_i w_i x_i \frac{\partial f}{\partial x_i} = df, \qquad d = d_1 = d_2. \tag{XII.7.16}$$

It puts the single vector $(f_1, f_2)^T$ in the derivative image. It does not put all Cf there. The quadratic example shows what would go wrong: the first coordinate column only gives the relation

$$[x_1 e_1] = -[x_1 e_2] \qquad \text{modulo } \operatorname{im}_R Df. \tag{XII.7.17}$$

It does not kill either term individually. Restrict the derivative-only quotient to the x_1 axis and project the equation slots with the row $(-1, 1)$. The first column is annihilated and the others vanish along that axis. The image of $x_1^k e_2$ is x_1^k for every $k \geq 1$. Thus the ambient derivative-only quotient is infinite-dimensional, despite isolation of the singularity on the fiber. Taking a scalar ideal of all partial derivatives would make the opposite error. It would kill x_1 directly and would forget which equation changed.

There is a second diagnostic for the defining-ideal part of the quotient. In the quadratic case the Euler relation is obtained with $b_i = x_i/2$, so $Df\, b = f$. On the x_1 axis, however, the row $(-1, 1)$ used above evaluates the separate equation generator as

$$(-1,1) f\big|_{x_2=\cdots=x_5=0} = 0, \qquad (-1,1)(f_2 e_1)\big|_{x_2=\cdots=x_5=0} = -x_1^2. \tag{XII.7.18}$$

The first identity is compatible with f being in the derivative image. The nonzero second value shows that $f_2 e_1$ is not in that image, since the row annihilates every derivative column after restriction. Thus Euler removes the simultaneous rescaling of the pair, but cannot replace the four equation-generator relations. After quotienting by I, the surviving powers on the axis are truncated. This is how the deformation problem becomes localized on the isolated fiber even though the ambient derivative-only module was infinite.

The two-component description also tells us how to translate between choices of equations. If B is an invertible constant matrix and $f' = Bf$, then the ideal I is unchanged, $Df' = BDf$, and

$$f + \epsilon v \longmapsto Bf + \epsilon B v, \qquad [v] \longmapsto [Bv]. \tag{XII.7.19}$$

For $B = \left(\begin{smallmatrix} 2 & 1 \\ -1 & 3 \end{smallmatrix}\right)$, the representative $x_2 e_2$ becomes $x_2(e_1 + 3e_2)$. The representative changes even though it describes the same direction after transport. Equal equation weights ensure that this change preserves the polynomial grade. We will see how the same operation changes the residue used to normalize the physical periods.

XII.7.4 The nine deformation directions

We now reduce the quadratic pair in (XII.7.1). What are the independent perturbations after the two redundancies have been removed? Give every variable weight one and both equations weight two. The relations are homogeneous, so it is enough to solve one grade at a time. There is no constant in any Jacobian column or equation, leaving e_1 and e_2 in grade zero. In grade one each column gives its own relation $x_i e_1 + i x_i e_2 = 0$. There are five independent classes $x_i e_2$, one for each variable.

In grade two, for $i \neq j$, multiplying each linear relation by the other variable gives

$$x_i x_j (e_1 + i e_2) = 0, \qquad x_i x_j (e_1 + j e_2) = 0 \quad \Longrightarrow \quad x_i x_j e_1 = x_i x_j e_2 = 0. \tag{XII.7.20}$$

Only pure squares remain. Use $u_i = [x_i^2 e_2]$ for these square classes. The derivative columns already give $[x_i^2 e_1] = -iu_i$. The four ideal generators now give three independent rows:

$$[f_1 e_2] = \sum_i u_i, \qquad [f_2 e_2] = -[f_1 e_1] = \sum_i i u_i, \qquad [f_2 e_1] = -\sum_i i^2 u_i. \tag{XII.7.21}$$

Here the expressions are reduced by the Jacobian columns before imposing the ideal. Setting the rows to zero, the first three columns of the moment matrix have determinant 2:

$$\begin{pmatrix} 1 & 1 & 1 & 1 & 1 \\ 1 & 2 & 3 & 4 & 5 \\ 1 & 4 & 9 & 16 & 25 \end{pmatrix} \begin{pmatrix} u_1 \\ u_2 \\ u_3 \\ u_4 \\ u_5 \end{pmatrix} = 0, \qquad \begin{pmatrix} u_1 \\ u_2 \\ u_3 \end{pmatrix} = \begin{pmatrix} -1 & -3 \\ 3 & 8 \\ -3 & -6 \end{pmatrix} \begin{pmatrix} u_4 \\ u_5 \end{pmatrix}. \tag{XII.7.22}$$

The moment equations can be solved by ordinary elimination. Subtract the first row from the second and subtract the second row from the third in (XII.7.22). One obtains

$$\begin{aligned} u_1 + u_2 + u_3 &= -u_4 - u_5, \\ u_2 + 2u_3 &= -3u_4 - 4u_5, \\ 2u_2 + 6u_3 &= -12u_4 - 20u_5. \end{aligned} \tag{XII.7.23}$$

The last row minus twice the middle row gives $2u_3 = -6u_4 - 12u_5$. Back substitution gives the other two lines of the solution in (XII.7.22). This calculation identifies representatives, not only their number. In particular, a perturbation of a discarded square still contributes to the retained coefficients.

For a concrete reduction, consider a vector containing constants, a linear term, a mixed quadratic and two pure squares,

$$v = 3e_1 - 2e_2 + 7x_2 e_1 + x_1 x_3 (e_1 + 2e_2) + x_2^2 e_1 + 2x_3^2 e_2. \tag{XII.7.24}$$

First use the linear column to replace $7x_2 e_1$ by $-14x_2 e_2$. The mixed quadratic vanishes in both slots. In the remaining square part, $x_2^2 e_1 = -2u_2$, so the moment solution gives

$$\begin{aligned} [x_2^2 e_1 + 2x_3^2 e_2] &= -2u_2 + 2u_3 \\ &= -2(3u_4 + 8u_5) + 2(-3u_4 - 6u_5) \\ &= -12u_4 - 28u_5. \end{aligned} \tag{XII.7.25}$$

The complete answer is therefore

$$[v] = 3[e_1] - 2[e_2] - 14[x_2 e_2] - 12u_4 - 28u_5. \tag{XII.7.26}$$

This vector would shift the five corresponding coefficients in the local family. A representative is allowed to have entries in both equations even though most of the chosen basis happens to occupy only the second slot. The reduction, rather than the appearance of a representative, determines which coefficients it changes.

A useful check is to start with an actual redundancy. For example,

$$[x_2^2(e_1+2e_2)] = -2u_2 + 2u_2 = 0, \qquad [f_2 e_1] = -\sum_i i^2 u_i = 0. \tag{XII.7.27}$$

The first vanishes because it is a coordinate-change column times $x_2/2$. The second vanishes by an equation change, using the third moment row. Both must reduce to zero, but they use different relations. This distinction is useful when repeating the method for the cube.

The nonzero determinant shows that the two retained square representatives are free of further grade-two relations. In grade three any term involving two different variables already vanishes. Multiplying the first moment row by x_j leaves just one term,

$$0 = x_j \sum_i u_i = x_j^3 e_2 \qquad \text{in } T^1. \tag{XII.7.28}$$

The derivative relation kills $x_j^3 e_1$ as well. All higher monomials are multiples of the cubic ones.

Let us separate spanning from independence in this calculation. At grade one there are ten vectors $x_i e_a$. The five derivative relations have disjoint monomial supports, so their rank is five. At grade two, every mixed monomial is eliminated by two independent column relations because the slopes differ. For each pure square the derivative relation leaves one class u_i. The ideal then imposes the three moment rows, whose rank is three. Hence

$$\dim T_0^1 = 2, \qquad \dim T_1^1 = 10 - 5 = 5, \qquad \dim T_2^1 = 5 - 3 = 2, \qquad T_g^1 = 0 \ (g \geq 3). \tag{XII.7.29}$$

The displayed eliminations show spanning, while these relation ranks show that no retained coefficient can be removed. Truncation has a further consequence for analytic perturbations. A convergent series has infinitely many monomials, but every term of degree at least three belongs to the submodule of redundancies. Its class is represented by its degree-at-most-two part, reduced by the same finite linear algebra. This is why a finite polynomial basis controls the analytic deformation problem here.

The basis and the corresponding local family are therefore

$$\mathcal{B}_2 = \{e_1, e_2,\ x_i e_2 \ (1 \leq i \leq 5),\ x_4^2 e_2, x_5^2 e_2\}, \qquad \sum_g \dim T_g^1 \, t^g = 2 + 5t + 2t^2, \tag{XII.7.30}$$

$$F_1 = f_1 + U_1, \qquad F_2 = f_2 + U_2 + \sum_{i=1}^{5} M_i x_i + K_4 x_4^2 + K_5 x_5^2. \tag{XII.7.31}$$

Each symbol U_i, M_i or K_i is a coefficient of one representative, not a change of coordinates on the ambient space. Figure XII.7.2 keeps track of the three groups. The right column anticipates their coefficient dimensions; we will derive it from the residue.

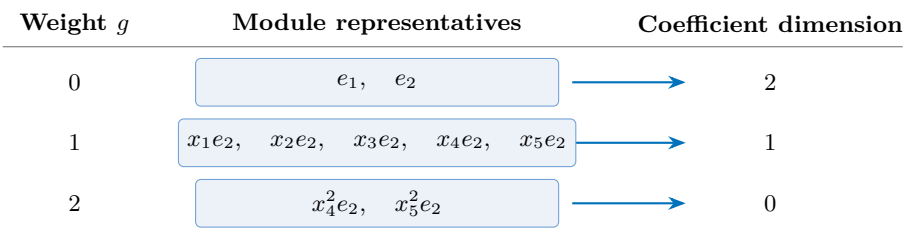


Figure XII.7.2: The basis of the two-quadric deformation module, arranged by monomial weight in the frame $w_i = 1$. Each listed vector represents one class in the quotient. Its associated coefficient has dimension $2 - g$ when the representative has weight g, as derived below.

A scalar ring can give the right total and still give the wrong answer. The ideal generated by I and the Jacobian minors describes the rank-drop scheme on X_0. For these quadrics its minors kill mixed monomials, and f_1, f_2 impose two scalar square relations. Cubics then vanish just as in (XII.7.28), but there is only one constant and there are three independent squares. Its graded count is

$$\mathrm{Hilb}_{R/(I,\,\Delta_{ij})}(t) = 1 + 5t + 3t^2, \qquad \mathrm{Hilb}_{T^1}(t) = 2 + 5t + 2t^2. \tag{XII.7.32}$$

Both totals are nine. Only the vector module distinguishes the two constant equation shifts. The scalar ring is useful for studying where rank drops; its graded basis does not parametrize the family in (XII.7.31).

The dimension $\tau = \dim_{\mathbb{C}} T^1$ is the Tjurina number. The Milnor number μ is instead the rank of the middle homology of a smooth local Milnor fiber. They agree for the positive-dimensional quasihomogeneous isolated complete intersections considered here. Thus $\mu = \tau = 9$ for the two quadrics. One can obtain the same topological count without finding a deformation basis. For this weighted threefold, the Euler characteristic of the Milnor fiber $\mathcal{F}$ is given by the coefficient formula

$$\chi(\mathcal{F}) = \frac{d_1 d_2}{\prod_i w_i}[t^3]\frac{\prod_i (1 + w_i t)}{(1 + d_1 t)(1 + d_2 t)} = 4(10 - 40 + 60 - 32) = -8 \tag{XII.7.33}$$

at $w_i = 1$, $d_1 = d_2 = 2$. Here $[t^3]$ means the coefficient of t^3 about $t = 0$. The local Milnor fiber has the homotopy type of a bouquet of three-spheres, so $\chi(\mathcal{F}) = 1 - \mu$. This recovers $\mu = 9$ as a homology rank. It counts possible topological charge directions, not stable wrapped particles.

To repeat the independent Euler calculation, expand numerator and denominator separately to the needed order. Only the cubic coefficient matters:

$$\begin{aligned} (1 + t)^5 &= 1 + 5t + 10t^2 + 10t^3 + O(t^4), \\ (1 + 2t)^{-2} &= 1 - 4t + 12t^2 - 32t^3 + O(t^4), \\ [t^3]\frac{(1 + t)^5}{(1 + 2t)^2} &= 10 - 4 \cdot 10 + 12 \cdot 5 - 32 = -2. \end{aligned} \tag{XII.7.34}$$

Multiplication by four gives $\chi = -8$. For a bouquet of μ three-spheres the single connected component contributes 1 to Euler characteristic and each three-sphere

contributes -1, giving $1-\mu$. The two calculations count different objects before the weighted-ICIS theorem relates them. The agreement is a check of the length, while the explicit module remains necessary to recover the grading and the equation slots.

XII.7.5 The residue sets the physical scale

A geometric weight tells us how a deformation scales relative to the defining equations. How do we turn that weight into a mass dimension? In the direct IIB construction, the scale comes from periods of a holomorphic three-form. With two equations the residue must remove both normal directions.

Fix a smooth fiber $X_{\boldsymbol{\lambda}}$ of $F=(F_1,F_2)^T$. The differentials in this section are taken in the ambient coordinates with the coefficients fixed on that fiber. Suppose $\Delta_{ij}=\det\bigl(\partial(F_1,F_2)/\partial(x_i,x_j)\bigr)$ is nonzero for $i<j$. The complementary coordinates x_k,x_l,x_m in increasing order are local coordinates along the fiber. In the ambient order $dx_1\wedge\cdots\wedge dx_5$, the ordered residue is represented by

$$\Omega_{ij}=(-1)^{i+j-3}\frac{dx_k\wedge dx_l\wedge dx_m}{\Delta_{ij}}\Bigg|_{X_{\boldsymbol{\lambda}}}. \tag{XII.7.35}$$

To derive the formula, wedge the complementary differentials with $d_xF_1\wedge d_xF_2$. The only surviving term of the latter is $\Delta_{ij}dx_i\wedge dx_j$. Bringing (i,j,k,l,m) back to the ambient order gives the displayed sign. For the ambient representative $\widetilde{\Omega}_{ij}$ this gives

$$d_xF_1\wedge d_xF_2\wedge\widetilde{\Omega}_{ij}=dx_1\wedge\cdots\wedge dx_5. \tag{XII.7.36}$$

The condition fixes the restriction of $\widetilde{\Omega}_{ij}$ to the tangent space. Indeed, choose ordered normal vectors N_a with $d_xF_b(N_a)=\delta_{ba}$. Evaluating (XII.7.36) on those two normals and three tangent vectors leaves the desired evaluation of Ω. Changing a normal lift by a tangent vector adds a volume evaluation with four tangent vectors in a three-dimensional space, which vanishes. This is why different chart formulas describe the same form on the fiber even though their ambient representatives differ.

On the quadratic fiber $f(p)=(6,15)^T$ considered earlier, a tangent frame at p is

$$T_1=(2,-4,1,0,0)^T,\qquad T_2=(0,0,0,1,0)^T,\qquad T_3=(0,0,0,0,1)^T. \tag{XII.7.37}$$

The first Jacobian row gives $4-8+4=0$ on T_1 and the second gives $4-16+12=0$. The last two vectors are tangent because $x_4=x_5=0$ at p. On charts $(1,2)$, $(1,3)$ and $(2,3)$ the minors are $4,16,8$. Evaluating the signed complementary differentials on the frame gives $1,4,2$, respectively. Thus

$$\Omega(T_1,T_2,T_3)=\frac{1}{4}=\frac{4}{16}=\frac{2}{8}. \tag{XII.7.38}$$

The signs in the chart formula can be checked directly on this frame. In chart $(1,3)$ the complement is $(2,4,5)$ and $(-1)^{1+3-3}=-1$. The restriction of $dx_2\wedge dx_4\wedge dx_5$ evaluates to -4 on (T_1,T_2,T_3). Thus its signed value is 4. In chart $(2,3)$ the complement

is $(1,4,5)$, the sign is positive and the numerator evaluates to 2. The three chart calculations are

(i,j)	$(1,2)$	$(1,3)$	$(2,3)$
$(-1)^{i+j-3}$	$+1$	-1	$+1$
$(dx_k \wedge dx_l \wedge dx_m)(T_1,T_2,T_3)$	1	-4	2
$\Delta_{ij}(p)$	4	16	8

(XII.7.39)

The entries differ because each chart solves for a different pair of normal coordinates. Their ratios agree because the resulting form is evaluated on the same tangent vectors. In particular, comparing numerator coefficients alone would not compare the same residue. The nonzero minor is part of the chart, not an optional multiplicative constant.

Now change the equations to $F' = BF$. Their conormal wedge is multiplied by $\det B$, so their ordered residue becomes

$$\Omega' = \frac{\Omega}{\det B}. \tag{XII.7.40}$$

In the determinant-seven frame of (XII.7.19) this gives $1/28$ on the same tangent frame. Swapping the equations instead reverses the sign. These are changes of the representative three-form, not changes of the fiber. An independently fixed physical normalization would compensate the common factor.

We now let the coefficients vary again. Write the weight of x_i as w_i, the weight of equation F_j as d_j, and the monomial weight of a representative $p_\alpha e_j$ as Q_α. For its term to scale with F_j, its coefficient must carry weight $d_j - Q_\alpha$. Under the combined action,

$$x_i \longmapsto t^{w_i} x_i, \qquad \lambda_\alpha \longmapsto t^{d_j - Q_\alpha}\lambda_\alpha, \qquad F_j \longmapsto t^{d_j} F_j. \tag{XII.7.41}$$

A coefficient that is held fixed at a generic nonzero value with nonzero weight breaks coordinate scaling on that fiber. A weight-zero coefficient is different: if only such coefficients are nonzero, the equations remain homogeneous with the coefficients held fixed.

Under the combined action, each relative differential $d_x F_j$ scales with its equation. In (XII.7.36) the volume form contributes $\sum_i w_i$ and the two conormals contribute $d_1 + d_2$. The weight left for the residue is

$$Q_\Omega = \sum_i w_i - d_1 - d_2. \tag{XII.7.42}$$

For the two quadrics this is $5 - 2 - 2 = 1$. Using degree-one equations instead, with $w_i = 1/2$, gives $Q_\Omega = 1/2$. This common rescaling of all algebraic weights cannot change a ratio of weights.

The next step uses the physical local limit. The proposed construction first sends the IIB string coupling to zero at fixed string length and then sends the string length ℓ_s to zero. The selected four-dimensional sector is assumed to survive this low-energy limit. The deformation calculation does not establish this decoupling. In that sector a D3-brane wrapped on a suitable three-cycle γ has central charge proportional to the

period of Ω. For a BPS particle the mass is the modulus of its central charge. Thus we assign the period mass dimension one:

$$Z_\gamma \;\propto\; \int_\gamma \Omega, \qquad [Z_\gamma] = 1, \qquad [\Omega] = 1. \tag{XII.7.43}$$

When the scaling transports both fiber and cycle, the period scales with the form. We can therefore divide geometric weights by the positive residue weight to obtain

$$[\lambda_\alpha] = \frac{d_j - Q_\alpha}{Q_\Omega}. \tag{XII.7.44}$$

It is helpful to perform this conversion with a coefficient already present in the equations. Take the term $M_2 x_2$ in F_2 of the quadratic family. In the integer-weight frame it must transform as a quadratic term, so

$$x_2 \longmapsto t x_2, \qquad M_2 \longmapsto t M_2, \qquad M_2 x_2 \longmapsto t^2 M_2 x_2, \qquad \Omega \longmapsto t\Omega. \tag{XII.7.45}$$

The period and M_2 therefore scale by the same power, giving $[M_2] = 1$. For a constant U_2, no coordinate factor supplies any of the equation weight, and $U_2 \mapsto t^2 U_2$, giving dimension two. For $K_4 x_4^2$ the monomial already supplies the full weight, so K_4 has dimension zero.

The degree-one frame gives exactly the same conclusion without assigning the coordinates unit weight. There the two equation weights are one, each coordinate has weight $1/2$, and the residue has weight $1/2$. Thus

$$[U_2] = \frac{1}{1/2} = 2, \qquad [M_2] = \frac{1 - 1/2}{1/2} = 1, \qquad [K_4] = \frac{1-1}{1/2} = 0. \tag{XII.7.46}$$

Equation weight one is a convenient algebraic convention; it is not a declaration that every coefficient has mass dimension one. The residue fixes the conversion because a transported period is the physical quantity whose mass dimension is prescribed. Multiplying Ω by a fixed nonzero constant rescales both its pointwise evaluations and its periods, while leaving these scaling ratios unchanged. The value $1/4$ computed above is its evaluation on the tangent frame (T_1, T_2, T_3), rather than a cycle integral. Changing equation generators and changing units of mass are correspondingly distinct operations.

There are also two uses of scaling in these formulas. On the total family, x and the coefficients transform together, sending one fiber to another. On a fixed fiber with $M_2 \neq 0$, coordinate scaling alone changes the relative coefficient of $M_2 x_2$ and the quadrics. Only in the homogeneous slice with all positive-weight coefficients set to zero does this scaling act with those coefficients held fixed. Keeping these operations distinct makes the dimension calculation meaningful even when an individual smooth deformed fiber has no scaling symmetry.

The rule sets dimensions. It does not fix an overall period prefactor or guarantee that a stable BPS particle exists on every cycle.

XII.7.6 Vacuum parameters, masses, and couplings

Which coefficients label a vacuum of the four-dimensional theory, and which change the theory? In the IIB parameter dictionary, a coefficient of dimension greater than one is

a local Coulomb-branch expectation value, with the same dimension as its Coulomb operator. A dimension-one coefficient is a mass. To understand the remaining positive dimensions, recall the chiral deformation of the action. The four supercharges in its top component contribute two units of mass dimension, while the spacetime measure contributes minus four:

$$\delta S = \lambda \int d^4x\, \widetilde{Q}^4 \mathcal{O} + \text{complex conjugate}, \qquad [\lambda] + [\mathcal{O}] + 2 - 4 = 0. \tag{XII.7.47}$$

Here $\mathcal{O}$ is the Coulomb chiral operator and $\widetilde{Q}^4\mathcal{O}$ denotes its chiral top component. When $1 < [\mathcal{O}] < 2$, the coefficient has $0 < [\lambda] < 1$ and is a relevant coupling. For example, a dimension-3/2 operator has a dimension-7/2 top component, so its coupling has dimension 1/2. The cubic example below realizes this pairing. A dimension-two operator allows a dimensionless coefficient in this counting; the argument does not prove that a dimensionless direction is exactly marginal. Negative coefficient dimensions label formal irrelevant directions of the geometric family. They do not specify independent ultraviolet-complete deformations.

In the quadratic example $d_j = 2$ and $Q_\Omega = 1$. The three grades in Figure XII.7.2 now acquire their physical dimensions:

$$[U_a] = \frac{2-0}{1} = 2, \qquad [M_i] = \frac{2-1}{1} = 1, \qquad [K_4] = [K_5] = \frac{2-2}{1} = 0. \tag{XII.7.48}$$

For example, the shift U_2 and the coefficient K_4 both change the second equation. Their weights differ because U_2 multiplies a constant and K_4 multiplies a square. Setting the normalization by the residue rather than by the equation alone makes this difference a difference in physical role. Counting directions yields

$$\begin{gathered} r = 2, \qquad \{\Delta_{\text{Coulomb}}\} = \{2, 2\}, \\ \#\{\text{mass coordinates}\} = 5, \qquad \#\{\text{dimensionless coefficients}\} = 2. \end{gathered} \tag{XII.7.49}$$

The rank r is the dimension of the Coulomb branch, not the dimension nine of the whole deformation base. The five coefficients M_i provide mass coordinates in this local description; the module does not identify them with a preferred basis of the flavor Cartan. Likewise the dimension pairing does not select a preferred pairing of the two U coefficients with the two K coefficients.

We can see what the dimensionless coefficients do directly in the equations. Set all U_a and M_i to zero and vary K_4, K_5. Then $F_1 = f_1$ and the slopes of F_2 are

$$(1, 2, 3, 4, 5) \longmapsto (1, 2, 3, 4 + K_4, 5 + K_5). \tag{XII.7.50}$$

The equations remain quadratic, and sufficiently small changes leave the slopes distinct. The rank calculation in (XII.7.3) then proves that the central singularity remains isolated. This explains geometrically why this slice has a fixed-coefficient scaling symmetry. It does not by itself determine a quantum conformal manifold.

XII.7.7 Following a mass deformation

What does one of the five mass coefficients actually do to the two-equation geometry? We can answer this without changing the underlying example. Turn on $M = M_5$, retain

the two Coulomb coordinates $U = U_1$ and $V = U_2$, and set the other masses and the two dimensionless coefficients to zero. With $y = x_5$, the resulting slice of (XII.7.31) is

$$\begin{aligned} F_1 &= \sum_{i=1}^{4} x_i^2 + y^2 + U, \\ F_2 &= \sum_{i=1}^{4} i x_i^2 + 5y^2 + My + V. \end{aligned} \tag{XII.7.51}$$

The coefficient M has mass dimension one. We will fix a nonzero value of M and study which choices of the vacuum coordinates leave a singular fiber. This is a deformation of the original pair, rather than a replacement of one exponent by another.

The fifth quadratic terms have the same ratio in both equations. Subtracting five times the first equation from the second removes them. To keep the remaining terms visible, define

$$a_i = i - 5, \qquad A = \sum_{i=1}^{4} x_i^2, \qquad B = \sum_{i=1}^{4} a_i x_i^2, \qquad C = V - 5U. \tag{XII.7.52}$$

The ordered change $(F_1, F_2) \mapsto (F_1, G)$ has determinant one and gives

$$G = F_2 - 5F_1 = My + B + C, \qquad y = -\frac{B + C}{M}. \tag{XII.7.53}$$

For $M \neq 0$ this solves for an actual ambient coordinate. Substitution in F_1 gives a hypersurface in four coordinates,

$$H(x; U, C, M) = A + \frac{(B + C)^2}{M^2} + U = 0, \qquad \operatorname{Res}_y(F_1, F_2) = M^2 H. \tag{XII.7.54}$$

Projection to $x_1, \ldots, x_4$ and the graph in (XII.7.53) are inverse maps of these fibers. The hypersurface retains the full geometry of this fixed-mass slice. It also retains the vacuum parameters in both its quadratic and constant coefficients. The chart contains inverse powers of M and therefore does not extend to the original $M = 0$ singularity.

The inverse powers are compatible with the ultraviolet dimensions already assigned. Each x_i has dimension one, B, C, U have dimension two, and every term of H has dimension two. One can keep the singular points inside an arbitrarily small representative of the original germ by taking

$$x_i = M\xi_i, \qquad y = M\eta, \qquad U = M^2 u, \qquad C = M^2 c. \tag{XII.7.55}$$

At bounded ξ_i, η, u, c, all five coordinates approach the original origin as $M \to 0$. We use these ratios to locate the nearby fibers; this observation does not make the elimination chart regular at $M = 0$.

Elimination also explains how the two-component deformation module becomes a scalar one on this slice. Use $g = G$ as the fifth ambient coordinate. The first equation then reads

$$F_1 = H - \frac{2(B + C)}{M^2} g + \frac{g^2}{M^2}, \qquad G = g. \tag{XII.7.56}$$

An original infinitesimal perturbation $v = (v_1, v_2)^T$ becomes $(v_1, v_2 - 5v_1)^T$ in this equation basis. Write $w_2 = v_2 - 5v_1$ and evaluate the perturbations on the unperturbed graph. The perturbed second equation sets $g = -\epsilon w_2 + O(\epsilon^2)$, so the first becomes

$$F_1 + \epsilon v_1 = H + \epsilon \left(v_1 + \frac{2(B+C)}{M^2}(v_2 - 5v_1) \right) + O(\epsilon^2). \tag{XII.7.57}$$

Thus the remaining scalar normal direction is the displayed combination of both slots. A perturbation of the first equation survives even when the second original slot is zero. Conversely, after the coordinate g and its equation have been removed, scalar coordinate changes add derivatives of H. The local deformation quotient is therefore the hypersurface quotient by H and its derivatives. It is obtained by this elimination, not by retaining just one slot of the old module.

We can now find every singular fiber in the (U, C) plane at fixed M. Differentiating the actual hypersurface gives

$$H_i = 2x_i \left(1 + \frac{2a_i(B+C)}{M^2} \right), \qquad i = 1, \dots, 4. \tag{XII.7.58}$$

If two coordinates x_i, x_j were nonzero at a critical point, the parentheses would require $a_i = a_j$. The four slopes are distinct. Every critical point therefore lies either at the origin of the x chart or on a single x_i axis. This exhausts the possibilities, rather than selecting a few particularly symmetric critical points.

At $x = 0$ the remaining equation and its original-coordinate location are

$$D_0 = M^2 U + C^2 = 0, \qquad (x_1, x_2, x_3, x_4, y) = (0, 0, 0, 0, -C/M). \tag{XII.7.59}$$

This point is the original ambient origin only when $C = 0$. Its Hessian in the four-variable chart is diagonal, with entries $2(1 + 2a_i C/M^2)$. When none vanishes the local quadratic form is nondegenerate, so the singularity is an ordinary node.

For $x_i \neq 0$, (XII.7.58) first fixes $B + C = -M^2/(2a_i)$. Imposing $H = 0$ then gives

$$\begin{aligned} D_i &= a_i^2 U - a_i C - \frac{M^2}{4} = 0, \\ x_i^2 &= -U - \frac{M^2}{4a_i^2}, \qquad x_{j \neq i} = 0, \qquad y = \frac{M}{2a_i}. \end{aligned} \tag{XII.7.60}$$

If the displayed square is nonzero there are two distinct points over $\mathbb{C}$. At either point the axial and transverse Hessian entries are

$$H_{ii} = \frac{8a_i^2 x_i^2}{M^2}, \qquad H_{jj} = 2\left(1 - \frac{a_j}{a_i}\right) \quad (j \neq i), \qquad H_{jk} = 0 \quad (j \neq k). \tag{XII.7.61}$$

All four diagonal entries are nonzero. The generic fiber on D_i therefore has two ordinary nodes. This count concerns singular points of that fiber, rather than stable particles in the associated four-dimensional theory.

There is a direct check in the original pair. Its minors are

$$\Delta_{ij} = 4(j - i)x_i x_j, \qquad \Delta_{i5} = 2x_i(M - 2a_i y), \qquad i, j \leq 4. \tag{XII.7.62}$$

The first minors again exclude two nonzero x coordinates, and the second give $y = M/(2a_i)$ on the nonzero-axis branch. On that nonzero-axis branch, a finite multiplier $dF_2 = \lambda dF_1$ gives the same result, with $\lambda = i$. One must separate the original origin: there $dF_1 = 0$ and $dF_2 = M\,dy$, so the rank is one although no finite λ exists. It belongs to the fiber at $U = V = 0$ and is already included by (XII.7.59). The minors and the hypersurface gradient both cover this exception.

The reduced discriminant of this fixed-mass slice is consequently the union $D_0 \cup D_1 \cup \cdots \cup D_4$. In the dimensionless variables of (XII.7.55), its components take a useful form,

$$D_0 : \quad u = -c^2, \qquad D_i : \quad u = \frac{c}{a_i} + \frac{1}{4a_i^2}, \qquad (c_i^*, u_i^*) = \left(-\frac{1}{2a_i}, -\frac{1}{4a_i^2}\right). \tag{XII.7.63}$$

Each line is tangent to the parabola at the displayed point. These are precisely the points where the axis square in (XII.7.60) vanishes and the two axis nodes meet the x-origin node. Figure XII.7.3 displays this collision in a real slice. Intersections of two distinct lines instead give two node pairs; their D_0 value is $M^4(a_i - a_j)^2/(16a_i^2a_j^2) \neq 0$. The description determines the reduced set of singular fibers. It assigns no discriminant scheme multiplicities.

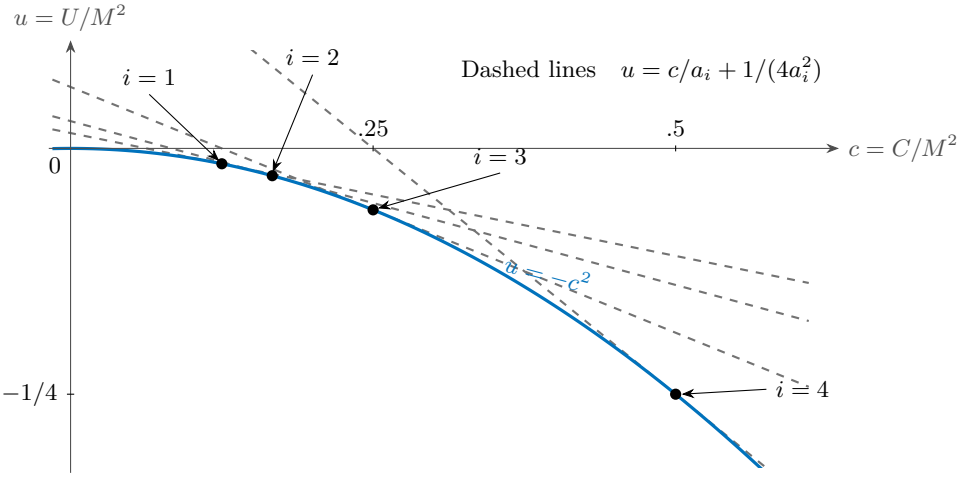


Figure XII.7.3: A real slice of the reduced discriminant at fixed nonzero M. The solid parabola is the component with a node at $x = 0$; the dashed tangent lines are the four components with a pair of axis nodes. A black point labels the tangency associated with that index i, where the three nodes coalesce into the quartic local singularity derived below. The equations define complex curves; the drawing shows only their real plane and this restricted mass slice.

XII.7.8 The residue near a selected node

The eliminated equation still controls the normalization of the three-form. How does the original ordered residue compare with the hypersurface residue, and which small parameter does a local period measure? Fix $M \neq 0$ throughout. Define Ω_H with the same normal-first convention used earlier,

$$dH \wedge \Omega_H = dx_1 \wedge \cdots \wedge dx_4, \qquad dF_1 \wedge dG \wedge \Omega = dx_1 \wedge \cdots \wedge dx_4 \wedge dy. \tag{XII.7.64}$$

The second equality retains Ω because the equation change to (F_1, G) has determinant one. In coordinates (x, g), the ambient volume is $M^{-1} d^4x \wedge dg$, while $dF_1 \wedge dg = dH \wedge dg$ on $g = 0$. Moving dg past the three-form gives

$$dH \wedge dg \wedge \Omega_H = -d^4x \wedge dg, \qquad \boxed{\Omega = -\frac{1}{M}\Omega_H}. \tag{XII.7.65}$$

The sign follows from the equation and ambient orders. The factor $1/M$ is the Jacobian for removing y. Neither is supplied merely by recognizing the resulting hypersurface.

The coordinate charts give an independent way to recover both factors. Substituting the graph into (XII.7.62) gives

$$\begin{aligned} \Delta_{i5}|_{G=0} &= M H_i, \\ \Omega &= \frac{(-1)^i \, dx_1 \wedge \cdots \widehat{dx_i} \cdots \wedge dx_4}{M H_i}, \\ \Omega_H &= \frac{(-1)^{i-1} \, dx_1 \wedge \cdots \widehat{dx_i} \cdots \wedge dx_4}{H_i}. \end{aligned} \tag{XII.7.66}$$

These formulas are used only where the denominator is nonzero. They agree with the wedge calculation on every such chart. A reversal of the solved sign of y would satisfy the even equation F_1 but fail $G = 0$; a missing factor $1/M$ would instead preserve the zero set and change its periods. The graph and residue are separate parts of the construction.

Choose the node at $U = C = 0$ and approach it through the smoothing path $C = 0$. Write

$$\begin{aligned} x_i = \sqrt{M}\, q_i, \qquad U = M\varepsilon, \qquad B(q) = \sum_{i=1}^{4} a_i q_i^2, \\ h = \frac{H}{M} = \sum_{i=1}^{4} q_i^2 + \frac{B(q)^2}{M} + \varepsilon. \end{aligned} \tag{XII.7.67}$$

A branch of $\sqrt{M}$ is chosen locally for this fixed nonzero mass. Since $d^4x = M^2 d^4q$ and $dH = M\, dh$ along a fixed fiber, (XII.7.65) becomes

$$\Omega = -\operatorname{Res}_{h=0} \frac{d^4q}{h}. \tag{XII.7.68}$$

The two factors of M in the coordinate volume cancel the equation factor and the elimination Jacobian. The resulting coefficient $\varepsilon = U/M$ has ultraviolet mass dimension

one, while q_i has dimension $1/2$. These statements retain $[U] = 2$ and $[M] = 1$; they do not change the ultraviolet assignment of U.

There is an explicit compact cycle on which to measure this scale. Take $M > 0$, set $\varepsilon = -t$ with $t > 0$, and assume $t/M \ll 1$. The real locus

$$\sum q_i^2 + \frac{B(q)^2}{M} = t, \qquad q_i = \sqrt{t}\, w_i, \qquad \sum w_i^2 + \frac{t}{M} B(w)^2 = 1 \tag{XII.7.69}$$

is a smooth deformation of a three-sphere. Along each real radial direction its left side is strictly increasing with the radius. The cycle shrinks to the node as $t \to 0$, and the quartic term is a controlled correction to its shape. Under this substitution the residue contributes an overall factor t, since its four coordinate differentials give t^2 and the equation gives t.

To find the leading coefficient, first set the quartic correction to zero. For the homogeneous node $h_0 = \sum q_i^2 - t$, let $E = \sum q_i \partial_{q_i}$ be the radial vector and let d^4q be the oriented Euclidean volume form. On the sphere, $dh_0(E) = 2t$, so its residue and integral are

$$\Omega_{h_0} = \frac{\iota_E d^4 q}{2t}, \qquad \int_{S^3_{\sqrt{t}}} \Omega_{h_0} = \frac{\mathrm{Area}(S^3_{\sqrt{t}})}{2\sqrt{t}} = \pi^2 t. \tag{XII.7.70}$$

The orientation is the boundary orientation with the outward radial normal first. The factor $2\sqrt{t}$ in the denominator is the radial derivative of h_0. The sign for the original complete intersection is the minus sign in (XII.7.68).

The correction is regular in the small ratio $\kappa = t/M$. Indeed, write $w = rn$ with $n \in S^3$ and put $b = B(n)$. The level equation and positive radial solution are

$$\begin{aligned} &r^2 + \kappa b^2 r^4 = 1, \qquad r^2 = \frac{2}{1 + \sqrt{1 + 4\kappa b^2}}, \\ &\frac{r^3}{\partial_r (r^2 + \kappa b^2 r^4)} = \frac{r^2}{2 + 4\kappa b^2 r^2} = \frac{1}{2} + O(\kappa). \end{aligned} \tag{XII.7.71}$$

The expansion is uniform on the compact unit sphere for sufficiently small positive κ. If Γ_t is the deformed real vanishing cycle with the same outward orientation, the original form therefore has the period

$$\Pi(t) = \int_{\Gamma_t} \Omega = -\pi^2 t \left[1 + O\left(\frac{t}{M} \right) \right]. \tag{XII.7.72}$$

This is a local period with a stated residue normalization. Under the IIB premise of (XII.7.43), it is proportional to a central charge, with the same unspecified overall physical prefactor as before. The calculation shows which small scale a shrinking cycle measures. It does not infer a stable particle on every cycle or identify the complete infrared theory of the mass-deformed rank-two construction.

XII.7.9 Tuning the quartic local singularity

At a tangency in Figure XII.7.3, two axis nodes meet the node at $x = 0$. What singularity replaces them? The tuned coordinates for index i are

$$U_i^* = -\frac{M^2}{4a_i^2}, \qquad C_i^* = -\frac{M^2}{2a_i}, \qquad V_i^* = C_i^* + 5U_i^*, \qquad y_i^* = \frac{M}{2a_i}. \tag{XII.7.73}$$

There is one vanishing Hessian entry, in the x_i direction. To determine the singularity one must retain the first nonzero term in that direction. Set $z = x_i$ for this original, unrescaled axial coordinate. At the tuned values, the actual polynomial is

$$H_* = \sum_{j\neq i}\left(1 - \frac{a_j}{a_i}\right)x_j^2 + \frac{1}{M^2}\left(a_i z^2 + \sum_{j\neq i} a_j x_j^2\right)^2. \tag{XII.7.74}$$

Its restriction to the axis is $a_i^2 z^4/M^2$, which is nonzero for fixed M. The transverse quadratic coefficients are nonzero because the slopes are distinct. Thus the collision has retained a quartic axial term rather than another ordinary node.

We can remove the mixed terms by constructing analytic coordinates. Order the three indices different from i increasingly and assign each mixed square to its earlier index. Define

$$\begin{aligned} P_j &= 1 - \frac{a_j}{a_i} + \frac{2a_i a_j z^2 + a_j^2 x_j^2 + 2a_j \sum_{\substack{k>j \\ k\neq i}} a_k x_k^2}{M^2}, \\ H_* &= \frac{a_i^2 z^4}{M^2} + \sum_{j\neq i} x_j^2 P_j, \qquad Z_j = x_j\sqrt{P_j}. \end{aligned} \tag{XII.7.75}$$

Every $P_j(0) = 1 - a_j/a_i$ is nonzero. Choose analytic square roots in a neighborhood of the selected point. The derivative of $(x_{j\neq i}, z) \mapsto (Z_j, z)$ there is diagonal, with entries $\sqrt{1 - a_j/a_i}$ and 1. It is invertible, so these are genuine local analytic coordinates. In them the polynomial is exactly three squares plus $a_i^2 z^4/M^2$. No global polynomial coordinate change is required.

Follow one endpoint in detail. For $i = 4$ we have $a_4 = -1$ and

$$(U^*, C^*, V^*) = \left(-\frac{M^2}{4}, \frac{M^2}{2}, -\frac{3M^2}{4}\right), \qquad H_* = -3x_1^2 - 2x_2^2 - x_3^2 + \frac{B^2}{M^2}. \tag{XII.7.76}$$

The transverse coefficients are $-3, -2, -1$, while the coefficient of $z^4 = x_4^4$ is $1/M^2$. With a fixed branch of $\sqrt{M}$, introduce a separately named canonical coordinate

$$\zeta = \frac{z}{\sqrt{M}}, \qquad W = Z_1^2 + Z_2^2 + Z_3^2 + \zeta^4. \tag{XII.7.77}$$

This is the H_1 hypersurface polynomial of the local IIB classification. Here the equivalence to it has been obtained from the original mass-deformed pair, including the transverse coordinate change. The local residue in these coordinates is its canonical

residue multiplied by a nonvanishing analytic function. The constant term of that function is nonzero, so the leading homogeneous residue has the same scaling weight.

The local deformation algebra is now especially small:

$$\frac{\mathbb{C}\{Z_1, Z_2, Z_3, \zeta\}}{(\partial_{Z_1} W, \partial_{Z_2} W, \partial_{Z_3} W, \partial_\zeta W)} \simeq \frac{\mathbb{C}\{\zeta\}}{(\zeta^3)}, \qquad \{1, \zeta, \zeta^2\}. \tag{XII.7.78}$$

This length three concerns the selected local germ. The original two-quadrics deformation module still has length nine. The mass deformation and choice of singular fiber have led us to a new local expansion point.

Which original parameters supply the three new local directions? Restore one further original mass coefficient $N = M_4$, multiplying $z = x_4$ in F_2, and vary U, C about the tuned values. It is useful first to keep a general axis i, with Nx_i in the second equation. Its exactly eliminated hypersurface is

$$H_\delta = A + \frac{(B + C_i^* + \delta C + Nz)^2}{M^2} + U_i^* + \delta U. \tag{XII.7.79}$$

At first order in $\delta U, \delta C, N$, the effective scalar perturbation of (XII.7.57) restricts to the axis as

$$\begin{aligned} \delta H\big|_{x_{j\neq i}=0} &= \delta U + \frac{2}{M^2}\left(a_i z^2 - \frac{M^2}{2a_i}\right)(\delta C + Nz), \\ [\delta H] &= \left(\delta U - \frac{\delta C}{a_i}\right) - \frac{N}{a_i} z + \frac{2a_i \delta C}{M^2} z^2. \end{aligned} \tag{XII.7.80}$$

The transverse variables vanish in the local quotient and the cubic term is a multiple of z^3, hence zero there. The square-root change leaves the axis fixed, so this restriction computes the same tangent classes as the analytic normal form. In the unrescaled basis $(1, z, z^2)$, the coefficient map has determinant

$$\det \frac{\partial(\lambda_0, \lambda_1, \lambda_2)}{\partial(\delta U, \delta C, N)} = \det \begin{pmatrix} 1 & -1/a_i & 0 \\ 0 & 0 & -1/a_i \\ 0 & 2a_i/M^2 & 0 \end{pmatrix} = \frac{2}{M^2} \neq 0. \tag{XII.7.81}$$

The original two constant directions and one original mass direction therefore cover all three local infinitesimal deformations. Setting $N = 0$ would miss the odd direction. The even slice used to draw the discriminant was enough to reach the quartic singularity, but it was not its full local deformation family.

For the selected $i = 4$ example the unrescaled coefficients are $\lambda_0 = \delta U + \delta C$, $\lambda_1 = N$ and $\lambda_2 = -2\delta C/M^2$. The canonical coordinate in (XII.7.77) changes them. Writing tildes for its coefficients gives

$$\begin{aligned} [\delta H] &= \widetilde{\lambda}_0 + \widetilde{\lambda}_1 \zeta + \widetilde{\lambda}_2 \zeta^2, \\ \widetilde{\lambda}_0 &= \delta U + \delta C = \delta V - 4\delta U, \\ \widetilde{\lambda}_1 &= \sqrt{M}\, N, \qquad \widetilde{\lambda}_2 = -\frac{2\delta C}{M} = -\frac{2(\delta V - 5\delta U)}{M}. \end{aligned} \tag{XII.7.82}$$

These are tangent coordinates at fixed nonzero M. At finite parameter displacement the squared expression in (XII.7.79) contributes nonlinear shifts, including a constant $(\delta C)^2/M^2$. The displayed linear combinations must not be used as an exact finite-parameter discriminant equation.

The remaining physical step applies the same local IIB period premise to this selected homogeneous limit. It assumes that the sector associated with the quartic singularity is retained in the appropriate local low-energy limit. The analytic coordinate reduction alone does not prove its decoupling from the rest of the original rank-two system. Under this premise, the degree-one weights and leading residue weight are

$$(q_{Z_1}, q_{Z_2}, q_{Z_3}, q_\zeta) = \left(\frac{1}{2}, \frac{1}{2}, \frac{1}{2}, \frac{1}{4}\right), \qquad Q_{\Omega,\mathrm{local}} = \frac{3}{2} + \frac{1}{4} - 1 = \frac{3}{4}. \tag{XII.7.83}$$

Requiring a local residue period to have mass dimension one gives

$$[\widetilde{\lambda}_0]_{\mathrm{local}} = \frac{4}{3}, \qquad [\widetilde{\lambda}_1]_{\mathrm{local}} = 1, \qquad [\widetilde{\lambda}_2]_{\mathrm{local}} = \frac{2}{3}. \tag{XII.7.84}$$

Thus the constant class is the local Coulomb direction, the odd class is a mass direction, and the quadratic class is a relevant coupling. The Coulomb and coupling dimensions add to two. These are dimensions under the new homogeneous action about the tuned point, with M fixed. They do not replace the original ultraviolet dimensions of U, V, N or the factors of M in (XII.7.82).

There is a useful independent distinction between a local Coulomb direction and a parameter at its boundary. For a threefold hypersurface with these weights, the sourced strict local normalizability criterion is

$$\widehat{c} = 4 - 2\sum q_i = \frac{1}{2}, \qquad Q_\phi < \frac{\widehat{c}}{2} = \frac{1}{4}, \qquad Q_1 = 0, \quad Q_\zeta = \frac{1}{4}, \quad Q_{\zeta^2} = \frac{1}{2}. \tag{XII.7.85}$$

Only the constant representative satisfies the strict inequality. The odd representative lies exactly at the mass boundary; counting it as a normalizable Coulomb mode would give the wrong local rank. In this selected local description the two original Coulomb-coordinate variations supply both a Coulomb direction and a relevant coupling, while the restored original mass supplies the odd local mass direction. This is the physical use of the tangent map. It identifies the parameter roles of the local H_1 geometry under the stated IIB premise, without specifying the complete infrared decomposition, stable spectrum or flavor group of the original construction.

XII.7.10 Changing one exponent

What changes when the fifth power in the pair is a cube? Write $y = x_5$. The first four variables still occur quadratically and y occurs through y^3. The rank criterion still isolates the origin because the columns have the same distinct slopes. For the module calculation, choose the smallest common positive integer weights of this form:

$$(w_1, w_2, w_3, w_4, w_y) = (3, 3, 3, 3, 2), \qquad (d_1, d_2) = (6, 6), \qquad Q_\Omega = 14 - 12 = 2. \tag{XII.7.86}$$

The difference is in the derivative with respect to y. Up to nonzero scalar factors, the columns now give

$$x_i(e_1 + ie_2) = 0 \quad (i \le 4), \qquad y^2(e_1 + 5e_2) = 0. \tag{XII.7.87}$$

For $i, j \le 4$ and $i \ne j$, the same subtraction used for the quadrics kills $x_i x_j$ in both components. Multiplying the ith relation by y^2 and the last by x_i kills $x_i y^2$ in both components. But the y column begins at y^2. It does not kill $x_i y$. The surviving representative $x_i y e_2$ has weight five, below the equation weight six, so no ideal relation can remove it. Similarly, ye_1 and ye_2 both survive in weight two.

To transfer the quadratic calculation systematically, first list the monomial shapes left after column reduction. Distinct x_i still cannot occur in the same surviving monomial. A monomial involving x_i and y can contain at most one y, since $x_i y^2$ vanishes. The derivative relation removes the first slot whenever x_i occurs, but for pure powers of y it starts only at y^2. Before imposing the defining ideal, the candidates therefore have the shapes

$$\begin{aligned} &e_1, e_2, \quad ye_1, ye_2, \quad y^b e_2 \ (b \ge 2), \\ &x_i^a e_2, \quad x_i^a y e_2 \quad (a \ge 1,\ 1 \le i \le 4). \end{aligned} \tag{XII.7.88}$$

These are possible classes, not yet a basis. The ideal relations will remove most of the large powers. This intermediate list makes visible exactly what changed when the square became a cube: the derivative starts one power later, so one extra power of y can accompany the x_i terms, and the two slots at y remain independent.

For example, work at weight five, where the possible mixed terms are $x_i y e_1, x_i y e_2$. Multiplying the ith derivative relation by y gives just one relation per i. For the specific vector $x_2 y(e_1 + e_2)$ it gives

$$[x_2 y(e_1 + e_2)] = -2[x_2 y e_2] + [x_2 y e_2] = -[x_2 y e_2]. \tag{XII.7.89}$$

The defining equations have weight six, so they cannot supply a relation at weight five using holomorphic multipliers of nonnegative weight. The relation involving the y derivative has weight four, but multiplication by x_2 raises it to weight seven, not five. Thus this reduction leaves a nonzero class. At weight seven the extra relation is available, and subtraction gives

$$\begin{aligned} &[x_2 y^2(e_1 + 2e_2)] = 0, \\ &[x_2 y^2(e_1 + 5e_2)] = 0 \quad \Longrightarrow \quad 3[x_2 y^2 e_2] = 0. \end{aligned} \tag{XII.7.90}$$

Over $\mathbb{C}$ the factor three is invertible. Both slots of $x_2 y^2$ vanish, while $x_2 y$ survives. This is the step that would be lost if one merely reused the quadratic list of representatives.

In weights six and eight the remaining relations can again be written with moment rows. Let $u_i = [x_i^2 e_2]$ for $i \le 4$ and $u_5 = [y^3 e_2]$. These classes have weight six and their y multiples have weight eight:

$$\sum_{i=1}^{5} i^a u_i = 0, \qquad \sum_{i=1}^{5} i^a y u_i = 0, \qquad a = 0, 1, 2. \tag{XII.7.91}$$

The equation generators have weight six. Their only multipliers at weights six and eight are a constant and y, respectively. After the derivative relations have been imposed, there are therefore precisely the three moment rows in each of these grades, and the same Vandermonde minor as before leaves two classes in each. To see that the list stops, multiply the first moment row by x_i or by y^2. The mixed monomials vanish and leave

$$x_i^3 e_2 = 0 \quad (i \le 4), \qquad y^5 e_2 = 0. \tag{XII.7.92}$$

The corresponding e_1 classes vanish by (XII.7.87).

At weight six the moment matrix is identical to the quadratic matrix because it acts on the five terms h_i, not on their exponents separately. Its solution can therefore be reused, now with $u_5 = [y^3 e_2]$. For example,

$$\begin{aligned} [x_1^2 e_1] &= -u_1 = u_4 + 3u_5, \\ [x_3^2 e_1 + y^3 e_2] &= -3u_3 + u_5 = 9u_4 + 19u_5. \end{aligned} \tag{XII.7.93}$$

Multiplication by y gives the corresponding reduction at weight eight. This multiplication would not be legitimate as a new independent basis construction without checking the relations at the new grade. Here it works because the only equation multipliers of weight two are multiples of y, so the weight-eight ideal relations are exactly the y multiples of the three moment rows. Their coefficients still have rank three.

The cutoffs in (XII.7.92) also give $x_i^3 y e_2 = 0$ by multiplication by y. Combining them with the mixed relations reduces the intermediate list to the following possible surviving pure or singly mixed powers,

$$\begin{gathered} x_i e_2,\ x_i y e_2,\ x_i^2 e_2,\ x_i^2 y e_2, \\ y^2 e_2,\ y^3 e_2,\ y^4 e_2, \end{gathered} \tag{XII.7.94}$$

together with the two constants and two linear y classes. The five weight-six powers reduce to two representatives, and so do the five weight-eight powers. All other shapes are killed by a mixed relation or the power cutoffs. This proves exhaustion rather than inferring it from a finite list of low grades.

We can now count all grades and convert each one using $[\lambda] = (6-g)/2$. Table XII.7.1 gives the representatives so that the count and dimension can be read independently.

Weight g	Representatives	Count	$[\lambda]$
0	e_1, e_2	2	3
2	ye_1, ye_2	2	2
3	$x_i e_2$ for $i \leq 4$	4	3/2
4	$y^2 e_2$	1	1
5	$x_i y e_2$ for $i \leq 4$	4	1/2
6	$x_4^2 e_2, y^3 e_2$	2	0
8	$x_4^2 y e_2, y^4 e_2$	2	-1

Table XII.7.1: The cubic example. The representative weight uses the integer frame in (XII.7.86). The last column uses the same period normalization as for the quadratic pair.

The result is the weighted Hilbert polynomial and count

$$\mathrm{Hilb}_{T^1}(t) = 2 + 2t^2 + 4t^3 + t^4 + 4t^5 + 2t^6 + 2t^8, \qquad \tau = \mu = 17. \tag{XII.7.95}$$

For the topological calculation, the prefactor of (XII.7.33) is $2/9$, and the numerator through third order has coefficients $1, 14, 78, 216$. This gives

$$\chi(\mathcal{F}) = \frac{2}{9}(216 - 12 \cdot 78 + 108 \cdot 14 - 864) = -16. \tag{XII.7.96}$$

The Coulomb and mass assignments follow from the last column of Table XII.7.1:

$$r = 2 + 2 + 4 = 8, \qquad \#\{\text{mass coordinates}\} = 1, \qquad \#\{[\lambda] = 1/2\} = 4. \tag{XII.7.97}$$

In particular, the four $x_i y$ classes are relevant couplings, paired in dimension with the four Coulomb directions of dimension $3/2$. The single mass coordinate now comes from $y^2 e_2$. This is why raising one exponent need not increase every type of parameter along with the total number of deformations.

The conversion can also be checked directly in the cubic equations. Write L_i for the coefficient of $x_i e_2$ and H_i for the coefficient of $x_i y e_2$. The monomials have weights three and five, respectively. Keeping the equation at weight six requires

$$\mathrm{wt}(L_i) = 6 - 3 = 3, \qquad \mathrm{wt}(H_i) = 6 - 5 = 1, \qquad [L_i] = \frac{3}{2}, \quad [H_i] = \frac{1}{2}. \tag{XII.7.98}$$

Their dimensions add to two, as required by the chiral action deformation. The common variable label i is useful for this calculation but does not fix a canonical physical pairing when several operators have the same dimension. Similarly, ye_a has monomial weight two and coefficient dimension two, whereas $y^2 e_2$ has weight four and coefficient dimension one. The latter is the mass direction. A monomial's ordinary polynomial degree would give the wrong answer because x_i and y now have different weights.

For the highest representatives $x_4^2 y e_2$ and $y^4 e_2$, the monomial weight is eight. Their coefficient dimension is $(6-8)/2 = -1$. These terms belong to the miniversal geometric

family even though their coefficient dimensions are negative. The calculation retains them so that the deformation basis is complete. The physical role statement is narrower: they are formal irrelevant directions under the imported scaling dictionary, without an independent ultraviolet-complete deformation assigned to each one.

A final comparison explains when the one-equation method really does return. Outside the source family $n \geq 2$, replace the fifth square by a linear term in both equations. Now the first equation solves for x_5, and the second becomes

$$x_5 = -\sum_{i=1}^{4} x_i^2, \qquad \sum_{i=1}^{4} (i-5)x_i^2 = 0. \tag{XII.7.99}$$

The remaining quadric is nondegenerate in four variables, hence equivalent over $\mathbb{C}$ to the ordinary node of Chapter 2. In the unreduced pair the fifth Jacobian column is $(1, 5)^T$, so $e_1 = -5e_2$. The other columns give $(i-5)x_i e_2 = 0$, leaving one constant class, as in the hypersurface calculation. Here a reduction to one equation is justified by actual elimination. For the original two quadrics at zero mass no such linear coordinate was available. The fixed nonzero mass in (XII.7.53) supplied a different route to elimination within that same family.

The two-equation examples supply local deformation data for the atlas in Chapter 9. The conformal anomaly coefficients require an additional calculation and are treated in the planned atlas of four-dimensional SCFTs.

XII.7.11 Exercises

In the following exercises, use the equation and ambient coordinate orders of this chapter. Use `benchmark/tasks.json` to find the question IDs and `benchmark/PROTOCOL.md` for submission. Include explanations and proofs.

1. **Rank and the fiber.** For the two quadrics, compute the minor Δ_{24} as a numerical multiple of x_2x_4. Give the set of slopes of the critical-value lines in the constant slice. Explain why rank drop in the ambient space does not give a singular line on the central fiber with distinct slopes. Then change the slope of x_2^2 in the second equation to 1. Find a nonzero singular point and give the rank of the Jacobian there.

2. **Change the generators.** Take $B = \left(\begin{smallmatrix} 2 & 1 \\ -1 & 3 \end{smallmatrix}\right)$ and transport x_2e_2 to the new equation basis. Give the two components of its representative in units of x_2, the determinant of B, and the residue of BF evaluated on the same frame as in (XII.7.37). Now swap the two equations of BF. Predict what happens to the transported vector and to the residue. Explain why checking only the dimension of the deformation module would not verify the transport.

3. **Two ways to get the wrong module.** For the two quadrics, compare the scalar quotient by all partial derivatives with the scalar quotient by the defining ideal and the maximal minors. Explain why neither supplies the two-equation miniversal family. In particular, use the constants and squares to show why equal

total dimension in one of these comparisons does not suffice. This exercise is assessed as a written explanation.

4. **Change a basis in the cubic fixture.** List the nonzero graded dimensions of T^1 in the frame (XII.7.86), and give the full coefficient dimensions with multiplicities, including negative dimensions. In weight six change to the ordered basis $(x_2^2e_2, y^3e_2)$. Use the moment relations to give the two coordinates of $x_4^2e_2$ in this basis. Explain which derivative relations distinguish x_iy from x_iy^2.

Further written practice

Use the same quotient to reduce

$$v_2 = x_3e_1 + x_1^2e_1 + 2x_5^2e_2, \qquad v_3 = x_3ye_1 + x_1^2ye_1 + 2y^4e_2. \tag{XII.7.100}$$

The first vector belongs to the quadratic example, and the second to the cubic example. Give the coordinates of their classes in the bases used in this chapter, keeping separate terms of different weights. Explain why the same numerical square-reduction coefficients recur, while the physical coefficient dimensions attached to those coordinates change. This practice asks for a written reduction; it adds no new numerical submission to the preceding exercises.

For the mass-deformed family, carry out the following two written calculations using the fixed nonzero M convention.

1. Choose $i = 2$ in (XII.7.73). Find the original five-coordinate singular point and the transverse quadratic coefficients. Construct the three square-root factors in (XII.7.75), and derive the tangent map from $(\delta U, \delta V, N)$ when Nx_2 is restored in F_2. Keep its unrescaled axial coordinate distinct from a coordinate in which the fourth-power coefficient is one.

2. On the node smoothing path, derive (XII.7.68) directly from the coordinate volume and the equation degree. Compare the resulting leading period with what would follow if the elimination factor $1/M$ were omitted. Explain why U/M can measure a local mass scale while the original Coulomb coordinate U retains ultraviolet dimension two. State which additional physical premise is needed to interpret a local period as a central charge.

Status and sources

§§7.1–7.2. Geometry and scope. The defining family is ICIS (1) in Wang et al. 2017, arXiv:1606.06306v1, §3.3, printed page 12 (PDF page 13), and the explicit quadratic pair is also displayed in Chen et al. 2017, arXiv:1604.07843v1, PDF page 4 immediately before (2.9). The isolation and constant-value slice in (XII.7.3)–(XII.7.6) are exact local calculations [MATH]. The singular-line control is the collision of the first two square slopes, including when the fifth monomial is cubic. The critical-value equations are the reduced set in the constant slice.

§§7.3–7.4. Module and length. For the analytic quotient and miniversal family in (XII.7.13), see Greuel 2019, arXiv:1903.03661v1, pages 15–17 (Theorem 1.22 and Remark 1.24). The coordinate and equation equivalences and the computed graded quotients are [MATH]. Equation (2.9) of Wang et al. 2017, PDF page 6, prints an ambient polynomial numerator with a derivative-column denominator. Literally over that ambient ring this quotient lacks the defining-ideal relations; the intrinsic cokernel is over R/I. The nine representatives and quadratic coefficient dimensions agree with (2.9)–(2.10) of Chen et al. 2017, PDF page 4. The Milnor number and the quasihomogeneous equality with the Tjurina number use the discussion after Definition 2.22 and Theorem 2.26(2) of Greuel 2019, pages 42–45. The independent Euler calculation uses Greuel and Hamm 1978, Satz 3.7(c) and Korollar 3.8(b), printed pages 74 and 76, read as indexed text of the original scan. These are topological and algebraic counts [MATH], not particle counts.

§7.5. Residue and physical scale. The ordered three-form and coefficient dimension are anchored in Wang et al. 2017, PDF page 6, (2.11)–(2.12), and Chen et al. 2017, PDF page 3, (2.4)–(2.8). The chart formula, change of equation basis and relative scaling in (XII.7.35)–(XII.7.42) are [MATH]. The local string and low-energy limits are a [DEC] premise, following Wang et al. 2017, §2.2, PDF pages 4–5. The identification of the residue period with central-charge scaling in (XII.7.43) is [GEO-E], without an absolute normalization or a stability statement.

§7.6 and §7.10. Parameter roles and the cubic comparison. The roles of the coefficients and the chiral dimension pairing use Wang et al. 2017, (2.1)–(2.2), PDF pages 3–4, and Chen et al. 2017, the discussion following (2.8), PDF page 3. These role identifications are [GEO-E]. The quadratic dimensions, cubic graded quotient, residue arithmetic and linear elimination control are [MATH]. Equation (3.10) of Wang et al. 2017, PDF page 13, corroborates the cubic Coulomb/mass sub-spectrum only. The four coefficients of dimension 1/2, the dimensionless coefficients and the negative dimensions come from the module calculation with (2.12). The sources discuss physical marginality; the result used here is the computed zero dimension and the persistence of an isolated homogeneous pencil for small changes of its two slopes. No global flavor group or conformal anomaly is deduced.

§§7.7–7.9. Mass deformation and the selected local singularity. The starting mass and constant directions are the representatives in Chen et al. 2017, arXiv:1604.07843v1, PDF page 4, (2.9)–(2.10). The elimination, scalar normal-direction map, reduced discriminant of the fixed-mass slice, signed residue conversion, node-period calculation, analytic square extraction and tangent coefficient maps in (XII.7.51)–(XII.7.82) are [MATH]. The finite-multiplier exception at the original origin is included by the direct minors. The reduced discriminant assigns no scheme multiplicities. The map in (XII.7.82) is at fixed $M \neq 0$ and first order; it distinguishes $z = x_4$ from $\zeta = z/\sqrt{M}$. The local hypersurface residue and coefficient rule use Xie and Yau 2015, arXiv:1510.01324v1, PDF pages 6–9, (2.4)–(2.8); its (2.17) identifies the canonical polynomial as H_1. The strict normalizability input is Shapere and Vafa 1999, arXiv:hep-th/9910182v2, PDF page 5, (2.4)–(2.5), with the threefold discussion on PDF pages 6–7. It is the strict criterion, not the nonstrict Coulomb threshold printed on PDF page 8 of Xie and Yau

2015, that is used in (XII.7.85). The selected local parameter roles are conditional [GEO-E]; sector decoupling retains its [DEC] status. No complete infrared factorization, stable BPS spectrum, global charge embedding, flavor group or anomaly value is inferred.

References

Chen, B. et al. (2017). "4D N=2 SCFT and singularity theory. Part II: Complete intersection". In: *Adv. Theor. Math. Phys.* 21, pp. 121–145. arXiv: 1604.07843 [hep-th].

Greuel, G.-M. (2019). *Deformation and Smoothing of Singularities*. arXiv: 1903.03661 [math.AG].

Greuel, G.-M. and H. A. Hamm (1978). "Invarianten quasihomogener vollständiger Durchschnitte". In: *Invent. Math.* 49, pp. 67–86. DOI: 10.1007/BF01399511.

Shapere, A. D. and C. Vafa (1999). *BPS Structure of Argyres-Douglas Superconformal Theories*. arXiv: hep-th/9910182.

Wang, Y. et al. (2017). "4d N=2 SCFT from Complete Intersection Singularity". In: *Adv. Theor. Math. Phys.* 21, pp. 801–855. arXiv: 1606.06306 [hep-th].

Xie, D. and S.-T. Yau (2015). *4d N=2 SCFT and singularity theory Part I: Classification*. arXiv: 1510.01324 [hep-th].

Chapter XII.8

Four-dimensional $\mathcal{N} = 1$ engineering and geometric transitions

XII.8.1 From a wrapped brane to a glueball variable

A D5-brane wrapped on a rigid two-sphere leaves four extended directions. A stack then gives a gauge field without an adjoint scalar zero mode. The conifold also has a different smooth filling, with a three-sphere in place of the two-sphere. Can the second filling retain any of the gauge physics when there are no longer D5-branes at the tip?

The magnetic charge can be measured far from the tip. We first track this measurement through the two fillings and then compute the superpotential in the corresponding flux sector. The finite period sets a chiral coordinate. A second period, which reaches the cutoff, supplies the logarithm that combines with the bare gauge coupling. We will use this logarithm to find the phases of the pure gauge theory and then repeat the period calculation with two cuts, where the cutoff is shared.

We assume the conifold geometry of Volume IV, Chapter 5, and the use of quantized flux from Volume IV, Chapter 10. Chapter 2 of this volume supplied the marked conifold cycles and their orientations. We recall the pieces of that calculation that enter the superpotential. From Volume I we use rigid four-dimensional superspace, instanton number, and the one-loop running of a gauge coupling. The flux superpotential is the protected input from Volume V, Chapter 10.

XII.8.2 A rigid sphere and its four-dimensional gauge fields

Which light fields remain when a D5 stack wraps the exceptional sphere? Take $N \geq 2$ coincident D5-branes on a calibrated holomorphic curve C, with a trivial worldvolume

bundle and no other branes. The branes fill $\mathbb{R}^{1,3}$. To count their scalar zero modes we need the normal bundle, since a displacement transverse to the curve must fit together on its two coordinate patches.

Choose the small resolution of $uv - zw = 0$ that remembers the right kernel of the matrix of conifold coordinates:

$$X_{\text{res}} = \left\{ (u, v, z, w; [s : t]) : \begin{pmatrix} u & z \\ w & v \end{pmatrix} \begin{pmatrix} s \\ t \end{pmatrix} = 0 \right\}. \tag{XII.8.1}$$

A nonzero matrix of determinant zero has one kernel line. Above the zero matrix all lines are possible, so the fiber there is $C = \mathbb{P}^1$. On $s \neq 0$ let $q = t/s$ and solve for (u, w); on $t \neq 0$ let $p = s/t$ and solve for (z, v):

$$(u, w) = -q(z, v), \qquad (z, v) = -p(u, w), \qquad p = q^{-1}. \tag{XII.8.2}$$

For a single fiber coordinate of the tautological line, the local frames $(1, q)$ and $(p, 1)$ differ by q. Thus its coordinate in the second frame is q times its coordinate in the first. Absorbing a constant minus sign in the coordinates of one chart gives exactly this transition for both coordinates in (XII.8.2):

$$X_{\text{res}} = \text{Tot}_{\mathbb{P}^1}\big(\mathcal{O}(-1) \oplus \mathcal{O}(-1)\big), \qquad H^0(C, N_{C/X_{\text{res}}}) = 0, \quad H^1(C, \mathcal{O}_C) = 0. \tag{XII.8.3}$$

The first vanishing follows from negative degree on $\mathbb{P}^1$. The second is the genus-zero condition. In the ordinary calibrated reduction, the first excludes a normal-position chiral zero mode and the second excludes an internal Wilson-line chiral zero mode. The trivial bundle supplies a constant Chan–Paton mode for the gauge field.

One can see the obstruction to a normal displacement directly in the overlap. Let $h_0(q)$ describe one component of a putative holomorphic displacement in the first chart. Its component in the other chart is, up to the constant sign already removed, $h_\infty(p) = p^{-1} h_0(p^{-1})$. Regularity at both origins forces every Taylor coefficient to vanish:

$$\begin{gathered} h_0(q) = \sum_{m \geq 0} c_m q^m, \qquad h_\infty(p) = \sum_{m \geq 0} c_m p^{-m-1}, \\ h_\infty \text{ holomorphic at } p = 0 \implies c_m = 0. \end{gathered} \tag{XII.8.4}$$

Equivalently, the Laurent coefficients of a holomorphic section must satisfy the negative-degree transition. Thus a local transverse displacement on one patch cannot become a massless field by itself. It must extend over the entire wrapped curve. A gauge field in the extended directions has a constant wavefunction on C and passes this test. The Wilson-line question instead asks for an internal harmonic one-form; genus zero removes that possibility. The four preserved supercharges organize the retained $U(N)$ gauge fields into one $\mathcal{N} = 1$ vector multiplet. There is no matter chiral multiplet, tree-level chiral superpotential, or classical scalar modulus in this reduction.

The identity matrix commutes with all the traceless generators, so the diagonal gauge field has no charged light matter and no nonabelian self-interaction. In the selected rigid local sector it is a free Maxwell multiplet if retained. The interacting sector is pure $SU(N)$ gauge theory; this separation of local dynamics does not choose

the global lattice of line operators. For a stack of three branes, for example, the eight traceless generators interact and the ninth is the free diagonal direction.

How does the same wrapping encode an instanton weight? Use the leading two-derivative brane action of Volume III, Chapter 3. Take the smooth calibrated curve to have curvature radii much larger than the string length $\sqrt{\alpha'}$, so curvature corrections are suppressed. Use weak, slowly varying worldvolume fields, constant g_s, zero NS two-form pullback, and no internal flux. Write $A_C = \int_C \mathrm{vol}_C$ in string frame and $\lambda = 2\pi\alpha'$ for the factor multiplying the gauge curvature. Use the fundamental trace $\mathrm{Tr}_f(T^a T^b) = \delta^{ab}/2$. The tension T_5 and RR charge μ_5 are

$$T_5 = \frac{1}{(2\pi)^5 g_s \alpha'^3}, \qquad \mu_5 = g_s T_5. \tag{XII.8.5}$$

The curvature F of the four-dimensional connection has components only in the extended directions. For an antisymmetric matrix $F_\mu{}^\nu$, the linear term in the spacetime determinant vanishes, while $\mathrm{tr}_{\mathrm{st}}(F^2) = -F_{\mu\nu}F^{\mu\nu}$. Hence the square root of the determinant contributes $\lambda^2 F_{\mu\nu}F^{\mu\nu}/4$ at quadratic order. Multiplying by $T_5 A_C$ gives

$$\mathcal{L}^{(2)}_{\mathrm{DBI}} = -\frac{T_5 A_C \lambda^2}{4}\,\mathrm{Tr}_f\, F_{\mu\nu}F^{\mu\nu} = -\frac{1}{2g_4^2}\,\mathrm{Tr}_f\, F_{\mu\nu}F^{\mu\nu}, \qquad \frac{1}{g_4^2} = \frac{T_5 A_C \lambda^2}{2}. \tag{XII.8.6}$$

At this order the Chan–Paton trace is unambiguous. The RR two-form C_2 contributes through the quadratic term of the Wess–Zumino exponential:

$$I^{(2)}_{\mathrm{WZ}} = \frac{\mu_5 \lambda^2}{2}\left(\int_C C_2\right)\int_{\mathbb{R}^{1,3}} \mathrm{Tr}_f\, F\wedge F = \theta k, \qquad k = \frac{1}{8\pi^2}\int \mathrm{Tr}_f\, F\wedge F. \tag{XII.8.7}$$

The integral defining k is evaluated on the Euclidean instanton. With positive orientation a unit instanton has Euclidean gauge action $8\pi^2/g_4^2 - i\theta$. Inserting the constants of (XII.8.5) gives

$$\frac{8\pi^2}{g_4^2} = \frac{A_C}{2\pi g_s \alpha'}, \qquad \theta = \frac{1}{2\pi\alpha'}\int_C C_2, \qquad e^{-I_{k=1}} = \exp\!\left(-\frac{A_C}{2\pi g_s\alpha'} + i\theta\right). \tag{XII.8.8}$$

The real term is the area times the Euclidean D1 tension. The phase is the D1 coupling to C_2 with the same orientation. This checks the normalization using one wrapped D1, with both the area and α' in units of length squared. It also fixes the sign of the instanton exponent that we will use to match the flux-side coupling.

It is useful to vary the area while keeping the brane number fixed. Define the dimensionless smooth-cycle area $a = A_C/[(2\pi)^2\alpha']$. The same coefficients give

$$\frac{1}{g_4^2} = \frac{a}{4\pi g_s}, \qquad \frac{8\pi^2}{g_4^2} = \frac{2\pi a}{g_s}, \qquad q_{\mathrm{inst}} = e^{-2\pi a/g_s + i\theta}. \tag{XII.8.9}$$

For example, $a = 80$ and $g_s = 1/10$ give $g_4^2 = \pi/200$ and a unit-instanton suppression $e^{-1600\pi}$ at zero angle. Doubling a at the same dilaton halves g_4^2 and squares this suppression. It does not change the rank or the D5 charge. Conversely, changing N at fixed smooth area leaves the displayed tree-level coefficient in the fundamental-trace

action unchanged, while changing the interacting algebra and the integer measured at the end. These are distinct parameters in the construction. Their subsequent relation through the strong scale uses quantum gauge running and the protected boundary prescription, not a second expansion of the smooth brane determinant.

This smooth-cycle calculation uses weak, slowly varying fields; it cannot be used at the collapsing sphere. For a rigid four-dimensional comparison we assume that the energies of interest and the retained strong scale lie below the relevant string and Kaluza–Klein thresholds. Couplings to unwanted bulk, end-continuum, and gravitational modes must also be suppressed. A coordinate cutoff, or the noncompactness of the space, does not establish those conditions.

XII.8.3 Which charge crosses the conifold transition?

How can a D5 magnetic charge still be measured when the wrapped sphere is gone? On the resolved side, take a small sphere in the four real normal directions at a point of C. This linking S^3 is the fiber of the normal sphere bundle over C. One can move the measurement outward through the end of the local geometry. The same end can then be filled by the deformed conifold, as in Figure XII.8.1.

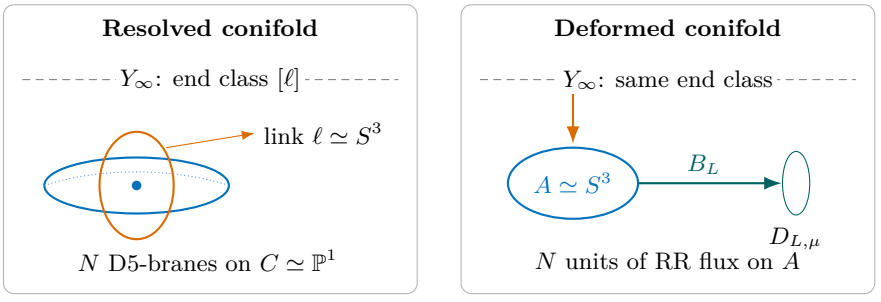


Figure XII.8.1: Two fillings of the conifold link. The resolved side has the zero-section C and a normal linking three-sphere ℓ. The deformed side has the real zero-section A; the matched boundary class maps to A. The relative chain B_L ends at a marked fiber $D_{L,\mu}$ and is separate from the linking measurement. The sketch shows homology data, with no metric radii assigned.

For the topology on the deformed side use

$$X_\mu = \{x^2 + y_1^2 + y_2^2 + y_3^2 = \mu\}, \qquad \mu > 0. \tag{XII.8.10}$$

Writing the coordinate vector as $a + ib$ with $a, b \in \mathbb{R}^4$ separates the equation into a length and an orthogonality constraint:

$$a \cdot b = 0, \quad |a|^2 = \mu + |b|^2, \qquad (n, b) \longmapsto \sqrt{\mu + |b|^2}\, n + ib, \quad n \in S^3,\ b \in T_n S^3. \tag{XII.8.11}$$

The round metric identifies the tangent fibers with cotangent fibers. Scaling b to zero retracts X_μ to its outward-oriented real zero-section A. On the resolution, contracting the normal fibers instead retracts the total space to C.

The retraction on the deformation can be written without choosing coordinates on the sphere. For $0 \le t \le 1$, use

$$H_t(n,b) = \sqrt{\mu + t^2|b|^2}\, n + itb, \qquad H_1(n,b) = a + ib, \qquad H_0(n,b) = \sqrt{\mu}\, n. \tag{XII.8.12}$$

The constraints in (XII.8.11) hold throughout this path. The zero-section stays fixed. On the resolution the corresponding path multiplies both normal fiber coordinates by t. Therefore the homology groups that distinguish the fillings are

$$\begin{array}{c|cc} & H_2 & H_3 \\ \hline X_{\mathrm{res}} & \mathbb{Z}[C] & 0 \\ X_\mu & 0 & \mathbb{Z}[A] \end{array}. \tag{XII.8.13}$$

A cycle supported near the common end can consequently have different images in the two interiors. This is the topological operation needed for the charge comparison. There is no path of smooth fillings in this argument that keeps both homology generators.

Let Y_∞ be the common large-radius link, of topology $S^2 \times S^3$. On the resolution it is the unit normal sphere bundle over S^2, up to the identification of ends. In the homology sequence for an S^3 bundle over S^2, the only contribution in degree three comes from the fiber: the base has no group in degree three or four. Hence $[\ell]$ generates $H_3(Y_\infty)$. On the deformation the end is a unit cotangent sphere bundle over S^3. Its S^2 fibers carry no third homology. The base is parallelizable, so the projection is the product projection in a trivialization and induces an isomorphism on H_3. Choose the matching positive orientation. The two inclusions of the link therefore act as

$$H_3(Y_\infty) = \mathbb{Z}[\ell], \qquad [\ell] \longmapsto \begin{cases} 0 & \text{in } H_3(X_{\mathrm{res}}), \\ [A] & \text{in } H_3(X_\mu). \end{cases} \tag{XII.8.14}$$

The resolved fiber can bound a normal ball whose center meets the branes. On the smoothing the same end class is represented by a compact cycle, even though there is no brane at its center.

For constant RR axion C_0 and no other magnetic sources, write F_3 for the RR member of the three-form doublet, locally dC_2 away from the D5. In the Bianchi identity the current δ_C is normalized to integrate to one over a positive normal ball D^4; κ_0 is the bulk gravitational normalization before including the dilaton:

$$dF_3 = 2\kappa_0^2 \mu_5 N\, \delta_C, \qquad 2\kappa_0^2 = (2\pi)^7 \alpha'^4, \qquad 2\kappa_0^2 \mu_5 = (2\pi)^2 \alpha'. \tag{XII.8.15}$$

Integrating over D^4 with $\partial D^4 = \ell$ gives the brane-side flux. On the source-free smoothing, $dF_3 = 0$ and the two cycles in (XII.8.14) are homologous there. With the same boundary charge and with no compact NS three-form flux, this gives

$$\frac{1}{(2\pi)^2\alpha'} \int_\ell F_3 = N, \qquad \frac{1}{(2\pi)^2\alpha'} \int_A F_3 = N, \qquad \int_A H_3 = 0. \tag{XII.8.16}$$

For the stack of three branes, the measured integral is $3(2\pi)^2\alpha'$ on the link. In the second filling Stokes' theorem assigns that same integral to A. Its compact quantization is independent of any relative period at the noncompact end.

To make the use of Stokes' theorem explicit, take two homologous representatives ℓ_1 and ℓ_2 in a region containing no D5 source. An oriented four-chain Q between them satisfies

$$\partial Q = \ell_2 - \ell_1, \qquad \int_{\ell_2} F_3 - \int_{\ell_1} F_3 = \int_Q dF_3 = 0. \tag{XII.8.17}$$

On the resolved side this equality stops being source-free if one moves the chain through the wrapped stack. The normal ball in (XII.8.15) then supplies exactly the charge. On the deformed side it holds all the way to the representative A of the end class. No division by the volume of a representative appears. A larger sphere can have the same integral with a different local flux density, but the integral alone does not determine that density or a metric solving the flux equations. This explains both what charge conservation fixes and why it does not determine the deformation parameter μ. In particular, the NS contribution to a relative period is not a second compact flux integer.

The large-N geometric transition proposes replacing the wrapped-brane filling by the flux filling. The charge argument selects the required flux sector. To compare gauge physics at a specified integer N, we also use the proposed matching of protected holomorphic data. The no-flux conifold of Chapter 2 used the same smoothing for different dynamics. We now compute the periods needed for the flux comparison.

XII.8.4 Computing the compact and regulated periods

Why does the period through the end remember the compact period? Both chains are swept out by two-spheres over intervals in x. The compact interval shrinks at both ends. On the relative interval only one end shrinks, and the large-x expansion of the fiber integral gives a logarithm. Figure XII.8.2 shows the two paths.

Let $F = x^2 + \sum_{j=1}^{3} y_j^2 - \mu$. With ambient order (x, y_1, y_2, y_3), define the residue by wedging dF first and divide it by $4\pi^2$. In the $y_3 \neq 0$ chart this fixes

$$4\pi^2 dF \wedge \Omega = dx \wedge dy_1 \wedge dy_2 \wedge dy_3, \qquad 4\pi^2 \Omega = -\frac{dx \wedge dy_1 \wedge dy_2}{2y_3}. \tag{XII.8.18}$$

Take initially $0 < \mu < L^2$ with $L > 0$. Write $y = \rho(x)n$, with n on the unit real sphere and outward area form ω_2. On A, $\rho = \sqrt{\mu - x^2}$ and the outward orientation is $-dx \wedge \omega_2$. On B_L, take $\rho = i\sqrt{x^2 - \mu}$ and orient by $dx \wedge \omega_2$ as x increases. Substituting in the residue, the terms containing $d\rho$ vanish against dx. Using $\omega_2 = dn_1 \wedge dn_2/n_3$ on this chart gives

$$4\pi^2 \Omega\big|_{y=\rho n} = -\tfrac{1}{2}\rho\, dx \wedge \omega_2, \qquad \int_{S^2} \omega_2 = 4\pi. \tag{XII.8.19}$$

At the common endpoint $x = +\sqrt{\mu}$, the oriented real and imaginary y planes meet once. Placing all three real axes before all three imaginary axes differs by three swaps from the complex orientation, so $I(A, B_L) = -1$. As in Chapter 2, the period pairing uses the negative of this raw intersection sign. The mark for the relative cycle is the fiber $D_{L,\mu} = X_\mu \cap \{x = L\}$, not the whole link in (XII.8.14).

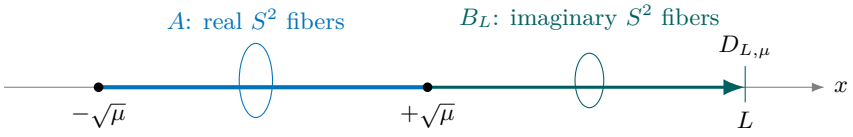


Figure XII.8.2: Projection of A and B_L to x on the initial positive real slice. The real fibers over the compact interval close at both branch points. The imaginary fibers over the outward ray close at $+\sqrt{\mu}$ and end at $D_{L,\mu}$. The orientation of A includes its outward sphere orientation as specified in the text.

Integrating the real fibers gives a semicircle area. For B_L the same normalization keeps the factor of $-i$ from the imaginary radius:

$$S := \int_A \Omega = \frac{1}{2\pi} \int_{-\sqrt{\mu}}^{\sqrt{\mu}} \sqrt{\mu - x^2}\, dx = \frac{\mu}{2\pi} \int_{-\pi/2}^{\pi/2} \cos^2 t\, dt = \frac{\mu}{4}, \tag{XII.8.20}$$

$$P_B := \int_{B_L} \Omega = \frac{I}{2\pi i}, \qquad I = \int_{2\sqrt{S}}^{L} \sqrt{x^2 - 4S}\, dx. \tag{XII.8.21}$$

Here I denotes the integral, whereas $I(A, B_L)$ denotes the crossing. The common residue normalization is essential: it fixes the logarithmic period relative to S. This choice fixes the holomorphic coordinate. Chapter 2 used a different conversion, to a wrapped-D3 particle mass.

The primitive must be evaluated at both ends. For positive S, set $x = 2\sqrt{S}\cosh t$. The integrand times dx becomes $4S\sinh^2 t\, dt$, with t running from zero to $t_L = \operatorname{arcosh}(L/(2\sqrt{S}))$. Thus

$$I = S\sinh(2t_L) - 2St_L = \frac{L}{2}\sqrt{L^2 - 4S} - 2S\operatorname{arcosh}\frac{L}{2\sqrt{S}}, \tag{XII.8.22}$$

$$t_L = \log\frac{L + \sqrt{L^2 - 4S}}{2\sqrt{S}}. \tag{XII.8.23}$$

The denominator in (XII.8.23) is the lower-end contribution: the logarithm vanishes when $L = 2\sqrt{S}$. Dropping it would erase the $\log S$ in the superpotential. For the four-dimensional normalization we will use the subtracted dual period

$$\Pi_B = -2\pi i P_B + \frac{L^2}{2} = \frac{L^2 - L\sqrt{L^2 - 4S}}{2} + 2St_L. \tag{XII.8.24}$$

The added term cancels the part of $-I$ that survives at $S = 0$. It is independent of the glueball coordinate.

We can check the dependence on both endpoints before making any large-cutoff approximation. Differentiate the integral defining I at fixed positive S or L. The lower-limit term vanishes because the square root is zero there. The remaining integral

is elementary in the same hyperbolic variable:

$$\left.\frac{\partial I}{\partial S}\right|_L = -2\int_{2\sqrt{S}}^{L}\frac{dx}{\sqrt{x^2-4S}} = -2t_L, \qquad \left.\frac{\partial \Pi_B}{\partial S}\right|_L = 2t_L, \tag{XII.8.25}$$

$$\left.\frac{\partial \Pi_B}{\partial L}\right|_S = L - \sqrt{L^2-4S} = \frac{4S}{L+\sqrt{L^2-4S}}. \tag{XII.8.26}$$

Although the differentiated integrand in the first line is singular at the branch point, its inverse-square-root singularity is integrable. The second line also follows by extending the relative chain by a thin segment at its outer end and varying the subtraction $L^2/2$. On the positive slice its sign is positive. At large L it is $2S/L$ to leading order, so the logarithm can already be anticipated without evaluating the primitive. The first line will instead determine the stationary equation when S is varied. These two variations answer different questions.

To see which terms survive at large L, set $z = L^2$ for this calculation and write the exact expression as

$$\Pi_B = \frac{z}{2}\left(1-\sqrt{1-4S/z}\right) + S\log\frac{z}{S} + 2S\log\frac{1+\sqrt{1-4S/z}}{2}. \tag{XII.8.27}$$

The first term is $S + S^2/z + 2S^3/z^2 + O(S^4/z^3)$. The last term contributes $-2S^2/z - 3S^3/z^2 + O(S^4/z^3)$. The expansion is therefore

$$\Pi_B = S\left(1+\log\frac{L^2}{S}\right) - \frac{S^2}{L^2} - \frac{S^3}{L^4} + O(S^4/L^6), \qquad |4S| \ll |L^2|. \tag{XII.8.28}$$

For instance, in numerical units with $S = 1$ and $L = 5$, the leading term $1 + \log 25$ is about 4.21888. Including the two inverse powers gives 4.17728, close to the exact 4.17716. The corrections are analytic in S at fixed L; a finite term linear in S could be moved between the period and the coupling, whereas these nonlinear terms cannot be absorbed by that move.

The expansion parameter is the dimensionless ratio S/L^2, rather than $1/L$ by itself. At fixed $S = 1$, doubling L makes the first omitted correction after the two displayed inverse powers about 2^6 times smaller. Direct evaluation at $S = 1$ gives

	$L = 5$	$L = 10$
Π_B exact	4.17715924	5.59506848
$S(1+\log(L^2/S))$	4.21887582	5.60517019
exact minus improved	$-1.16588\cdot 10^{-4}$	$-1.70253\cdot 10^{-6}$

. (XII.8.29)

Here the two-power approximation includes both $-S^2/L^2$ and $-S^3/L^4$. The decrease tests the first neglected order, not merely agreement between two rounded numbers. Close to $L = 2\sqrt{S}$ the ratio is no longer small; the exact hyperbolic expression remains the appropriate calculation on the positive slice. In particular, the existence of a simple primitive does not make its large-L truncation uniformly accurate near the branch point.

The exact form also separates the branch behavior from the asymptotic approximation. The square root in (XII.8.27) is the branch equal to one at $S/z = 0$. Its first term

and the last logarithm are single-valued for $|4S/z| < 1$, with $z \neq 0$. Thus the shifts for positive circuits come from the middle logarithm:

$$\begin{aligned} \Delta\Pi_B &= -2\pi i S \quad (S \text{ at fixed } L), \\ \Delta\Pi_B &= +2\pi i S \quad (z = L^2 \text{ at fixed } S), \\ \Delta\Pi_B &= +4\pi i S \quad (L \text{ at fixed } S). \end{aligned} \tag{XII.8.30}$$

The S circuit is a closed loop of the marked family at fixed L and shifts P_B by $+S$. One z circuit takes the lifted endpoint L to $-L$ with the mark transported. It is not a closed loop of the literal x endpoint. A closed positive circuit of L winds z twice.

For the pure gauge comparison, assign mass dimensions

$$[S] = [\mu] = 3, \qquad [x] = [L] = \tfrac{3}{2}, \qquad L = \Lambda_0^{3/2} \quad \text{on the positive slice.} \tag{XII.8.31}$$

The symbol Λ_0 has units of energy. The period Π_B has dimension three and L^2/S is dimensionless. The scale prescription identifies the power of the energy cutoff in the logarithm; it gives no proper radius of the conifold.

XII.8.5 Flux pairing and the four-dimensional scale

How does the cutoff logarithm become a finite strong scale? The compact flux multiplies the divergent dual period. A relative flux coefficient multiplies the compact period. As the cutoff moves, the second coefficient must change to cancel the first contribution.

Set $H_3 = dB_2$ locally and $\tau_{\mathrm{IIB}} = C_0 + i/g_s$. Use the normalized complex flux and its periods

$$G = \frac{F_3 - \tau_{\mathrm{IIB}} H_3}{(2\pi)^2 \alpha'}, \qquad G_A = \int_A G = N, \qquad G_B = \int_{B_L} G. \tag{XII.8.32}$$

The last integral refers to the specified relative chain and end data. It can include a boundary RR angle as well as an NS contribution. The compact integer in (XII.8.16) does not fix this relative period.

Use the local flux superpotential with the relative boundary prescription held fixed. In the orientation of §XII.8.4 the bilinear, with Ω ordered before G, is minus the determinant of the period columns on (A, B_L):

$$\mathcal{W}_{\Omega,G} = -\det \begin{pmatrix} S & G_A \\ P_B & G_B \end{pmatrix} = G_A P_B - G_B S. \tag{XII.8.33}$$

The use of this relative pairing is part of the flux prescription. An unrestricted noncompact bulk integral need not reproduce it without a choice of boundary term. Multiplying by $-2\pi i$ and adding the S-independent subtraction in (XII.8.24) yields the four-dimensional normalization

$$W_{\mathrm{eff}} = N\Pi_B + \alpha S, \qquad \alpha = 2\pi i G_B. \tag{XII.8.34}$$

The sign between the original periods in (XII.8.33) is what gives the plus sign in (XII.8.34) after the change of normalization.

In the Wilsonian matching prescription, take $G_B = \tau_h(\Lambda_0)$, where τ_h is the holomorphic coupling of the interacting gauge theory. A finite threshold may be absorbed into this scheme. The instanton weight has the orientation fixed by (XII.8.8):

$$\tau_h(\Lambda_0) = \frac{\theta}{2\pi} + \frac{4\pi i}{g_h^2(\Lambda_0)}, \qquad \alpha = i\theta - \frac{8\pi^2}{g_h^2(\Lambda_0)}. \tag{XII.8.35}$$

At weak coupling e^α is small. Although G contains the IIB axiodilaton, τ_h matches a relative period of G. The two couplings describe different operations.

At fixed S, insert (XII.8.28) with $L^2 = \Lambda_0^3$. For a reference mass $M > 0$, the coefficient linear in S combines with the log of the cutoff:

$$\begin{aligned} W_{\text{eff}} &= NS[1 - \log(S/M^3)] + S[3N\log(\Lambda_0/M) + \alpha(\Lambda_0)] \\ &\quad - NS^2/\Lambda_0^3 + O(NS^3/\Lambda_0^6), \\ \Lambda^{3N} &= \Lambda_0^{3N} e^{\alpha(\Lambda_0)}. \end{aligned} \tag{XII.8.36}$$

Hold the nonzero complex quantity Λ^{3N} fixed when removing the cutoff in this holomorphic expression. On a continuous branch for a positive change $\Lambda_0 \to r\Lambda_0$, the surviving period change and the required boundary change are

$$\Delta\Pi_B = 3S\log r + O(S^2/\Lambda_0^3), \qquad \Delta\alpha = -3N\log r. \tag{XII.8.37}$$

The factor N counts compact flux. The factor three comes from the relation between the energy cutoff and the geometric endpoint. For $N = 3$ and $r = 3$, the surviving changes in $N\Pi_B$ and αS are $+9S\log 3$ and $-9S\log 3$. At finite cutoff the first power correction still changes by $NS^2(1 - r^{-3})/\Lambda_0^3$. A shift of a coefficient linear in S does not remove this dependence.

The same cancellation can be stated as a differential equation for the boundary coefficient, with the energy variable used explicitly:

$$\frac{d\alpha}{d\log\Lambda_0} = -3N, \qquad \frac{d}{d\log\Lambda_0}\left[\alpha + 3N\log(\Lambda_0/M)\right] = 0. \tag{XII.8.38}$$

Its integration constant is a logarithm of Λ^{3N}/M^{3N} on a continuous branch. At fixed angle the real part says that $8\pi^2/g_h^2$ increases toward the ultraviolet. Thus the small instanton factor at a higher matching scale is compensated by the power of that scale. Neither e^α nor Λ_0^{3N} is separately held fixed in the cutoff removal.

A finite linear subtraction illustrates the role of the holomorphic scheme. If c is a dimensionless constant and one replaces the period by $\Pi_B + cS$, the same superpotential is written using

$$\widetilde{\Pi}_B = \Pi_B + cS, \qquad \widetilde{\alpha} = \alpha - Nc, \qquad N\widetilde{\Pi}_B + \widetilde{\alpha}S = N\Pi_B + \alpha S. \tag{XII.8.39}$$

The matched scale must then be defined using the matching constant as well as $\widetilde{\alpha}$. If one instead changes the period while keeping the original numerical α, one changes W by NcS and hence changes its stationary equation. This is why a linear convention has to be transported together with its source coefficient. A nonlinear correction has a nonzero second derivative with respect to S and cannot be canceled by this operation.

The pure gauge multiplet provides an independent weak-coupling check of the exponent. In the fundamental trace convention the adjoint index is $T_{\rm adj} = N$. The gauge boson and one adjoint Weyl fermion give

$$b_0 = \left(\frac{11}{3} - \frac{2}{3}\right) T_{\rm adj} = 3N. \tag{XII.8.40}$$

This checks the one-loop Wilsonian coefficient in the four-dimensional window. Taking the cutoff out of the holomorphic expression does not extend that gauge running above the string or Kaluza–Klein thresholds, or prove their decoupling.

There is a second way to change the coefficient of S. Continuing S once around zero and treating the resulting period as a new basis element at the same point shifts Π_B by $-2\pi i S$. Its coefficient in W is N, so the inverse change in α must be $+2\pi i N$. Table XII.8.1 separates this passive change from changing the physical angle at fixed period frame. The latter can permute stationary points.

Operation	Change of Π_B	Change of α
Energy cutoff $\Lambda_0 \to r\Lambda_0$	$3S \log r$ (surviving term)	$-3N \log r$
Period frame after one positive S loop	$-2\pi i S$	$+2\pi i N$
Active $\theta \to \theta + 2\pi$ at fixed frame	0 at fixed S	$+2\pi i$

Table XII.8.1: Three operations on the same one-cut expression. The first preserves the renormalized scale, the second preserves the pairing exactly, and the third winds the physical coupling along a path.

XII.8.6 One superpotential and the holomorphic vacua

How can a single logarithm give several phases of the gauge theory? Before solving for them we need to identify what the period is a coordinate for. The compact period has dimension three, as does a gaugino bilinear. The identification also requires a normalization: the coefficient that varies with the bare coupling must couple to the same operator on the two sides.

Use the traceless gauge-field-strength superfield $\mathcal{W}_{\rm WB} = \mathcal{W}^a T^a$, with the same generators as in the DBI calculation. In this component convention the microscopic chiral gauge density is

$$\mathcal{L}_{\rm chiral} = \frac{\tau_h}{16\pi i} \mathcal{W}^{a\alpha} \mathcal{W}^a_\alpha = \frac{\tau_h}{8\pi i} \operatorname{Tr}_f \mathcal{W}^2_{\rm WB}, \tag{XII.8.41}$$

where the action also contains its conjugate and the square contracts spinor indices. The chiral operator conjugate to $\alpha = 2\pi i \tau_h$ is obtained by differentiation at fixed component fields:

$$S_{\rm gauge} = -\frac{1}{16\pi^2} \operatorname{Tr}_f \mathcal{W}^2_{\rm WB} = -\frac{1}{32\pi^2} \operatorname{Tr}_f \mathcal{W}^2_{\rm match}, \qquad \mathcal{W}_{\rm match} = \sqrt{2}\, \mathcal{W}_{\rm WB}. \tag{XII.8.42}$$

This is why the frequently used $32\pi^2$ form requires the rescaled matrix superfield with this choice of trace. In either notation the microscopic source is αS_{gauge}. The field strength $\mathcal{W}$ and the scalar superpotential W are different objects.

The protected brane-to-flux dictionary identifies $S = \int_A \Omega$ with this interacting composite in the selected F-term. The trace here omits the free diagonal vector. The identification is an additional physical input; the residue integral computed S as a period and the DBI action checked the normalization of the weak brane-side instanton exponent. Neither calculation derives the operator match. Nor does the match assign a finite kinetic term to S at an unwarped noncompact end. The free wrapped-D3 hypermultiplet of the no-flux conifold also cannot be carried over: a D3 on A in the flux background has a tadpole for N fundamental-string endpoints.

Write C_Λ for a chosen logarithm of Λ^{3N}/M^{3N}, with $M > 0$. To retain all the branches of the logarithm of the scale, take the branchwise rigid superpotential

$$W_k(S) = NS\big[1 - \log(S/M^3)\big] + (C_\Lambda + 2\pi i k)S, \qquad k \in \mathbb{Z}. \tag{XII.8.43}$$

Use a local branch of $\log(S/M^3)$ on each patch with $S \neq 0$. Rigid supersymmetry imposes $\partial_S W_k = 0$; it does not require the value of W_k to vanish. Differentiation gives

$$\partial_S W_k = -N\log(S/M^3) + C_\Lambda + 2\pi i k, \qquad \partial_S^2 W_k = -N/S. \tag{XII.8.44}$$

Exponentiating the stationary equation removes the integer from the exponent. To check the converse, insert each candidate root in a local log patch where the log has the required value:

$$S^N = \Lambda^{3N}, \qquad S_k = M^3 e^{C_\Lambda/N} e^{2\pi i k/N}, \qquad \log(S_k/M^3) = \frac{C_\Lambda + 2\pi i k}{N}. \tag{XII.8.45}$$

A change of the S logarithm by $2\pi i$ relabels k by N in the stationarity equation. Thus k is distinct modulo N, and at fixed k a single logarithm branch has at most one stationary point.

A convenient way to follow the branches is to use the logarithm itself as a local coordinate. Put $u = \log(S/M^3)$, so that $S = M^3 e^u$ on the covering space of the punctured S plane. Since $S \neq 0$, stationarity in u and stationarity in S are equivalent:

$$\frac{\partial W_k}{\partial u} = S\,(-Nu + C_\Lambda + 2\pi i k) = 0, \qquad u_k = \frac{C_\Lambda + 2\pi i k}{N}. \tag{XII.8.46}$$

Shifting u by $2\pi i$ returns to the same S, and shifts the corresponding branch label by N. This gives exactly N points after projection to the S plane. It also shows why exponentiation alone is insufficient: it loses the integer specifying which local logarithm and source branch made a particular root stationary. The nonzero roots must be lifted back to compatible patches, as in (XII.8.45). The point $S = 0$ is not reached by this coordinate and is outside this local glueball calculation. The roots are distinct and the holomorphic Hessian is nonzero when $\Lambda^{3N} \neq 0$. Using the first equation of (XII.8.44) in W_k gives

$$W_k(S_k) = NS_k. \tag{XII.8.47}$$

This value uses our subtraction convention. The N isolated holomorphic vacua refer to the interacting pure sector; the free Maxwell multiplet, if kept, has no extra glueball branch.

For an active angle change $\theta \to \theta + 2\pi$, keep the period frame fixed. Equation (XII.8.36) winds Λ^{3N} once, so along that path C_Λ increases by $2\pi i$. Equation (XII.8.45) then sends S_k to S_{k+1}. For $N = 3$ choose Λ^9/M^9 initially positive and set $s_* = (\Lambda^9)^{1/3} > 0$ on this initial slice. The three solutions are

$$S_0 = s_*, \qquad S_1 = s_* \left(-\tfrac{1}{2} + i\tfrac{\sqrt{3}}{2}\right), \qquad S_2 = s_* \left(-\tfrac{1}{2} - i\tfrac{\sqrt{3}}{2}\right). \tag{XII.8.48}$$

Figure XII.8.3 shows the continuation by one angle turn. The final coupling is the same point of the angle circle. Following an individual vacuum distinguishes this path from a change of period frame.

For transfer to a different rank, take $N = 2$ and an initial scale $\Lambda^6/M^6 = 1$. Parametrize a continuous angle path by $\theta(t) = t$, $0 \le t \le 2\pi$, while retaining the local period frame. One continuous logarithm of the scale is $C_\Lambda(t) = it$, and the two solutions are

$$S_0(t) = M^3 e^{it/2}, \qquad S_1(t) = -M^3 e^{it/2}, \qquad (S_0(2\pi), S_1(2\pi)) = (-M^3, M^3). \tag{XII.8.49}$$

For the second solution the continuous log coordinate is $u_1(t) = i(t + 2\pi)/2$. Replacing it by a principal logarithm in the middle of the path would require a branch relabeling. The two final values reproduce the original set of vacua, while the followed solutions have exchanged places. A second angle winding returns each solution individually. This explicit example separates the periodicity of the coupling from the continuation of a state at that coupling.

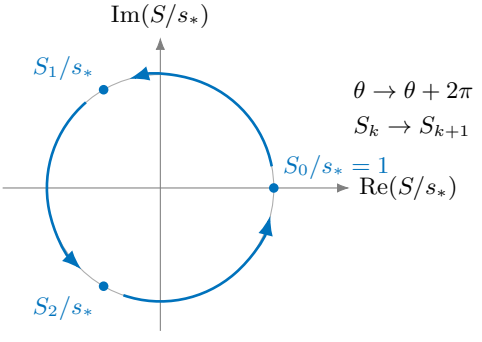


Figure XII.8.3: Three stationary roots in the complex S plane, normalized by the initial positive root s_*. A positive physical 2π winding of θ at fixed period frame rotates each root to the next one counterclockwise.

There is a separate symmetry check on these phases. The adjoint Weyl index in one unit of $SU(N)$ instanton number is $2T_{\rm adj} = 2N$. A gaugino rotation by β thus acts on the instanton measure with a phase whose exponent is $2N\beta$ up to the sign of the

transformation convention. The unbroken rotations of the measure and their action on the bilinear include

$$e^{2iN\beta} = 1, \qquad \beta = \frac{\pi}{N} : \quad S_{\text{gauge}} \longmapsto e^{2\pi i/N} S_{\text{gauge}}. \tag{XII.8.50}$$

Once a nonzero condensate is selected, this step agrees with the action on the phases in (XII.8.45). The anomaly does not prove that a condensate forms. The flux calculation agrees with the Veneziano–Yankielowicz superpotential and its stationary values in the stated holomorphic scheme.

A calculation with one other chiral coordinate makes the scope of the comparison concrete. Take a dimension-one coordinate Z, $W = mZ^2/2$ with $m \neq 0$, and either of two metrics from $K = c|Z|^2$, $c > 0$. Eliminating the auxiliary field uses the inverse metric; the canonically normalized variable is $Z_{\text{can}} = \sqrt{c}\, Z$. Therefore

$$V = c^{-1}|mZ|^2 = \frac{|m|^2}{c^2}|Z_{\text{can}}|^2, \qquad m_{\text{can}} = \frac{|m|}{c}. \tag{XII.8.51}$$

Choosing $c = 1$ and $c = 2$ keeps the holomorphic Hessian m but halves the canonical mass. The protected comparison gives neither a kinetic metric nor a confining spectrum or mass gap. The planned treatment of nonperturbative objects treats the broader gauge dynamics and confinement questions.

XII.8.7 Two cuts share one cutoff logarithm

Which period information is shared if two cuts run to the same end? The common part can be read from a single expansion at infinity. The difference samples a finite path between the cuts. To see both in one example, change the theory: start with an adjoint chiral field with a cubic tree-level superpotential and two distinct critical points. The polynomial construction uses

$$\begin{aligned} &W'_{\text{tree}}(x) = g(x-a_1)(x-a_2), \quad P(x) = W'_{\text{tree}}(x)^2 + f(x), \quad f = b_1 x + b_0, \\ &y_1^2 + y_2^2 + y_3^2 + P(x) = 0, \qquad Y(x)^2 = P(x), \quad Y \sim W'_{\text{tree}} \text{ at infinity.} \end{aligned} \tag{XII.8.52}$$

Here $g \neq 0$, $a_1 \neq a_2$ and the two cuts join pairs of branch points connected by continuation to the two nodes at $f = 0$. The example has distinct roots. Write the fiber radius as iY on the chosen sheet. Substituting it for ρ in (XII.8.19) leaves the same reduced differential $Y\,dx$ with its overall factor $1/(2\pi i)$ for the increasing-x orientation. Let γ_i be counterclockwise around the ith cut on the chosen sheet. Its upper lip goes from right to left, while the integral defining the filling S_i uses the upper lip left to right:

$$S_i = -\frac{1}{4\pi i}\oint_{\gamma_i} Y\,dx = \frac{1}{2\pi i}\int_{\text{upper lip},i}^{\text{left to right}} Y\,dx, \qquad \Pi_i = -\int_{B_i} Y\,dx + W_{\text{tree}}(L). \tag{XII.8.53}$$

The contour integral is twice the upper-lip contribution with the opposite orientation, since the two lips have opposite values of Y. Each B_i starts at the right end of its

cut, runs on the chosen sheet, and goes outward to the same large positive L. The left path passes above the right cut. We use $[x] = [L] = 1$, $[Y] = 2$ and $[S_i] = 3$ here. This engineering coordinate belongs to the cubic parent and does not use $L = \Lambda_0^{3/2}$ from the pure conifold.

To apply this construction to another quartic, first extract its polynomial square part. This step removes a restriction hidden by centered examples. Let

$$P = x^4 + c_3x^3 + c_2x^2 + c_1x + c_0, \qquad W'_{\text{tree}} = x^2 + ux + v. \tag{XII.8.54}$$

Matching the cubic and quadratic coefficients in $P - {W'_{\text{tree}}}^2$ forces

$$u = \frac{c_3}{2}, \qquad v = \frac{c_2}{2} - \frac{c_3^2}{8}, \qquad f = (c_1 - 2uv)x + (c_0 - v^2). \tag{XII.8.55}$$

The remainder has degree at most one, as required. A shift of all four roots changes c_3 and therefore the linear term of W'_{tree}; setting it to zero without first centering the roots would give the wrong f and the wrong total filling. The monic examples here have $g = 1$. They must also have distinct critical points of the extracted quadratic to lie in the stated parent construction.

At infinity the square root admits an expansion at fixed f:

$$Y = W'_{\text{tree}} + \frac{f}{2W'_{\text{tree}}} + O(f^2/(W'_{\text{tree}})^3) = W'_{\text{tree}} + \frac{b_1}{2gx} + O(x^{-2}). \tag{XII.8.56}$$

Deform the sum of the two contours into a large counterclockwise contour. The polynomial part integrates to zero, and the $1/x$ coefficient gives

$$S_{\text{tot}} := S_1 + S_2 = -\frac{1}{4\pi i}\left(2\pi i \frac{b_1}{2g}\right) = -\frac{b_1}{4g}. \tag{XII.8.57}$$

For a local check at small f, take fixed disjoint circles about the two simple zeros of W'_{tree}, with $|f| \ll |W'_{\text{tree}}|^2$ on the circles. Expanding on those contours gives the contribution of a single pole:

$$S_i = -\frac{f(a_i)}{4W''_{\text{tree}}(a_i)} + O(f^2), \qquad \sum_i \frac{f(a_i)}{W''_{\text{tree}}(a_i)} = \frac{f(a_1) - f(a_2)}{g(a_1 - a_2)} = \frac{b_1}{g}. \tag{XII.8.58}$$

Here $O(f^2)$ denotes second and higher orders in the deformation coefficients at fixed critical points. The local residues depend on the individual cuts; their sum already gives the coefficient measured at infinity.

In the dual period the polynomial part is canceled by $W_{\text{tree}}(L)$. The sign in (XII.8.53) leaves the same log coefficient for both paths:

$$\Pi_i = 2S_{\text{tot}} \log(L/M) + p_i + O(1/L). \tag{XII.8.59}$$

Here p_i is finite and depends on the chosen path, and M is a fixed reference mass. In this marked frame the flux prescription uses N_i units for cut i and one common boundary coefficient α. Thus

$$W = \sum_i N_i\Pi_i + \alpha S_{\text{tot}}, \qquad W\big|_{\log L} = 2(N_1 + N_2)S_{\text{tot}} \log(L/M). \tag{XII.8.60}$$

In particular the two ranks do not weight two separate end logarithms proportional to their own fillings. At fixed fillings a positive dilation $L \to rL$ requires $\Delta\alpha = -2(N_1 + N_2)\log r$ at surviving order. This agrees with the cubic parent's one-loop coefficient: an adjoint chiral multiplet subtracts $T_{\rm adj}$ from the pure vector coefficient $3T_{\rm adj}$. Finite relative terms can depend on both fillings. Independent pure-glueball stationary equations would miss this dependence.

The next term in the tail provides a useful finite-cutoff diagnostic. Write $W'_{\rm tree} = g(x^2 - \sigma x + \eta)$, with $\sigma = a_1 + a_2$. Expanding its reciprocal, while keeping $f = b_1 x + b_0$, gives

$$Y - W'_{\rm tree} = \frac{b_1}{2gx} + \frac{b_0 + b_1\sigma}{2gx^2} + O(x^{-3}), \tag{XII.8.61}$$

$$\Pi_i = 2S_{\rm tot}\log(L/M) + p_i + \frac{b_0 + b_1\sigma}{2gL} + O(L^{-2}). \tag{XII.8.62}$$

Indeed, differentiating the second line with respect to L gives $W'_{\rm tree}(L) - Y(L)$, the change of either subtracted relative path. Every coefficient that comes only from this exterior segment is common to the two periods. Subtracting the periods therefore cancels more than their logarithms: it cancels the entire shared exterior integral at finite cutoff. The ranks still weight the finite path-dependent constants separately.

Consider the four roots $(-4, -1, 2, 3)$ in fixed x units. For a monic quartic with no cubic term, the polynomial square part has no linear term, and its constant is half the quadratic coefficient of P. Multiplication gives

$$P = x^4 - 15x^2 + 10x + 24, \qquad W'_{\rm tree} = x^2 - \tfrac{15}{2}, \qquad f = 10x - \tfrac{129}{4}. \tag{XII.8.63}$$

To reproduce the lip signs, start with positive Y at $x > 3$ and take the boundary value from the upper half-plane. Each negative factor $x - e_j$ contributes $+i$ to its own square root. There are three such factors on the left lip, two on the gap and one on the right lip. The resulting values of $Y/\sqrt{|P|}$ are $-i, -1, +i$, respectively. Figure XII.8.4 marks the lips and the common exterior path.

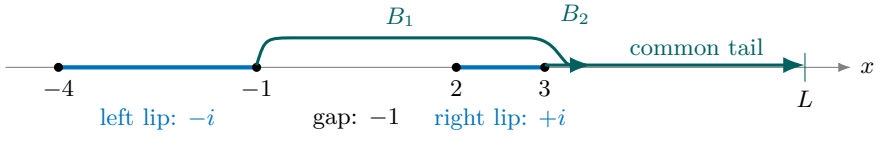


Figure XII.8.4: The two relative paths on the upper side of the cuts in the example. B_1 starts at -1, crosses the gap and passes above the right cut; B_2 starts at 3. The paths share the exterior segment ending at L. The labels $-i, -1, +i$ are the upper-side phases of $Y/\sqrt{|P|}$ on the indicated intervals.

Integrating the left lip with its negative phase and the right lip with its positive

phase gives

$$S_1 = -\frac{1}{2\pi}\int_{-4}^{-1}\sqrt{-P(x)}\,dx \simeq -2.798065,$$
$$S_2 = \frac{1}{2\pi}\int_{2}^{3}\sqrt{-P(x)}\,dx \simeq 0.298065. \tag{XII.8.64}$$

These are signed periods for the indicated contour frame, not a positivity condition on a vacuum. Their sum is $-5/2$ by (XII.8.57). Subtracting the two dual integrals cancels their common exterior segment, leaving a real gap contribution and a right-lip contribution:

$$\begin{aligned}\Pi_1 - \Pi_2 &= -\int_{-1}^{2} Y(x+i0)\,dx - \int_{2}^{3} Y(x+i0)\,dx \\ &= \int_{-1}^{2}\sqrt{P(x)}\,dx - i\int_{2}^{3}\sqrt{-P(x)}\,dx \simeq 11.518572 - 1.872799i.\end{aligned} \tag{XII.8.65}$$

The imaginary part is $-2\pi S_2$. Changing how the left path passes the right cut changes this finite comparison. For a direct check on the common tail, increase L from 4000 to 8000. Rationalizing $W'_{\text{tree}} - Y = -f/(W'_{\text{tree}} + Y)$ avoids subtracting two large nearly equal numbers. The subtracted period changes by about -3.463721 for either path, close to $-5\log 2 \simeq -3.465736$. With $(N_1, N_2) = (2, 5)$ the coefficient of $\log(L/M)$ in the flux sum is -35, whereas the finite periods still enter with their separate weights.

In this example the next term in (XII.8.62) is $-129/(8L)$. Its change between the two quoted endpoints is $129/64000 \simeq 0.002015625$. Adding this to $-5\log 2$ gives -3.46372028, already close to the direct tail integral. Thus the discrepancy at finite endpoints has a determined sign and size. It is not evidence for two different logarithmic slopes.

A second smooth input tests what is actually measured by the sum of fillings. Take the four distinct roots $(-3, -1, 1, 3)$, with the same upper-sheet convention. Now

$$P = x^4 - 10x^2 + 9, \qquad W'_{\text{tree}} = x^2 - 5, \qquad f = -16, \qquad b_1 = 0. \tag{XII.8.66}$$

The critical points $\pm\sqrt{5}$ are distinct. Reflection relates the two cut magnitudes, while the upper-sheet phases remain $-i$ and $+i$. Consequently

$$S_1 = -s, \qquad S_2 = s, \qquad S_{\text{tot}} = 0,$$
$$s = \frac{1}{2\pi}\int_{1}^{3}\sqrt{(9-x^2)(x^2-1)}\,dx \simeq 0.96768751. \tag{XII.8.67}$$

Neither cut has collapsed. The zero sum is a cancellation of signed periods in this frame. It removes the common logarithm, but leaves a finite comparison between the based paths:

$$\Pi_1 - \Pi_2 = \int_{-1}^{1}\sqrt{P(x)}\,dx - 2\pi i s \simeq 4.64599691 - 6.08015995i. \tag{XII.8.68}$$

The exterior correction is $-8/L$ at leading order. Increasing L from 20 to 40 changes either period by about 0.20147255, close to $4/20 = 0.2$; increasing it from 40 to 80 gives

about 0.10018273. These changes decay rather than approach a nonzero multiple of $\log 2$. Taking absolute values of the two compact periods before summing would destroy this check. This is a calculation on the specified polynomial family; no stationarity equation has selected this curve as a gauge vacuum.

At the distinct degeneration with roots $(-2,-2,1,3)$ the left cut shrinks to the double root. The right cut stays open. There $Y=(x+2)\sqrt{(x-1)(x-3)}$ with the inherited branch. Putting $u=x-2$ on the right lip gives

$$S_1=0, \qquad S_2=\frac{1}{2\pi}\int_{-1}^{1}(u+4)\sqrt{1-u^2}\,du=\frac{4}{2\pi}\frac{\pi}{2}=1. \tag{XII.8.69}$$

The odd part integrates to zero. The remaining filling sets the common tail in the limit of the two-cut family. This is a boundary with a collapsed cut, not another smooth two-cut example. Volume V, Chapter 9 develops the matrix-model formulation, and the planned treatment of nonperturbative objects addresses the general coupled gauge problem.

XII.8.8 The IIA and M-theory versions of the integer

The conifold charge also has a useful description in a different string frame. In the IIA counterpart the D6-branes wrap the deformed three-sphere, and the resolved side instead carries RR two-form flux through its two-sphere. This reverses the roles of the resolved and deformed geometries relative to the IIB example. The IIA comparison has its own boundary data; there is no direct M-theory lift of the IIB D5 in this argument.

The selected M-theory circle gives a geometric way to count the IIA flux. On the D6 side the circle degenerates at the source locus; the stack gives an ordinary transverse A_{N-1} quotient. On the other side of the M-theory flop the quotient acts freely on the finite S^3. The circle of this S^3 is the Hopf fiber over S^2. To count its degree, use overlapping northern and southern charts and take the oriented transition $e^{i\phi}$ on the equator. Dividing the fiber by $\mathbb{Z}_N$ identifies angles that differ by $2\pi/N$. The new angle of period 2π is N times the old angle. Its equatorial transition and first Chern number are therefore

$$e^{i\phi}\longmapsto e^{iN\phi}, \qquad c_1=\frac{1}{2\pi i}\oint (e^{iN\phi})^{-1}d(e^{iN\phi})=N. \tag{XII.8.70}$$

Kaluza–Klein reduction reads this degree as N units of RR two-form flux. The degree is independent of the length of the circle.

For instance, an order-three quotient starts with an old angle $\psi\sim\psi+2\pi$ and identifies $\psi\sim\psi+2\pi/3$. The normalized new angle $\widehat{\psi}=3\psi$ has its usual 2π period. An old chart shift by ϕ is therefore a new chart shift by 3ϕ, giving degree three. This uses the gluing of the circle, not a choice of its circumference. In the explicit M-theory metric the circle grows toward the asymptotic end; the IIA comparison with a finite asymptotic radius is conditional. The bundle calculation identifies the integer without identifying a finite-coupling metric or equating the IIA area with the IIB glueball period.

XII.8.9 Exercises

Use the cycle and coupling conventions of this chapter. Use `benchmark/tasks.json` to find the question IDs and `benchmark/PROTOCOL.md` for submission. Include explanations and derivations for Exercises 1–6.

1. **Energy cutoff versus coordinate endpoint.** Take $N = 3$ and double the energy cutoff Λ_0 at fixed nonzero S on the positive cutoff branch. At fixed Λ^{3N}, find the surviving change of Π_B in units of $S \log 2$ and the change of α in units of $\log 2$. For positive S, give the sign of the leading cutoff-suppressed term in Π_B. Show where it comes from in the elementary integral. Why does shifting α leave a difference between the two exact finite-cutoff superpotentials? Submit `delta_pi`, `delta_alpha` and `finite_sign`.

2. **Four isolated holomorphic vacua.** Set $M = 1$ in mass units and take $N = 4$ with $\Lambda^{12} = 16$ at $\theta = 0$. Compute the four roots from branchwise stationarity. Follow them under a positive 2π winding of θ at fixed period frame. In the initial ordering $k = 0, 1, 2, 3$ starting at the positive real root and going counterclockwise, give the destination index of each root. Explain why a single logarithm branch with fixed k does not enumerate all vacua and why the diagonal photon gives no additional branch. Submit `roots` as four real-imaginary pairs in any order and `permutation` in initial index order.

3. **Two fillings, one end logarithm.** In the dimension-one x units use roots $(-5, -2, 3, 4)$, the corresponding monic quartic P, and $Y = \sqrt{P} \sim x^2$. Take $N_1 = 2$ and $N_2 = 5$. Extract W'_{tree} from the polynomial part of Y at infinity and compute $f = P - {W'_{\text{tree}}}^2$. With the marked compact cycles, find S_{tot}, the coefficient of $\log(L/M)$ in each subtracted Π_i, and the coefficient of $\log(L/M)$ in the flux sum divided by S_{tot} before coupling compensation. Explain why the two tail coefficients coincide even with unequal fillings. Submit `f` as the ordered linear and constant coefficients, `total_s`, `log_pi` and `log_w_over_total_s`.

4. **A period frame change is not a theta experiment.** For $N = 5$, keep L fixed and wind S twice counterclockwise within $|4S| < |L|^2$. Give the change of the transported Π_B in units of $2\pi i S$. Give the simultaneous compensating change of α in units of $2\pi i$. Contrast this with a physical positive 2π continuation of θ at fixed period frame. Submit `period_shift` and `alpha_shift`.

5. **What the protected comparison leaves undetermined.** Using $W = mZ^2/2$ and two different positive constant kinetic coefficients, test the inference that two constructions with the same W must have the same canonical mass and confining spectrum. Identify one prerequisite for the weak brane-side four-dimensional limit and one missing piece of flux-side information needed for spectroscopy. Distinguish the large-N transition proposal, the finite-rank holomorphic comparison and a putative full gauge-theory equivalence.

6. **Translate the cuts without changing the compact periods.** Translate the original roots $(-4, -1, 2, 3)$ by $+2$, obtaining $(-2, 1, 4, 5)$. Compute P, the

polynomial square part and f without recentering the answer. By changing the integration variable in the compact integrals, show that both signed fillings and the based finite difference equal those of the original curve. Compare dual periods at L in the translated coordinate and $L-2$ in the old coordinate, taking $W^{\mathrm{new}}_{\mathrm{tree}}(x) = W^{\mathrm{old}}_{\mathrm{tree}}(x-2)$. Explain why using the same numerical endpoint in both coordinates instead leaves a finite tail change, and why that change tends to zero at large L despite the individual logarithms. Give a written derivation.

Status and sources

§8.2. Wrapped D5 fields and couplings. The two-chart resolution and cohomology in (XII.8.1)–(XII.8.3) are local calculations [MATH]. The ordinary calibrated wrapped-stack field content and free diagonal local sector use Vafa 2001, arXiv:hep-th/0008142v2, §4, PDF pp. 22–23, and Cachazo et al. 2001, arXiv:hep-th/0103067v2, §§2–2.1, PDF pp. 5–8 [GEO-E]. The quadratic DBI and Wess–Zumino coefficients apply Myers 1999, arXiv:hep-th/9910053v2, §2, (7)–(10), and §7, (90)–(92), with the string-frame RR normalization of Volume III, Chapter 3 [SUGRA]. The isolated low-energy sector assumes the stated hierarchy and suppression of couplings to unwanted modes; the weak wrapped action does not establish a collapse limit [DEC].

§8.3. Boundary charge and the two fillings. The link maps in (XII.8.14) are topological [MATH]. The Bianchi and flux normalization in (XII.8.15)–(XII.8.16) use the RR units of Giddings et al. 2002, arXiv:hep-th/0105097v2, §2.1, (2.1)–(2.5), and (3.4) [SUGRA]. Matching the boundary charge determines the flux sector. The transition in the protected regime is the proposal of Vafa 2001, §4, PDF pp. 21–23, and Cachazo et al. 2001, §2, PDF pp. 5–7 [GEO-E].

§8.4. Periods and marked loops. The exact residues, cutoff expansion, and branch transports in (XII.8.18)–(XII.8.30) are [MATH]. Chapter 2 fixes the raw residue and intersection orientation. The period normalization and endpoint scale are matched to Cachazo et al. 2001, §2, PDF pp. 6–7. Its cutoff loop acts on the reduced cutoff L^2 with a transported mark. The exact power corrections follow from the explicit integral here.

§8.5. Relative flux and running. The relative pairing prescription and the identification of G_B with the Wilsonian τ_h are separate inputs [GEO-E]: Vafa 2001, §4, final unnumbered superpotential, and Cachazo et al. 2001, (1.7) and §2, PDF pp. 6–7. Their NS flux sign convention is translated rather than identified term by term with the minus-sign convention of Giddings et al. 2002, §2.1. The latter uses the opposite wedge order in (3.7) for a compact pairing. In the present relative frame the coefficient denoted α in Cachazo et al. 2001 corresponds to $-G_B$ before rescaling W by $-2\pi i$. The signed determinant, cutoff cancellation and period-frame compensation are calculations in that prescription [MATH]. The pure gauge one-loop coefficient is a check within the Volume I four-dimensional running regime.

§8.6. Operator, vacua, and comparison. The operator identification is an additional protected dictionary [GEO-E]; see Cachazo et al. 2001, the bilinear definition following (4.5), and §2.1 for the distinct flux-side wrapped-D3 object. The component-trace translation

follows from the microscopic chiral density with the same instanton convention as the brane calculation. The branchwise roots, values, and mass counterexample are [MATH] for the stated rigid superpotentials. The independent discrete phase check matches one adjoint instanton index coefficient [ANOM], Witten 2002, arXiv:hep-th/0006010v1, §3.1, (3.1)–(3.3). The one-variable superpotential and its stationary values agree in the given scheme [BPS:1/8|holo]; see Cachazo et al. 2001, §2, PDF p. 7, for the comparison to Veneziano and Yankielowicz 1982. This is a function-level holomorphic comparison in the local pure sector at nonzero Λ^{3N}, not a state count across chambers. It does not establish bulk equivalence or the metric needed for an unprotected mass.

§8.7. Two compact cycles and one end. The cubic family and common boundary coupling use Cachazo et al. 2001, (4.2)–(4.7) and (7.2)–(7.5) [GEO-E]. The contour sums, finite difference, and double-root limit are computations in the specified frame [MATH]. Both paths here end at the same positive L. The opposite ends used in Appendix B of that source, PDF pp. 43–44, are not an identification of the individual finite terms. No general coupled vacuum classification or normalizability statement is inferred.

§8.8. The IIA and M-theory bridge. The D6/flux counterpart follows Vafa 2001, §3, PDF pp. 9–12. The selected circle, singular and free quotients, and qualifications on the IIA comparison follow Atiyah et al. 2001, arXiv:hep-th/0011256v2, §§3–4, PDF pp. 8–12, and Appendix A, (A.6)–(A.8) [GEO-E]. The Hopf quotient degree in (XII.8.70) is a circle-bundle calculation [MATH].

The angle-three example is the same transition-function calculation at $N = 3$ [MATH].

Additional calculations within the same scope. The normal-section overlap test, normalized-area comparison, explicit retraction and source-free four-chain calculation develop the calculations in §§8.2–8.3 with the stated smooth-action and source hypotheses. Equations (XII.8.25)–(XII.8.29) are calculus and numerical consequences of the exact marked period, on its specified positive branch [MATH]. Equations (XII.8.38)–(XII.8.39) and (XII.8.46)–(XII.8.49) develop the existing cutoff, scheme and branch equations [MATH]; their physical use retains the premises of §§8.5–8.6. The quartic square-part calculation, the next tail term and the symmetric distinct-root example in §8.7 use the same polynomial family and upper-sheet paths [MATH]. The symmetric curve is not asserted to be a stationary gauge vacuum. No new physical identification, kinetic metric, normalizability claim or general duality statement is used.

References

Atiyah, M., J. M. Maldacena, and C. Vafa (2001). "An M-theory flop as a large N duality". In: *J. Math. Phys.* 42, pp. 3209–3220. DOI: 10.1063/1.1376159. arXiv: hep-th/0011256.

Cachazo, F., K. A. Intriligator, and C. Vafa (2001). "A large N duality via a geometric transition". In: *Nucl. Phys. B* 603, pp. 3–41. DOI: 10.1016/S0550-3213(01)00228-0. arXiv: hep-th/0103067.

Giddings, S. B., S. Kachru, and J. Polchinski (2002). "Hierarchies from fluxes in string compactifications". In: *Phys. Rev. D* 66, p. 106006. DOI: 10.1103/PhysRevD.66.106006. arXiv: hep-th/0105097.

Myers, R. C. (1999). "Dielectric-branes". In: *JHEP* 12, p. 022. DOI: 10.1088/1126-6708/1999/12/022. arXiv: hep-th/9910053.

Vafa, C. (2001). "Superstrings and topological strings at large N". In: *J. Math. Phys.* 42, pp. 2798–2817. DOI: 10.1063/1.1376161. arXiv: hep-th/0008142.

Veneziano, G. and S. Yankielowicz (1982). "An effective Lagrangian for the pure N=1 supersymmetric Yang–Mills theory". In: *Phys. Lett. B* 113, pp. 231–236. DOI: 10.1016/0370-2693(82)90828-0.

Witten, E. (2002). "Supersymmetric index in four-dimensional gauge theories". In: *Adv. Theor. Math. Phys.* 5, pp. 841–907. DOI: 10.4310/ATMP.2001.v5.n5.a1. arXiv: hep-th/0006010.

Chapter XII.9

Atlas of direct Type IIB constructions

XII.9.1 What distinguishes two construction records?

A D3-brane on the vanishing three-sphere of a fluxless conifold gives a light particle. The same smoothing equation can describe the closed side of a D5-brane transition, where its compact period enters a four-dimensional superpotential. What distinguishes the two uses of the same integral? The choice of local sector includes the flux, the normalization of the period, and the fields held fixed at the end of the space. These choices determine which four-dimensional quantity the integral measures. In each case we assume that the stated local limit isolates the retained sector from gravity and unwanted bulk modes.

We will use the residue, vanishing-cycle and period calculations of Chapters 2–4 and the fixed-end analysis of Chapter 5. The first comparison asks how many Coulomb parameters survive when the compact homology changes. The next holds the Milnor number fixed and changes the deformation algebra. We then keep track of the ends of a fibration and of the flux on the conifold. Finally, a mirror presentation and an ALE surface show why the origin of the equation and the dimension of the wrapped cycle belong in the record. Figure XII.9.1 identifies the four settings before we compare their outputs.

XII.9.2 Compact charges and relative periods

Which coefficients are Coulomb coordinates, and which cycles can supply their electric and magnetic charges? The two counts start from different objects. For the first, consider the isolated hypersurfaces

$$f_n = y_1^2+y_2^2+y_3^2+x^n, \qquad (q_{y_1}, q_{y_2}, q_{y_3}, q_x) = \left(\frac{1}{2}, \frac{1}{2}, \frac{1}{2}, \frac{1}{n}\right), \qquad n = 2, 3, 4. \tag{XII.9.1}$$

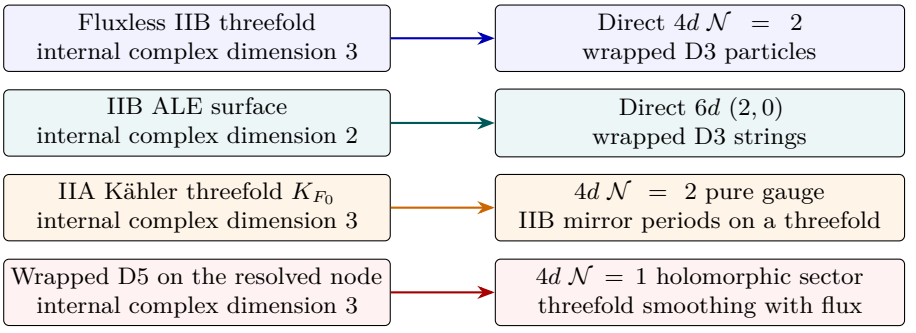


Figure XII.9.1: Each arrow follows an input to its use in this chapter. A direct Type IIB construction uses the specified surface or threefold and its boundary conditions. The mirror branch begins with a Type IIA Kähler construction. The transition changes the resolved brane geometry to the smoothing with flux. The internal dimensions label the geometric spaces used in the corresponding branch.

Here the q_i are geometric weights with f_n of degree one. The partial derivatives set each y_i and x^{n-1} to zero in the Jacobi algebra. Weighted Euler implies $f_n = \sum_i q_i z_i \partial_{z_i} f_n$, so adding f_n to the gradient ideal leaves the same quotient. The basis and the residue weight are

$$\mathcal{J}_n = \mathbb{C}[x]/(x^{n-1}), \qquad \mu = n-1, \qquad Q_\Omega = \sum_i q_i - 1 = \frac{1}{2} + \frac{1}{n}. \tag{XII.9.2}$$

A term $c_k x^k$ has coefficient weight $1 - k/n$. In the local Type IIB sector, a retained calibrated D3 measures its central charge by a common multiple of the period. Assigning that period dimension one fixes the mass dimensions

$$[c_k] = \frac{1-k/n}{1/2+1/n} = \begin{cases} 1 & (n=2,\ k=0), \\ 6/5,\ 4/5 & (n=3,\ k=0,1), \\ 4/3,\ 1,\ 2/3 & (n=4,\ k=0,1,2). \end{cases} \tag{XII.9.3}$$

In this local dictionary a coefficient of dimension greater than one is a Coulomb vev, a coefficient of dimension one is a mass, and a coefficient with dimension strictly between zero and one is a relevant coupling. In particular the dimension $4/5$ belongs to the source paired with the dimension-$6/5$ operator. It gives one entry of the deformation spectrum and no additional vev. We next ask how this distinction appears in the periods and charges.

For $n = 2$ smooth by $f_2 = s$ on the positive real slice. Take $X_s = \{f_2 = s\}$, the real sphere A with outward orientation, and the marked complex fiber $D_{L,s} = X_s \cap \{x = L\}$ with $L > \sqrt{s}$. The deformed quadric retracts to A. The fiber is a smooth quadric surface and retracts to a two-sphere. The homology sequence at degree three therefore reads

$$0 \longrightarrow \mathbb{Z}A \longrightarrow H_3(X_s, D_{L,s}; \mathbb{Z}) \xrightarrow{\partial} \mathbb{Z}[S^2] \longrightarrow 0, \qquad \partial B_L = [S^2]. \tag{XII.9.4}$$

The chain B_L is swept from $x = \sqrt{s}$ to L with the outward imaginary sphere in the y_i. At the first endpoint that sphere collapses. At the second endpoint it gives the nonzero boundary in (XII.9.4). The absolute compact lattice has just one generator, hence its alternating self-pairing is zero. Figure XII.9.2 compares this endpoint with the two compact matching cycles in the cubic.

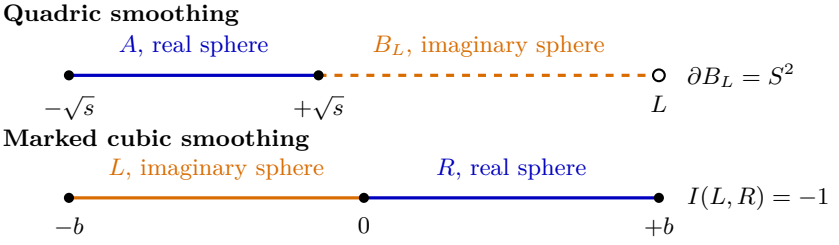


Figure XII.9.2: Base intervals of the sphere sweeps. Filled points denote collapse of the fiber sphere. The open point at L is the marked fiber carrying the two-sphere boundary. In the cubic both matching intervals end at collapses. Near $x = 0$ their tangent planes in the y_i are imaginary on the left and real on the right.

Use the residue $df_2 \wedge \Omega = dx \wedge dy_1 \wedge dy_2 \wedge dy_3$. Integrating over the oriented real fiber gives $2\pi\sqrt{s - x^2}\, dx$. On the relative interval the imaginary outward sphere contributes $-2\pi i\sqrt{x^2 - s}\, dx$ in the same residue frame. Thus

$$\begin{aligned} P &= 2\pi \int_{-\sqrt{s}}^{\sqrt{s}} \sqrt{s - x^2}\, dx = \pi^2 s, \\ Q &= -\pi i \left(L\sqrt{L^2 - s} - s \log \frac{L + \sqrt{L^2 - s}}{\sqrt{s}} \right). \end{aligned} \tag{XII.9.5}$$

To wind the smoothing parameter, continue from the positive slice at fixed L. The factors $L + \sqrt{L^2 - s}$ and $\sqrt{L^2 - s}$ admit the marked analytic branches near $s = 0$. The only winding term comes from $\log \sqrt{s}$, giving

$$Q = \frac{P}{2\pi i} \log \frac{s}{4L^2} + H_L(s), \qquad (P, Q) \longmapsto (P, Q + P). \tag{XII.9.6}$$

Here H_L is holomorphic on the local marked disk. The geometric crossing has $I(A, B_L) = -1$, and the reversed, period-ordered pairing is $+1$. The shear acts in a relative frame and the nonzero boundary of B_L survives it.

There is a kinetic distinction even for A. On the unwarped asymptotically conical end, a link three-cycle maps to A. For a closed three-form ω with fixed nonzero period on that cycle, the harmonic projection of its restriction to the unit link has a nonzero norm bounded away from zero. Rescaling the metric on the link to radius r supplies r^{-6} in the squared norm of a tangential three-form. The radial volume is proportional to $r^5\, dr$, so

$$\|\omega\|^2_{L^2(r_0 < r < R)} \;\geq\; c \int_{r_0}^{R} \frac{dr}{r}, \qquad c > 0. \tag{XII.9.7}$$

The bound gives at least logarithmic growth. In the chosen unwarped metric the complex-structure kinetic variation itself has a logarithmic divergence. With the asymptotic data fixed, the RR mode with nonzero A-period supplies a background field. The dimension-one coefficient s controls the mass of the retained hypermultiplet. In the isolated sector this gives a rank-zero free hypermultiplet at zero mass. A compact embedding can instead retain a normalizable vector and a cycle closing outside the local patch. The associated photon then belongs to that enlarged charge and kinetic problem.

For $n = 3$, use $f_3 - 3a^2x - t = 0$ with $a > 0$ and $t = 0$. Set $b = \sqrt{3}\,a$. The sphere equation in the y_i has right-hand side $x(b^2 - x^2)$. It is negative on $(-b, 0)$ and positive on $(0, b)$. Denote the two matching spheres by L, R, with interval orientation followed by outward sphere orientation. At the shared endpoint the imaginary radius is decreasing on the left, while the real radius increases on the right. In the real coordinate order $(\operatorname{Re} y_1, \operatorname{Im} y_1, \ldots, \operatorname{Re} y_3, \operatorname{Im} y_3)$, an oriented left basis can be chosen as $(-ie_1, ie_2, ie_3)$ and the right basis as (e_1, e_2, e_3). Taking the determinant of the concatenation gives

$$J_{(L,R)} = \begin{pmatrix} 0 & -1 \\ 1 & 0 \end{pmatrix}, \qquad B = -J_{(L,R)}, \qquad \det J_{(L,R)} = 1. \tag{XII.9.8}$$

Here J is the raw oriented intersection and B is the Dirac pairing in the declared frame. The distinguished compact matching basis has a unit symplectic block. In the local charge dictionary it can supply one electric and one magnetic charge, and the nonzero pairing prevents both vanishing charges from being electric in any polarization. The result agrees with the one Coulomb coordinate t of dimension $6/5$.

In the cubic use the residue order (y_1, y_2, y_3, x). On the right interval the sphere integral is real and positive, and on the left it carries phase i. The common real integral reduces by $x = b\sqrt{u}$ to a beta integral,

$$(P_L, P_R) = (iA_0, A_0), \qquad A_0 = 2\pi \int_0^b \sqrt{x(b^2 - x^2)}\, dx = \pi b^{5/2}\, \mathrm{B}(3/4, 3/2). \tag{XII.9.9}$$

A common conversion to central charges Z_L, Z_R leaves the relative phase unchanged. For the local light sector with the two adjacent primitive charges as the positive basis, the one-arrow quiver has the linear map $R \to L$. Linear algebra decomposes any single linear map into its kernel, cokernel and identity blocks. The only possible additional indecomposable besides the two simple representations is thus the dimension-$(1, 1)$ identity block. Its only nontrivial proper subrepresentation is the left simple. In a common open half-plane strict stability requires that the left simple precede the total phase, so the test is

$$\arg Z_L < \arg(Z_L + Z_R) \quad \Longleftrightarrow \quad \operatorname{Im}(\overline{Z_L} Z_R) > 0. \tag{XII.9.10}$$

Equation (XII.9.9) gives a negative value. Only the two simples are stable at this point. Under the positive-basis and quiver assumptions these are the two light hypermultiplets, together with their charge conjugates. Reversing the phase order in the abstract quiver adds the identity block. This variation of phases by itself specifies no path in the geometric family.

The quartic suspension $f_4 = 0$ gives a nearby test of the charge count. For the four-real-root matching chain, the sheet choices along successive intervals are real, imaginary, real. The adjacent tangent determinants alternate, and nonadjacent intervals are disjoint. Thus

$$J_{(d_1,d_2,d_3)} = \begin{pmatrix} 0 & 1 & 0 \\ -1 & 0 & -1 \\ 0 & 1 & 0 \end{pmatrix}, \qquad \ker_{\mathbb{Z}} J = \mathbb{Z}(d_1 - d_3). \tag{XII.9.11}$$

The kernel generator is primitive and the quotient has the unit pair represented by d_1, d_2. The middle ranks for the node, cubic and quartic suspension are respectively $1, 2, 3$, while their compact skew ranks are $0, 2, 2$. The parameter counts in (XII.9.3) give Coulomb ranks $0, 1, 1$. The cubic calculation shows what extra phase and representation data a spectrum statement requires. For the quartic, Chapter 4 supplies that additional information on its controlled four-real-simple-root slice. In the fixed residue and positive charge basis the periods have the form A_L, iB, A_R, with $A_L, B, A_R > 0$, and the two linear maps are $V_1 \to V_2 \leftarrow V_3$. Strict stability leaves the three simple representations. With the sourced local D3 and quiver interpretation these give three light hypermultiplets and their charge conjugates in this chamber. The five- and six-state assignments obtained from other abstract quiver rays are representation-theory comparisons; no geometric quartic chamber is assigned to those rays.

The quartic row makes the three counts especially easy to separate. Let $r_0 = d_1 - d_3$, and use the ordered basis (d_1, d_2, r_0). The change-of-basis matrix has columns equal to these vectors in the old basis, so the intersection matrix changes by congruence rather than similarity:

$$T = \begin{pmatrix} 1 & 0 & 1 \\ 0 & 1 & 0 \\ 0 & 0 & -1 \end{pmatrix}, \qquad \det T = -1, \qquad T^{\mathsf{T}} J T = \begin{pmatrix} 0 & 1 & 0 \\ -1 & 0 & 0 \\ 0 & 0 & 0 \end{pmatrix}. \tag{XII.9.12}$$

Because the determinant is a unit, this operation preserves the integral lattice. It exhibits one compact symplectic pair and a primitive radical direction. No division by two or rational change of charge units has entered. In the same example the coefficient calculation gave one Coulomb vev and one mass. The agreement of the nondegenerate compact rank with twice the Coulomb rank is a comparison of the two explicit calculations in this row. It does not identify a general formula from the Milnor number alone.

Writing Δ for the mass dimension of a deformation coefficient, the first three entries give

	$n = 2$	$n = 3$	$n = 4$
$\operatorname{rk} H_3$	1	2	3
$\operatorname{rk} J$	0	2	2
$\operatorname{rk} \ker J$	1	0	1
$\#\{\Delta > 1\}$	0	1	1

(XII.9.13)

Going from the cubic to the quartic adds a middle cycle without adding a second Coulomb vev. The additional cycle participates in a degenerate compact form. The

node shows a different reason to keep the groups separate: its relative chain has a nonzero boundary even though its period has a logarithm. In fact the shear preserves that boundary,

$$\partial(B_L + A) = \partial B_L = [S^2] \neq 0. \tag{XII.9.14}$$

The logarithm consequently supplies no missing compact magnetic charge. To decide which background fields become dynamical, one must still use the kinetic and end conditions, as in the node calculation above.

XII.9.3 Equal Milnor rank and different parameter roles

How much of the deformation spectrum can one infer from nine vanishing cycles? Compare the binary quartic suspension and the ordered pair of quadrics. Both have a Milnor fiber with middle rank nine. Their deformation grades, and hence the physical uses of their parameters, differ.

In the hypersurface start from

$$f_\lambda = x^2 + y^2 + z^4 + w^4 + \lambda z^2 w^2, \qquad (q_x, q_y, q_z, q_w) = (1/2, 1/2, 1/4, 1/4). \tag{XII.9.15}$$

With $w = 1$ the binary factor is $p(z) = z^4 + \lambda z^2 + 1$. At a root of p its derivative can vanish only when $z^2 = -\lambda/2$, since $p(0) = 1$. More explicitly the product of p over the roots of p', multiplied by the fourth power of the leading coefficient of p', gives

$$\operatorname{disc}(p) = 4^4 p(0) \left(1 - \frac{\lambda^2}{4}\right)^2 = 16(\lambda^2 - 4)^2. \tag{XII.9.16}$$

At $\lambda = \pm 2$ the binary form is $(z^2 \pm w^2)^2$. The vanishing partial derivatives then extend along two lines in the plane $x = y = 0$. Away from those values the two cubic partials have no common projective zero. They are a regular sequence in $\mathbb{C}[z, w]$, and removing them from the two-variable polynomial ring gives the ordinary-grade Hilbert polynomial

$$H_{\text{quartic}}(h) = \frac{(1 - h^3)^2}{(1 - h)^2} = 1 + 2h + 3h^2 + 2h^3 + h^4. \tag{XII.9.17}$$

The two quadratic variables disappear from the quotient. Since $Q_\Omega = 1/2$, grade k in (XII.9.17) gives coefficient dimension $2 - k/2$. In decreasing order the dimensions with multiplicities are

$$2, \quad (3/2)^{\times 2}, \quad 1^{\times 3}, \quad (1/2)^{\times 2}, \quad 0. \tag{XII.9.18}$$

Here the superscript $\times m$ denotes multiplicity. The zero-dimensional direction preserves the weight of the equation. Its existence is a geometric statement. The failure of isolation at two finite λ values gives no period calculation for a weak gauge tube.

A different use of this family is to add az^2 at fixed $a \neq 0$ and study the tuned origin. A holomorphic square root of $a + z^2 + \lambda w^2$ is defined near that point. Multiplying z by

this root yields a nonsingular coordinate change that puts the equation locally in the form $x^2+y^2+Z^2+w^4$. To see the scaling of its residue, choose a branch of $\sqrt{a}$ and set

$$(x,y,z,w)=(a\epsilon^2X,a\epsilon^2Y,\sqrt{a}\,\epsilon^2Z,\sqrt{a}\,\epsilon W). \tag{XII.9.19}$$

Dividing the equation by $a^2\epsilon^4$ gives $X^2+Y^2+Z^2+W^4+\lambda\epsilon^2Z^2W^2+\epsilon^4Z^4$. The ambient volume acquires $a^3\epsilon^7$. Dividing this factor by the equation scaling gives the residue factor $a\epsilon^3$. In the limiting local germ the residue weight is $3/4$. The same w^2 monomial therefore gives

$$[c_{w^2}]_{\text{quartic}}=\frac{1-2/4}{1/2}=1,\qquad [c_{w^2}]_{A_3\text{ germ}}=\frac{1-2/4}{3/4}=\frac{2}{3}. \tag{XII.9.20}$$

With the local IIB scaling dictionary this compares a mass in the original grading with a relevant coupling in the tuned local sector. The calculation concerns the germ and its retained period scaling near the tuned point.

For the complete intersection take $R=\mathbb{C}\{x_1,\dots,x_5\}$ and the ordered equations

$$F=(F_1,F_2)^{\mathsf{T}},\qquad F_1=\sum_{i=1}^{5}x_i^2,\qquad F_2=\sum_{i=1}^{5}i\,x_i^2,\qquad F_1=F_2=0. \tag{XII.9.21}$$

The i in the sum is the integer index. A rank drop of DF would require all nonzero x_i to have the same slope i. Because the slopes are distinct, a rank drop on the zero set occurs only at the origin. The deformation varies both equations. At first order a coordinate change contributes a column of DF times a function. An equation change can add any multiple of the defining equations to either component. This gives the normal deformation module

$$T^1=\frac{Re_1\oplus Re_2}{\operatorname{im}DF+(F_1,F_2)(Re_1\oplus Re_2)}. \tag{XII.9.22}$$

For $i\neq j$, the two ways of removing $x_ix_je_1$ differ by $(i-j)x_ix_je_2$. Therefore the mixed products vanish and all positive-degree classes can be represented in the second component. In degree two the original equation multiples in each component give the three independent moments

$$\sum_{i=1}^{5}i^kx_i^2e_2=0,\qquad k=0,1,2. \tag{XII.9.23}$$

The three rows are independent by the Vandermonde determinant for any three distinct slopes. Multiplying the $k=0$ row by x_j kills the cube $x_j^3e_2$, since the mixed products already vanish. The surviving classes can be chosen as

$$\underbrace{e_1,e_2}_{0},\qquad \underbrace{x_1e_2,\dots,x_5e_2}_{1},\qquad \underbrace{x_4^2e_2,x_5^2e_2}_{2}. \tag{XII.9.24}$$

The independent weighted Euler count of the Milnor fiber gives

$$\chi=4[t^3]\frac{(1+t)^5}{(1+2t)^2}=4(10-40+60-32)=-8,\qquad \mu=1-\chi=9. \tag{XII.9.25}$$

Here the odd-dimensional Milnor fiber has the homotopy type of a bouquet of three-spheres. Its middle rank and the module length agree in this example. A scalar singular scheme of equal length would not reproduce the two equation components in (XII.9.24).

In the ordered residue $dF_1 \wedge dF_2 \wedge \Omega = d^5x$, the two equation differentials have weight two and the five variables have weight one. Consequently $Q_\Omega = 1$ and the coefficient dimensions are $2, 1, 0$ by grade, with multiplicities $2, 5, 2$. A change $F' = BF$ for constant invertible B transports v to Bv and changes the ordered residue by

$$dF_1' \wedge dF_2' = (\det B)\, dF_1 \wedge dF_2, \qquad \Omega' = (\det B)^{-1}\Omega. \tag{XII.9.26}$$

Thus even when the base space is unchanged, the ordering and scale of the defining pair enter the period frame. The two spectra give three Coulomb and three mass directions in the quartic, versus two and five in the complete intersection. Their zero-weight directions count geometric deformations. In Table XII.9.1 these are listed separately from the dimensionless coupling of the four-ended gauge family.

We can now compare the equal-rank rows without identifying their deformation spaces. Keep track of a coefficient by its grade and the number of independent classes in that grade:

	graded dimensions	coefficient dimension at grade k
binary quartic	$1 + 2h + 3h^2 + 2h^3 + h^4$	$2 - k/2$
two quadrics	$2 + 5h + 2h^2$	$2 - k$

(XII.9.27)

Both polynomials take the value nine at $h = 1$. That evaluation removes all the grading information needed to determine parameter roles. Keeping the grading, count the classes above, at and below dimension one:

	Coulomb	mass	relevant	weight zero
binary quartic	$1 + 2 = 3$	3	2	1
two quadrics	2	5	0	2

(XII.9.28)

For example, the five grade-one classes of the ordered pair all have dimension one. Treating their grades with the quartic normalization would assign dimension $3/2$ and change five mass directions into vevs. The error occurs before any question about stability or periods. It comes from forgetting which residue fixes the mass unit.

One can also change the presentation while preserving the ordered-pair problem. Choose a constant equation change with determinant different from one:

$$B = \begin{pmatrix} 1 & 1 \\ 1 & -1 \end{pmatrix}, \qquad F' = \begin{pmatrix} F_1 + F_2 \\ F_1 - F_2 \end{pmatrix}, \qquad \det B = -2, \qquad \Omega' = -\frac{1}{2}\Omega. \tag{XII.9.29}$$

A deformation $ge_2 = (0, g)^{\mathsf{T}}$ becomes $B(0, g)^{\mathsf{T}} = (g, -g)^{\mathsf{T}}$. Thus the two components must be transported together, although the zero set is unchanged. The constant common residue factor preserves relative period ratios and homogeneity dimensions. It changes the absolute period normalization until the physical conversion is transported as well. This example separates a change of equation frame from a new choice of physical sector, which is the next distinction needed for comparing table rows.

XII.9.4 Four ordinary ends and a weak tube

What replaces the finite Jacobi quotient when the singular locus is a curve? Fix a sphere with the four marked points $0, q, 1, \infty$, with $q \neq 0, 1$, and let C be its complement. The threefold is

$$X_Q = \{uv + x^2 = Q\} \subset \mathrm{Tot}(K_C \oplus K_C \oplus K_C), \qquad Q = \phi_z\, dz^2. \tag{XII.9.30}$$

The three fiber coordinates are coefficients of one-forms in a base chart, and both sides of the equation take values in $K_C^{\otimes 2}$. If the base coordinate changes from z to $\zeta(z)$, the three coefficients each acquire $dz/d\zeta$. The equation scales by its square. In $d(uv + x^2 - \phi_z) \wedge \Omega = dv \wedge du \wedge dx \wedge dz$, the ambient volume acquires this same square, since one factor of $d\zeta/dz$ comes from the base. The residue consequently patches over the curve.

At $Q = 0$ the gradient in the fiber directions sets u, v, x to zero, while every function of z survives on the zero section. At a simple zero of ϕ_z the total space is instead smooth because $\partial_z \phi_z \neq 0$. The deformation problem comes from a meromorphic quadratic differential with prescribed behavior at the punctures. With $P = z(z-q)(z-1)$, take

$$\begin{aligned}\phi_z = \frac{m_0^2}{z^2} + \frac{m_q^2}{(z-q)^2} + \frac{m_1^2}{(z-1)^2} \\ + \frac{m_\infty^2 - m_0^2 - m_q^2 - m_1^2}{z(z-1)} + \frac{U}{P}.\end{aligned} \tag{XII.9.31}$$

The double poles describe ordinary ends with the indicated mass squares. The sheet residues of $\lambda = x\, dz$ are $\pm m_p$ at an ordinary massive end. At zero mass the marked point remains part of the boundary data.

For any differential with these allowed poles, $N(z) = P(z)^2 \phi_z$ has degree at most four. The leading pole map has five polynomial coefficients as its domain and four values as its target,

$$N \longmapsto \left(\frac{N(0)}{P'(0)^2}, \frac{N(q)}{P'(q)^2}, \frac{N(1)}{P'(1)^2}, [z^4]N \right). \tag{XII.9.32}$$

The kernel has degree at most three by the infinity condition and vanishes at all three finite marks. It is therefore exactly the span of P, so the rank is four and the fixed-mass direction is U. The positions of the four ends contribute the separate marked cross-ratio q.

For a concrete use of this map, place the moving mark at $q = 1/2$ and write $N(z) = n_0 + n_1 z + n_2 z^2 + n_3 z^3 + n_4 z^4$. In coefficient order $n_0, \ldots, n_4$, the four leading squares are

$$\begin{pmatrix} m_0^2 \\ m_q^2 \\ m_1^2 \\ m_\infty^2 \end{pmatrix} = M_{1/2} \begin{pmatrix} n_0 \\ n_1 \\ n_2 \\ n_3 \\ n_4 \end{pmatrix}, \qquad M_{1/2} = \begin{pmatrix} 4 & 0 & 0 & 0 & 0 \\ 16 & 8 & 4 & 2 & 1 \\ 4 & 4 & 4 & 4 & 4 \\ 0 & 0 & 0 & 0 & 1 \end{pmatrix}. \tag{XII.9.33}$$

The entries follow from $P'(0) = P'(1) = 1/2$ and $P'(1/2) = -1/4$. Solving the homogeneous equations first sets $n_0 = n_4 = 0$. The remaining two independent equations leave one vector,

$$\delta\mathbf{n} = \delta U(0, 1/2, -3/2, 1, 0)^{\mathsf{T}}, \qquad \delta N = \delta U\, z(z - 1/2)(z - 1). \tag{XII.9.34}$$

This is a direct instruction for varying the Coulomb parameter without changing any leading mass square. In contrast, adding a constant to N changes three finite pole values. Polynomial coefficients by themselves have no fixed physical role until the boundary map is applied.

For equal end masses $m_0 = m_q = m_1 = m_\infty = m \neq 0$, the numerator obtained from (XII.9.31) is

$$N = m^2(z^4 - 2z^3 + 2z^2 - z + 1/4) + U(z^3 - 3z^2/2 + z/2). \tag{XII.9.35}$$

Substitution into (XII.9.33) gives the four values m^2, independently of U. Choose U away from repeated roots of N when applying the smooth-cover period discussion below. The fixed-mass parameter direction exists independently of that extra smoothness requirement.

Now move the mark to $q = 1/3$, retaining distinct ends. The entries of the pole map change, but its kernel is still generated by the divisor polynomial:

$$\delta\mathbf{n} = \delta U(0, 1/3, -4/3, 1, 0)^{\mathsf{T}}, \qquad \delta N = \delta U\, z(z - 1/3)(z - 1), \qquad \operatorname{rk} M_{1/3} = 4. \tag{XII.9.36}$$

The one-dimensional kernel therefore survives this change of marked base. Moving q changes the boundary geometry; varying U at fixed q lies in the kernel of its mass map. The two operations cannot be combined into a count of two Coulomb coordinates.

The compact spectral cover can be written $y^2 = N(z)$ with $y = Px$. On a smooth cover, varying U while fixing the end data gives

$$\lambda = \frac{y}{P}\, dz, \qquad \omega_U = \partial_U \lambda = \frac{dz}{2y}. \tag{XII.9.37}$$

The differential ω_U extends across simple branch points and is holomorphic on the compact genus-one curve. In the reduced spectral norm this is a finite variation. Changing a massive residue by δm_p contributes $\delta m_p\, dz/(z - p)$. Its reduced squared norm diverges by $\int dr/r$ at the end. These are statements in the reduced curve description. To identify the threefold periods in that description, fiber the oriented sphere along an interval γ with the endpoint collapses as in Chapter 5. Its normalized integral is

$$\frac{1}{2\pi i}\int_{\Gamma_\gamma} \Omega = \int_{\gamma_+ - \gamma_-} \lambda, \tag{XII.9.38}$$

where the two lifts are first oriented as γ. The sheet difference closes on the curve. A retained D3 central charge is proportional to this period, which fixes $[\lambda] = 1$. The base coordinate z and the marked cross-ratio q are dimensionless, so $\lambda = x\, dz$ gives $[x] = 1$. Then $x^2 = \phi_z$ and the term U/P in (XII.9.31) give $[U] = 2$. In the local gauge dictionary the one finite reduced variation at fixed masses gives a rank-one Coulomb

branch with coordinate U. Changing a residue instead changes the corresponding fixed mass. The compact spectral pair supplies the gauge quotient over $\mathbb{Q}$ in the period description. The primitive integral threefold lattice is a separate problem.

To find a weak tube, take q small while keeping the two ends $0, q$ distinct in the rescaled coordinate $w = z/q$. Define $a^2 = m_0^2 + m_q^2 - U$ and assume $a \neq 0$ with the ordinary smooth massive component data. Equation (XII.9.31) has the two limits

$$\begin{aligned} \lim_{q\to 0} \phi_z &= \frac{a^2}{z^2} + \frac{m_1^2}{(z-1)^2} + \frac{m_\infty^2 - a^2 - m_1^2}{z(z-1)}, \\ \lim_{q\to 0} q^2 \phi_z(qw) &= \frac{m_0^2}{w^2} + \frac{m_q^2}{(w-1)^2} + \frac{a^2 - m_0^2 - m_q^2}{w(w-1)}. \end{aligned} \tag{XII.9.39}$$

The node has square a^2 at $z = 0$ in the outer chart and at $w = \infty$ in the inner one. The inner limit retains the mass information that a substitution $q = 0$ at fixed z would lose. Figure XII.9.3 shows how the cover has two lifts of the connecting annulus.

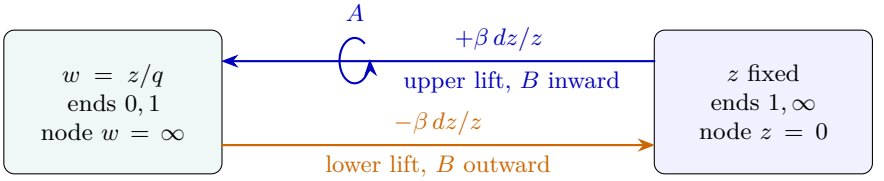


Figure XII.9.3: The two limiting components retain the indicated ends. The two sheets of the neck carry opposite signs of ω_U. A cycle joining the components traverses the two annuli in opposite directions, so their logarithms add. An oriented circumference on the upper annulus gives the A-period in the denominator.

On a neck with $|q| \ll |z| \ll 1$, one has $x \simeq \pm a/z$, $P \simeq -z^2$, and $y = Px \simeq \mp az$. Thus the leading variation is $\pm\beta\, dz/z$ with $\beta = -1/(2a)$. Orient A counterclockwise on the upper sheet and B inward on that sheet and outward on the lower sheet. Integrating the two terms on B gives

$$\oint_A \omega_U = 2\pi i\beta + O(\sqrt{|q|}), \qquad \oint_B \omega_U = 2\beta \log q + O(1), \qquad \tau_{\mathrm{per}} = \frac{\log q}{\pi i} + O(1). \tag{XII.9.40}$$

For A the error follows by taking a radius of order $\sqrt{|q|}$. On each B path the relative corrections $O(|z| + |q/z|)$ integrate to bounded terms in a fixed sector of $\log q$. The two limiting component contributions are bounded under the stated smoothness assumptions. The period ratio here is the ratio of derivatives at fixed ends. As $\operatorname{Im} \tau_{\mathrm{per}}$ grows without bound, the gauge sector in this frame becomes weakly coupled.

At zero masses and $U \neq 0$ the cover becomes the Legendre curve $Y^2 = z(z-1)(z-q)$ after dividing y by $\sqrt{U}$. Its four branch points include infinity, so its genus is one. The Legendre invariant gives a separate check on the logarithm,

$$j(q) = \frac{256(1 - q + q^2)^3}{q^2(1-q)^2}, \qquad \lim_{q\to 0} q^2 j(q) = 256. \tag{XII.9.41}$$

Since $j(\tau)$ has a simple pole in $e^{2\pi i\tau}$, the double pole in q checks the coefficient in (XII.9.40).

Under the ordinary-end matter dictionary each three-ended component supplies a half-hypermultiplet in the tensor product of the three doublets. As seen by the node algebra, the other two doublets give four copies of its doublet. The two components therefore supply four full fundamentals after diagonal gauging. For $\mathfrak{su}(2)$ their contribution cancels the adjoint term in the one-loop coefficient, $2h^\vee - 4 = 0$. The exact marginality of the marked q in the massless family is a separate physical input.

XII.9.5 One quadric with and without flux

Keep the algebraic smoothing equation fixed and change the brane and end data. Which period relations survive? On the resolved side of the transition take N wrapped D5-branes on the exceptional $\mathbb{P}^1$ in $\mathrm{Tot}(\mathcal{O}(-1)\oplus\mathcal{O}(-1))$. This is the last branch of Figure XII.9.1. Their charge is measured on the linking sphere at the common end. In the specified smoothing without localized D5 sources, that sphere maps to the compact cycle A. With zero compact NS period, the normalized complex flux obeys

$$G = \frac{F_3 - \tau_{\mathrm{IIB}} H_3}{(2\pi)^2 \alpha'}, \qquad G_A = \int_A G = N. \tag{XII.9.42}$$

The period G_B is instead fixed in a regulated relative frame. Its boundary prescription supplies the holomorphic coupling $\alpha = 2\pi i G_B$. The compact charge and this complex coupling play different roles in the superpotential.

Use μ_{def} for the algebraic smoothing coefficient on the flux side. At $\mu_{\mathrm{def}} = s$ the raw compact integral in (XII.9.5) is the same. The flux period convention and four-dimensional matching scale give

$$S = \frac{P}{4\pi^2} = \frac{\mu_{\mathrm{def}}}{4}, \qquad L = \Lambda_0^{3/2}, \qquad [L] = \frac{3}{2}, \qquad [S] = 3. \tag{XII.9.43}$$

The dimension of S follows from the assigned dimension of the endpoint and the relation $[\mu_{\mathrm{def}}] = 2[L]$ in the quadric. In the fluxless D3 sector the same algebraic coefficient was normalized by a particle mass. Here the physical identification is with the holomorphic glueball composite of the interacting gauge sector. It uses the coupling to that composite and the brane-to-flux dictionary.

In the relative period on the flux side first use the residue normalization in (XII.9.43). Multiplying the resulting B-period by $-2\pi i$ gives minus the real square-root integral. Adding $L^2/2$ removes its S-independent leading part. On the positive starting slice one obtains

$$\begin{aligned} \Pi_B &= \frac{L^2}{2} - \int_{2\sqrt{S}}^{L} \sqrt{x^2 - 4S}\, dx \\ &= S\left(1 + \log\frac{L^2}{S}\right) + O(S^2/L^2). \end{aligned} \tag{XII.9.44}$$

For the expansion one can evaluate the integral using the square-root primitive in (XII.9.5) with $s = 4S$. Its lower endpoint fixes the $S\log S$ term. The primitive and the sign specify the analytic continuation from the positive slice.

In the local holomorphic transition prescription $W = N\Pi_B + \alpha S$ up to the stated subtraction. Since $L^2 = \Lambda_0^3$, rescaling Λ_0 to $r\Lambda_0$ adds $3NS\log r$ to the surviving period part. Holding the interacting scale fixed gives

$$\Lambda^{3N} = \Lambda_0^{3N} e^{\alpha}, \qquad \Delta\alpha = -3N\log r. \tag{XII.9.45}$$

The rank-three example needs $\Delta\alpha = -9\log r$. After taking this matched limit, the local branch of the superpotential has the form

$$W_k(S) = NS\big(1 - \log(S/M^3)\big) + S\big(\log(\Lambda^{3N}/M^{3N}) + 2\pi i k\big), \tag{XII.9.46}$$

with M a fixed mass for writing the logarithms. Differentiation cancels the two constant N terms and exponentiation gives

$$S^N = \Lambda^{3N}, \qquad S_k = M^3 \exp\!\left(\frac{\log(\Lambda^{3N}/M^{3N}) + 2\pi i k}{N}\right). \tag{XII.9.47}$$

For $\Lambda^{3N} \neq 0$ there are N distinct nonzero roots. At fixed period frame, a positive 2π winding of the physical theta angle winds Λ^{3N} once. For $N = 3$ the roots move from $0, 1, 2$ to $1, 2, 0$ in the initial counterclockwise ordering. An S-plane loop at fixed L instead changes Π_B by $-2\pi i S$ through (XII.9.44). The roots are information about the selected F-term. Their calculation does not determine the glueball kinetic term or a spectrum of particles.

To use the flux row, it helps to perform three different continuations separately. A change of relative period frame may replace the subtracted period by $\Pi'_B = \Pi_B + cS$, with constant c. The same superpotential is written in that frame only if the boundary coefficient changes at the same time:

$$\Pi'_B = \Pi_B + cS, \qquad \alpha' = \alpha - Nc, \qquad N\Pi'_B + \alpha' S = N\Pi_B + \alpha S. \tag{XII.9.48}$$

For an S-plane loop the local logarithm gives $c = -2\pi i$. The corresponding compensating change is $\alpha' = \alpha + 2\pi i N$. A cutoff rescaling instead has $c = 3\log r$ in the surviving linear term and gives the real-scale compensation in (XII.9.45). These transformations preserve the selected F-term when the accompanying boundary coefficient is transported. Holding α fixed while changing the period frame would change the expression being compared.

A physical theta winding at fixed period frame varies Λ^{3N} and follows the roots continuously. For example, change the rank from three to four in the already stated stationary equation, take $\Lambda^{12} = \rho^4 e^{i\theta}$ with $\rho > 0$, and follow

$$S_k(\theta) = \rho \exp\!\left(\frac{i(\theta + 2\pi k)}{4}\right), \qquad k = 0, 1, 2, 3, \qquad S_k(2\pi) = S_{k+1 \pmod 4}(0). \tag{XII.9.49}$$

At $\theta = 0$ these are $\rho, i\rho, -\rho, -i\rho$. The winding permutes them counterclockwise and returns the unordered set. The compensating cutoff coefficient is now $-12\log r$. Changing N changes both the flux integer and this stationary-point arithmetic. Neither operation supplies the normalization of a kinetic term or a mass for fluctuations of S. Those require information absent from this holomorphic record.

XII.9.6 When the presentation or spacetime dimension changes

Two genus-one period problems can come from different gauge constructions. To distinguish them, follow the inputs to the Laurent family of the Type IIA local-F_0 model. The compact surface is $\mathbb{P}^1 \times \mathbb{P}^1$ in its canonical bundle. The two toric relations can be written

$$\ell_b = (-2,1,1,0,0), \qquad \ell_f = (-2,0,0,1,1). \tag{XII.9.50}$$

Relative to the interior monomial, the first pair of monomials has product one and the second pair does as well. Thus the two pairs may be represented by z, z^{-1} and w, w^{-1}. The mirror presentation of the selected Type IIA limit uses

$$\begin{aligned} UV &= H(z,w), \qquad H = w + w^{-1} - K + c(z + z^{-1}), \\ K &= 2 + \epsilon^2 u, \qquad c = \epsilon^2 L/2, \qquad z, w \in \mathbb{C}^*. \end{aligned} \tag{XII.9.51}$$

The symbols U, V are the extra affine coordinates of this presentation. The scale $L \neq 0$ and the scaled Coulomb variable u belong to this limit. This L is unrelated to the cutoff in the conifold record.

For $\epsilon \neq 0$, the torus critical points have $w, z = \pm 1$. At $w = 1$ the two critical values are $\epsilon^2(-u \pm L)$. At $w = -1$ they are $-4 + \epsilon^2(-u \pm L)$. Multiplication gives

$$\prod_{z,w=\pm 1} H(z,w) = \epsilon^4 (u^2 - L^2)\big[(4 + \epsilon^2 u)^2 - \epsilon^4 L^2\big]. \tag{XII.9.52}$$

The first factor gives the two finite singular fibers $u/L = \pm 1$. The other two zeros move to infinity in the scaled u-plane. The surviving curve follows by setting $w = e^{\epsilon p}$ near $w = 1$,

$$\lim_{\epsilon \to 0} \frac{H(z, e^{\epsilon p})}{\epsilon^2} = p^2 - u + \frac{L}{2}(z + z^{-1}). \tag{XII.9.53}$$

The full threefold carries the form $dU/U \wedge d\log w \wedge d\log z$ in the marked torus chart. Its gauge periods depend on cycles that close in the relative construction.

For example, A', B' are a unit pair on the compactified mirror curve. In the punctured curve A' has torus winding $(1,0)$, whereas B' has $(0,0)$. At the punctures over $z = 0, \infty$, one sheet has a simple zero of w and the other has a simple pole. The winding vectors are

$$(\operatorname{ord} z, \operatorname{ord} w) = (1, \pm 1), \ (-1, \pm 1). \tag{XII.9.54}$$

Their two entries have the same parity. An odd multiple of A' cannot be canceled by such loops. The two unit-circle lifts A', A_- both wind by $(1,0)$. Their difference has zero ambient winding, so it bounds a relative chain in the torus. Their sum bounds the inside of the lifted circle after filling the punctures. Hence $A' - A_-$ projects to $2A'$, and the projected gauge lattice and pairing are

$$\mathbb{Z}(2A') \oplus \mathbb{Z}B' \subset \mathbb{Z}A' \oplus \mathbb{Z}B', \qquad [H_1(\overline{\Sigma}) : \mathbb{Z}(2A') \oplus \mathbb{Z}B'] = 2, \qquad (2A') \cdot B' = 2. \tag{XII.9.55}$$

The inherited mirror dictionary identifies the retained sector with the pure $\mathfrak{su}(2)$ solution. The direct four-ended fibration has four full fundamentals at its weak tube and its comparison was made in a spectral gauge quotient. The gauge algebra alone cannot carry that matter or primitive lattice information from one presentation to the other.

A further comparison uses the same D3-brane with a different internal dimension. For the A_2 ALE surface take

$$(u, v, w) = (a^3, b^3, ab), \qquad uv = w^3 \quad \text{for} \quad (a, b) \longmapsto (\zeta a, \zeta^{-1} b), \quad \zeta^3 = 1. \tag{XII.9.56}$$

Every invariant monomial has exponent difference divisible by three, so these three generate the invariant ring. In the smooth resolution there are two compact rational curves Σ_1, Σ_2. Adjunction gives square -2 for each curve and the adjacent transverse intersection is $+1$. The symmetric intersection and its determinant are

$$I_{\mathrm{ALE}} = -C_{A_2} = \begin{pmatrix} -2 & 1 \\ 1 & -2 \end{pmatrix}, \qquad \det I_{\mathrm{ALE}} = 3. \tag{XII.9.57}$$

This is the middle pairing in real dimension four. In the threefold the middle cycles have real dimension three and the pairing is alternating.

In the aligned tensor-branch slice the wrapped D3 tension coordinates are $T_i = T_{\mathrm{D3}} \int_{\Sigma_i} J$. For $(T_1, T_2) = (2, 3)$ in common tension units the three positive root coordinates are $2, 3, 5$. The last value is the linear pairing with the sum root. It does not assert an independently stable string with that charge. The spacetime worldvolume dimension follows directly by subtracting the internal real wrapping dimension d from four,

$$\dim_{\mathbb{R}} W_{\mathrm{ext}} = 4 - d = \begin{cases} 2 & (d = 2, \ \text{ALE two-cycle}), \\ 1 & (d = 3, \ \text{threefold three-cycle}). \end{cases} \tag{XII.9.58}$$

Figure XII.9.1 separates the resulting six-dimensional string from the four-dimensional particle. In the smooth ALE description the two localized harmonic two-forms supply the tensor branch. The interacting $(2, 0)$ origin uses the ordinary Type IIB identification with the periods tuned to the origin and the local sector isolated.

XII.9.7 The atlas by construction route

The records below separate coefficient, charge and period information. Within the direct four-dimensional entries the isolated examples use graded deformation algebras. The four-ended example uses boundary conditions on a base curve. The other three panels use different geometric or physical inputs, so a common symbol need not measure a common quantity. A question left open in a panel is outside that record's calculation.

In Table XII.9.1, the conifold and cubic entries specify local particle content only in the settings of Section XII.9.2. The A_3 entry additionally uses the local collinear-root chamber of Chapter 4 just described. The binary quartic and two-quadric entries leave stability chambers open. For the last two the explicit middle rank is known while the marked compact polarization and relative lattice are unspecified. Table XII.9.2 uses a reduced spectral norm for the fibration and a holomorphic flux superpotential for the

Geometry	Vev / mass / coupling / zero	Charge and physical scope
Node f_2 $\mu = 1$	$\varnothing$ 1 $\varnothing$ $\varnothing$	One compact A, skew rank 0. Relative B_L ends on the marked sphere. Fixed-end free hyper.
(A_1, A_2), f_3 $\mu = 2$	$\frac{6}{5}$ $\varnothing$ $\frac{4}{5}$ $\varnothing$	Compact unit pair (L, R). Two light hypers at the marked real-root point under the stated assumptions.
(A_1, A_3), f_4 $\mu = 3$	$\frac{4}{3}$ 1 $\frac{2}{3}$ $\varnothing$	Skew rank 2 with primitive radical $d_1 - d_3$. Three simple light hypers in the collinear-root local chamber under the stated assumptions.
Binary quartic f_λ $\mu = 9$	$2, \frac{3}{2}^{\times 2}$ $1^{\times 3}$ $\frac{1}{2}^{\times 2}$ 0	Isolated for finite $\lambda \neq \pm 2$. Middle homology rank nine. Pairing and chamber unspecified.
ICIS (1), $n = 2$ $\mu = 9$	$2^{\times 2}$ $1^{\times 5}$ $\varnothing$ $0^{\times 2}$	Ordered two quadrics in $\mathbb{C}^5$. Middle homology rank nine. Pairing and chamber unspecified.

Table XII.9.1: Direct Type IIB on isolated threefold singularities with four-dimensional $\mathcal{N} = 2$. Coefficient dimensions are grouped as Coulomb vevs, masses, relevant couplings and geometric weight-zero directions. The empty-set symbol denotes an empty group. Repeated values carry their multiplicities. The last column concerns compact cycles unless a relative chain is explicitly named.

Route and sector	Geometric input	Selected output and boundary
Direct $4d$ $\mathcal{N} = 2$ Four punctures	$uv + x^2 = Q$ in $\mathrm{Tot}(K_C \oplus K_C \oplus K_C)$. Ordinary ends at $0, q, 1, \infty$.	Genus 1, 1 vev U. Four masses and massless marginal q. Four full fundamentals at the weak tube. Integral D3 lift unspecified.
Transition $4d$ $\mathcal{N} = 1$ Conifold	Resolved D5 input. Marked smoothing $f_2 = \mu_{\mathrm{def}}$ with $G_A = N$, regulated G_B.	$S = \mu_{\mathrm{def}}/4$ and $[S] = 3$. Theta sends the rank-three roots to $(1, 2, 0)$. Kinetic term unspecified.
Direct $6d$ $(2, 0)$ ALE A_2	Surface $uv = w^3$. Two compact rational curves on the resolved tensor branch.	$\det I = 3$. Aligned root tension coordinates $(2, 3, 5)$. D3 wrapping gives strings.
Mirror $4d$ $\mathcal{N} = 2$ Local F_0	Type IIA on K_{F_0}, with the IIB threefold $UV = H$ of (XII.9.51).	Pure gauge sector. Finite $u/L = -1, 1$. Gauge projection index 2. Absolute line lattice unspecified.

Table XII.9.2: The direct four-ended fibration and three separate comparison settings. The row headings indicate which geometry and supersymmetry enter each calculation.

transition. Neither column supplies the corresponding full threefold kinetic metric. The only finite-coupling modulus identified here as exactly marginal is the marked q of the massless four-ended family, under its sourced physical dictionary.

Let us use the panels to answer a practical selection question. Suppose a local construction has a rank-one Coulomb branch. Which row could describe it? This condition first selects two isolated rows with different coefficient roles and the four-ended gauge row:

record	one Coulomb coordinate	other specified inputs
cubic	$[t] = 6/5$	one relevant source
quartic suspension A_3	$[c_0] = 4/3$	one mass, one relevant source
four ordinary ends	$[U] = 2$	four masses, marked q

(XII.9.59)

Here the isolated quartic suspension is the $n = 4$ example, distinct from the binary quartic with Milnor rank nine. The mirror comparison also has a rank-one gauge sector, with the scaled variable u. To select that row one must specify its Type IIA Kähler origin and the mirror limit. The table distinguishes these cases before any claim about a BPS chamber. The four-ended row includes exactly marginal q under its stated massless dictionary; the cubic and quartic-suspension rows have relevant sources instead.

If the question is narrowed to a weak $\mathfrak{su}(2)$ description, the two gauge constructions remain distinct. The four ordinary ends give four full fundamentals. The local-F_0 mirror presents the pure sector, with the index-two projected particle lattice. A unit pair on a compact spectral curve is insufficient to identify these charge problems. Indeed the actual mirror projection gives

$$D = \begin{pmatrix} 2 & 0 \\ 0 & 1 \end{pmatrix}, \qquad J_0 = \begin{pmatrix} 0 & 1 \\ -1 & 0 \end{pmatrix}, \qquad D^{\mathsf{T}} J_0 D = 2J_0, \qquad |\det D| = 2. \quad \text{(XII.9.60)}$$

The factor two comes from the allowed winding kernel and is retained when comparing particle charges. The direct four-ended calculation was made in a spectral gauge quotient over $\mathbb{Q}$; it did not perform this integral projection. Reading the entries together therefore tells us which further lattice computation a comparison would require.

The ALE entry provides a different selection test. Two compact cycles and a nonzero determinant occur both for the ALE A_2 surface and for the cubic threefold matching pair. The symmetry of their intersections already separates the wrapping problems:

$$I_{\mathrm{ALE}}^{\mathsf{T}} = I_{\mathrm{ALE}}, \qquad J_{(L,R)}^{\mathsf{T}} = -J_{(L,R)}, \qquad \det I_{\mathrm{ALE}} = 3, \qquad \det J_{(L,R)} = 1. \quad \text{(XII.9.61)}$$

For transverse middle cycles of real dimension d, exchanging their order gives the intersection sign $(-1)^{d^2}$. The two-cycle and three-cycle cases accordingly have different symmetry. The D3 wrapping then leaves a string worldsheet or a particle worldline as in (XII.9.58). Counting cycles first and declaring a common gauge sector would discard precisely this information.

These examples suggest an order for using either panel. First specify the geometric dimension and construction route, then the allowed deformations and their normalization. Next read the compact or relative charge frame and the end conditions. Only then use the displayed physical dictionary and any stated stability data. Each step answers a

different question. A missing lattice, norm or chamber calculation remains visible in its own column and identifies the next calculation to perform.

The deeper examples provide a further way to select a construction without enlarging the two panels into a classification. Chapter 3 holds the sources fixed in the complete family $x_1^2 + x_2^2 + x^p + z^q + \sum c_{ij} x^i z^j = 0$. Its three worked choices separate a larger Coulomb rank from a larger number of deformation parameters. In the following count, a source is a coefficient held fixed while the Coulomb vevs vary. Positive sources have $0 < \Delta < 1$; the last two columns retain sources with $\Delta = 0$ and $\Delta < 0$:

(p, q)	μ	vevs	masses	positive sources	zero	negative
$(3, 5)$	8	4	0	4	0	0
$(3, 6)$	10	4	2	3	1	0
$(4, 6)$	15	7	1	5	1	1

(XII.9.62)

The first two choices have the same Coulomb rank four, yet their external parameters differ. In the last choice the dimension-zero and negative-dimension coefficients remain part of the full local miniversal deformation space. They are fixed along a chosen local Coulomb family. Their algebraic existence does not provide a quantum conformal manifold or a continuum theory at finite irrelevant coupling. For the undeformed conformal theory the sources and masses are set to zero; its conformal vacuum also has all vevs zero. Fixing the external parameters therefore differs from choosing a vacuum.

For the binary quartic, the useful question is instead which singular point and period scale a deformation selects. The local choices constructed in Chapter 6 can be read side by side. Use its Fermat representative $\lambda = 0$ for the critical counts and two-mass period windows below:

Changed input	Selected geometry	Conditions for the selection
Mass az^2	Local A_3 germ	$a \neq 0$, tuned origin; the same w^2 coefficient changes from UV mass dimension one to local dimension 2/3.
Relevant hz^2w	Principal D_5 sector	$h \neq 0$ fixed, origin selected; its localized Milnor count is five, while the full critical algebra has length nine.
Masses $az^2 + bw^2$	Local node	$a, b \neq 0$, smoothing δ with $\lvert\delta\rvert \ll \lvert a\rvert^2, \lvert b\rvert^2$.

For a hierarchy $|b| \ll |a|$, the same two-mass family has an intermediate A_3 period window $|b|^2 \ll |\delta| \ll |a|^2$. Finer smoothing enters the node window in the last row. These comparisons use transported compact cycles in smooth fibers, consistent roots and nonzero finite normalized periods. One must keep the selected fiber and the period window when passing from a UV coefficient role to a local one. Counting all stationary points as singularities of a single chosen fiber would mix the selected origin with remote critical levels.

Chapter 7 reaches a local quartic from a different UV input. Giving the fifth mass M a nonzero fixed value in the same two-quadric family permits exact elimination to a graph hypersurface $H = 0$. With Ω_H its residue in the declared graph coordinates, the

ordered original residue is $\Omega_{\mathrm{ICIS}} = -\Omega_H/M$. Selected Coulomb fibers give a node or a tuned quartic germ. Applying the stipulated fixed-M local IIB premise to the quartic gives coefficient dimensions $4/3, 1, 2/3$. This selected rank-one sector does not describe the complete infrared theory of the UV rank-two construction. The equation-module map tracks infinitesimal directions; it is not a finite parameter map.

Changing the ends gives a different operation. In Chapter 5 the fixed-mass limit $q \to 0$ produces the weak tube of the four-ordinary-ended family. Its one-heavy-flavor limit instead takes $H \to \infty$, $q = \Lambda/H$ and tunes the Coulomb coefficient. The full-hyper masses are arranged as $m, H, b+c, b-c$, so removing H leaves three finite masses. The allowed pole orders and retained Coulomb count are

$$(2,2,2,2) \;\longrightarrow\; (4,2,2), \qquad \#\{\text{finite masses}\} = 3, \qquad \#\{\text{Coulomb vevs}\} = 1. \tag{XII.9.63}$$

The new fourth-order pole is at the irregular end; the two ordinary poles are exactly double for nonzero b, c. Holding the polar part of the selected square root fixed holds Λ, m fixed, together with the ordinary residues. The scale $\Lambda = qH$ has mass dimension one and depends on the stated mass and marked-coordinate convention. It replaces the separate marked-base modulus in this three-ended boundary problem. The finite interior compact periods survive under the smooth-cycle transport proved there. Equal Coulomb rank therefore does not turn heavy-flavor removal into the fixed-mass weak-tube operation.

XII.9.8 Exercises

1. **Three counts for the suspended singularities.** In the order conifold, marked A_2, nearby A_3, compute the Milnor numbers, compact skew ranks, and Coulomb ranks. Give a primitive generator of the A_3 radical up to overall sign in the matching basis. State whether B_L is compact and use its boundary to explain your answer.

2. **An ordered pair of equations.** Compute the multiplicities and normalized coefficient dimensions of T^1 in grades $0, 1, 2$. With the same ambient order, change the equations to $F' = \mathrm{diag}(2,1)F$ and give the factor Ω'/Ω. Does the weight-zero slice by itself establish exact marginality? Explain what goes wrong if one replaces the normal module by a scalar minors quotient.

3. **Which geometry is the mirror?** An entry calls the Laurent threefold of (XII.9.51) a direct construction and assigns it the four fundamentals of the four-puncture fibration. Repair the route label and find the finite u/L singular values. Compare the numbers of full fundamentals in the order local F_0, four punctures. State whether the common rank and weak algebra establish a QFT identity. Identify the Type IIA input to the mirror presentation.

4. **The same quadric at rank three.** For $N = 3$ give S/μ_{def}, the mass dimension of S, and G_A. Compute the coefficient of $\log r$ in the compensating $\Delta\alpha$. Give the destination of each of the roots $0, 1, 2$ under a positive theta winding. Explain the two physical uses of the compact period in the presence and absence of flux.

5. **Geometric and physical coupling data.** Find the exceptional finite λ values of the binary quartic and the number of fixed-mass differential directions of the four-ended fibration. In the order binary quartic, two quadrics, massless four-ended family, state whether the chapter identifies a physical exactly marginal coupling. Explain what further information a BPS spectrum would need.

For further written practice, consider the following variations. At $q = 1/3$, write the four-by-five leading-pole matrix and verify the kernel in (XII.9.36). Explain why adding a constant to the numerator changes mass squares. For the equation change in (XII.9.29), transport a perturbation in the first component and check the ordered residue factor directly. Finally, at rank four compare a positive theta winding with an S-plane loop at fixed cutoff. State which boundary coefficient must be transported to leave W unchanged. These written questions extend the five exercises above.

Take-home message of this chapter

To compare two constructions, retain the equation and its deformation space, the oriented period and charge frame, and the physical boundary conditions. The Milnor number counts middle cycles of a smoothing. The Coulomb rank counts vevs in the chosen local theory. A relative period, a flux integral or a spectral curve only acquires its physical meaning with the accompanying choice of sectors and boundary data.

Status and sources

§XII.9.2. Compact charges and relative periods. The Jacobi quotients, weight and middle-rank arithmetic in (XII.9.1)–(XII.9.3) are [MATH], with the period-mass and local parameter dictionary [GEO-E] from Chapter 3 and Xie and Yau 2015, (2.16), (2.19)–(2.22), Example I. The conifold pair, residue and shear in (XII.9.4)–(XII.9.6) are [MATH] in Chapter 2's marked frame. The compact monodromy comparison is Strominger 1995, (2.1)–(2.4). The lower bound (XII.9.7) is [MATH] for the stipulated AC end. The concrete metric variation uses the unwarped calculation of Koroteev et al. 2016, §5.3, [SUGRA]. The isolated fixed-end rank-zero hyper is [GEO-E]. The ordinary compact nodal charged hypermultiplet has different boundary hypotheses.

The oriented matching forms and the one-arrow strict stability test in (XII.9.8)–(XII.9.11) are [MATH] in Chapter 4's marked frames. The period-to-charge and light-quiver identification are [GEO-E] for the selected local sector. See Shapere and Vafa 1999, §5.1, (5.3) and the collinear-root example, and Alim et al. 2013, §2. The linear term of the cubic uses its dimension-4/5 coupling role here.

§XII.9.3. Equal Milnor rank and different parameter roles. The quartic discriminant, Hilbert polynomial and local germ in (XII.9.16)–(XII.9.20) are [MATH] as in Chapter 6. Compare the coefficient weights in Buican et al. 2015, (3.7)–(3.10). Its stronger cusp and marginality analysis requires additional input. The ordered normal module, Euler calculation and residue change in (XII.9.22)–(XII.9.26) are [MATH] from Chapter 7, Chen et al. 2017, (2.9)–(2.10), Greuel 2019, Thm. 1.22 and Def. 2.22, and Greuel and Hamm 1978, §3. The coefficient-role interpretations in the two local IIB settings are [GEO-E].

§XII.9.4. Four ordinary ends and a weak tube. The bundle and patching, the end map, sweep and compact curve period calculations in (XII.9.30)–(XII.9.41) are [MATH] from Chapter 5 and Alim et al. 2013, (3.1)–(3.6). The ordinary-end matter and exact marginality of massless q are separate [GEO-E] inputs, Alim et al. 2013, §3.4.2, and Gaiotto 2009b, §2.1–2.2, (2.11), (2.18). The comparison concerns compact spectral periods and the reduced norm.

§XII.9.5. One quadric with and without flux. The ratio of residues and the branchwise computations (XII.9.43)–(XII.9.47) are [MATH] with the stated holomorphic prescription. The transition, compact charge sector and composite match are [GEO-E] in the frame of Chapter 8. See Cachazo et al. 2001, §2, for the relative flux superpotential and stationary points, and Giddings et al. 2002, (2.2), (2.25), for the flux doublet and integer units. The regulated relative period is distinct from a compact flux integer.

§XII.9.6. Presentation and dimension. The local mirror toric, scaling and winding calculations in (XII.9.50)–(XII.9.55) are [MATH] in the marked chart of XI.6. The identification of the Type IIA engineered pure gauge sector by mirror periods is [GEO-E] as used there, with Katz et al. 1997, §4.2–5. This comparison uses that route and makes no new duality transfer. The ALE pairing and wrapping dimensions in (XII.9.56)–(XII.9.58) are [MATH]. The ordinary Type IIB identification and wrapped string interpretation are [GEO-E] from Chapter 1 and Witten 1995, (1.4)–(1.5) and the wrapped D3 discussion. Isolation of the retained sectors is assumed separately for each construction [DEC].

Comparative calculations. Equations (XII.9.12)–(XII.9.14) are integral linear algebra and the boundary map applied to the compact and relative forms above, [MATH]. Equations (XII.9.27)–(XII.9.29) are grade counts and constant equation transport, [MATH]. The fixed-end examples (XII.9.33)–(XII.9.36) are polynomial substitutions, [MATH]. The period-frame compensation and changed-rank root arithmetic in (XII.9.48)–(XII.9.49) use the same holomorphic prescription, [MATH] conditional on its imported [GEO-E] dictionary. The selection comparisons in (XII.9.59)–(XII.9.61) reuse the coefficient, winding and intersection calculations above; they introduce no additional identification of sectors.

Further local selections. The count comparison in (XII.9.62) reuses Chapter 3's two-exponent calculation, [MATH], with its imported [GEO-E]/ [DEC] coefficient dictionary and local limit; see Xie and Yau 2015, §2.2 and §3.1. The quartic three-simple chamber uses the positive basis, signed periods and strict-subobject calculation of Chapter 4; its physical light-hyper identification is [GEO-E] under the stipulated local isolation [DEC]. The local mass/relevant and period-window comparisons reuse Chapter 6, with [MATH] local geometry and conditional [GEO-E]/ [DEC] interpretation. The end change in (XII.9.63) reuses Chapter 5, with [MATH] confluence and polar constraints; the sourced three-flavor interpretation is [GEO-E] and local isolation remains [DEC]. These comparisons introduce no new global BPS, kinetic, primitive lattice or exact coupling-normalization claim. The mass-deformed complete-intersection pointer uses Chapter 7; the exact elimination, signed residue and local singularities are [MATH]; the selected local coefficient-role interpretation is conditional [GEO-E]/ [DEC]. It identifies neither a complete IR decomposition nor a BPS stability chamber. The new end prescription and three-flavor family use Gaiotto et al. 2009, (10.19), and Gaiotto 2009a, §6–7, as

translated in Chapter 5.

References

Alim, M. et al. (2013). "BPS Quivers and Spectra of Complete $\mathcal{N} = 2$ Quantum Field Theories". In: *Commun. Math. Phys.* 323.3, pp. 1185–1227. DOI: 10.1007/s00220-013-1789-8. arXiv: 1109.4941 [hep-th].

Buican, M. et al. (2015). "Argyres-Douglas Theories and S-Duality". In: *JHEP* 02, p. 185. DOI: 10.1007/JHEP02(2015)185. arXiv: 1411.6026 [hep-th].

Cachazo, F., K. A. Intriligator, and C. Vafa (2001). "A large N duality via a geometric transition". In: *Nucl. Phys. B* 603, pp. 3–41. DOI: 10.1016/S0550-3213(01)00228-0. arXiv: hep-th/0103067.

Chen, B. et al. (2017). "4D N=2 SCFT and singularity theory. Part II: Complete intersection". In: *Adv. Theor. Math. Phys.* 21, pp. 121–145. arXiv: 1604.07843 [hep-th].

Gaiotto, D. (2009a). *Asymptotically free $\mathcal{N} = 2$ theories and irregular conformal blocks*. arXiv: 0908.0307 [hep-th].

Gaiotto, D. (2009b). "N=2 Dualities". In: arXiv: 0904.2715 [hep-th].

Gaiotto, D., G. W. Moore, and A. Neitzke (2009). *Wall-crossing, Hitchin Systems, and the WKB Approximation*. arXiv: 0907.3987 [hep-th].

Giddings, S. B., S. Kachru, and J. Polchinski (2002). "Hierarchies from fluxes in string compactifications". In: *Phys. Rev. D* 66, p. 106006. DOI: 10.1103/PhysRevD.66.106006. arXiv: hep-th/0105097.

Greuel, G.-M. (2019). *Deformation and Smoothing of Singularities*. arXiv: 1903.03661 [math.AG].

Greuel, G.-M. and H. A. Hamm (1978). "Invarianten quasihomogener vollständiger Durchschnitte". In: *Invent. Math.* 49, pp. 67–86. DOI: 10.1007/BF01399511.

Katz, S. H., A. Klemm, and C. Vafa (1997). "Geometric engineering of quantum field theories". In: *Nucl. Phys. B* 497, pp. 173–195. DOI: 10.1016/S0550-3213(97)00282-4. arXiv: hep-th/9609239.

Koroteev, P., M. Shifman, and A. Yung (2016). "Non-Abelian vortex in four dimensions as a critical string on a conifold". In: *Phys. Rev. D* 94, p. 065002. DOI: 10.1103/PhysRevD.94.065002. arXiv: 1605.08433 [hep-th].

Shapere, A. D. and C. Vafa (1999). "BPS structure of Argyres–Douglas superconformal theories". In: arXiv: hep-th/9910182.

Strominger, A. (1995). "Massless black holes and conifolds in string theory". In: *Nucl. Phys. B* 451, pp. 96–108. DOI: 10.1016/0550-3213(95)00287-3. arXiv: hep-th/9504090.

Witten, E. (1995). "Some Comments on String Dynamics". In: arXiv: hep-th/9507121.

Xie, D. and S.-T. Yau (2015). "4d N=2 SCFT and singularity theory Part I: Classification". In: arXiv: 1510.01324 [hep-th].